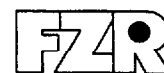


FORSCHUNGSZENTRUM ROSSENDORF



WISSENSCHAFTLICH-TECHNISCHE BERICHTE

**FZR-247**

Januar 1999

**Annual Report 1998**  
**Institute of Radiochemistry**

**Editors:** Prof. Dr. H. Nitsche  
PD Dr. G. Bernhard

**Editorial staff:** Dr. H.-J. Engelmann  
PD Dr. G. Bernhard

## Foreword

We have made further progress in achieving the Institute's goal of contributing to an improved understanding of radionuclide transport in the environment through basic and applied research. We are describing the radionuclide interactions in ground and surface waters on a molecular level by closely combining laboratory and field experiments with modeling. Our interests focus on the interactions of radionuclides on interfaces between the aqueous phase and geological materials such as rocks, soil, and minerals, and on the effect of these interactions on radionuclide transport. We are studying in particular speciation in solution, sorption on geological material, microbial interaction, and the formation and distribution of colloids.

We are very happy and proud to report two major achievements of the Institute. First, the Rossendorf Beam Line (ROBL) at the European Synchrotron Radiation Facility (ESRF) in Grenoble, France, was officially opened in June 1998 and is now fully operational. ROBL EXAFS measurements with uranium, neptunium and technetium confirmed the beamline's superb performance. A collaboration at ROBL was successfully initiated with the Paul Scherrer Institute (PSI), Switzerland. And second, the Radiochemical Laboratory Building at Rossendorf was commissioned. Major parts of the Institute have moved to the new laboratories where neptunium was already successfully handled in the glove boxes.

We accomplished many new scientific results including the synthesis of C-14-labeled humic acid with a specific radioactivity that is high enough to enable radiometric studies of these substances at environmentally relevant concentration levels. Two different kinds of colloidal humic acid particles were identified by atomic force microscopy and photocorrelation spectroscopy that are in accordance with the random coil model. The influence of phenolic hydroxyl groups in humic acids on the complexation of U(VI) was studied for the first time by using designed humic acids with chemically blocked phenolic hydroxyl groups. The laser-induced photoacoustic spectroscopy is now fully established and was successfully used to show that a reduction of U(VI) to U(IV) occurs in the environment under certain conditions.


The Institute organized three large conferences in the past year. The Vortragstagung der Fachgruppe Nuklearchemie in der Gesellschaft Deutscher Chemiker (GDCh) (conference of the Nuclear Chemistry Section of the German Chemical Society) was held at the Technische Universität Dresden in September, followed by the Euroconference and NEA Workshop on Speciation, Techniques, and Facilities for Radioactive Materials at Synchrotron Light Sources at Grenoble, France, in October and the Euroconference on Bacterial-Metal/Radio-nuclide Interaction: Basic Research and Bioremediation in December in Rossendorf. The conference of the German Chemical Society is held every four years and both Euroconferences will be organized again by the Institute in two years.

This past year has also brought some changes to the Institute. Professor Nitsche has pursued a call from the University of California at Berkeley and the Lawrence Berkeley National Laboratory. Beginning November 1, 1998, Dr. Bernhard has assumed the role of Acting Director of the Institute. Professor Nitsche would like to take this opportunity to express his gratitude to all members of the Institute for their excellent work and dedication that made it possible, in just five years, to establish the Institute as an international player in the field of nuclear and environmental chemistry. He also would like to wish Dr. Bernhard and the members of the Institute the very best of luck for the future and he hopes to maintain close ties in form of many future collaborations.

Dr. Bernhard would like to take the opportunity to thank Professor Nitsche on behalf of all members of the Institute for his excellent and successful scientific work here in Rossendorf. Under his leadership the Institute has made significant progress in achieving scientific results in the field of Radioecology and getting an international reputation. All members of the Institute would like to wish him all the best for his further scientific work. We also would like to continue our close collaboration in future.

We would like to thank the visitors, German and international, for their interest in our research and for their participation in the Institute's seminars. We would also like to thank our scientific collaborators and the visiting scientists for coming to Rossendorf in 1998 to share their knowledge and experience with us. We continue to strongly encourage the collaborations and visits by scientists in the future.

Rossendorf, January 1999



Prof. Dr. Heino Nitsche



PD Dr. Gert Bernhard

# CONTENTS

## I. SCIENTIFIC CONTRIBUTIONS

### 1. SPECIATION AND MIGRATION OF RADIONUCLIDES

A new Radiochemical Building for the Institute of Radiochemistry - Constructional and Radiation Protection Aspects - H. Friedrich, G. Bernhard, H. Nitsche	1
The Department of Analytical Chemistry W. Wiesener, D. Birnstein, K. Krogner	2
The Natural $\alpha$ -Activity of Concrete Caused by Natural Uranium and Thorium C. Nebelung, H. Nitsche	3
Separation of Contaminated Concrete into Fine Cement and Added Particles C. Nebelung, H. Nitsche	4
Tailing Water Helmsdorf: pH Titration and Determination of Solution Species G. Geipel, M. Rutsch, G. Bernhard, H. Nitsche	5
Time-Resolved Laser-Induced Fluorescence Spectroscopy of Uranium Minerals Part I: Earth Alkaline Uranyl Phosphates G. Geipel, G. Bernhard, H. Nitsche	6
Time-Resolved Laser-Induced Fluorescence Spectroscopy of Uranium Minerals Part II: Uranyl Arsenates G. Geipel, M. Rutsch, G. Bernhard, H. Nitsche	7
Time-Resolved Laser-Induced Fluorescence Spectroscopy of Uranium Minerals Part III: Copper in Uranyl Minerals G. Geipel, M. Rutsch, G. Bernhard, H. Nitsche	8
Determination of the Speciation of Uranium in Plant Samples by Time-Resolved Laser-Induced Fluorescence Spectroscopy (TRLFS) A. Günther, G. Bernhard, G. Geipel, V. Brendler, H. Nitsche	9
Increase in the Ionic Strength of Uranyl Containing Solutions G. Geipel, M. Rutsch, G. Bernhard, H. Nitsche	10
Validation of the Complex Formation Between $\text{Ca}^{2+}$ , $\text{UO}_2^{2+}$ and $\text{CO}_3^{2-}$ Using EDTA to Adjust the $\text{Ca}^{2+}$ Concentration G. Geipel, G. Bernhard, H. Nitsche	11
Solubility of $\text{Ca}_2[\text{UO}_2(\text{CO}_3)_3] \cdot 10\text{H}_2\text{O}$ , Liebigite S. Amayri, G. Bernhard, H. Nitsche	12
Initial Laser-Induced Photoacoustic Spectroscopic Studies of Uranium(IV) G. Geipel, A. Abraham, G. Bernhard, H. Nitsche	13
Time-Resolved Laser-Induced Fluorescence Spectroscopy with Ultra-short Pulses Part I: Setup of the Laser System M. Rutsch, G. Geipel, G. Bernhard, H. Nitsche	14
Time-Resolved Laser-Induced Fluorescence Spectroscopy with Ultrashort Pulses Part II: Testing of the new Laser System M. Rutsch, G. Geipel, S. Pompe, K. Schmeide, G. Bernhard, H. Nitsche	15
Characterization of Ferrihydrite with AFM and TEM T. Arnold, G. Hüttig, A. Mücklich, Zänker	16
Determination of the Acidity Constant and the Number of Surface Sites of Schwertmannite T. Arnold, G. Bernhard, H. Nitsche	17

Sorption of Uranium(VI) onto Schwertmannite T. Arnold, G. Bernhard, H. Nitsche	18
Distribution of Uranium (VI) on Biotite Surfaces G. Mainka, T. Zorn, T. Arnold, G. Bernhard, H. Nitsche	19
Adsorption Isotherm and Potentiometric Titrations of Quartz T. Zorn, T. Arnold, G. Bernhard, H. Nitsche	20
Sorption of Tetravalent Uranium on Metamorphic Rocks and Sediments A. Abraham, L. Baraniak, H. Neubert, G. Bernhard, H. Nitsche	21
Influence of Hydrothermal Wood Degradation Products on the Uranium Sorption on Rocks and Sediments under Anaerobic Conditions L. Baraniak, A. Abraham, G. Bernhard, H. Nitsche	22
Computation of Distribution Coefficients ( $K_d$ ) for Risk Assessment Studies V. Brendler, Y. Stiglund, S. Nordlinder	23
Distribution Coefficients for Uranium: Modeling of the Ranstad Tailing Site V. Brendler, Y. Stiglund, T. Arnold	24
<b>2. ORGANIC MATTER AND ITS INTERACTION WITH RADIONUCLIDES</b>	
Synthesis of Isotopically Labeled Synthetic Humic Acids M. Bubner, S. Pompe, M. Meyer, K.H. Heise, H. Nitsche	25
Complexation of Uranium(VI) with Kranichsee Humic Substances K. Schmeide, G. Geipel, K.H. Heise, H. Nitsche	26
Effect of Humic Substances on the Sorption of Uranium(VI) onto Site-Specific Rock Material K. Schmeide, S. Pompe, R. Jander, K.H. Heise, H. Nitsche	27
The Influence of Phenolic Hydroxyl Groups on the Complexation Behavior of Humic Acids with Uranyl(VI) Ions Studied with Modified Synthetic Humic Acids S. Pompe, M. Bubner, G. Geipel, K.H. Heise, H. Nitsche	28
Comparison of the Model Humic Acids M1 and M42 with Aldrich Humic Acid and their Uranyl Complexes by Infrared Spectroscopy K.H. Heise, R. Nicolai, S. Pompe, M. Bubner, H. Nitsche	29
Reduction of Hexavalent Uranium by Natural Polyelectrolytes A. Abraham, L. Baraniak, G. Bernhard, H. Nitsche	30
Complex Formation of Hexavalent Uranium with Protocatechuic Acid L. Baraniak, G. Bernhard, H. Nitsche	31
Iron(III) Reduction by Synthetic and Natural Humic Acids B. Mack, K.H. Heise, L. Baraniak, G. Bernhard, H. Nitsche	32
Experimental Studies for the Disposal of Carbon-14-Labeled Organic Material: 4. Results of the Photocatalytic Mineralization E. Förster, S. Heller, K.H. Heise, H. Nitsche	33
The Structural <i>trans</i> -Influence - 6-Coordination vs. 5-Coordination U. Abram	34
Synthesis, Characterization and Structure of Amminetris(dimethylphenylphosphine)-diiodidorhenium(III) Triiodid B. Schmidt-Brücken, U. Abram	35
Synthesis, Characterization and Structure of Dichlorobis(triphenylphosphine)pyridine-2-thiolatorhenium(III) and Dichlorobis(triphenylphosphine)pyrimidine-2-thiolatorhenium(III) B. Schmidt-Brücken, U. Abram	36

[Re(NGaCl <sub>3</sub> )Cl(Me <sub>2</sub> PhP) <sub>2</sub> (H <sub>2</sub> Et <sub>2</sub> tcb)][GaCl <sub>4</sub> ] (H <sub>2</sub> Et <sub>2</sub> tcb = N,n-Diethylthiocarbamoylbenzamidine) A Complex with a Covalent Re-N-Ga Bridge U. Abram, S. Ritter	37
Stabilisation of Au <sup>I</sup> and Au <sup>III</sup> in the Same Complex Molecule U. Abram, K. Ortner, L. Hilditch, J.R. Dilworth	38
<b>3. INTERACTION OF MICROORGANISM WITH RADIONUCLIDES</b>	
Bacterial Diversity in Two Uranium Mine Waste Piles in Saxony S. Selenska-Pobell, K. Flemming	39
Diversity in Natural Bacterial Communities in Uranium Wastes as Examined by 16S rDNA Retrieval G. Satschanska, S. Selenska-Pobell	40
Investigation of Bacterial Diversity in a Soil Sample of a Depleted Saxonian Uranium Mining Area Via Sequencing of PCR Amplified and TA-Cloned 16S rRNA Genes C. Puers, S. Selenska-Pobell, H. Nitsche	41
Comparison of Environmental <i>Desulfovibrio</i> Isolates Using RAPD and rep-APD Analyses J. Wober, S. Selenska-Pobell	42
Classification of <i>Desulfovibrio</i> Isolates Recovered From a Uranium Waste Pile K. Flemming, J. Wober, B. Hard, S. Selenska-Pobell	43
Molecular Characterization of <i>Thiobacillus</i> Strains Recovered From a Uranium Mining Waste Pile S. Kutschke, V. Groudeva, S. Selenska-Pobell	44
Characterization of the Surface Layer Protein of the <i>Bacillus Sphaericus</i> Isolate JG A-12 From a Uranium Waste Pile J. Raff, R. Kirsch, S. Kutschke, T. Maier, M. Mertig, S. Selenska-Pobell, G. Bernhard, U. Hahn, W. Pompe	45
Complex Formation of <i>Thiobacillus Ferrooxidans</i> With U(VI) P. Panak, S. Kutschke, S. Selenska-Pobell, G. Bernhard, H. Nitsche	46
Spectroscopic Characterization of U(VI)-Complexes With <i>Thiobacillus Ferrooxidans</i> P. Panak, S. Kutschke, S. Selenska-Pobell, G. Geipel, G. Bernhard, H. Nitsche	47
Interaction of <i>Bacillus</i> Isolates From a Uranium Mining Waste Pile With U(VI) P. Panak, V. Miteva, I. Boudakov, S. Selenska-Pobell, G. Bernhard, H. Nitsche	48
Selective Accumulation of Metal Ions in a Drain Water of a Uranium Mining Waste Pile by Indigenous <i>Bacillus</i> Isolates P. Panak, V. Miteva, I. Boudakov, S. Selenska-Pobell, G. Bernhard, H. Nitsche	49
<b>4. APPLICATION OF X-RAY ABSORPTION SPECTROSCOPY</b>	
The Radiochemistry End Station for XAS Measurements at the Rossendorf Beamline (ROBL) T. Reich, G. Bernhard, M.A. Denecke, S. Dienel, H. Funke, C. Hennig, H. Krug, W. Neumann, W. Oehme, H. Nitsche	51
An EXAFS Study of Uranium(VI) Sorption onto Ferrihydrite T. Reich, T. Arnold, C. Hennig, M.A. Denecke, G. Bernhard, H. Nitsche	52
EXAFS Investigations of the Complexation Behavior of UO <sub>2</sub> <sup>2+</sup> With Model Compounds of Phenolic Wood Degradation Products A. Roßberg, T. Reich, C. Hennig, L. Baraniak, G. Bernhard, H. Nitsche	53
EXAFS Investigations of Uranium Complexes in Plant Samples A. Günther, A. Roßberg, T. Reich, G. Bernhard, H. Nitsche	54

Crystal Structure Comparison of Uranium Arsenates Using EXAFS C. Hennig, T. Reich, M. Rutsch, A. Roßberg, H. Funke, G. Geipel, G. Bernhard, H. Nitsche	55
Coordination Geometry of Ferrihydrite C. Hennig, T. Reich, H. Funke, T. Arnold, H. Nitsche	56
Chromium(III) Sulfate - Collagen Interaction: An EXAFS-Study T. Reich, A. Roßberg, C. Hennig, M.A. Denecke, G. Reich	57
Texture Analysis of Powder Samples Using the Rietveld Method C. Hennig, W. Kraus, G. Nolze	58
<b>5. BEHAVIOR OF COLLOIDS AND AEROSOLS</b>	
Dynamic Light Scattering on Filtered Humic Acid Solutions H. Zänker, G. Hüttig, M. Böttger, H. Nitsche	59
Migration Behavior of Uranium in a Humic-Colloids-Rich Aquifer System: Laboratory Studies With Column Experiments S. Pompe, R. Artinger, K. Schmeide, K.H. Heise, J.I. Kim, H. Nitsche	60
Characterization of Colloid Particles in Mining Water (Rothschönberger Stolln) W. Richter, H. Zänker, H. Nitsche	61
Colloid-Borne Heavy Metals in the Water of a Mining Drainage Gallery (Rothschönberger Stolln) H. Zänker, V. Brendler, W. Richter, H. Nitsche	62
Rothschönberger Stolln: Modeling of Reaction Pathways With EQ3/6 V. Brendler, H. Zänker, W. Richter	63
Detection of Iron and Aluminium Hydroxide Colloids in a Suspension of Ground Phyllite H. Zänker, G. Hüttig, T. Arnold, T. Zorn, H. Nitsche	64
Photolysis of Silicic Acid and New Particle Formation D. Rettig, V. Berghof, P. Merker, N. Schwentner	65
<b>6. CHEMISTRY OF HEAVIEST ELEMENTS</b>	
Physico Chemical Characterization of Seaborgium as Oxide Hydroxide S. Hübener, A. Vahle, S. Taut, H. Nitsche et al.	67
CORA - A New Control Program for the ROMA Detection System S. Taut	68
<b>II. PUBLICATIONS, PATENTS, LECTURES AND POSTERS</b>	69
<b>III. SEMINARS, CONFERENCES AND WORKSHOPS</b>	81
<b>IV. PERSONELL</b>	83
<b>V. ACKNOWLEDGMENTS</b>	85

# **I. SCIENTIFIC CONTRIBUTIONS**

## **Speciation and Migration of Radionuclides**



## A NEW RADIOCHEMICAL BUILDING FOR THE INSTITUTE OF RADIOCHEMISTRY - CONSTRUCTIONAL AND RADIATION PROTECTION ASPECTS -

H. Friedrich, G. Bernhard, H. Nitsche

*A new building devoted to radiochemical work was commissioned in 1998. It is home to 24 radiochemical laboratories and additional 10 rooms for technical service rooms. In accordance to the German Radiation Protection Ordinance (§3) we are licensed to handle 135 different radionuclides, including transuranium elements. The alpha-laboratories are equipped with glove boxes allowing experiments with gram amounts of the actinide elements under ambient or inert gas atmosphere.*

This new radiochemical building is designed for studying the behavior of radionuclides such as uranium, thorium, neptunium, americium, curium, radium, technetium, carbon-14 and tritium, which are important for the environment and for the life sciences.

The cover picture of this report shows a view on the radiochemistry building (background) and the office building complex (front). The laboratory building has 24 radiochemical laboratories and 10 service rooms (rooms for short-term storage of solid and liquid radioactive waste, and waste water, a room for safely storing radioactive samples in special safes, a control room with devices for measuring and signalization of safety and

treatment. The ventilation system guarantees an increasing negative pressure gradient from the hall-ways to the laboratories and from the laboratories to the glove boxes and hoods. The laboratories (Fig. 2) are equipped with 22 alpha-boxes, laminar-boxes, hoods, dish washers for cleaning glass-ware, refrigerators, and drying cupboards. Glove box systems (Fig. 3) are installed for handling gram amounts of various actinide elements under air or inert gas conditions. Several boxes are foreseen for experiments under special gas atmosphere (humidity, CO<sub>2</sub> content). Modern analytic methods are established in the laboratories. These are nuclear magnetic resonance spectroscopy, different methods of



Fig. 1: Frame structure of the building radiation protection relevant data, a separate top floor which houses all equipment for air conditioning, ventilation and filtering). The building is constructed from prefabricated standard room containers. The dimension of such a container is 3.3 x 6.6 x 8.3 m (height x width x



Fig. 2: Inside a standard laboratory length). Fig. 1 shows a photograph of this frame construction during the building phase. Laboratories and service rooms were installed in the first and second floor, in the third floor all technique is located for air



Fig. 3: View on alpha-glove boxes laser spectroscopy, UV-vis/FTIR-spectroscopy, photon correlation spectroscopy, field flow fractionation, equipment for electrochemical measurements, and ultra centrifugation. Modern equipment for  $\alpha$ -,  $\beta$ - and  $\gamma$ -spectrometry is also available.

All laboratories are connected to a central gas supply station located outside the building. Up to four different gases can be used in each laboratory at the same time. All rooms are located in one controlled area. Radioactivity and the dose rate of the air are constantly monitored. The exhaust air is automatically surveyed for tritium, carbon-14, radioactive iodine,  $\alpha$ -,  $\beta$ - and  $\gamma$ -activity in aerosols. All safety related data are monitored by an automated survey system.

The entrance system to the building is controlled by an automated dosimetry system. This ensures a permanent overview and radiation exposure record for the personnel. According to the licence given by the Saxon Ministry of Environment in March 1998, we are licensed to handle 135 nuclides with a maximum of activity for each nuclide of  $10^{11}$  Bq. Concerning the kind and number of radionuclides, the permission for handling radioactivity varies for each laboratory.

## THE DEPARTMENT OF ANALYTICAL CHEMISTRY

W. Wiesener, D. Birnstein, K.Krogner

*The quantitative determination of elements and components is an essential part of many research projects. The methods available in the Department of Analytical Chemistry are used in close cooperation with the scientists.*

Since 1998 the former Central Department of Analytical Chemistry of the Research Center Rossendorf is part of the Institute of Radiochemistry and is involved in the chemical and physico-chemical characterization of many different types of samples coming from the Institute's scientific group.

Elemental analyses, especially at trace level, are conducted out by ICP-MS (inductively coupled plasma mass spectrometry), various techniques of AAS (atomic absorption spectroscopy) and for some light elements by combustion followed by ion chromatography (IC), which is also used for the determination of anions. The sum parameters for adsorbable organic halogens (AOX) and total organic carbon (TOC) are mostly the focus of investigation in environmental samples. Various methods of thermal analysis and surface determination are also used.

The samples cover a wide field, e. g. natural waters, soils, biological and geological materials, substances and solutions from basic research programs of the Institute. Various methods of sample digestion and sample preparation are therefore applied. Besides the major work for the Institute of Radiochemistry other institutes of the Forschungszentrum Rossendorf are also assisted with the analytical methods. Samples from the Rossendorf territory are investigated if they meet the requirements of environmental and radiation protection. The AAS and AOX methods are used for commercial samples of the Nuclear Engineering and Analytics Rossendorf (VKTA).

Close interactions exist between the analysts and the users of the analytical facilities. The requirements for the specific samples, e. g., the purity of the vessels and the chemicals used for preparation and often also the results of the analyses, are discussed. These discussions result in a better understanding of the problems concerning the scientific tasks and the specific requirements for the analytical methods.

The variety of samples poses a permanent challenge to the analysts. The matrices and main components often interfere in various ways with the determination of minor components or traces. ICP-MS measurements for example, can be impeded by high acid and/or salt causing not only an overload of the mass detector, but also interference with the plasma itself and may form molecule ions having the same mass as the elements to be determined. This leads to wrong results by pile up effects. The influence of the matrix must therefore be corrected, for example, by the standard addition method. Quality control and quality assurance is carried out by measurements of certified standard materials and participation in inter-laboratory comparison studies.

In 1998 the following elemental analysis methods were mainly performed for research projects of the Institute:

- element determination of isolated humic acids;
- determination of heavy metals in humates;
- determination of heavy metals in geological materials to investigate their exchange capacity;
- comparison of various humic acids for their complex forming behavior with uranyl ions and arsenates;
- determination of element composition of calcium uranyl carbonate related to their different syntheses and characterization;
- determination of 36 elements in mining related water samples as a basis for species calculations;
- determination of 16 elements in waters and separated colloids from former mines in Saxony;
- determination of uranium and other metals to investigate their interaction with microorganisms.

Other elemental analyses were carried out for the Institute of Bioinorganic and Radiopharmaceutical Chemistry, the Institute of Safety Research, the Institute of Ion-Beam Physics and Material Research, the Nuclear Engineering and Analytics Rossendorf and the Institute of Analytical Chemistry at Dresden Technical University.

More than 1,600 samples from the Institute of Radiochemistry were analyzed for anions (IC) and/or DOC/TOC, often in close combination with the above-mentioned samples for elemental analyses. The analyses were conducted for the following research projects:

- Colloid organic particles in mining related waters (SMWK project);
- Characterization of colloid particles in water systems of former mines in Saxony (DFG project);
- Interaction of radionuclides with anthropogenic and natural organics;
- Colloid research.

These methods are also used for samples from the Rossendorf territory (environmental protection).

The analytical results are integrated into scientific publications, e. g. *Radiochimica Acta*, *J. Phys.*, *Journal of Applied Bacteriology*.

# THE NATURAL $\alpha$ -ACTIVITY OF CONCRETE CAUSED BY NATURAL URANIUM AND THORIUM

C. Nebelung, H. Nitsche

The measurement of low contaminations of  $\alpha$ -active nuclides in concrete are of interest during the dismantling of nuclear installations. The contamination levels are close to the level of the concrete's natural radioactivity. Therefore the determination of natural radioactivity levels in uncontaminated concrete are measured.

## Experimental

Alpha-active nuclides in concrete can be measured by  $\alpha$ -spectrometry after mechanical preparation [1,2]. The concrete is crushed in two steps. It is first crushed with a jaw breaker to 0.1 mm particles and then second wet milled to 0.1  $\mu$ m particles. The suspension is sprayed or poured to thicknesses between 0.5  $\mu$ m to 2  $\mu$ m onto steel plates with 200 mm diameter. The samples are measured in a grid ionization chamber (GIC).

## Results

Fig. 1, 2, 3 show the GIC spectra of three uncontaminated concretes (columns) and the peakfitting functions (lines). The measuring time was 20 h and the spectra are corrected for background. The measured alpha-activity is due to natural uranium and thorium and their decay products. The Table shows the activity of different nuclides that were detected in three different samples coming from construction concrete of the radiochemistry laboratory in Rossendorf (RCNS), the zero energy research reactor in Rossendorf (RRR) and the nuclear power plant in Greifswald (BGI).

Nuclide	specific $\alpha$ -activity Bq/g		
	RCNS	RRR	BGI
$^{232}\text{Th}$	$0.007 \pm 0.002$	$0.004 \pm 0.004$	$0.019 \pm 0.007$
$^{238}\text{U}$	$0.017 \pm 0.003$	$0.039 \pm 0.008$	$0.030 \pm 0.007$
$^{230}\text{Th}$	$0.019 \pm 0.005$	$0.047 \pm 0.012$	$0.056 \pm 0.005$
$^{234}\text{U} / ^{226}\text{Ra}$	$0.014 \pm 0.004$	$0.046 \pm 0.012$	$0.030 \pm 0.009$
$^{210}\text{Po}$	$0.012 \pm 0.003$	$0.022 \pm 0.004$	$0.026 \pm 0.003$
$^{228}\text{Th}$	$0.004 \pm 0.004$	$0.002 \pm 0.002$	$0.026 \pm 0.001$
$^{222}\text{Rn}$	$0.009 \pm 0.003$	$0.020 \pm 0.007$	$0.024 \pm 0.012$
$^{224}\text{Ra}$	$0.012 \pm 0.002$	$0.006 \pm 0.004$	$0.020 \pm 0.005$
$^{218}\text{Po}$	$0.007 \pm 0.003$	$0.022 \pm 0.004$	$0.016 \pm 0.004$
$^{212}\text{Bi}$	$0.011 \pm 0.005$	$0.007 \pm 0.003$	$0.017 \pm 0.005$
$^{220}\text{Rn}$	$0.012 \pm 0.002$	$0.007 \pm 0.003$	$0.022 \pm 0.001$
$^{216}\text{Po}$	$0.015 \pm 0.002$	$0.010 \pm 0.001$	$0.020 \pm 0.003$
$^{214}\text{Po}$	$0.011 \pm 0.003$	$0.022 \pm 0.005$	$0.019 \pm 0.002$
$^{212}\text{Po}$	$0.011 \pm 0.002$	$0.006 \pm 0.001$	$0.014 \pm 0.003$
all nuclides	$0.162 \pm 0.020$	$0.261 \pm 0.023$	$0.339 \pm 0.018$

The overall activity of these three concrete samples varies by a factor of two. The activity of the  $^{232}\text{Th}$ - and the  $^{238}\text{U}$ -decay products are nearly equal in the BGI and RCNS concrete. For the RRR-concrete most of the activity is caused by  $^{238}\text{U}$  and its decay products. We have shown to 20 hours measuring time are sufficient to determine the  $\alpha$ -activity of all nuclides in the concrete by

peak fitting the spectra with a Gaussian function and an exponential tailing [2].

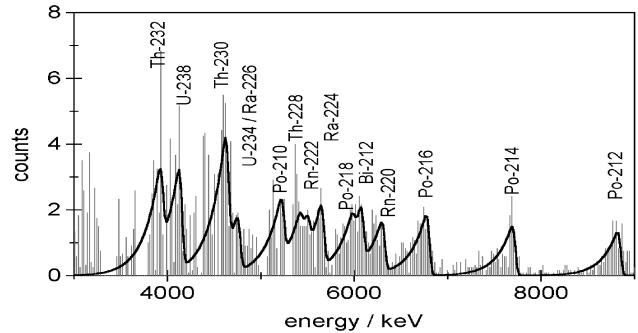


Fig. 1:  $\alpha$ -spectrum of 50 mg RCNS-concrete

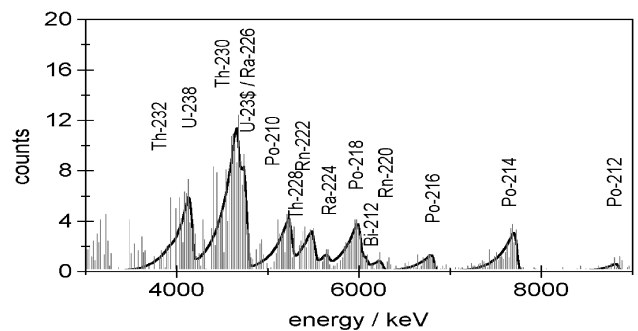


Fig. 2:  $\alpha$ -spectrum of 50 mg RRR-concrete

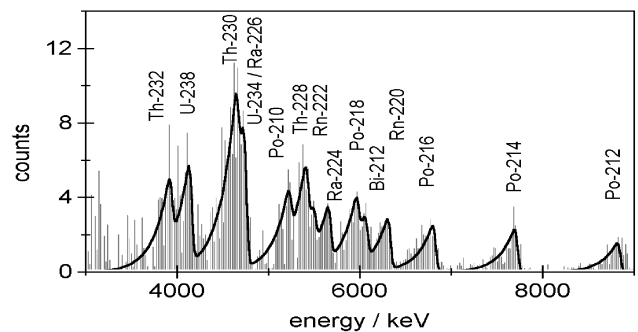


Fig. 3:  $\alpha$ -spectrum of 50 mg BGI-concrete

## Acknowledgments

This work was supported by the Bundesministerium für Bildung, Wissenschaft, Forschung und Technologie of the Federal Republic of Germany under the contract number 02 S 7655A8.

## References

- 1/ Nebelung, C., Hübener, S., Bernhard, G.: *Methodenentwicklung zur Freimessung von Bauschutt auf alpha-aktive Nuklide (Th, U, Np, Pu, Am)*. Schlußbericht zum Fördervorhaben BMBF 02 S 7442 2, 1995
- 2/ Nebelung, C., Nitsche, H., Bernhard, G.: V. Stilleungskolloquium Hannover und IV. Statusbericht Stilleung und Rückbau kerntechnischer Anlagen. 24.-25.6.1997 Hannover Tagungsband S. 293-301

# SEPARATION OF CONTAMINATED CONCRETE INTO FINE CEMENT AND ADDED PARTICLES

C. Nebelung, H. Nitsche

We separated contaminated concrete in fine-grained cement particles and coarse grained additive particles and found that uranium and americium is mostly associated with the fine-grained particles of the concrete.

## Experimental

In order to determine to which fraction of concrete radioactivity binds the most, we treated the surface of concrete pieces with radioactive solutions. Two peaces were treated with  $^{233}\text{U}$  (sample No. 1:  $0.02 \text{ Bq g}^{-1}$ , sample No. 2:  $2 \text{ Bq g}^{-1}$ ) and two pieces with  $^{241}\text{Am}$  (sample No. 3:  $0.225 \text{ Bq g}^{-1}$  and sample No. 4:  $0.222 \text{ Bq g}^{-1}$ ) two untreated concrete pieces (sample no. 5 and 6) were also used for comparison. The samples were decomposed into a fine cement fraction and into coarse grained particles by two different methods except sample No. 6 which was not separated. Samples 1,2 and 3 were decomposed by heating to  $700^\circ\text{C}$  and then immediately cooled in liquid nitrogen. Samples 4 and 5 were decomposed by pulsed electrical discharge /1/. The fine and coarse fraction were separated and prepared for  $\alpha$ -counting. The processing involved grinding to 0.1 mm and wet milling to  $0.1 \mu\text{m}$ -sized particles which were sprayed thin and evenly onto counting plates of 200 mm diameter. The  $\alpha$ -spectra of the samples were measured with a grid ionization chamber/2/.

## Results

The table shows the measured specific activity of samples 1 to 6. The total activity of the other samples is the sum of the activities of fine and coarse grained fractions considering the percentages of the masses. The main activity of the added actinides was found in the fine fraction of the concrete. The total activity represents the expected specific activity (added activity + concrete activity without contamination).

No	added actinides in $\text{Bq g}^{-1}$	specific activity in $\text{Bq g}^{-1}$ [mass content in %]		
		fine	coarse	total
1	0.02 U-233	$0.279 \pm 0.020$ [65.1]	$0.131 \pm 0.012$ [34.9]	$0.227 \pm 0.017$ [100]
2	2.0 U-233	$2.830 \pm 0.061$ [60.7]	$0.729 \pm 0.036$ [39.3]	$2.004 \pm 0.051$ [100]
3	0.225 Am-241	$0.565 \pm 0.044$ [72.3]	$0.226 \pm 0.017$ [27.7]	$0.471 \pm 0.036$ [100]
4	0.222 Am-241	$0.678 \pm 0.052$ [57,2]	--	--
5	--	$0.185 \pm 0.012$ [39.1]	$0.205 \pm 0.021$ [60.9]	$0.197 \pm 0.017$ [100]
6	--	--	--	$0.191 \pm 0.018$ [100]

Fig. 1 shows the  $\alpha$ -spectrum of the coarse-grained particles and fig. 2 of the fine fraction (with the higher Am-241 peak) of the concrete piece No. 4. Fig. 3 shows a comparison with the uncontaminated concrete.

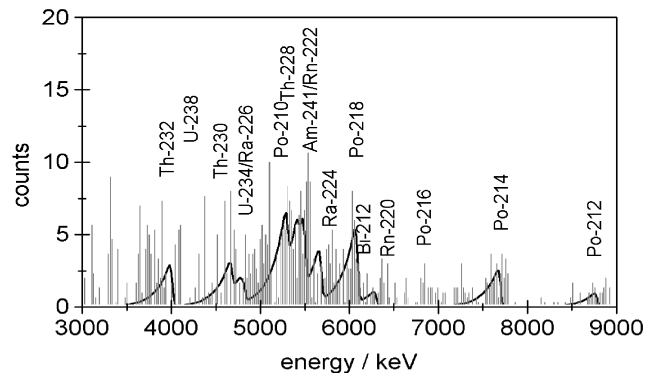


Fig. 1:  $\alpha$ -spectrum of the coarse grained fraction of a concrete with  $0.2 \text{ Bq g}^{-1} \text{ } ^{241}\text{Am}$

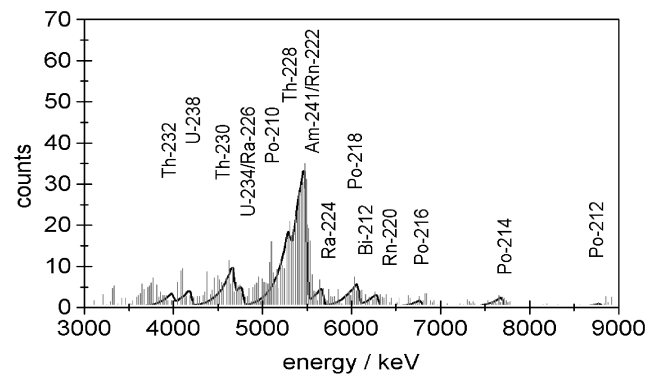


Fig. 2:  $\alpha$ -spectrum of the fine fraction of a concrete with  $0.2 \text{ Bq g}^{-1} \text{ } ^{241}\text{Am}$

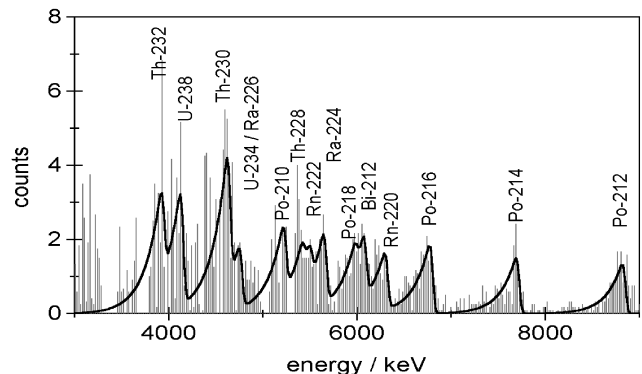


Fig. 3:  $\alpha$ -spectrum of the concrete without contamination

## Acknowledgments

This work was supported by the Bundesministerium für Bildung, Wissenschaft, Forschung und Technologie of the Federal Republic of Germany under the contract number 02 S 7655A8.

## References

- Neubert, V. et al. "Process and device for electrodynamic fragmentation of solids"; in: Report FZKA 5840, Forschungszentrum Karlsruhe
- Nebelung, C., Nitsche, H., Bernhard, G.: V. Stilleungskolloquium Hannover und IV. Statusbericht Stilleung und Rückbau kerntechnischer Anlagen. 24.-25. 6.1997 Hannover Tagungsband S. 293-301

# TAILING WATER HELMSDORF: pH TITRATION AND DETERMINATION OF SOLUTION SPECIES

G.Geipel, M. Rutsch, G. Bernhard, H. Nitsche

The tailing water Helmsdorf was studied by Time-Resolved Laser-Induced Fluorescence Spectroscopy (TRLFS) to validate the different uranium species at several pH values. In the pH range below 6.0, an increase of the fluorescence intensity was found. Deconvolution of these spectra showed that the predominant species are in agreement with newer speciation calculations including the uranyl arsenate species.

Uranium mill tailings play an important role in the assessment of environmental contaminations from uranium mining and ore processing activities. The tailing water has a pH of about 9.6. A substantial change of the pH due to dilution by rain water will not occur because of the large volume of tailing water. However the relatively small amounts of seepage water can easily undergo pH changes due to changing of environment. Thus, changes in speciation will occur when the pH of the tailing water decreases. This speciation change is subject of our studies.

We used the tailing water and added perchloric acid to adjust the pH to the desired value. The solution was always adjusted to a constant volume. The pH was measured with a glass electrode (Ingold) and a pH meter (WCW Weinheim).

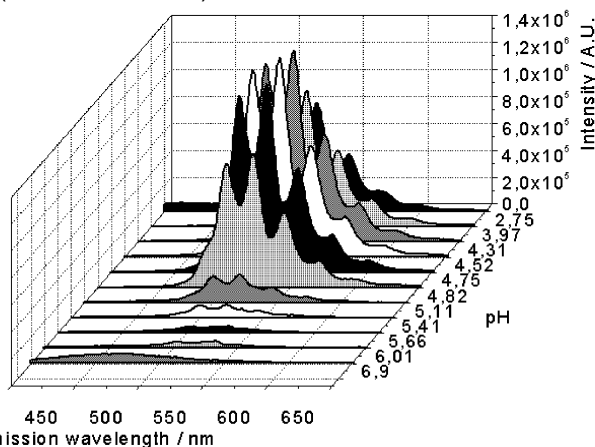


Fig. 1: Fluorescence Spectra of tailing water as function of pH. We studied the pH range from 1.5 to 9.6. Fig 1 shows the fluorescence spectra obtained with the TRLFS setup, that was described earlier /1/. The fluorescence intensity increases with decreasing pH and shows a structure which is significant for most uranyl species. We were able to deconvolute the measured spectra by

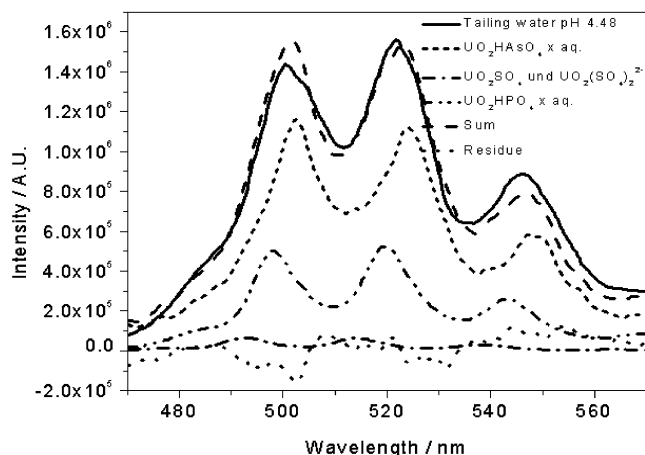


Fig. 2: Deconvolution of the fluorescence spectrum of the tailing water at pH 4.43

using the data from model solutions containing only one anion /1,2,3/. Fig. 2 shows the deconvolution at pH 4.43. We determine two main species UO<sub>2</sub>HPO<sub>4</sub>(aq.) and UO<sub>2</sub>HAsO<sub>4</sub>(aq.), and two minor species UO<sub>2</sub>SO<sub>4</sub>(aq.) and UO<sub>2</sub>(SO<sub>4</sub>)<sub>2</sub><sup>2-</sup>.

When we lower the pH to 1.5, the measured spectrum changes only very little and the intensity decreases slightly. The deconvolution of this spectrum shows an important change in the composition of the different uranyl species. The main fluorescence intensity is now

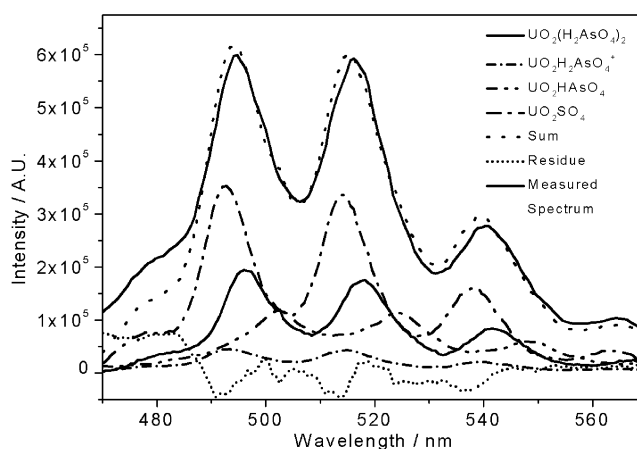


Fig. 3: Deconvolution of the fluorescence spectrum of the tailing water at pH 1.5

caused by the two sulfate species UO<sub>2</sub>SO<sub>4</sub>(aq.) and UO<sub>2</sub>(SO<sub>4</sub>)<sub>2</sub><sup>2-</sup> which cannot be deconvoluted by their spectral properties /2/. A deconvolution is only possible if one can include the fluorescence lifetimes of the uranyl species. This was impossible because substances are present in the tailing water, that quench the fluorescence of the different uranyl species. The other determined uranyl species at pH 1.5 are UO<sub>2</sub>[H<sub>2</sub>AsO<sub>4</sub>]<sup>+</sup> and UO<sub>2</sub>[H<sub>2</sub>AsO<sub>4</sub>]<sub>2</sub>(aq.). Because these two species show very intensive fluorescence properties, it is possible to detect them even in such small amounts as predicted by the speciation calculation. In summary we find very good qualitative agreement between the measured fluorescence spectra at different pH values and speciation calculations including the uranyl arsenate complex formation.

A quantitative analysis of the uranyl species is at this time still impossible due to quenching. Further studies are planned to estimate the influence of quenchers on the fluorescence of uranyl species.

## References

- /1/ Geipel,G., Brachmann,A., Brendler,V., Bernhard,G., Nitsche,H. ; Radiochim. Acta **75**, 199 (1996)
- /2/ Brendler,V., Geipel,G., Bernhard,G., Nitsche,H.; Radiochim. Acta **75**, 75 (1996)
- /3/ Rutsch,M., Geipel,G., Bernhard,G., Nitsche,H.; Report FZR-218 (1998) p.12

# TIME-RESOLVED LASER-INDUCED FLUORESCENCE SPECTROSCOPY OF URANIUM MINERALS - PART I: EARTH ALKALINE URANYL PHOSPHATES

G.Geipel, G.Bernhard, H. Nitsche

The fluorescence properties of the minerals saleeite, autunite and uranocircite were studied by TRLFS. The fluorescence lifetimes increase in this series. Changes in the main fluorescence emission bands between saleeite and the other two minerals were also observed. This can possibly explained with the difference crystal lattice parameters of these minerals.

The minerals saleeite  $[\text{Mg}(\text{UO}_2\text{PO}_4)_2 \cdot 10 \text{H}_2\text{O}]$ , autunite  $[\text{Ca}(\text{UO}_2\text{PO}_4)_2 \cdot 10 \text{H}_2\text{O}]$  and uranocircite  $[\text{Ba}(\text{UO}_2\text{PO}_4)_2 \cdot 8 \text{H}_2\text{O}]$  are alkaline earth uranyl phosphates /1/. These minerals differ only in the alkaline earth cation and in the number of crystal waters. Saleeite (the mineral containing Mg) came from Capeterra, Italy, autunite (the Ca mineral) and uranocircite (the Ba mineral) were from Saxony, Germany. All these minerals were on loan from the Mineral Collection of the Mining Academy Freiberg, Germany.

The fluorescence lifetimes increase from saleeite ( $2.2 \pm 0.2 \mu\text{s}$ ) to autunite ( $5.1 \pm 0.3 \mu\text{s}$ ) and to uranocircite ( $30.5 \pm 1.0 \mu\text{s}$ ). This increase of the lifetime may have two causes. First, the fluorescence lifetime is strongly influenced by the structure and quality of the crystal lattice. Monocrystalline minerals such as liebigite show very long fluorescence lifetimes of more than  $300 \mu\text{s}$ . Second, the crystal water in the minerals acts as a quencher of the fluorescence. The number of crystal water molecules per unit decreases from ten in autunite to eight in uranocircite. A less quenching can therefore be expected. We assume that the sixfold lifetime increase between autunite and uranocircite is due to this decrease in water.

The main fluorescence emission bands are listed in Tab. 1.

Mineral	Fluorescence emission bands / nm				
saleeite	500.9	522.1	545.8	571.6	600.5
autunite	504.1	524.2	547.9	574.1	604.7
uranocircite	503.1	524.1	548.0	574.0	604.8

Tab. 1: Fluorescence emission bands of alkaline earth uranyl phosphate minerals

We found a wavelength shift of about 2.2 nm between saleeite and autunite. The differences between autunite and uranocircite are very small. This spectra look very similar. Only the relative intensity of the first fluorescence emission is much more intensive in saleeite than in autunite.

We calculated the wave numbers of the vibration in the ground state from the band spacing of these three minerals.

The data for saleeite, autunite and uranocircite are  $828 \text{ cm}^{-1}$ ,  $825 \text{ cm}^{-1}$  and  $820 \text{ cm}^{-1}$ . From these data, we can calculate the relative axial U-O distance. A slight increase of about  $0.01 \text{ \AA}$  in the U-O distance from saleeite to uranocircite. This effect is due to the increase in the atomic radius of the alkaline earth metal bound in the minerals.

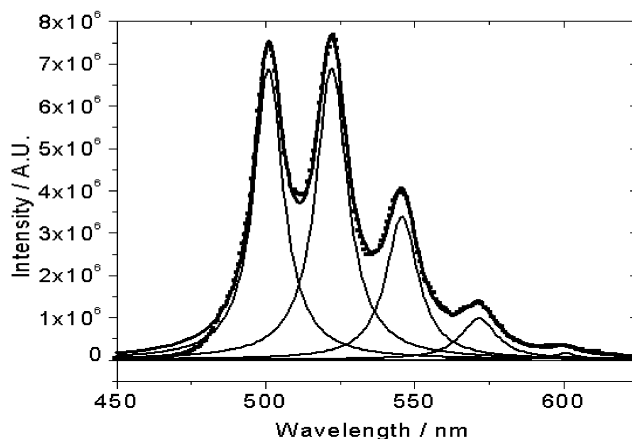


Fig. 1: Fluorescence spectrum of saleeite

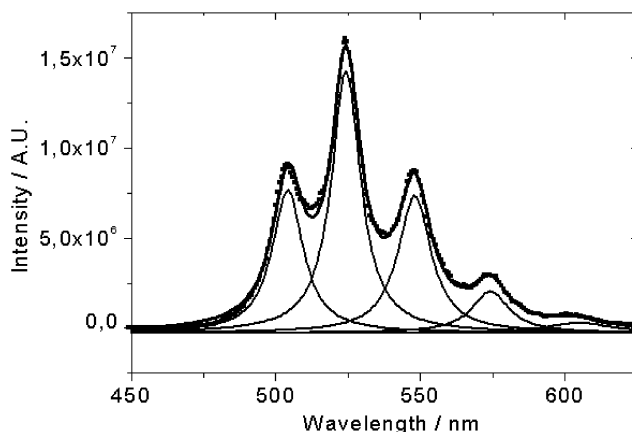


Fig. 2: Fluorescence spectrum of autunite

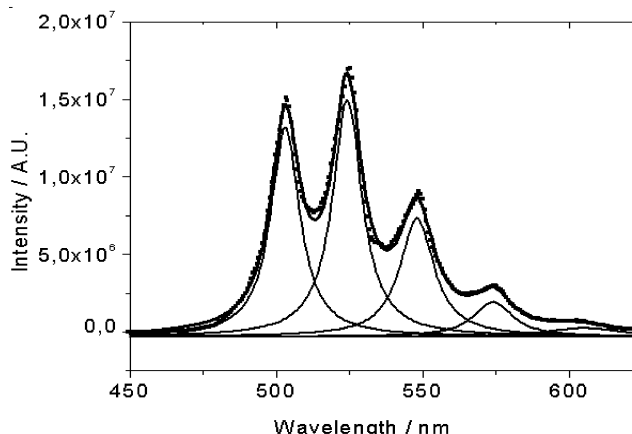


Fig. 3: Fluorescence spectrum of uranocircite

## References

- /1/ Rösler, H.J.: *Lehrbuch der Mineralogie*, DVG, Leipzig, 1991, p. 649-651
- /2/ Gabriel, U.: *Transport reactif de l'uranyle*. Dissertation, Grenoble 1998
- /3/ Frondel, C.: *Mineralogy of uranium and thorium*. Geol. Survey Bull. 1064, 1958

# TIME-RESOLVED LASER-INDUCED FLUORESCENCE SPECTROSCOPY OF URANIUM MINERALS - PART II: URANYL ARSENATES

G.Geipel, M. Rutsch, G.Bernhard, H. Nitsche

The Helmsdorf tailing water forms various uranyl arsenate complexes at pH 5. Such arsenates can also be found as minerals. Fluorescence measurements of troegerite, novacekite and abernathyite showed a good agreement between the main fluorescence emission bands.

We used the same equipment as in the other fluorescence studies of minerals. We applied only low laser energies to the solid samples (< 300  $\mu\text{J}$  per pulse) to avoid any damage to the minerals structure. Thus all the laser energy was absorbed by the sample and the actual laser power could only be measured before application to the sample using a simple quartz beam splitter. This beam splitter divides the laser beam power into one 10% beam which is directed to the power meter, and one 90% beam which is applied to the mineral. No visible change was observed in all minerals during the measuring time.

Fluorescence spectroscopic studies of a pH titration between about 3.0 and 5.5 of the Helmsdorf tailing water identified uranyl arsenate /1,2/. The fluorescence properties of several uranyl arsenate minerals were used as major species in this pH range to characterize the uncharged uranyl species.

From the Mineral Collection of the Mining Academy Freiberg obtained several minerals containing the uranyl arsenate group. These minerals were: troegerite ( $\text{H}_2[\text{UO}_2/\text{AsO}_4]_2 \cdot 8\text{H}_2\text{O}$ ), novacekite ( $\text{Mg}[\text{UO}_2/\text{AsO}_4]_2 \cdot 10\text{H}_2\text{O}$ ), abernathyite ( $\text{K}_2[\text{UO}_2/\text{AsO}_4]_2 \cdot 8\text{H}_2\text{O}$ ). The fluorescence properties of a fourth mineral of this group, zeunerite ( $\text{Cu}[\text{UO}_2/\text{AsO}_4]_2 \cdot 10\text{H}_2\text{O}$ ), were studied and the results are described together with other copper-containing minerals /3/. The troegerite was from Schneeberg, Germany, the novacekite from Brumado, Brasilia, and the abernathyite from Rivalal Lodere, France.

Fig. 1 to Fig. 3 show the fluorescence spectra of these minerals. The main fluorescence emission bands are listed in Tab. 1. Slight differences were found between the main fluorescence emission bands. These differences are caused by the different second cation, hydrogen, magnesium and potassium. The differences are less than three nanometers for the three most intensive emission bands. The agreement between the troegerite and the uranyl arsenate is very good.

Mineral	Fluorescence emission bands / nm			
troegerite	501.6	524.4	548.1	572.4
novacekite	502.8	523.1	546.3	571.7
abernathyite	503.1	526.3	549.2	576.0
$\text{UO}_2(\text{HAsO}_4)\text{aq.}$	504	525	547	

Tab. 1: Main fluorescence emission bands of uranyl arsenate minerals

The fitted fluorescence lifetime for the mineral troegerite was  $126 \pm 12$  ns. Values in this range were also found for the chemical analogue  $\text{UO}_2(\text{HAsO}_4)(\text{aq.})$  /1/. For novacekite, we calculated a fluorescence lifetime of  $5.2 \pm 0.4$   $\mu\text{s}$ . This mineral shows also a second shorter lifetime of  $560 \pm 50$  ns, which we have not yet assigned. The fluorescence intensity of abernathyite is not very high. Also, the spectra show more noise than the other fluorescence spectra. The lifetime of this mineral is very

short, in the range of a few nanoseconds. For this reason the error for the fitted fluorescence lifetime is relatively high. A value for this lifetime is therefore omitted.

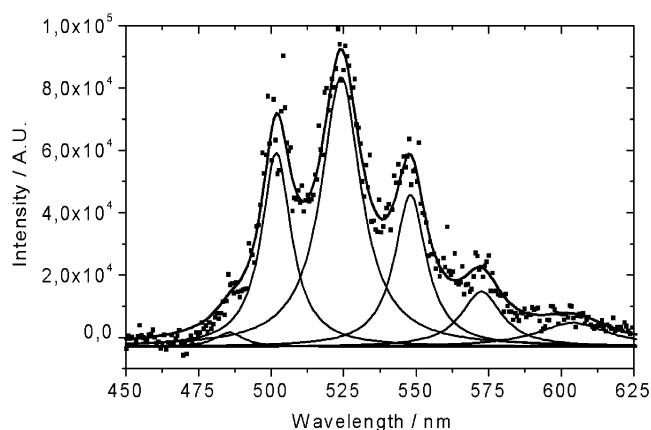


Fig. 1: Fluorescence spectrum of troegerite

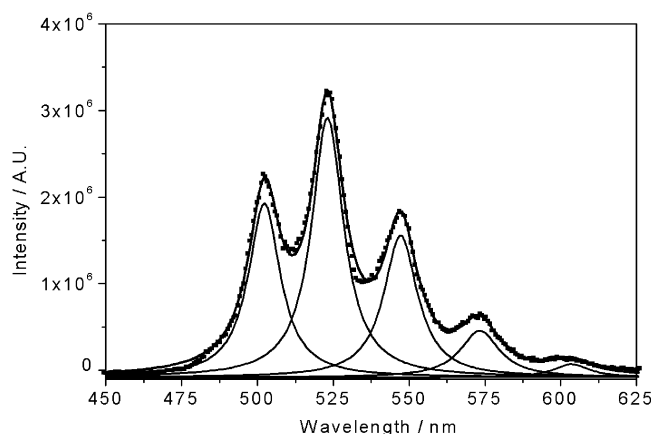


Fig. 2: Fluorescence spectrum of novacekite

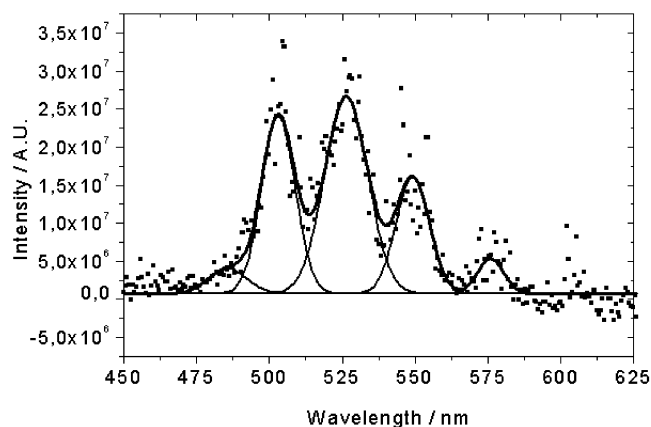


Fig. 3: Fluorescence spectrum of abernathyite

## References

- /1/ Rutsch, M. et al.; Report FZR-218 (1998) p.12
- /2/ Geipel, G. et al.; This report, p. 5
- /3/ Geipel, G. et al.; This report, p. 8

# TIME-RESOLVED LASER-INDUCED FLUORESCENCE SPECTROSCOPY OF URANIUM MINERALS - PART III: COPPER IN URANYL MINERALS

G.Geipel, M. Rutsch, G.Bernhard, H. Nitsche

*Additional cations such as copper, lead and iron in uranium minerals have an important influence on their fluorescence properties. The fluorescence properties of three copper-containing minerals are discussed as examples for fluorescence measurements of about 100 uranium minerals.*

In a series of studies of various uranium minerals, we measured the fluorescence properties of several copper-containing minerals. These minerals are members of various groups according to their chemical composition.

We compared voglite ( $\text{Ca}_2\text{Cu}[\text{UO}_2(\text{CO}_3)]_4 \cdot 6 \text{H}_2\text{O}$ ) from Jachymov, Czech Republic with a series of other uranyl carbonate minerals such as liebigite ( $\text{Ca}_2[\text{UO}_2(\text{CO}_3)]_3 \cdot 10 \text{H}_2\text{O}$ ), and we found very intensive fluorescence properties with sharp emission bands connected with long fluorescence lifetimes of several hundreds of microseconds. Voglite did not show such fluorescence properties. As shown in Fig.1, a broad emission was measured: a simple peak fit resulted in maxima at 520 nm and 542 nm. The fitted fluorescence lifetime is  $360 \pm 20$  ns. This lifetime is about 1000 times shorter than for liebigite.

We conclude that copper quenches the fluorescence properties of uranyl minerals.

Also metazeunerite ( $\text{Cu}[\text{UO}_2/\text{AsO}_4]_2 \cdot 8\text{H}_2\text{O}$ ) from Majuba Hill, USA, did not show any fluorescence properties. This confirmed our assumption on the quenching influence of copper because other uranyl arsenates such as troegerite and novacekite /1/ show fluorescence properties.

It was therefore surprising that the copper uranyl phosphates show relatively good fluorescence spectra. Fig. 2 and Fig. 3 show the fluorescence spectra of torbernite and metatorbernite. The chemical composition of these minerals is  $\text{Cu}[\text{UO}_2/\text{PO}_4]_2 \cdot 8\text{H}_2\text{O}$ , which is similar to zeunerite and metazeunerite where phosphorus has been replaced by arsenic. The torbernite came from Johannegeorgenstadt, Germany, and the metatorbernite was found in St. Symphorien, France. The main fluorescence emission bands for torbernite are 502.4 nm, 524.5 nm, 548.0 nm and 573.7 nm. For metatorbernite the peak fitting algorithm resulted in emission maxima at 502.4 nm, 524.6 nm, 547.7 nm and 573.9 nm. The fitted lifetimes are 0.7  $\mu\text{s}$  and 8.5  $\mu\text{s}$ , respectively. Comparing these data with data from alkaline earth uranyl phosphates, good agreement with the fluorescence maxima of autunite and urano-circite can be ascertained. Only the first emission band at about 502 nm is blue shifted by about 1 nm.

The measurements are still continuing and a more detailed description of the fluorescence properties of uranyl minerals will be given upon completion of the study.

## Acknowledgment

The authors wish to thank the Mineral Collection of the Mining Academy of Freiberg and mineralogist A. Massanek for their support of these studies.

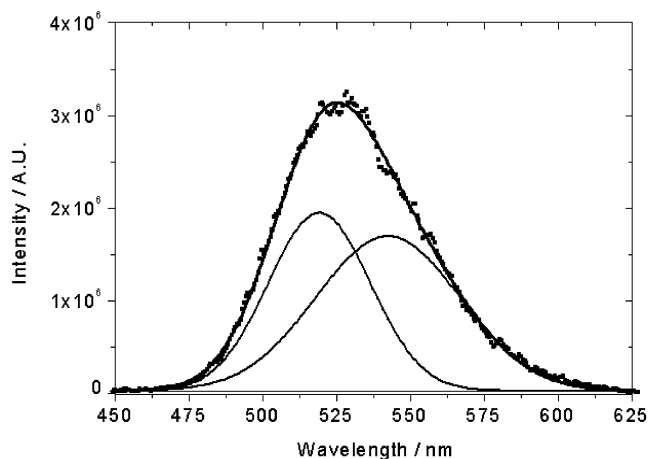


Fig. 1: Fluorescence spectrum of voglite

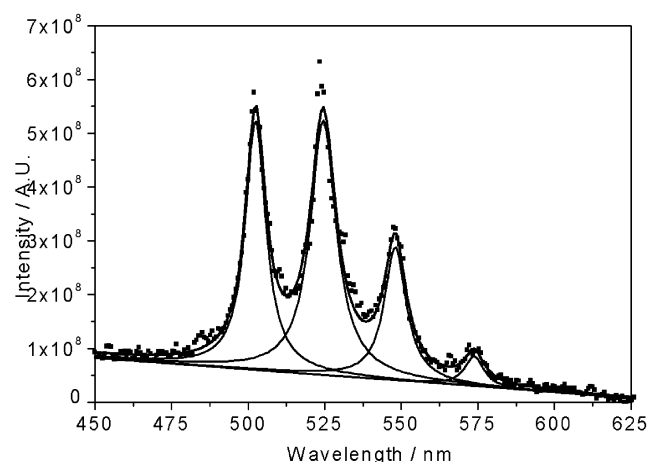


Fig. 2: Fluorescence spectrum of torbernite

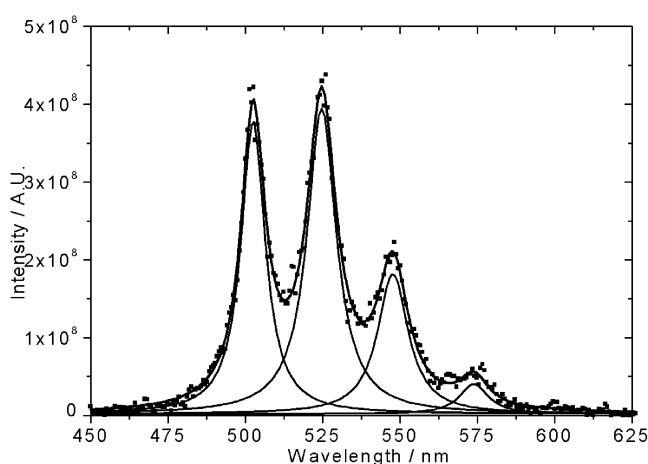


Fig. 3: Fluorescence spectrum of metatorbernite

## References

/1/ Geipel, G. et al.; This report p. 7



# DETERMINATION OF THE SPECIATION OF URANIUM IN PLANT SAMPLES BY TIME-RESOLVED LASER-INDUCED FLUORESCENCE SPECTROSCOPY (TRLFS)

A.Günther, G.Bernhard, G.Geipel, V.Brendler, H.Nitsche

*The influence of the chemical speciation of radionuclides on the transfer factors in the soil/plant systems are important parameters for risk assessment for the rehabilitation and remediation of contaminated soils. Time-resolved laser-induced fluorescence spectroscopy (TRLFS) can be used to experimentally determine the chemical speciation of uranium in plant samples*

## Experiments and Results

Various plants (e.g. blue and yellow lupins, dandelion, lamb's lettuce, buckwheat) were grown in an agricultural test field (Tharandt/Hartha) and in the laboratory on naturally and artificially contaminated soils to obtain samples for speciation measurements.

To increase the uptake of uranium compounds by the plant root and to determine the uranium speciation, soil cultures (dandelion, lamb's lettuce, lupin) were converted to hydroponics. The plant roots were exposed to either  $10^{-2}$ M uranium solution or  $10^{-2}$ M uranium/nutrient solutions. Additionally, uranium solution was injected into selected roots. These experimental conditions do not represent the natural living conditions of the plants. The most important results are demonstrated with a selected example where a hydroponics plant (lamb's lettuce) was grown in  $10^{-2}$ M  $UO_2(NO_3)_2$  solution and in addition injected into the roots of the plant.

Thermodynamic calculations of the uranium speciation in the initial solutions were performed with EQ 3/6 /1/, using the NEA data bank /2/. Various uranium species were offered to the plants. In a  $10^{-2}$ M  $UO_2(NO_3)_2$  solution at pH 3.55, 72% of the uranium occurs as  $UO_2^{2+}$  species, 16% as  $(UO_2)_2(OH)_2^{2+}$  species and 9% as  $(UO_2)_2(OH)^{3+}$  species. The maxima of the main emission bands in the fluorescence spectrum lie therefore at 495, 516 and 541nm (Tab 1). However, our measurements showed peaks of the uranyl hydroxides. These peaks superimpose the bands of the free uranyl ion because of their higher fluorescence intensity.

The fresh plant samples were thoroughly washed with water and cut into small pieces and subjected to laser fluorescence measurements. Good fluorescence spectra of the root and shoot axis samples were recorded. Furthermore, uranium species were also identified in leaf samples.

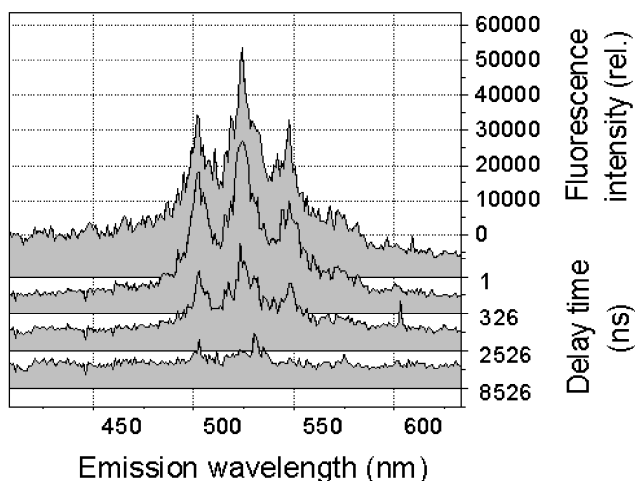


Fig. 1: Time-resolved laser-induced fluorescence spectrum of an uranium containing, fresh base of leaf-sample

As shown in Fig. 1 and Tab.1 of the selected example, the maxima of the three main bands in the fluorescence spectra of the fresh plant samples are near 499 to 502 nm, 521 to 528 nm and 543 to 549 nm. After drying and pulverizing of the fresh samples, the positions of the bands in the fluorescence spectra change only insignificantly. In some cases, however, a decrease of the starting fluorescence intensity was observed. During drying process, the solvating envelope of the individual uranium species changes and can be connected with the change of the fluorescence characteristics and a decrease of the fluorescence intensity. The visible emission bands in the fluorescence spectra of fresh plant samples are generally shifted to higher wavelengths in comparison with those of the initial solution. A change of the uranium speciation is therefore very probable.

As the quenching influences of the plants' compounds on the uranium species cannot be quantified, an analysis of the experimentally determined fluorescence lifetimes is not yet possible.

The position of the fluorescence bands in the spectrum is similar to the spectra of fluorescent uranyl carbonates. At the moment, however, it is not possible to assign these fluorescence bands to known species. Considering the chemical build-up and metabolism of the plants /3/, the formation of uranyl carbonate species and of complexes with organic compounds is imaginable in the pH range from 6 to 8.

Initial solution		495.3	516.2	541.2
plant - not injected	root	501.2	523.2	543.0
	shoot axis	501.3	528.0	549.0
plant - injected with initial solution	root	500.2	522.2	547.7
	shoot axis	499.4	520.7	545.3
	base of leaf	502.2	524.3	546.8

Tab.1: Wavelength (nm) of main peaks in the TRLFS-spectrum of uranium-containing hydroponics plant samples

## References

- /1/ Wolery, T.J.: *EQ3/6 A software package for the geochemical modeling of aqueous systems*. Report UCRL-MA-110662 Part1, Lawrence Livermore National Laboratory, California, USA, 1992
- /2/ Grenthe, I., Fuger, J. et al.: *Chemical Thermodynamics of Uranium*. Amsterdam, 1992
- /3/ Nultsch, W.: *Allgemeine Botanik*. Georg Thieme Verlag Stuttgart, New York, 1996

## INCREASE IN THE IONIC STRENGTH OF URANYL CONTAINING SOLUTIONS

G.Geipel, M. Rutsch, G. Bernhard, H. Nitsche

The influence of high concentrations of perchloric and sulfuric acid on the fluorescence properties of the uranyl ions was studied. Due to the decreasing water concentration of the solutions, an increase in the fluorescence lifetime was found for both media. Deconvolution and peak fitting of the perchloric medium showed no evidence for complex formation between uranyl and perchlorate ions.

It was recently discussed /1/ that time-resolved fluorescence spectroscopy of uranyl and uranyl species in aqueous solution may be hampered by the quenching properties of the water molecule. Because sodium perchlorate is frequently used as an ionic strength adjuster it was also important to study the influence of the perchlorate ion on the uranyl fluorescence.

Fig. 1 shows the increase in fluorescence lifetime as a function of increasing perchloric acid concentration. A linear dependence was found. At very high concentrations of perchloric acid no further decrease of the fluorescence lifetime occurred within the error limits. The same studies were repeated with sulfuric ions, because nearly water-free conditions can be reached in this medium. The measurements were begun with a 2 M solution of  $H_2SO_4$  because only the trisulfato complex exists as the major species in solution /2/. The fluorescence lifetime increased with increasing concentration of sulfuric acid.

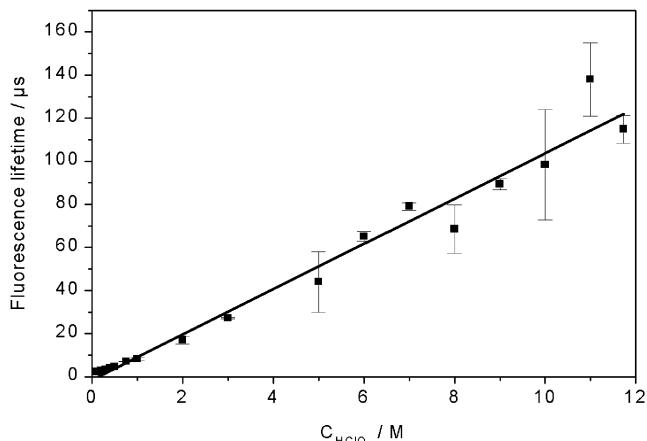


Fig. 1: Fluorescence lifetime of uranyl as function of concentration of perchloric acid

To compare the two measurements, we calculated the resulting water concentration each solution from the concentration of the acid and the density of the solution. The fluorescence lifetimes of both series nearly linearly dependent on the water concentration. The results of both series were fitted with the same equation parameters ( Fig. 2 ). Showing that the fluorescence lifetime of these uranyl systems is mainly influenced by the quenching of the water molecule. Taking the Stern-Vollmer mechanism as a basis for this effect, we calculate a quenching constant for the water molecule /3/ accordingly to the following equation.

$$\frac{J_M}{J_Q} = 1 + J_M(k_{QM}([Q]) \quad (1)$$

The quenching constant was in:

$$\begin{aligned} \text{sulfuric acid} & \quad k_{QM} = 6.3 \times 10^2 \text{ mol}^{-1}\text{s}^{-1} \\ \text{perchloric acid} & \quad k_{QM} = 7.2 \times 10^2 \text{ mol}^{-1}\text{s}^{-1}. \end{aligned}$$

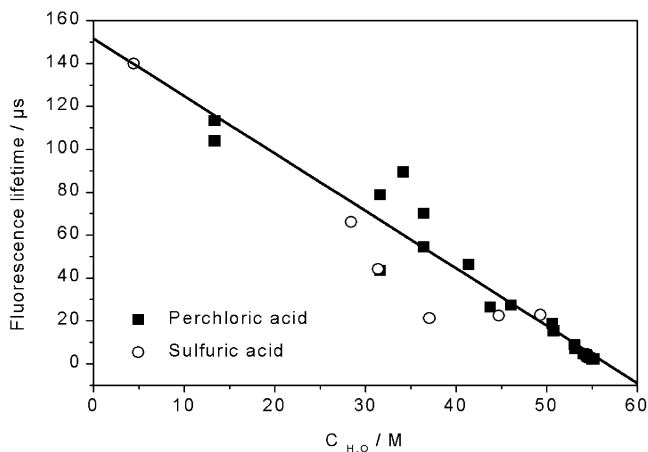


Fig. 2: Fluorescence lifetime of uranyl as function of calculated water concentration in perchloric and sulfuric acid

To investigate a possible complex formation between the uranyl and perchlorate ions, we studied the emission properties of the main fluorescence emission bands. All fluorescence lifetimes were found to follow a monoexponential decay mechanism and deconvolution of the spectra did not show any evidence of the formation of new emission bands. Fig. 3 shows the fitted wavelength of the third emission band as a function of the concentration of perchloric acid. The wavelength shift is smaller than 1 nm. This is significant evidence that no complex formation between uranyl and perchlorate ions occurs up to 11 M  $HClO_4$ .

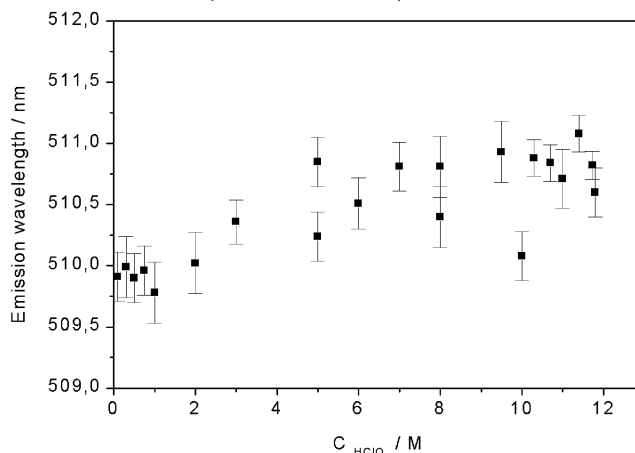


Fig. 3: Wavelength of the third emission band of uranyl ion as function of perchloric acid concentration

### References

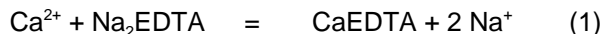
- /1/ Billard, I., Bouby, M. et al.; Abstracts 13<sup>th</sup> Radiochem. Conf., Marianske Lazne (1998), p. 283
- /2/ Geipel, G., Brachmann, A., Bernhard, G., Nitsche, H.; Radiochim. Acta **75**, 199 (1996)
- /3/ Perkampus, H.H.; *Encyclopedia of Spectroscopy*. VCH Weinheim, 1995, p. 200

# VALIDATION OF THE COMPLEX FORMATION BETWEEN $\text{Ca}^{2+}$ , $\text{UO}_2^{2+}$ AND $\text{CO}_3^{2-}$ USING EDTA TO ADJUST THE $\text{Ca}^{2+}$ CONCENTRATION

G. Geipel, G. Bernhard, H. Nitsche

The complex formation constant between calcium, uranyl and carbonate ions was reported in the last annual report /1/. To validate this formation constant against other complex formation reactions we used EDTA to adjust the concentration of free calcium ions in the solution. We included the complex formation between  $\text{Ca}^{2+}$  and EDTA in the calculation of the complex formation constant for  $\text{Ca}_2[\text{UO}_2(\text{CO}_3)_3]_{(\text{aq})}$  we obtained  $\log \beta_0 = 26.5 \pm 0.3$ . The slope was found to be  $1.66 \pm 0.35$ .

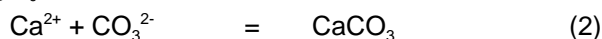
The validation of the formation constant of the species  $\text{Ca}_2[\text{UO}_2(\text{CO}_3)_3]_{(\text{aq})}$  is important to exactly calculate the speciation in the mining related waters. We studied the complex behavior at pH 8.0 and 9.0 and at a uranium concentration of  $5 \times 10^{-5}$  M. The concentration of added  $\text{Ca}^{2+}$  was kept constant at  $1 \times 10^{-2}$  M and  $1 \times 10^{-3}$  M. To form the uranyl-tris-carbonato complex, the concentration of  $\text{HCO}_3^-/\text{CO}_3^{2-}$  was kept constant at  $1 \times 10^{-2}$  M. The ionic strength in the solutions was constant at 0.1 M. Under these conditions more than 95% of the uranyl ions in the solution were bound in the  $\text{Ca}_2[\text{UO}_2(\text{CO}_3)_3]_{(\text{aq})}$  complex. To vary the concentration of uncomplexed  $\text{Ca}^{2+}$  and in consequence the concentration of the  $\text{Ca}_2[\text{UO}_2(\text{CO}_3)_3]_{(\text{aq})}$  complex, we added  $\text{Na}_2\text{EDTA}$ , which forms strong complexes with  $\text{Ca}^{2+}$ .



The formation constant for reaction (1) is given in the literature /1/ as  $\log \beta_0 = 10.59$ .

We also considered the formation of  $\text{CaCO}_3$ .

The formation constant for reaction (2) is given in /2/ as  $\log \beta_0 = 3.1$ .



To calculate the overall formation constant of the calcium uranyl-tris-carbonato complex we included the formation constant of the uranyl-tris-carbonato complex (reaction (3)), which is given in /3/ as  $\log \beta_0 = 21.6$ .



Fig 1. shows the fluorescence spectra of a series with initial  $1 \times 10^{-5}$  M  $\text{Ca}_2[\text{UO}_2(\text{CO}_3)_3]_{(\text{aq})}$  with an increasing amount of  $\text{Na}_2\text{EDTA}$ . The fluorescence intensities decrease with increasing  $\text{Na}_2\text{EDTA}$  concentration. This is

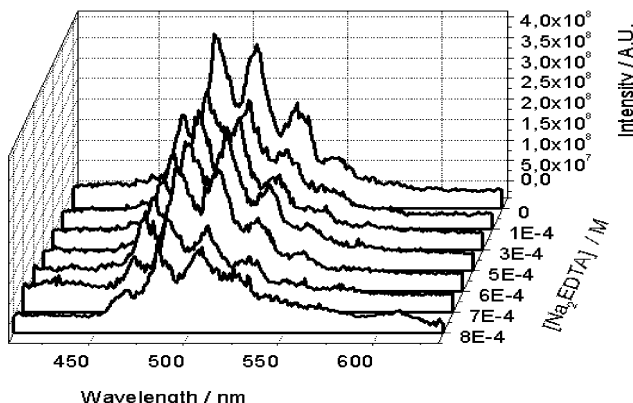
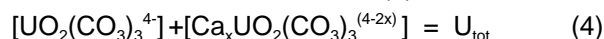


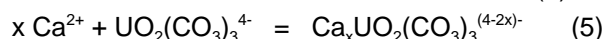
Fig. 1: Fluorescence spectra of  $5 \times 10^{-5}$  M  $\text{Ca}_2\text{UO}_2(\text{CO}_3)_3$  (aq) at pH 9.0 as function of added  $\text{Na}_2\text{EDTA}$  concentration

a result of the increasing  $\text{CaEDTA}$  formation, which reduces the concentration of free  $\text{Ca}^{2+}$  ions in the solution. The complex equilibrium of  $\text{Ca}_2[\text{UO}_2(\text{CO}_3)_3]_{(\text{aq})}$  is thus influenced, resulting in decreasing concentrations of the fluorescent  $\text{Ca}_2[\text{UO}_2(\text{CO}_3)_3]_{(\text{aq})}$  complex. Under

these conditions, we calculate the free  $\text{Ca}^{2+}$  concentration from the equilibria (1) and (2) and from the measured fluorescence intensity. The sum of the concentrations of  $\text{Ca}_x\text{UO}_2(\text{CO}_3)_3^{(4-2x)-}$  and  $\text{UO}_2(\text{CO}_3)_3^{4-}$  is the total uranium concentration of  $1 \times 10^{-5}$  M (4).



To calculate the formation constant for reaction (5):



we arrange the mass action law in the following expression:

$$\log \frac{[\text{Ca}_x\text{UO}_2(\text{CO}_3)_3^{(4-2x)-}]}{[\text{UO}_2(\text{CO}_3)_3^{4-}] \cdot \log K \cdot x \cdot (\log[\text{Ca}^{2+}])^x} \quad (6)$$

Fig. 2, for instance, shows the slope analysis of this equation for pH 8 and a total calcium concentration of  $1 \times 10^{-3}$  M. Using all measured series, the slope was

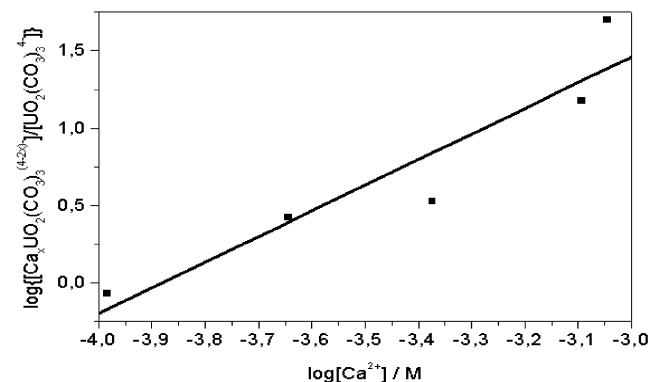
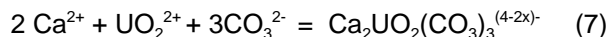


Fig. 2: Slope analysis for the validation of complex formation of  $\text{Ca}_2\text{UO}_2(\text{CO}_3)_3$  (aq) as function of the  $\text{Ca}^{2+}$  concentration.

found to be  $1.66 \pm 0.35$ . The agreement with the theoretical value of 2 for the  $\text{Ca}^{2+}$  ions involved in equation (5) is relatively good under the given experimental conditions. The value for  $\log K$  in equation (6) was found to be  $7.55 \pm 0.23$  at an ionic strength of 0.1 M. Recalculation for the complete formation reaction



using data for the  $\text{UO}_2(\text{CO}_3)_3^{4-}$  /3/ gives  $\log \beta_{213} = 29.15 \pm 0.3$ , the correction to zero ionic strength gives  $\log \beta_{213}^0 = 26.5 \pm 0.3$ . Within the error limits given by the varying experimental conditions, this value is in good agreement with the value of  $\log \beta_{213} = 25.7 \pm 0.7$  that we reported earlier /1/.

## References

- /1/ Geipel, G. et al.; Report FZR-218, (1998) p.16
- /2/ Anderegg, G.: *Critical survey of stability constants of EDTA complexes*. IUPAC Chemical Data Series No. 14, Pergamon Press, Oxford, 1977
- /3/ Grenthe, I. et al.: *Chemical Thermodynamics of Uranium*. Elsevier, Amsterdam, 1992.

# SOLUBILITY OF $\text{Ca}_2[\text{UO}_2(\text{CO}_3)_3] \cdot 10\text{H}_2\text{O}$ , LIEBIGITE

S. Amayri, G. Bernhard, H. Nitsche

The solubility of calcium uranyl carbonate  $\text{Ca}_2[\text{UO}_2(\text{CO}_3)_3] \cdot 10\text{H}_2\text{O}$  was studied at 25 °C and pH 8.0 from undersaturation in aqueous solution open to the atmosphere. The solubility of liebigite at pH 8.0 was determined to be  $9.9 \pm 0.5$  g/L.

## Experimental

Solubility experiments were carried out according to the guidelines given by Nitsche /1/. Liebigite was synthesized according to /2/. Five grams of calcium uranyl carbonate was transferred to a teflon cell containing 100 mL of 0.1 M  $\text{NaClO}_4$  (p.A., Merck). The pH-value was adjusted with  $\text{HClO}_4$  (Suprapur, Merck). The cells were thermostated at  $25 \pm 1$  °C and shaken at 100 rpm with an automatic agitator. The dependence of solubility on the time was determined by periodically analyzing the calcium and uranium content in solution. The samples were ultrafiltered through Minisart cellulose nitrate membrane filters of 25 nm pore size (Schleicher & Schuell, Dassel, Germany) and then analyzed by ICP-MS and AAS. The X-ray diffraction diagrams of the solid residues at steady-state were recorded in the  $2\theta$  range from 8° to 60° (URD 6, Freiburger Präzisionsmechanik, Freiberg, Germany). The soluble uranium (VI) species at steady-state were characterized by time-resolved laser-induced fluorescence spectroscopy (TRLFS). TRLFS measurements were performed with a Nd-YAG-laser system (Spectra Physics, Mountain View, CA, USA). The excitation wavelength was 266 nm /3/. For speciation calculations the software EQ3/6 /4/ was used. The calculation were carried out with the NEA data base /5/ including the species  $\text{Ca}_2[\text{UO}_2(\text{CO}_3)_3]_{(\text{aq})}$  /3/.

## Results and Discussion

In this report we will discuss only the solubility experiments at pH 8.0. This is the pH-value of natural seepage waters coming from an uranium mining area /3/. In these waters, the species  $\text{Ca}_2[\text{UO}_2(\text{CO}_3)_3]_{(\text{aq})}$  was identified. Fig. 1 depicts the uranium solubility at pH 8.0

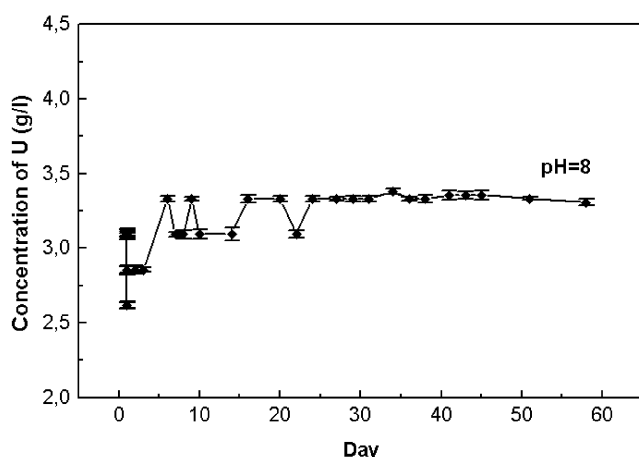


Fig. 1: Concentration of uranium in 0.1  $\text{NaClO}_4$  at 25 °C under air as function of time. (Starting solid phase:  $\text{Ca}_2[\text{UO}_2(\text{CO}_3)_3] \cdot 10\text{H}_2\text{O}$ ; undersaturation, error is within the size of the symbols)

as a function of time. The experimental results indicate that the steady-state is reached after about 30 days.

The observed decrease followed by an increase in uranium concentration may be due to changes of the calcium uranyl carbonate surface. XRD measurement of the initial solid phase and under steady-state conditions showed no change of the crystal structure.  $\text{Ca}_2[\text{UO}_2(\text{CO}_3)_3] \cdot 10\text{H}_2\text{O}$  was the solubility-controlling solid phase at pH 8.0. No phase change occurred and no secondary phase was formed. It was shown by TRLFS measurements that  $\text{Ca}_2[\text{UO}_2(\text{CO}_3)_3]_{(\text{aq})}$  dominates the uranium speciation in the aqueous phase at steady-state. Speciation calculation showed the same result (Fig. 2). The solubility of liebigite (0.1 M  $\text{NaClO}_4$ ,

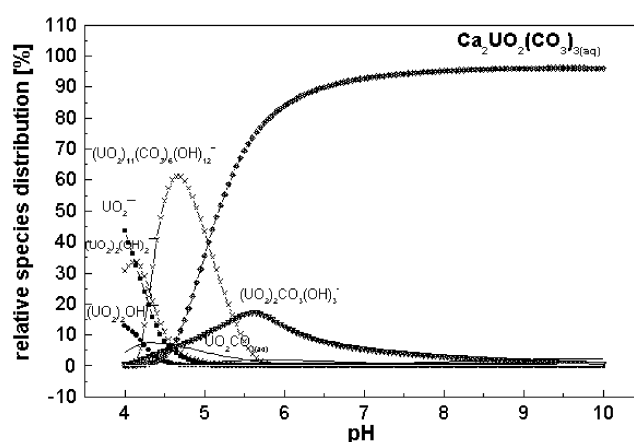


Fig. 2: Calculated species distribution of uranium as a function of pH (calculated with EQ3/6). ( $[\text{UO}_2^{2+}] = 1.26\text{E}-2$  M,  $[\text{Ca}^{2+}] = 2.52\text{E}-2$  M,  $[\text{CO}_3^{2-}] = 3.78\text{E}-2$  M)

under air atmosphere, 25 °C, pH 8.0) was determined to be  $9.9 \pm 0.5$  g/L. The U, Ca concentrations at steady-state are  $(3.33 \pm 0.05)$  g/L and  $(1.202 \pm 0.003)$  g/L respectively.

First results of solubility experiments at pH 6.0 and 11.0 show a change of the solid phase and also different uranium speciation in the aqueous phase.

## Acknowledgments

The authors thank Dr. G. Geipel for TRLFS, Dr. W. Wiesener and Ms. U. Schäfer for ICP-MS and AAS and Ms. A. Scholz for X-ray diffraction measurements.

## References

- 1/ Nitsche, H.: Radiochim. Acta **52/53**, 3-8 (1991)
- 2/ Amayri, S., et al.: Synthesis and characterization of calcium uranyl carbonate  $\text{Ca}_2[\text{UO}_2(\text{CO}_3)_3] \cdot 10\text{H}_2\text{O}$ , (liebigite). In: Report FZR-218, p.14 (1998)
- 3/ Bernhard, G., et al.: Radiochim. Acta **74**, 87 (1996)
- 4/ Wolery, T.G.: EQ3/6, A software package for the geochemical modeling of aqueous system. Report UCRL-MA-110662 Part I (1992)
- 5/ Grenthe, I., et al.: Chemical Thermodynamics of Uranium. Elsevier Science Publishers, Amsterdam 1992

# INITIAL LASER-INDUCED PHOTOACOUSTIC SPECTROSCOPIC STUDIES OF URANIUM(IV)

G. Geipel, A. Abraham, G. Bernhard, H. Nitsche

*Laser-Induced Photoacoustic Spectroscopy (LIPAS) is a powerful tool to study spectroscopic properties at very low concentrations /1/. We are currently studying the influence of organic compounds on the U(VI)/U(IV) potential. We use LIPAS as one of tools to investigate this phenomenon, and investigate the wavelength range between 510 nm to 590 nm. In addition to this range, the absorption band above 650 nm can be accessed by single beam LIPAS. These however, the light absorption of the solvent water studies at very low concentrations.*

Uranium(IV) does not display any fluorescence properties, thus only UV-vis or laser-induced photoacoustic spectroscopy can be used as non-invasive methods to study solution species and their complex formation.

The used laser-Induced photoacoustic spectroscopy (LIPAS) is already described elsewhere /1/.

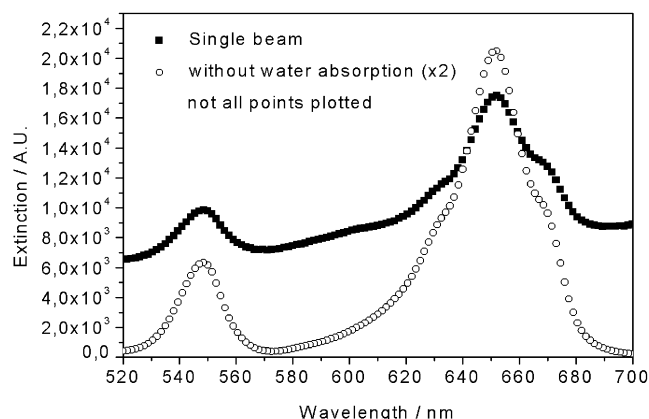


Fig. 1: Absorption spectrum of Uranium(IV)

The absorption spectrum of uranium(IV) shows several absorption bands over a wide wavelength range. Between 350 nm and 750 nm, we find four main absorption bands. The band near 650 nm should be the most useful absorption feature for analytical purposes, because it has the highest molar extinction coefficient in this wavelength region (Fig.1).

Unfortunately, in this range a concurrent absorption due to the solvent water occurs. We avoid this problem by using a two-cuvette LIPAS, which enables us to subtract the absorption of the solvent. This system is currently being built.

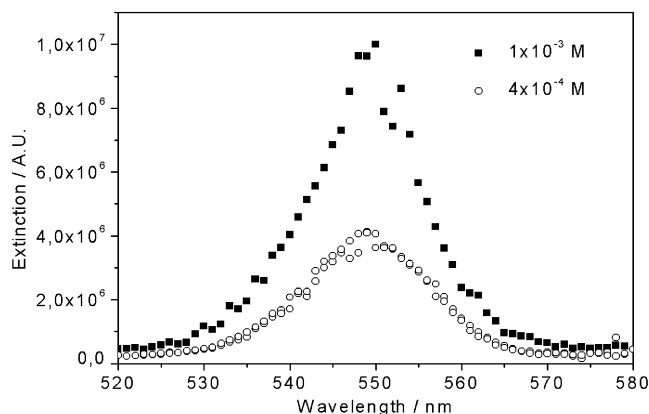


Fig. 2: LIPA Spectra of Uranium(IV) between 520 nm and 580 nm

Until then, we used the 548 nm absorption line of uranium(IV) for first studies. Also here, we find a slight solvent absorption, in this wavelength range the absorption

of the water increases nearly linearly with increasing wavelength. We therefore can correct for the background using the software package GRAMS'386.

Fig 1. shows that the absorption around 650 nm also consist of more than one absorption band. This behavior was also found between 450 nm and 500 nm. The absorption below 450 nm can be influenced by uranium(VI) when present in the solution. This limits the useful spectral range from 520 to 690 nm for studying in the uranium(IV) system.

Fig. 2 shows the photoacoustic spectra of two uranium(IV) solutions. Peak fitting shows us that the absorption consists of two absorption lines at  $536\pm 1$  nm and  $550\pm 1$  nm.

Fig.3 shows the dependence of the photoacoustic signal on the uranium(IV) concentration. The detection limit for uranium(IV) for our photo-acoustic setup is  $5\times 10^{-5}$  M at 550 nm.

This clearly shows the necessity for a two-cell design in order to detect lower concentrations of uranium(IV).

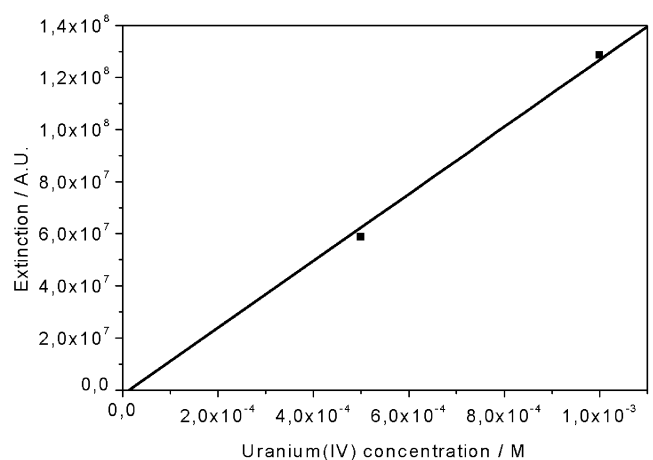


Fig. 3: Dependence of the photoacoustic signal on the uranium(IV) concentration

## References

/1/ Geipel, G. et al.; Complex Formation between  $\text{UO}_2^{2+}$  and  $\text{CO}_3^{2-}$ : Studied by Laser-Induced Photoacoustic Spectroscopy. *Radiochim. Acta* **82**, 59 (1998)

# TIME-RESOLVED LASER-INDUCED FLUORESCENCE SPECTROSCOPY WITH ULTRA-SHORT PULSES - PART I: SETUP OF THE LASER SYSTEM

M. Rutsch, G. Geipel, G. Bernhard, H. Nitsche

*A new pico- and femtosecond laser system was built up for time-resolved laser-fluorescence spectroscopy of metal-organic complexes by the fluorescence properties of the organic ligands.*

Many environmentally harmful metals and radionuclids, such as arsenic and neptunium, do not show fluorescence properties under ambient conditions. These elements form complexes with organic compounds, that are important for the migration in the environment. The use of ultra-short laser pulses, pulses of pico- or femtosecond duration for TRLF spectroscopy has opened up a new path for investigating of such metal complexes by studying the fluorescence properties of the organic ligands. The very short fluorescence lifetimes of the organic ligands require an excitation with ultra-short pulses, that are much shorter than the lifetimes of the organic ligands. We describe here briefly our new pico- and femtosecond laser system that will be used for such studies. Fig. 1 shows a scheme of the experimental setup.

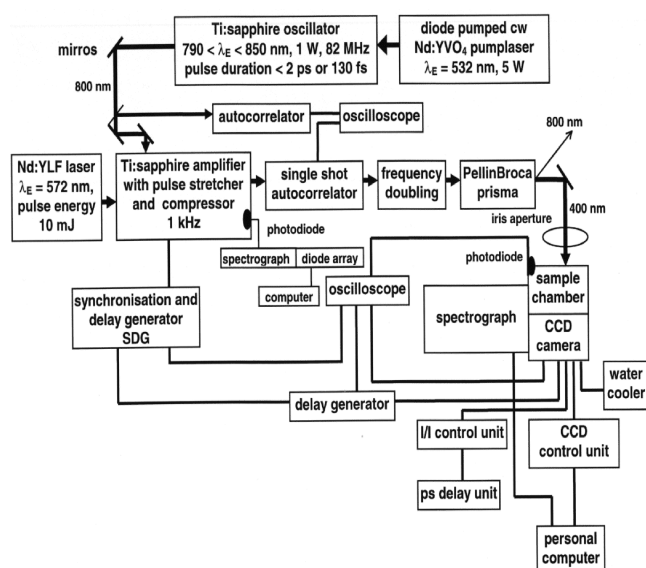


Fig. 1: Experimental Setup of the laser system for time-resolved laser-induced fluorescence spectroscopy with ultra-short pulses.

Time-resolved fluorescence measurements are carried out by using an amplified, frequency-doubled excitation pulse from a mode-locked pico- or femtosecond Ti:sapphire oscillator (Tsunami, Spectra Physics). The Ti:sapphire oscillator is pumped by the second harmonic of a diode pumped cw Nd:YVO<sub>4</sub> laser (Millenia, Spectra Physics) and delivers pulses of a duration smaller than 2 ps or than 130 fs and with some nJ output energy per pulse at 800 nm and a repetition rate of 80 MHz. The pulse is stretched by a grating and then used as seeding for the regenerative Ti:sapphire amplifier (Spitfire, Spectra Physics). The Ti:sapphire amplifier is pumped by the second harmonic of a Nd:YLF laser operating at a repetition rate of 1 kHz, with a pulse duration of 250 ns and an energy per pulse of 10 mJ (Merlin, Spectra Physics). The amplified pulse is then compressed to

obtain an output of pico- or femtosecond pulses with an energy of . 1mJ at 800 nm (Spitfire, Spectra Physics).

The pulse duration and the pulse shape is controlled by autocorrelation before amplification (Autocorellator 409, Positive Light) and after amplification (Single Shot Autocorrelator SSA, Positive Light). The amplified pulse is frequency-doubled in a beta barium-borate (BBO) crystal to generate the second harmonic. A Pellin Broca prism separates the residual of the wavelength at 800 nm from the generated 400 nm. The frequency-doubled pulse is directed with mirrors to the center of a sample chamber, which is mounted directly on the entrance slit of the spectrograph (M270, Spex). The fluorescence emission is focused on the slit spectrograph vertical to the excitation pulse without using an optical fiber cable.

The spectrograph has a turret with two gratings, 300 l/mm and 100 l/mm. Spectral resolutions of 0.46 nm or 1.4 nm and a spectral range of 178 nm and 534 nm are possible, respectively. The entrance slit is variable from 100 to 2,000  $\mu$ m.

The fluorescence signal is detected by a picosecond CCD camera system operating at 1 kHz (PicoStar, LaVision). The CCD camera system consists of a camera head with cooling water connectors, a water cooler, CCD control unit, image intensifier unit and ps delay. The CCD chip is cooled to +10°C for a low dark signal. The camera head is directly connected to the spectrograph over a multi-channel detector adapter. The CCD camera system has fixed gate times of 0.08, 0.12, 0.25, 0.5, 1, 2, 4 or 6 ns, the delay time can be varied between 0 and 25 ns. The CCD camera system and the spectrograph are connected with a computer for controlling and for recording the spectra (program WinSc4.5, LaVision). The CCD camera is triggered by the regenerative amplifier system (Spitfire). In order to start the recording of the spectra exactly at the same time when the laser pulse reaches the sample, a delay-generator (DG535, Stanford Research System) compensates the optical and electrical path of the pulse between the regenerative amplifier and the sample chamber. The signals from the camera, the regenerative amplifier and of the pulse at the sample measured with an ultrafast photodiode (UPD-300SP, Soliton) are sent to an oscilloscope (LC574A, LeCroy) to adjust the delay-generator.

By a photodiode at the regenerative amplifier on-line measurements of the wavelength of the pulses are also possible with an additional spectrograph (1235, EG&G) diode array (M1455, EG&G) system. The energy of the pulse can be measured by an analogue energy power meter (407A, Spectra Physics). Fluorescence spectra are obtained by accumulation of several numbers of laser shots.

# TIME-RESOLVED LASER-INDUCED FLUORESCENCE SPECTROSCOPY WITH ULTRA-SHORT PULSES - PART II: TESTING OF THE NEW LASER SYSTEM

M. Rutsch, G. Geipel, S. Pompe, K. Schmeide, G. Bernhard, H. Nitsche

The fluorescence properties of humic substances were investigated by time-resolved laser-induced fluorescence spectroscopy with ultra-short excitation pulses to test the new pico/femtosecond laser system.

## Experimental

The influence of different laser system parameters and some environmental factors on the fluorescence behavior of humic substances was studied.

Varied system parameters were: the number of the laser shots per spectrum (from 25 to 30000), the gate time of the CCD camera (from 0.120 to 6 ns) and the excitation energy (from 2  $\mu\text{J}$  to 80  $\mu\text{J}$ ). The following system parameters were held constant: the excitation wavelength of  $396 \pm 0.5$  nm, the excitation pulse duration of smaller than 10 ps and the slit of the spectrograph of 100  $\mu\text{m}$ . The time-resolved spectra were recorded between 0 and 15 ns after laser pulse excitation in the wavelength range between 410 and 588 nm with different delay steps.

Varied environmental factors were: the origin and the purity (purified or not purified) of the humic substances, the pH (from 1.5 to 12.0) and the concentration (from 0.25 to 25 mg/L) of the sample solutions. All sample solutions were prepared at an ionic strength of 0.1 M  $\text{NaClO}_4$ . The following samples were investigated: (a) commercial humic acid (Aldrich, purified /1/ and not purified), (b) synthetic humic acid (Maillard reaction type M42, /1/), (c) natural humic and (d) fulvic acid extracted from the Bog "Kleiner Kranichsee" in Saxony /2/.

## Results and Discussion

The fluorescence intensity increases exponentially with increasing gate time. For each measurement the expected linearity between fluorescence intensity and the number of laser shots and the excitation energy as well is observed.

At low concentrations, up to 8 mg/L, the fluorescence intensity increases linearly, with higher concentrations the fluorescence intensity reaches a maximum and then decreases. (Fig. 1). The fluorescence intensity shows a maximum around pH 7, corresponding to /3/. The life-

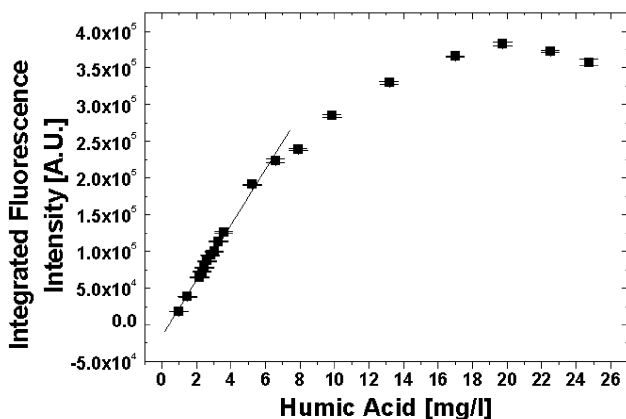


Fig. 1: Fluorescence intensity as function of humic acid concentration (Aldrich, purified, delay time 0 ps)

time is not affected by pH, concentration and system parameter. A typical time resolved spectrum is shown in

Fig. 2. All samples show a mono-exponential decay of the integrated fluorescence signal between 450 and 550 nm at the chosen experimental conditions. The determined lifetimes range from 3.5 to 5.0 ns. Differences between the lifetimes of the five samples are small but significant (Tab. 1).

sample	Fluorescence lifetime / [ps]	Integrated fluorescence signal / [A.U.] $\times 10^3$
(a) purified	$4612 \pm 283$	$331.0 \pm 6.1$
(a) not purified	$4336 \pm 265$	$134.1 \pm 4.8$
(b)	$4137 \pm 203$	$58.5 \pm 2.9$
(c)	$3935 \pm 209$	$51.3 \pm 2.0$
(d)	$3843 \pm 91$	$53.4 \pm 2.6$

Tab. 1: Fluorescence lifetime and integrated fluorescence signal of the different samples

The fluorescence intensity of the Aldrich humic acid is higher than that of the other samples, as shown in Tab. 1 as an example for a concentration of 7 mg/L. The differences can be explained by the diversity of cumulative structural effects /3/. Comparing the fluorescence intensity of unpurified Aldrich humic acid with purified Aldrich humic acid show that the presence of metal ions impurities decreases the fluorescence intensity by fluorescence quenching. At all experimental conditions, the spectra of the different samples are rather similar, showing a broad band between 410 and 588 nm (Fig. 2). This behavior can be explained by the large

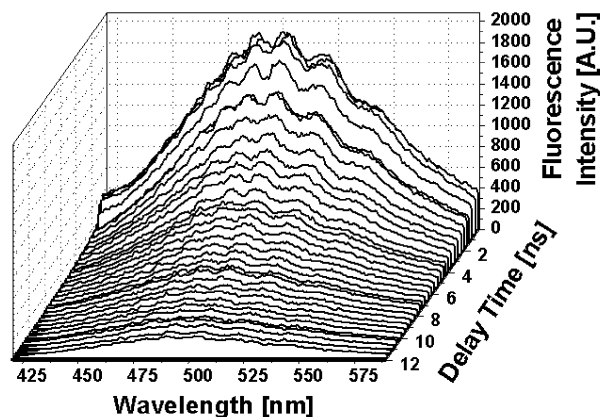


Fig. 2: TRLFS spectrum of purified Aldrich humic acid

number of identical chemical structural units and functional groups, such phenolic and carboxylic groups, resulting in a uniform wavelength shift for all samples.

We demonstrated that our new pico / femtosecond laser system is very suitable for investigating the fluorescence behavior of organic substances.

## References

- /1/ Pompe, S.; Radiochim. Acta **74**, 135-140 (1996)
- /2/ Schmeide, K., et al.; 1<sup>th</sup> Technical Progress Report EC Project F14W-CT96-0027, in press (1998)
- /3/ Senesi, N.; Analyt. Chim. Acta **232**, 77-106 (1997)

# CHARACTERIZATION OF FERRIHYDRITE WITH AFM AND TEM

T. Arnold, G. Hüttig, A. Mücklich<sup>1</sup>, H. Zänker

<sup>1</sup>Institute of Ion Beam Physics and Materials Research

AFM and TEM measurements on ferrihydrite showed that ferrihydrite consists of nano-size particles with a disc-like morphology. The small particles have a diameter of 2 to 5 nm. Ferrihydrite particles are usually made of agglomerates consisting of many of such nano-size particles.

## Experimental

A ferrihydrite suspension (1 mM) was prepared by slowly raising the pH of a  $(\text{Fe}(\text{NO}_3)_3 \cdot 9 \text{H}_2\text{O})$  solution to 7.3. The suspension was aged for 45 minutes before the pH was reduced to 5 in order to minimize the diffusion of  $\text{CO}_2$  into the suspension.  $\text{NaNO}_3$  was added to adjust an ionic strength to 0.1 M, and the pH was readjusted. The suspension was then aged for 65 hours. Prior to Atomic Force Microscopy (AFM) measurements, the ferrihydrite suspension was centrifuged and the centrifugate was washed with deionized water to remove  $\text{NaNO}_3$ . Atomic Force Microscopy (AFM) specimens were prepared by pipetting a drop of the suspension on a glass slide and evaporating the suspension to dryness under an IR-lamp. The sample was analyzed with a Nanoscope III AFM (Digital Instruments, Inc) working in tapping mode. Transmission electron micrographs (TEM) were taken in the magnification range from 110 K to 550 K using a Philips CM 300. From the # 50 nm filtrate Carbon Ultra-thin Support Films (PLANO, W. Plannet GmbH) were prepared.

## Results

Ferrihydrite is an intermediate solid that can form in aqueous solutions, and can be placed in the series from ferric aquo ions to hematite or goethite. It has  $\text{pK}_{\text{sp}}$  values ranging from 37 to 39 and is therefore metastable when compared to the thermodynamically more stable iron minerals goethite and hematite, which have  $\text{pK}_{\text{sp}}$  values in the range from 41 to 43 [1].

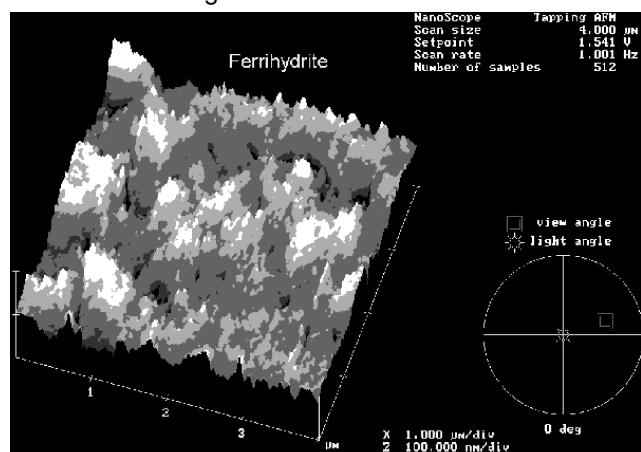


Fig. 1: AFM picture of ferrihydrite agglomerates.

Fig. 1 shows the AFM image of a ferrihydrite surface. The surface appears very rough and indicates the very high specific surface area of this mineral. Values of 100 to 700  $\text{m}^2/\text{g}$  were reported in the literature [1]. BET measurements of freeze dried ferrihydrite samples gave specific surface areas of  $316.6 \text{ m}^2/\text{g} \pm 10 \%$ . Because of this very high specific surface area ferrihydrite is a well-known sorbent for many toxic heavy metals [2]. We further examined the ferrihydrite particles by TEM

measurements. Consistent with the literature [3], we found that ferrihydrite consists of 2 to 5 nm particles.

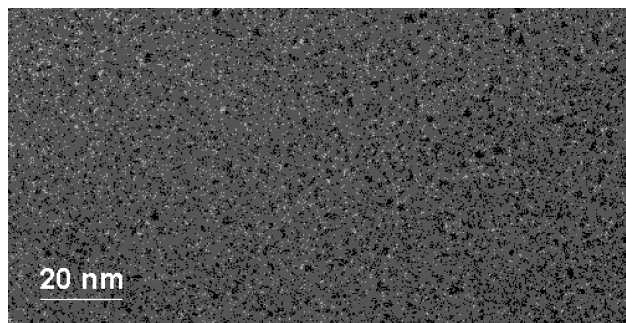


Fig. 2: TEM image of ferrihydrite particles.

The particles show a disc-like appearance (Fig. 2). Their size was determined on the base of TEM images of high magnification.

Transformation of ferrihydrite to goethite proceeds by crystallization within the aggregated ferrihydrite in the presence of free or surface-bound water [3]. However, when impurities, such as  $\text{SiO}_4^{4-}$  and/or anion groups from organic acids are present, which are very common in nature, they sorb preferentially to the surface, and block phase transformation [4] from ferrihydrite to hematite. When the ionic strength of a ferrihydrite suspension is low, the nano-sized particles can remain in solution, giving a colloidal dispersion or sol. However, when the ionic strength is increased, the electric double layer of the particles shrinks. Thus, the particles can approach each other more closely and van der Waals forces may lead to attraction of these nano-sized particles so that coagulation may occur. For a 5 nm particle, about one third of the atoms are at the surface. When ferrihydrite particles start to agglomerate or flocculate, cations and anions sorbed to these nano-sized particles are incorporated into the agglomerates and are removed from the solution by coprecipitation. The AFM image shown in Fig. 1 represents therefore an image of a heavily aggregated mass of many of these nano-sized ferrihydrite particles.

## Acknowledgments

D. Bosbach from the University of Münster, Institute of Mineralogy is thanked for taking the AFM image and G. Schuster for the BET measurement.

## References

- [1] Cornell, R.M., Schwertmann, U.: *The iron oxides*, VCH Verlag Weinheim, 1996
- [2] Dzombak, D.A., Morel, F.M.M., *Surface Complexation modeling*. Wiley, New York, 1990
- [3] Schwertmann, U., Friedl, J., Stanjek, H.: From Fe(III) to Ferrihydrite and then to Hematite. (submitted)
- [4] Zhao, J. et al.; *Physical Review B* **54** (5), 3403 (1996)



# DETERMINATION OF THE ACIDITY CONSTANT AND THE NUMBER OF SURFACE SITES OF SCHWERTMANNITE

T. Arnold, G. Bernhard, H. Nitsche

The surface site density on the schwertmannite surface was determined by potentiometric titrations. A value of 7.22 sites/nm<sup>2</sup> was calculated. In addition, the acidity constant, log k, of the reaction  $\text{SOH}_2^+ = \text{SOH} + \text{H}^+$  was determined to be 4.71.

## Introduction

Schwertmannite is an oxidation product of pyrite and forms only in the pH range from 2.5 to 4.5 /1/. It forms in nature by bacterial oxidation of Fe(II) in acid mine effluents or acid sulphate soils. Its general simplified formula is  $\text{Fe}_{16}\text{O}_{16}(\text{OH})_y(\text{SO}_4)_z \times n\text{H}_2\text{O}$  where  $16 - y = 2z$  and  $2.0 \leq z \leq 3.5$  /2/. The mineral has a characteristic "pincushion" morphology and a high specific surface area of 125 -225 m<sup>2</sup>/g for natural samples and 240 - 300 m<sup>2</sup>/g for synthetic samples.

## Experimental

Synthetic schwertmannite was prepared by dissolving 7.26 g of  $\text{K}_2\text{SO}_4$  in three liters of MILLIQ water. Then the solution was heated in a water bath to 60 EC. While constantly stirring the solution, 16.16 g of  $\text{Fe}(\text{NO}_3)_3 \times 9\text{H}_2\text{O}$  was added to the solution and the solution was left standing for an additional 12 minutes. Then the suspension was transferred into dialysis tubes and dialyzed until the salt content in the surrounding water showed no conductivity.

Potentiometric titrations were performed with a METROHM titrator and the software program TiNet 2.2. Fifty milligrams of schwertmannite were added to 40 mL of MILLIQ water and titrated with acid and base. Blank titrations were also carried out. Twenty-five  $\mu\text{L}$  of 0.1 N HCl or NaOH were added in two minute intervals to the schwertmannite suspension and the blank solutions and the pH was recorded.

## Results

From the results of the acid-base titrations the proton surface charge of schwertmannite was determined, and from that the concentration of ionizable hydroxyl groups was estimated. Hydrous metal oxides exhibit amphoteric behavior, which means that hydroxyl groups on oxide surfaces can bind and release protons. As a result of these proton transfer reactions, oxides acquire a surface charge. The proton surface charge on the schwertmannite surface in the pH range from 2.5 to 4.5 was determined by subtracting the titration curve of the background electrolyte in the absence of oxide from that of the oxide suspension /3/ in the following manner:

$$(C_A - C_B)_{\text{susp.}} = (\text{H}^+) - (\text{OH}^-) + (\text{SOH}_2^+) - (\text{SO}^-) + Y$$

$$(C_A - C_B)_{\text{Blank.}} = (\text{H}^+) - (\text{OH}^-) + (\text{SOH}_2^+) - (\text{SO}^-) + Y$$

$$(C_A - C_B) = (\text{SOH}_2^+) - (\text{SO}^-)$$

$C_A$  is the molar concentration of added acid and  $C_B$  is the molar concentration of added base. The molar concentrations of  $\text{H}^+$  and  $\text{OH}^-$  are calculated from the pH measurements. Y represents an unknown constituent that can react with  $\text{H}^+$  and  $\text{OH}^-$ . This method accounts for the effects of impurities and reactions with the vessel wall.

The results are graphically displayed in Fig. 1.

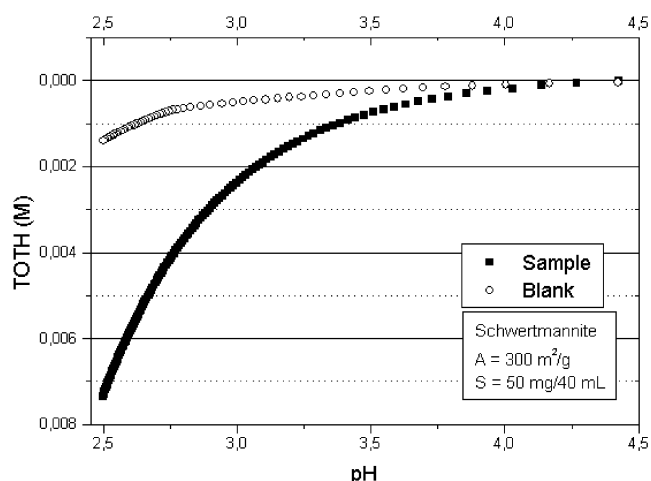


Fig. 1: Titration data of schwertmannite

$\text{SOH}_2^+$  and  $\text{SO}^-$  are the charged ionizable surface species. It is assumed that at pH 2.5 all surface species are positively charged ( $\text{SOH}_2^+$ ). The surface charge density in  $\text{C}/\text{m}^2$  is then given by:

$$F = F/(A \times S) [\text{SOH}_2^+]$$

where F is the Faraday constant; A the specific surface area; and S the solid concentration. The total number of surface sites was calculated as 7.22 sites/nm<sup>2</sup> from the calculated surface charge density and the known specific surface area of 300 m<sup>2</sup>/g. Furthermore, the acidity constant of schwertmannite was determined by applying the Diffuse Double Layer Model. In the acidic region where schwertmannite is stable, the  $\text{SOH}_2^+$  is the dominating surface species. Therefore, the following reaction was used to determine the acidity constant:



The formation constant of the above-listed reaction was determined as log k = 4.71 using the computer program FITEQL Version 3.2 /4/.

## Acknowledgments

The authors would like to thank G. Grambole for performing acid-base titrations.

## References

- /1/ Bigham, J.M. et al., *Geochim. Cosmochim. Acta* **60**, 2112 (1996)
- /2/ Cornell, R.M., Schwertmann, U.: *The iron oxide*. VCH, Weinheim (1996)
- /3/ Dzomak, D.A., Morel, F.M.M.: *Surface Complexation Modeling*. Wiley, New York (1990)
- /4/ Herbelin, A., Westall, J.: *FITEQL Version 3.2*. Report 96-01, Dep. of Chem., Oregon State University, Corvallis, Oregon 97331 (1996)

# SORPTION OF URANIUM(VI) ONTO SCHWERTMANNITE

T. Arnold, G. Bernhard, H. Nitsche

Sorption batch experiments with uranium(VI) and schwertmannite were conducted. The formation constant  $\log k$  for the sorbed U(VI) surface complex was determined using the computer code FITEQL and a value of 6.30 was obtained.

## Experimental

Schwertmannite was prepared as described in /1/. Two series of batch experiments were carried out by adding 50 mg of synthetically prepared schwertmannite to 40 mL of 0.1 and 0.01 M NaClO<sub>4</sub> solutions, respectively. Then, the suspension was aged for 24 hours. After this period the pH was adjusted to the desired value using appropriate amounts of HNO<sub>3</sub> or NaOH. The next day the pH was checked and if necessary readjusted. About 80 µL uranyl perchlorate [UO<sub>2</sub>(ClO<sub>4</sub>)<sub>2</sub>] solution, prepared in 5 × 10<sup>-3</sup> M HClO<sub>4</sub>, was added to the pH-adjusted samples to set the final U(VI) concentration in the suspension to the 1 × 10<sup>-6</sup> M. Immediately, after the uranium addition, the pH was readjusted. Then, the samples were rotated end-over-end at 1 to 5 rpm for about 50 hours to keep the solid material in suspension. At the end of a 50 hours period, the final pH values were taken. The aqueous and solid phase were separated by centrifugation at 3000 rpm for 7 minutes. Subsequently, the supernatant was filtered using Centriscart C 30 membranes (from Sartorius) with a molecular weight cut-off of 100,000 Dalton, which is approximately equivalent to 5 nm pore size. The filtrates were acidified to a pH of approximately 1.4 and the samples were analyzed for uranium and iron by ICP-MS. Uranium concentration in the filtrate was determined within an analytical error of 5-10 %. This was determined by two blanks accompanying each batch series. The difference between the concentration in the supernatant solution and the total uranium concentration was attributed to sorption onto schwertmannite.

## Results

The results of the batch experiments are shown in Fig. 1. No sorption of uranyl onto schwertmannite was

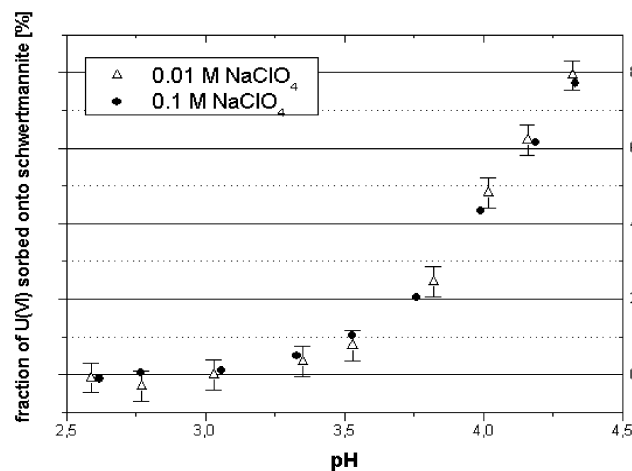
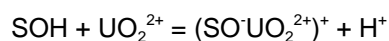


Fig. 1: Sorption of 1 × 10<sup>-6</sup> uranium(VI) onto schwertmannite in 0.1 M and 0.01 M NaClO<sub>4</sub> solution, respectively

detected below pH 3. However, with increasing pH the uranyl sorption increased. At pH 4.4, 80 % of the initially added uranium sorbed onto schwertmannite, indicating

that this secondarily formed iron mineral acts as strong sorbent for uranium(VI). Mineral dissolution above pH 2.6 was insignificant, clearly showing that the uptake of aqueous uranium was related to sorption. The two curves shown in Fig. 1 further indicate that the sorption of uranyl onto schwertmannite seems to occur by chemisorption rather than by physisorption, because variations in ionic strength have no influence on the uranium sorption behavior.

The DDLM (Diffuse Double Layer Model) was used together with the computer code FITEQL Version 3.2 /3/ to model the sorption results and to calculate formation constants for uranium surface complexes on the schwertmannite surface. The formation constants for aqueous uranium (VI) complexes /4/, the acidity constant determined in /1/, and the following reaction:



were included in the calculation. Based on the experimental results, the surface complex formation constant  $\log k$  was optimized with FITEQL and a value of 6.30 was obtained. The distribution of surface and aqueous uranium species in a system of 1.25 g/L schwertmannite, 1 × 10<sup>-6</sup> M U(VI), and 0.1 N NaClO<sub>4</sub> solution is shown in Fig. 2.

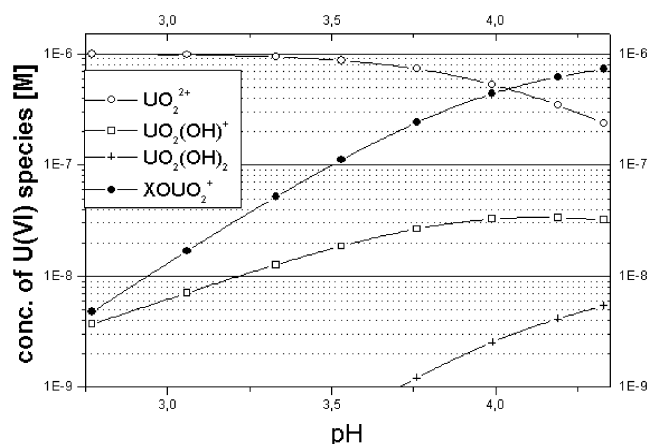


Fig. 2: Distribution of uranium species in a system containing schwertmannite (50 mg / 40 mL) and a solution containing 1 × 10<sup>-6</sup> M U(VI) and an ionic strength of 0.1 M (NaClO<sub>4</sub>)

## Acknowledgments

W. Wiesener is thanked for conducting the ICP-MS analyses.

## References

- /1/ Arnold, T., et al., This report p. 17
- /2/ Cornell, R.M., Schwertmann, U.: *The iron oxides*, VCH Verlag, Weinheim 1996
- /3/ Herbelin, A., Westall, J.: *FITEQL*, Report 96-01, Dep. of Chem., Oregon State University 1996
- /4/ Grenthe, I., et al.: *Chemical Thermodynamics of Uranium*, Elsevier Science, Amsterdam 1992

# DISTRIBUTION OF URANIUM(VI) ON BIOTITE SURFACES

G. Mainka, T. Zorn, T. Arnold, G. Bernhard, H. Nitsche

Uranium(VI) is not uniformly adsorbed on the biotite surface. Sorption of uranyl occurs preferentially on edge positions. The elemental composition of the surface changes when the mineral is pre-treated with sodium perchlorate solution.

## Experimental

Biotite specimen (mica, 2\*3\*0,5 cm pieces) [ K (Mg, Fe, Ti, Al)<sub>3</sub>(AlSi<sub>3</sub>O<sub>10</sub>) (OH, F)<sub>2</sub> ] were immersed for 48 hours in 0.1M sodium perchlorate solution containing 25 ppm uranyl perchlorate at pH 6.5. To distinguish the difference between uranyl sorption and the perchlorate-altered surface, reference pieces were treated only with 0.1 M perchlorate solution. The samples were rinsed with deionized water and dried at 80° C for 1 hour.

SEM (Scanning-Electron-Microscopy) pictures were taken from the surface and the edge of the biotite of non-treated, the reference and the uranyl treated samples. EDX (Energy-Dispersive-X-ray-fluorescence-analysis) measurements were carried out at different points of the surface and at the edge of the samples.

## Results

Fig.1 shows an SEM image of a biotite surface. The surface shows edges, damages and particles that are

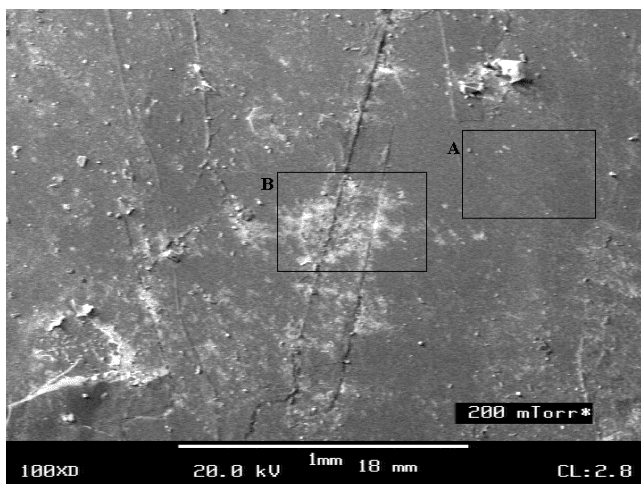


Fig. 1: SEM picture of a biotite surface 100xD

distributed over the whole surface. With the detection of recoil electrons a distinction is possible between different elements and their distribution on surfaces. The lighter elements are depicted in lighter grey colors than the heavier ones.

The EDX detection on the surface in fig. 2 shows different elemental distribution for two selected surface areas (Fig. 1 box A and B). The EDX measurements of

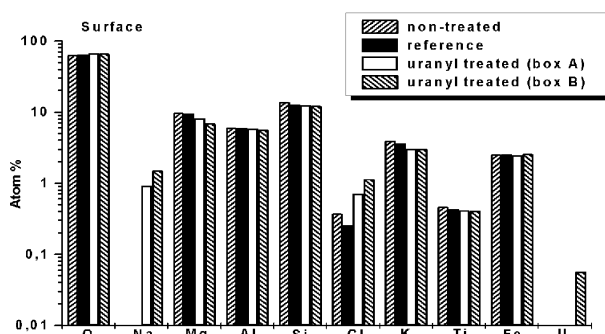


Fig. 2: EDX measurement of the biotite surface

the uranyl treated sample shows a slightly lower potassium and magnesium and much higher sodium and chloride concentrations on the surface than the non-treated sample. Uranium sorption could only be found with EDX measurements in the area of box B where the biotite surface is damaged.

Fig. 3 shows the elemental composition of the edge and their change by immersion into sodium perchlorate or uranyl solution. The sodium and the chloride concen-

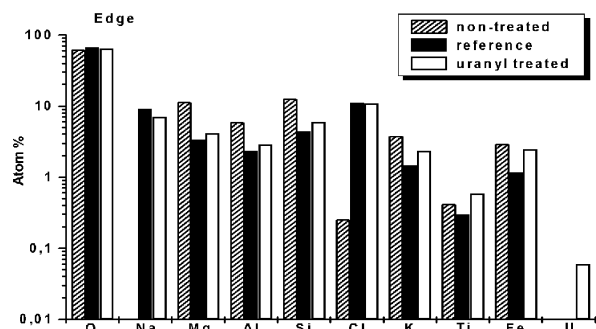


Fig. 3: EDX measurement of the biotite edge

trations of the edge samples are much higher for the reference and the contaminated sample than for the non-treated sample. The concentration of the other elements seems to be lower for the uranyl treated and the reference sample than for the non-treated sample.

## Discussion

The comparison between EDX measurements at different points of the surface shows that uranium is preferably adsorbed either at the edge or at points where the surface is damaged. At this points the surface is more reactive.

The immersion of biotite in solution leads to a loss of interlayer potassium at the edge which is replaced by hydrated cations. This immediately leads to a modification of the octahedral sheet with loss of iron. This iron not necessarily remains in solution. It also can precipitate as amorphous or crystallized oxyhydroxide at the surface /1/.

Iron-oxyhydroxide compounds are preferred adsorption sites for uranium(VI) /2/.

The adsorption of a sodium perchlorate layer may be the reason for the lower detection of the other elements on the edge.

## Acknowledgments

The authors are grateful to Prof. Dr. B.O. Kolbesen / J.W. Goethe-University Frankfurt/Main and his working group for the SEM pictures and EDX measurements.

## References

- /1/ Nahon, D.B. : *Introduction to the petrology of soils and chemical weathering*; Wiley & Sons 1991 p. 52
- /2/ Zorn,T., Arnold,T., Bernhard,G., Nitsche,H.: Sorption of uranium(VI) onto phyllite and its mineralogical constituents. In: Report FZR-218 (1998) p. 3

# ADSORPTION ISOTHERM AND POTENTIOMETRIC TITRATIONS OF QUARTZ

T. Zorn, T. Arnold, G. Bernhard, H. Nitsche

The adsorption isotherm at pH 6.5 indicates that the quartz surface possesses only one type of binding site. Based on potentiometric titrations, the total number of the surface sites was calculated and values of 3.44 and 3.55 sites/nm<sup>2</sup> were determined for I=0.1M and I=0.05M, respectively.

## Experimental

Potentiometric titrations of quartz were performed with a Schott-titrator under N<sub>2</sub> atmosphere. One gram of quartz (63-200µm) was titrated with acid and base in 80mL 0.1 M NaClO<sub>4</sub>-solution. Sixty micro liter of 10<sup>-3</sup>M NaOH or 10<sup>-3</sup>M HCl were added to the quartz suspension in intervals of two minutes. The adsorption isotherm of quartz was determined at pH 6.5 under the followings experimental conditions: Half a gram of quartz of the 63-200 µm fraction was added to 20 mL of 0.1 M NaClO<sub>4</sub> solution in 50 mL polypropylene centrifuge tubes. The mineral samples were conditioned for 24 hours with this solution. Then 20 mL of 0.1 M NaClO<sub>4</sub> solution were added to reach a final volume of 40 mL. The pH was adjusted to 6.5. The pH was checked after 24 hours and if necessary readjusted. This was repeated until the pH was stable. Then the uranyl perchlorate solution was added to set the final U(VI) concentration between 1x10<sup>-8</sup> M to 5x10<sup>-4</sup>M. Immediately after the addition of the uranium, the pH was readjusted to 6.5. Then the samples were rotated end-over-end at 1 - 5 rpm for about 60 hours to minimize abrasion and to keep the geomaterial in suspension. After 60 hours the final pH values were measured and the aqueous solid phases were separated by centrifugation at 3000 rpm for 7 minutes. Subsequently, the supernatant was filtered using Centrisart C 30 membranes with a pore size of 5 nm. The filtrate was acidified to a pH of about 1.5, and the sample was analysed for uranium by ICP-MS (Inductive Coupled Plasma-Mass Spectrometry).

## Results and Discussion

The proton surface charge on quartz was determine from acid-base titrations and the concentration of ionizable hydroxyl groups was estimated. The surface site density was estimated using the following equation /1/:

$$F = F/AxS[c_a - c_b - (H^+) + (OH^-)]$$

C<sub>a</sub> is the molar concentration of added acid and c<sub>b</sub> is the molar concentration of added base. The molar concentration of H<sup>+</sup> and OH<sup>-</sup> is calculated from the pH measurements. F is the Faraday constants, A is the specific surface area of quartz (0.2m<sup>2</sup>/g) and S is the solid concentration (g/L). SOH<sub>2</sub><sup>+</sup> and SO<sup>-</sup> are the charged ionizable surface species of quartz. The results are graphically displayed in Fig. 1. At pH 9.5 it is assumed that all surface species are negatively SO<sup>-</sup> surface species. For this assumption the total number of surface sites was determined as 3.44 and 3.35 sites/nm<sup>2</sup> for I=0.1M and I=0.05M, respectively.

The adsorption isotherm are shown in Fig. 2. The linear behavior in the concentration range between 1x10<sup>-8</sup>M and 1x10<sup>-4</sup>M of initially added uranium indicates that the ground quartz has a homogeneous surface with only one type of binding site.

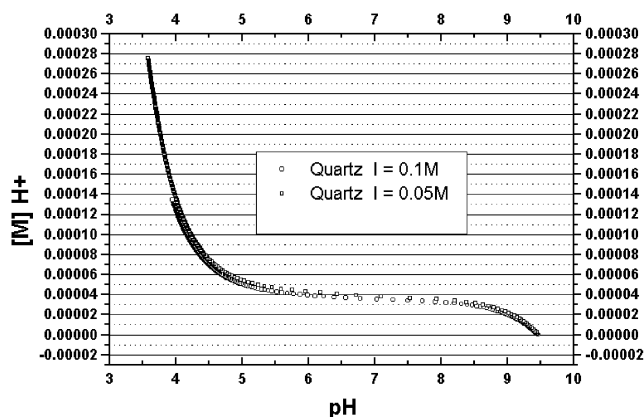


Fig. 1: Potentiometric titrations data of quartz

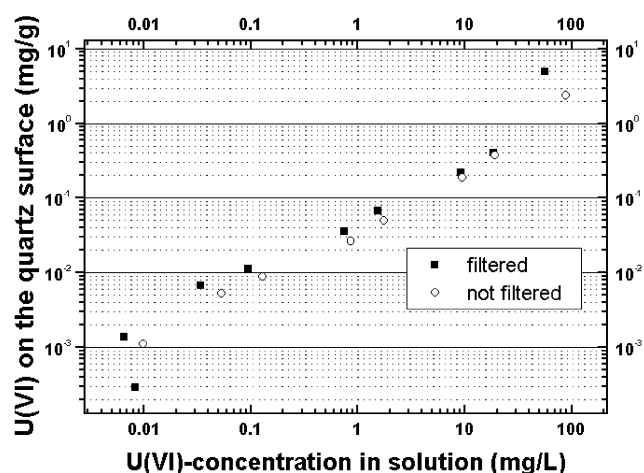


Fig. 2: Adsorption isotherm of quartz at pH 6.5

At an initial uranium concentration of 5x10<sup>-4</sup>M a yellow precipitate was observed, which can be attributed to the formation of a solid uranium hydroxide phase, thus causing the upslope of the adsorption isotherm.

The DDLM (Diffuse Double Layer Model) will be applied to model the sorption results and the optimisation program FITEQL will be used to determine surface complex formation constants.

## Acknowledgements

The authors would like to thank W. Wiesener for ICP-MS measurements and G. Grambole for performing acid-base titrations.

## References

/1/ Dzombak, D.A., Morel, F.M.M. *Surface complexation modeling*. Hydrous ferric oxide. Wiley, New York, 1990

# SORPTION OF TETRAVALENT URANIUM ON METAMORPHIC ROCKS AND SEDIMENTS

A. Abraham, L. Baraniak, H. Neubert, G. Bernhard, H. Nitsche

The uranium(IV) sorption studies under anoxic conditions showed that (1) in the transitional range the sorption is comparable with uranium(VI) and (2) under reducing conditions uranium is sorbed as  $U(OH)_4$  with high distribution ratios.

## Introduction

In continuation of the uranium sorption studies on rocks from the Erzgebirge and sediments from the Elbe Valley in Saxony, Germany, we investigated tetravalent uranium sorption under transitional and reducing conditions in the presence of organic materials such as wood degradation products (WDP), lignin (PWL) and humic acids (HUA).

The process of wood degradation in the flooded mines consumes oxygen which creates anoxic conditions. The organic compounds contribute to the decrease of the redox potential in deeper mine water layers. Potentials from 25 to 150 mV are found in the flooded Schlema mine at a depths below 20 m /1/.

Reducing conditions were simulated in sorption experiments in two steps: first under transitional conditions with an Eh between 200 and 400 mV, and then under reducing conditions with an Eh between 0 and 200 mV. After reaching steady state (4-6 weeks) and separating the liquid and solid phases the distribution ratios ( $R_s$  [mL/g]) were determined using  $^{234}U$  tracer and LSC measurements.

## Results

The  $R_s$  values for the rocks under transitional conditions are between 2 and 8 mL/g at pH 8 to 9 (Fig. 1).

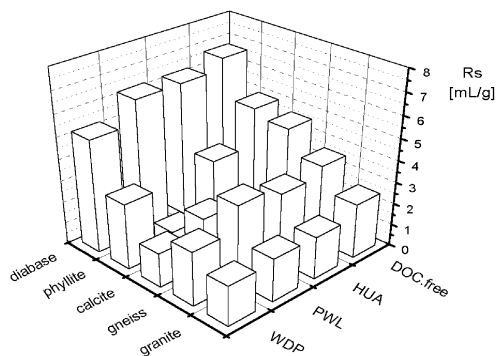


Fig. 1: Uranium sorption on metamorphic rocks under transitional conditions

We found the following gradation: *diabase* has the highest values followed by *phyllite/calcite*, *gneiss* and *granite*. We found no change in  $R_s$  for *diabase*, *gneiss* and *granite* in the presence of the organic substances. Only *phyllite* and *calcite* showed a slightly decreased sorption.

Under reducing conditions, the sorption on the rocks increases by two orders of magnitude (Fig. 2).

The  $R_s$  values range from  $1.4 \times 10^2$  to  $2.1 \times 10^3$  mL/g. The highest sorption is found on *phyllite* with  $R_s$  above  $10^3$ . The sorption on the other rocks is not as strong ( $R_s$ : 130-920 mL/g). Generally the organic compounds do not influence the sorption. In the case of *phyllite*, PWL increases the distribution ratio by about 22%, WDP and HUA decrease it by 24%.

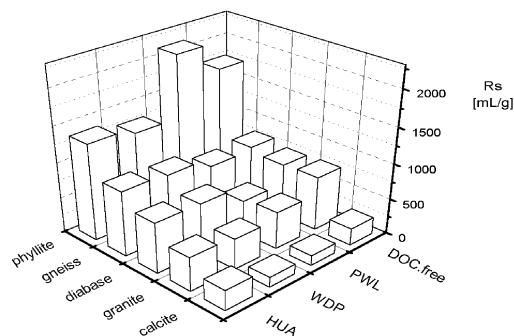


Fig. 2: Uranium sorption on metamorphic rocks under reducing conditions

The U(IV) sorption from the DOC-free mine water onto the sediments under reducing conditions is characterized by strong binding to *sandstone*, *lime marl* and *claystone* with the highest  $R_s$  values and the lowest sorption on *turonian sandstone* (B). The influence of DOC decreases the sorption, with the exception of *lime marl A* and *sandstone B* (Fig. 3).

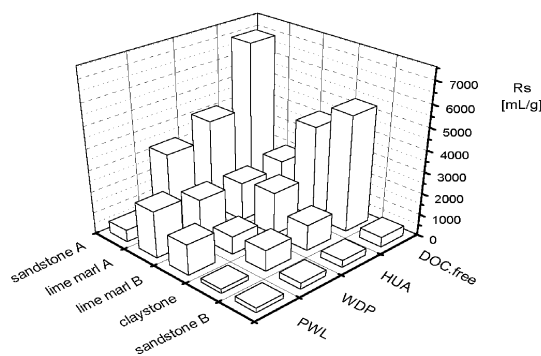


Fig. 3: Uranium sorption on Sediments under reducing conditions

Under weakly reducing conditions (around 400 mV), the  $R_s$  values are between 2 and 20 mL/g and the influence of DOC on the sorption is negligible.

## Conclusions

The sorption on the rocks and sediments increases strongly with decreasing redox potential. Uranium exists in neutral solution and Eh values below 100 mV in the tetravalent state /2/. U(IV) is oxidized to U(VI) at higher potentials. This results in relatively weak sorption (transitional potential range). Under strongly reducing conditions, tetravalent uranium precipitates as  $U(OH)_4$  causing high distribution ratios.

## Acknowledgments

This study was supported by the Sächsisches Ministerium für Wissenschaft und Kunst under contract No. 4-7541.83 -FZR/512.

## References

- /1/ Final Report Project 4-7541.83-FZR/512, 1998
- /2/ Brookins, D.G., *Eh-pH Diagrams for Geochemistry* Springer-Verlag Berlin 1988, p. 73

# INFLUENCE OF HYDROTHERMAL WOOD DEGRADATION PRODUCTS ON THE URANIUM ADSORPTION ON ROCKS AND SEDIMENTS UNDER ANAEROBIC CONDITIONS

L. Baraniak, A. Abraham, G. Bernhard, H. Nitsche

Uranium adsorption on rocks and sediments that are typical of the Saxon mining areas was studied in the presence of wood degradation products, pine wood lignin and humic acid under anaerobic conditions by batch experiments using  $^{234}\text{U}$  tracer and LSC.

## Introduction

Hydrothermal wood degradation introduces organic substances (DOC) into the water. This DOC complexes radionuclides and heavy metals /1/. That influences their adsorption on rocks and sediments. Under aerobic conditions an increase in U(VI) adsorption was found on rocks and minerals typical for the Erzgebirge in the presence of the wood degradation products. U(VI) adsorption on the Königstein sediments is less influenced by this organic matter /2/. Oxygen-consuming processes result in anaerobic conditions in deeper water layers, for example in flooded mines, that may influence the uranium adsorption on the geomaterials.

## Experimental

One gram of geomaterial was equilibrated in batch experiments with 5 mL water (corresponding to the water composition of the Schlema and Königstein mines) containing  $\text{UO}_2^{2+}$  ( $10^{-5}$  to  $10^{-4}$  mol/L) and DOC (20 mg/L). After 4-6 weeks gentle agitation under inert gas, the distribution ratios were determined by measuring the added  $^{234}\text{U}$  tracer (60 Bq/sample) in a liquid scintillation counter. The pH and Eh were determined in each sample at the end of the equilibration.

## Results

The anaerobic U(VI) adsorption on the rocks in the pH range 7.8-8.3 and at Eh 410-470 mV is generally characterized by a small decrease in DOC presence (Fig. 1), e.g., for *pyrite*,  $R_s$  diminishes from 10.4 to about 8 mL/g by pine-wood lignin (PWL) and humic acid (HUA), and to 4.8 mL/g by the wood degradation products (WDP). Adsorption on *gneiss* (PWL: 4.0, HUA: 3.4-3.9, WDP: 3.0 mL/g) and *granite* ( $R_s$ : 3.0/2.1-2.2/2.0 mL/g) shows the same tendency, but on a lower level. A comparably high adsorption is found on *diabase*. The WDP reduce the adsorption from 13 to 8.2 mL/g, whereas PWL and HUA have no influence. Adsorption on *calcite* is nearly unchanged by the organic matter ( $R_s$ :  $8.0 \pm 1.5$  mL/g).

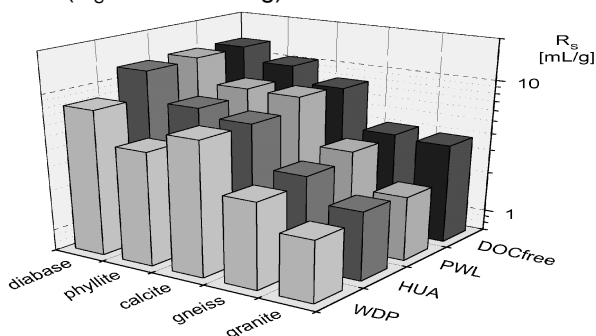


Fig. 1: Influence of wood degradation products on the U(VI) adsorption on metamorphic rocks under anaerobic conditions

There are only small differences in adsorption between the various rocks. We found the following gradation

under the influence of WDP:

*diabase* ( $R_s$ : 8.2 mL/g) > *calcite* (6.8) > *phyllite* (4.8) > *gneiss* (3.9) > *granite* (2.0).

The anaerobic U(VI) adsorption on the sediments in acidic solution (pH 3.0-3.8) and at decreased Eh (400-580 mV) shows no significant change in the presence of DOC (Fig. 2). But there is an evident gradation between the various sediments; adsorption decreases in the following order:

*lime marl A* /A/ ( $R_s$ : 14.9 mL/g) > *turonian sandstone B* /B/ (4.6) > *cenomanian sandstone A* /A/ = *claystone* (1.8).

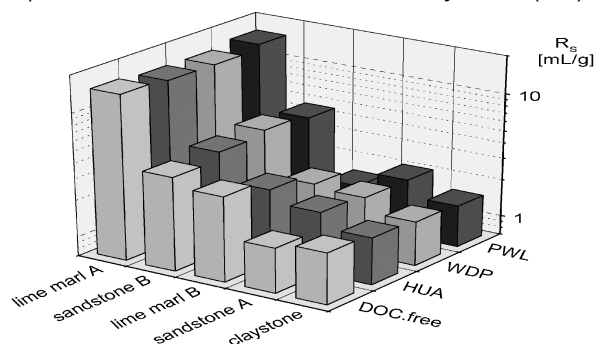


Fig. 2: Influence of wood degradation products on the U(VI) adsorption on sediments under anaerobic conditions

## Discussion

The exclusion of oxygen from the experiments caused a decrease in the redox potential: in rock samples by 300 mV and in sediments by about 500 mV. By relating these conditions to the Eh-pH dependency of the U(VI)/U(IV) system in the presence of carbonate /3/, we find that the reduction of  $[\text{UO}_2(\text{CO}_3)_2]^{2-}$  at pH 8 and of  $\text{UO}_2^{2+}$  at pH 3.4 takes place at Eh below 100 and 220 mV, respectively. That means, that no U(VI) was reduced and the determined  $R_s$  are uninfluenced by precipitated  $\text{U}(\text{OH})_4$ .

Comparing the anaerobic with the aerobic adsorption /2/, we find a stronger adsorption on *phyllite* (4.8 instead of #0.1 mL/g) that will contribute to the uranium retardation in subsurface waters near the mines. From the dominant influence of pH for the sandstone (4.8 mL/g at pH 3.8 and 150 at pH 6.8), we conclude that U(VI) is more and more immobilized at increasing pH in the mine flooding process.

## Acknowledgments

This study was supported by the Sächsisches Staatsministerium für Wissenschaft und Kunst under contract no. SMWK 4-7541.83-FZR/512.

## References

- /1/ Schmidt, M., et al.: Report FZR-180 (1997) p. 30
- /2/ Baraniak, L., et al.: Report FZR-218 (1998) p. 6
- /3/ Brookins, D.G.: *Eh-pH Diagrams for Geochemistry*, Springer-Verlag Berlin 1988, p. 154

# COMPUTATION OF DISTRIBUTION COEFFICIENTS ( $K_d$ ) FOR RISK ASSESSMENT STUDIES

V. Brendler, Y. Stiglund<sup>1</sup>, S. Nordlinder<sup>1</sup>  
<sup>1</sup>Studsvik Eco & Safety AB, Nyköping, Sweden

Geochemical speciation software (MINTEQA2) is integrated into a risk assessment code (PRISM / BIOPATH), unfolding the simplistic  $K_d$  concept into complex formation, heterogeneous phase equilibria and surface complexation. This allows the computation of a more realistic  $K_d$ , using an iterative approach to account for a changing chemical environment. Furthermore, those parameters are clearly identified that contribute most to the overall uncertainty.

## Methodology

World-wide activities focus on remediation of radioactively contaminated sites. An EU project (RESTRAT /1/) develops a generic methodology for ranking of restoration techniques. The risk assessment model used for RESTRAT is based on two programs:

- PRISM /2/ as outer shell performs uncertainty analysis, using the Latin Hypercube Sampling for input parameters, allowing arbitrary parameter distributions and correlations;
- BIOPATH /3/ computes the contaminant transport in geo- and biosphere based on compartment theory. It applies first order differential equations for kinetics. Up to now chemistry is included (like in other risk assessment codes) only through distribution coefficients ( $K_d$  values), the ratio of the sorbed (fixed, immobilized) and the unsorbed (free, truly dissolved) fraction of a given component under equilibrium conditions. This widely used concept is, however, too simplistic because many very different basic physico-chemical phenomena (hydrolysis and complexations, redox reactions, mineral precipitation and dissolution, adsorption and ion exchange, colloid formation) are subsumed into just one empirical parameter. Any  $K_d$  used in prognostic studies is just a snapshot for a specific combination of Eh, pH, concentrations, and mineral composition, and its value is sensitive to even slight changes in some parameters. This in turn assigns very large uncertainties to them.

A better strategy is to unfold the single  $K_d$  value into a parameter vector, i.e., the decomposition of the  $K_d$  into its underlying basic processes, knowing the functional relationships between them and how they contribute to the  $K_d$ . Then a  $K_d$  can be calculated, even for simulated hypothetical scenarios with long-term drifts in the chemical environment. Moreover, those parameters affecting the  $K_d$  strongest can be identified, and consequently, extra measurements can be designed specifically to reduce their uncertainty. A realization of this concept requires the integration of a geochemical speciation program, such as MINTEQA2 /4/, into the risk assessment code PRISM / BIOPATH.

## Results

Leaving the original codes for both risk assessment and chemical speciation mainly unchanged, an interface was created to connect them, together with software to handle the input setup. MINTEQA2 covers all chemical reactions in homogeneous aqueous solutions, including redox reactions, handles precipitation and dissolution equilibria, and incorporates surface complexation models (SCM). MINTEQA2 delivers a computed  $K_d$  whenever required, see Fig. 1 for internal flow of information and relationships between the various software modules. An application of this new approach is presented in

the article following this one.

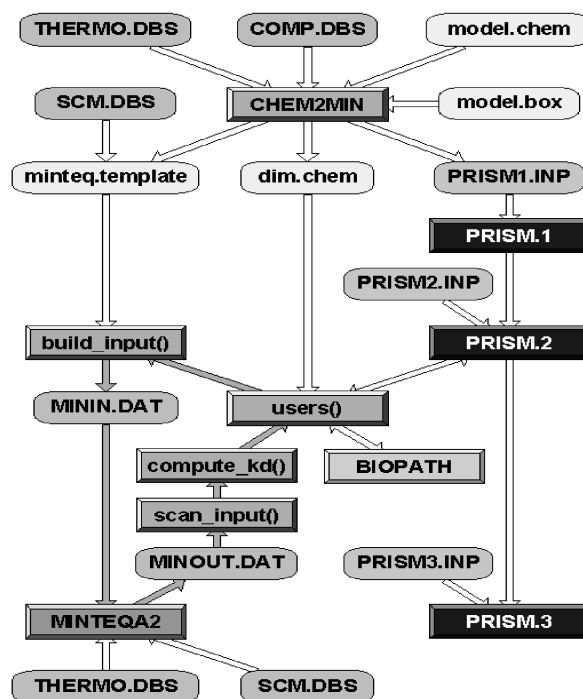


Fig. 1: Data flow and module interaction in the coupled PRISM / BIOPATH / MINTEQA2 software package

The chemical model is defined in a separate file that must be written by the user. It creates the input file for PRISM and a template for the speciation code, assuring a model description consistent for both parts of the modeling. The input file has a well defined, line-oriented structure. After some general comments (documentation information), detailed chemical data for each compartment follows. This includes the selected SCM with its intrinsic surface parameter, also pH, Eh and the concentrations for all components. Then reaction constants (for complexation, precipitation / dissolution, sorption) are listed that should be modified, also certain reactions can be suppressed totally.

## Acknowledgments

Financial support from the Nuclear Fission Safety Programme of the European Commission under contract F14P-CT95-0021a is gratefully acknowledged.

## References

- <http://www.fz-rossendorf.de/RESTRAT/>
- Gardner, R.H., et al., Studsvik Energiteknik AB, Report NW-83/555, Nyköping, 1983
- Bergstroem, U., et al., Studsvik Energiteknik AB, Report NW-82/261, Nyköping, 1982
- Allison, J.D., et al., U.S. EPA, Environ. Res. Lab., EPA/600/3-91/021, 1991

# DISTRIBUTION COEFFICIENTS FOR URANIUM: MODELING OF THE RANSTAD TAILING SITE

V. Brendler, Y. Stiglund<sup>1</sup>, T. Arnold  
<sup>1</sup>Studsvik Eco & Safety AB, Nyköping, Sweden

Distribution coefficients ( $K_d$ ) for uranium with hydrous ferric oxides were computed based on the MINTEQA2 geochemical speciation software and a newly developed interface to the risk assessment package PRISM / BIOPATH. The data were taken from the Ranstad Tailing Site in Sweden. The results are compared to literature data.

## Modeling

A newly developed approach to incorporate physico-chemical phenomena into risk assessment modeling (see previous article) is applied to the Ranstad Tailing site in Sweden, a former uranium milling facility. Fig. 1 and 2 illustrate the derivation of a compartmental structure for this site.

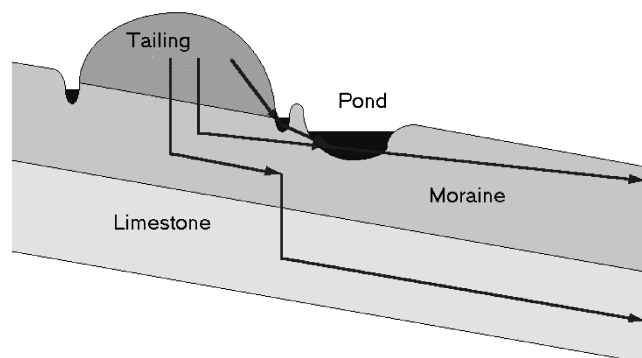


Fig. 1: Section through the Ranstad Tailing

structure for this site. The tailing layer (T) is situated above a moraine layer (M) and a limestone layer (L). It is surrounded by a collecting ditch that drains into a storage pond (P) and then into a river. Additionally, both moraine and limestone layers are aquifers.

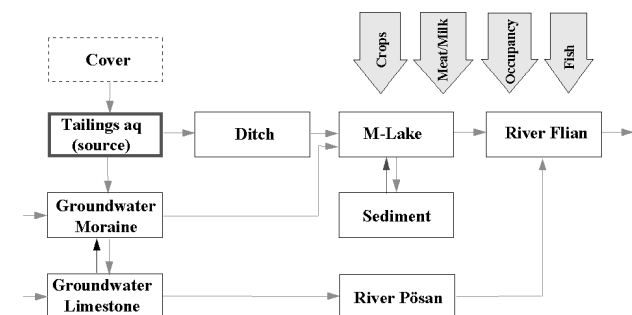


Fig. 2: Compartment scheme for the Ranstad Tailing site

The main contaminant is uranium. Samples from the site contained considerable amounts of freshly precipitated iron hydroxides. Their transformation into thermodynamically more stable minerals such as goethite or hematite has a very slow kinetics, thus ferrihydrite was chosen as the major adsorbing surface. The Diffuse Double Layer model /1/ is selected to describe surface complexation. The respective intrinsic surface parameters and the reaction constants for the ions competing with uranium for sorption sites were taken from Dzombak/Morel /1/, the uranium sorption parameters are those determined by Dicke/Smith /2/.

## Results

The results presented in Table 1 are based on a run with 1000 varied parameter sets. The calculated distri-

bution coefficients ( $K_d$  values) for uranium fall well into the range used so far for modeling of this site /3/, but exhibit much smaller uncertainties. Moreover, those parameters were identified contributing most to the uncertainty of the various computed  $K_d$  values: pH and solid concentration  $C_{solid}$  (and to a less amount the carbonate content for the storage pond). This reflects the uncertainty of the rock porosity. Also the portion of rock which is not accessible to sorption processes inside the various layers is not well known. The pH determines the uranium speciation in solution, controlling the amount of hydrolysis species and carbonate complexes that reduce the sorbed portion of uranium.

Box	$K_d \pm F$	1 <sup>st</sup> Factor	2 <sup>nd</sup> Factor
T	$(2.0 \pm 0.8) \cdot 10^{-2}$	pH: 76.4 %	$C_{solid}$ : 11.8 %
M	$(5.2 \pm 1.1) \cdot 10^{-2}$	$C_{solid}$ : 38.6 %	pH: 34.2 %
L	$(3.5 \pm 1.3) \cdot 10^{-3}$	pH: 70.2 %	$C_{solid}$ : 18.6 %
P	$2.37 \pm 0.43$	$C_{solid}$ : 50.7 %	pH: 13.2 %

Tab. 1: Computed  $K_d$  values for the Ranstad Tailing site compartments (for abbreviations see above) with the major uncertainty factors and how they contribute to the overall uncertainty.

These first results for the Ranstad Tailing site / Sweden prove the applicability of the concept and its software implementation. It will be expanded to several instead of just one mineral surface per compartment. Furthermore, the variation of the  $K_d$  due to the time-dependence of its determining parameters will be included.

## Acknowledgments

Financial support from the Nuclear Fission Safety Programme of the European Commission under contract FI4P-CT95-0021a is gratefully acknowledged.

## References

- /1/ Dzombak, D.A., Morel, F.M.M.: *Surface complexation modeling*. Hydrous ferric oxide; Wiley, New York (1990)
- /2/ Dicke, C.A., Smith, R.W.: Surface complexation modeling of uranium adsorption on naturally occurring iron coated sediments. ACS Meeting, New Orleans, March 1996
- /3/ Puigdomenech, I., Bergström, U.; SKB Technical Report 94-32, Stockholm (1994)



# **Organic Matter and its Interaction with Radionuclides**

# SYNTHESIS OF ISOTOPICALLY LABELED SYNTHETIC HUMIC ACIDS

M. Bubner, S. Pompe, M. Meyer, K.H. Heise, H. Nitsche

*Isotopically labeled synthetic humic acids are synthesized from reducing sugars and  $^{14}\text{C}$ -labeled  $\alpha$ -amino acids. These labeled compounds have functional properties that are comparable to those of natural humic acids and can be used as humic acid models.*

## Introduction

Isotopically labeled humic acids are very useful for investigating the migration behavior of metal-humic acid-complexes in column experiments, and for ligand exchange and complexation studies with metal ions.

## Experiments and results

We synthesized  $^{14}\text{C}$ -labeled humic acids (HA) via the Maillard reaction according to Pompe et al. [1,2] from xylose and  $^{14}\text{C}$ -labeled  $\alpha$ -amino acids, e. g., glycine and phenylalanine in a molar ratio of 1:1, or glutamic acid, respectively. The alkali-soluble and acid-insoluble components of the resulting [ $^{14}\text{C}$ ]melanoidines were isolated, dialyzed and lyophilized. These synthetic HA's were characterized by elemental analysis and by determination of functional carboxylic groups and phenolic hydroxyl groups. The results shown in Tab. 1 agree with the data obtained with non labeled HA.

starting material	synthesis product			
amino acid	HA type	Yield [% $^{14}\text{C}$ ]	COOH [meq/g]	phen. OH [meq/g]
[U- $^{14}\text{C}$ ]phenylalanine, glycine	M1	12	1.0	2.3
[2- $^{14}\text{C}$ ]glycine, phenylalanine	M1	30	1.0	2.3
[1- $^{14}\text{C}$ ]glutamic acid	M42	0	4.1	2.3
[U- $^{14}\text{C}$ ]glutamic acid	M42	5	4.1	2.3

Tab. 1:  $^{14}\text{C}$ -labeled synthetic humic acids from Maillard reaction

$^{14}\text{C}$ -labeled HA's were produced starting from 11.3 mmol xylose and 6.35 mmol labeled amino acid. The specific radioactivity obtained for the synthesized HA's are shown in Tab. 2.

starting material	synthesis product		
amino acid	MBq/mmol	HA type	MBq/g
[U- $^{14}\text{C}$ ]phenylalanine, glycine	40	M1	35.5
[2- $^{14}\text{C}$ ]glycine, phenylalanine	40	M1	104
[1- $^{14}\text{C}$ ]glutamic acid	40	M42	0
[U- $^{14}\text{C}$ ]glutamic acid	40	M42	102

Tab. 2: Specific radioactivity of  $^{14}\text{C}$ -labeled synthetic HA's starting from labeled amino acids

The products and by-products of the Maillard reaction were quantitatively isolated. [ $^{14}\text{C}$ ]Carbon dioxide is the only radioactive, volatile by-product of the melanoidine synthesis. Our experiments with [ $^{14}\text{C}$ ]amino acids with different labeled positions show that carbon dioxide is eliminated from the 1-position (carboxylic group) of the amino acids. The radioactivity of carbon dioxide eliminated during the reaction with uniformly labeled amino acids corresponds to the total amount of radioactivity introduced in the melanoidine. Labeled melanoidine can not be produced with amino acids labeled in the no.1 position. The nitrogen content of the melanoidine corresponds to the radioactivity introduced by the amino acid carbon atoms. The best results for  $^{14}\text{C}$ -labeled synthetic HA were obtained from Maillard reaction with [2- $^{14}\text{C}$ ]glycine.

## Conclusions

We synthesized  $^{14}\text{C}$ -labeled humic acids by the Maillard reaction with a specific radioactivity up to 100 MBq/g. Starting from [2- $^{14}\text{C}$ ]glycine with a specific radioactivity of 1,8 GBq/mmol it should be possible to obtain synthetic HA with a specific radioactivity of more than 4 GBq/g. Thus, we will be able to quantify less than 100 ng HA in a geological material or in a solution.

This synthesis procedure for  $^{14}\text{C}$ -labeling can also be applied for  $^{13}\text{C}$ -labeling of melanoidines and synthetic HA's.

The advantage of our labeling method for HA compared to other methods is the real isotopic labeling in the stable molecule skeleton without any damages in the functionality of the humic acid.

## Acknowledgments

This work was supported by the Bundesministerium für Bildung, Forschung und Technologie (BMBF) under contract number 02 E88 150.

## References

- 1/ Pompe, S. et al.; *Radiochim. Acta* **74**, 135 (1996)
- 2/ Bubner, M. et al.; *J. Labelled Cpd. Radiopharm.* **XLI**, 1057 (1998)

# COMPLEXATION OF URANYL(VI) WITH KRANICHSEE HUMIC SUBSTANCES

K. Schmeide, G. Geipel, K.H. Heise, H. Nitsche

The complexation of Kranichsee humic and fulvic acid with uranyl(VI) was studied by laser-induced fluorescence spectroscopy at pH 4 and an ionic strength of 0.1 M. The results were compared to the complexation behavior of other natural humic acids (Aldrich HA, GoHy-573 HA).

## Introduction

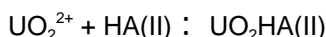
The determination of the effect of humic substances on the actinide migration in natural aquifer systems is of great interest and allows to assess their impact on the long-term safety of abandoned uranium mines. The solubility of actinides can be increased by complexation with humic substances and, thus, their mobility in the geosphere can be enhanced. Complexation constants can be used to quantify the interaction between radionuclides and humic substances.

The humic material, used for this study, was isolated from surface water of the mountain bog 'Kleiner Kranichsee' that is located in the vicinity of uranium mining sites at Johanngeorgenstadt (Saxony, Germany). The humic material was separated into humic and fulvic acid /1/.

## Experimental

The complexation of uranyl(VI) with Kranichsee humic acid (HA) and fulvic acid (FA) was studied by laser-induced fluorescence spectroscopy. The measurements were carried out in air at 20 °C in 0.1 M NaClO<sub>4</sub> at pH 3.96 ± 0.02. The fluorescence of uranyl(VI) ions was measured as a function of the total uranyl concentration at constant HA concentrations (5 mg/L). The uranyl concentration was varied from 0.5 to 5.1 µmol/L.

Further experimental conditions were: excitation wavelength - 266 nm, laser energy - about 500 µJ, delay time - 200 ns, and gate time - 1000 ns. Always 10 spectra were collected, each with 100 laser pulses, per sample. The experimental data were evaluated by means of the metal ion charge neutralization model /2/ assuming the following complexation equation:



## Results

The loading capacity (defined as the maximum fraction of proton exchanging sites of the HA that can be occupied by uranyl ions under the given experimental conditions) was determined graphically as shown in Fig. 1. The results, given in Tab. 1, indicate that there is only little difference between the complexation of UO<sub>2</sub><sup>2+</sup> with humic and fulvic acid of the Kranichsee site.

The complexation constants of the complexation of Kranichsee humic and fulvic acid and of Aldrich HA (commercial product) /3/ and GoHy-573 HA (isolated from Gorleben, Germany) /4/ with uranyl(VI) ions (Tab. 1) indicate a comparable complexation behavior with U(VI). The loading capacity of the Kranichsee humic substances is lower than that of Aldrich HA and GoHy-573 HA. That means, fewer proton exchanging

sites of the Kranichsee humic substances can be occupied by uranyl(VI) ions under the given experimental conditions.

	log β <sup>a</sup>	LC [%] <sup>a</sup>
Kranichsee HA	6.35 ± 0.22	14.0 ± 1.1
Kranichsee FA	6.21 ± 0.20	13.0 ± 1.2
Aldrich HA (A2) <sup>b</sup> /3/	5.86 ± 0.14	21.7 ± 2.1
GoHy-573 HA <sup>c</sup> /4/	6.16 ± 0.13	18.5 ± 0.3

<sup>a</sup> ± 2F <sup>b</sup> commercial product <sup>c</sup> isolated from Gorleben, Germany

Tab. 1: Complexation constants (log β) and loading capacities (LC) of the uranyl(VI) complexation of Kranichsee HA and FA compared to Aldrich HA /3/ and GoHy-573 HA /4/

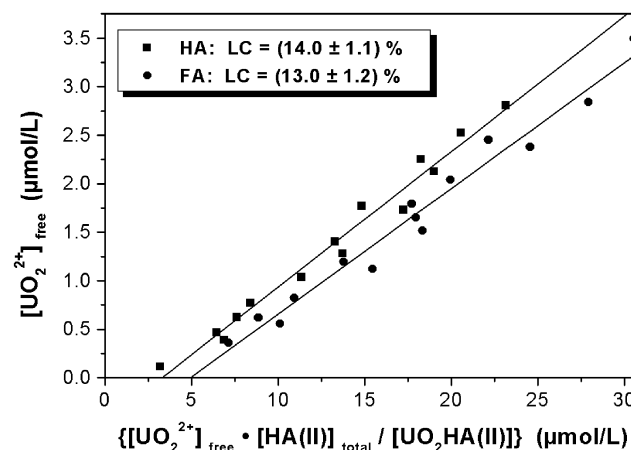


Fig. 1: Graphically determination of the loading capacity (LC) for the complexation of UO<sub>2</sub><sup>2+</sup> with Kranichsee humic substances

## Acknowledgments

This work was supported by Commission of the European Communities under contract no. F14W-CT96-0027.

## References

- /1/ Schmeide, K. et al.; Report FZKA 6124, Forschungszentrum Karlsruhe, 161 (1998)
- /2/ Kim, J.I., Czerwinski, K.R.; Radiochim. Acta **73**, 5 (1996)
- /3/ Pompe, S. et al.; Radiochim. Acta **82**, 89 (1998)
- /4/ Czerwinski, K.R. et al.; Radiochim. Acta **65**, 111 (1994)

# EFFECT OF HUMIC SUBSTANCES ON THE SORPTION OF URANIUM(VI) ONTO SITE-SPECIFIC ROCK MATERIAL

K. Schmeide, S. Pompe, R. Jander, K.H. Heise, H. Nitsche

The effect of humic material (Kranichsee humic acid) on the sorption of uranium(VI) onto phyllite and its individual main mineralogical components muscovite, albite and quartz was studied in air-equilibrated batch experiments as a function of pH.

## Introduction

Organic material, such as humic and fulvic acids, that are commonly present in natural aquifers can complex inorganic contaminants and change their sorption behavior on geological materials. Batch experiments were carried out in order to determine the effect of humic acid on the sorption behavior of uranium(VI) onto phyllite and its main mineralogical components muscovite, albite and quartz. The humic acid (HA), used for the experiments, was isolated from the bog 'Kleiner Kranichsee' /1/.

## Experimental

The experimental conditions were:  $[UO_2^{2+}] = 1 \mu M$ ,  $[HA] = 5 \text{ mg/L}$ ,  $I = 0.1 \text{ M (NaClO}_4)$ ,  $m/V = 500 \text{ mg mineral/40 mL}$ ,  $pH \text{ 3.5-9.5}$ , aerobic conditions, 60 h reaction period. The uranium sorption results were corrected for sorption on the walls of the experimental vials.

## Results

We compare the results of these experiments to results from previously conducted experiments where the sorption of U(VI) onto phyllite and its constituents was studied in the absence of humic material /2/.

Fig. 1 shows the pH-dependent U(VI) and HA uptake onto phyllite. The uranium adsorption curve in the presence of HA is similar to the adsorption curve obtained for the experiments in the absence of HA. The strong uranyl sorption on phyllite (95 - 97 % in the absence of HA) is not changed by HA in the pH range from 6.2 to 7.8. However, in the pH range from 3.6 to 6, the uranium uptake on phyllite is higher when HA is present. Above pH 8, the HA reduces the uranyl sorption on phyllite. Furthermore, HA is strongly taken up from pH 3.6 to 7.7: 78 to 88 % of the HA is adsorbed. The HA sorption decreases above pH 8.4 (to 59 % at pH 9.5).

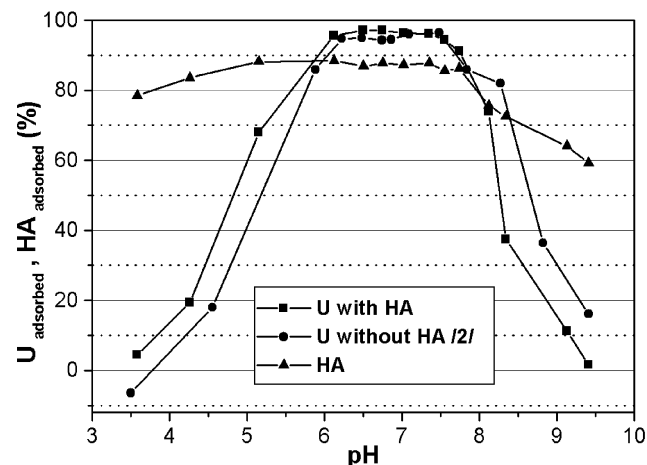


Fig. 1: Uranium and humic acid uptake on phyllite

The results for muscovite are depicted in Fig. 2. At pH

from 7.5 to 9.5, the uranium sorption on muscovite is unchanged by HA. At pH 7.5 to 6, the uranium sorption becomes smaller in the presence of HA. However, the uranium sorption is much stronger in the presence of HA below pH 6. That means, the maximum of the uranyl sorption (70 %) is shifted from pH 6.3 (without HA) to pH 5.5 (with HA). The sorption of HA on muscovite strongly depends on the pH of the solution: at pH 8 to 9.5 the HA is not sorbed; below pH 8, the HA sorption increases with decreasing pH and has a maximum at pH 4.5 to 5 (. 83 %).

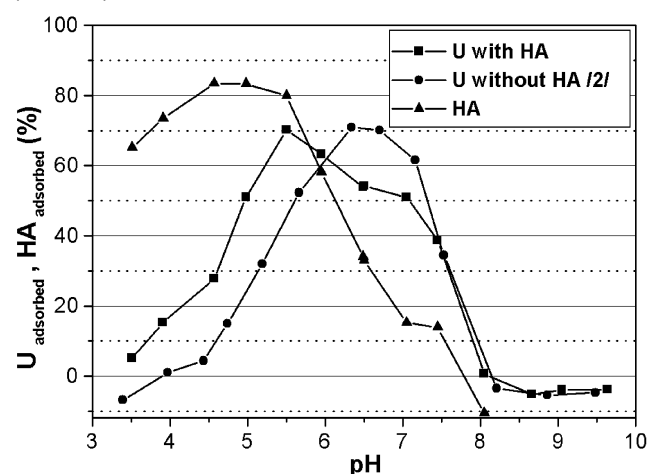


Fig. 2: Uranium and humic acid uptake on muscovite

The uranyl sorption on albite and quartz (further constituents of phyllite) in the presence of HA is similar to muscovite and can be summarized as follows:

- i) The uranium uptake increases in the presence of HA at acidic pH. This can be attributed to the fact that the HA is sorbed on the mineral surface thereby providing additional sorption sites through their complexing ability.
- ii) In the neutral pH range, the HA sorption decreases with increasing pH, thereby forming aqueous uranyl humate complexes and decreasing the uranyl uptake.
- iii) At alkaline pH values, the formation of weakly sorbing uranyl carbonate complexes predominate the influence of HA. /3/

We conclude that the uranium sorption is affected by both the pH and the presence of organic material.

## Acknowledgments

This work was supported by Commission of the European Communities under contract no. F14W-CT96-0027.

## References

- /1/ Schmeide, K. et al.; Report FZKA 6124, Forschungszentrum Karlsruhe, 161 (1998)
- /2/ Arnold, T. et al.; Chemical Geology **151**, 129(1998)
- /3/ Waite, T.D. et al.; Geochim. Cosmochim. Acta **58**, 5465 (1994)

# THE INFLUENCE OF PHENOLIC HYDROXYL GROUPS ON THE COMPLEXATION BEHAVIOR OF HUMIC ACIDS WITH URANYL(VI) IONS STUDIED WITH MODIFIED SYNTHETIC HUMIC ACIDS

S. Pompe, M. Bubner, G. Geipel, K.H. Heise, H. Nitsche

We investigated the influence of phenolic hydroxyl groups on the complexation behavior of humic acids at pH 4 using a modified synthetic humic acid with blocked phenolic hydroxyl groups. The modified humic acid, type M1-B with blocked phenolic hydroxyl groups, has a lower loading capacity with  $UO_2^{2+}$  at pH 4 than the non-modified synthetic humic acid.

Due to the heterogenous nature of humic acids (HA) there are numerous uncertainties in the description of their complexation behavior with metal ions. Therefore, it is necessary to investigate the complexation process with well-defined HA model substances. In this work, we investigated for the first time the influence of phenolic OH groups on the complexation behavior of HA with  $UO_2^{2+}$  ions.

## Experimental and Results

Starting from synthetic HA, type M1 /1/, we synthesized a HA with blocked phenolic OH groups (type M1-B) /2/. The modification process comprised two steps: a) the permethylation of carboxylic and phenolic OH groups with diazomethane resulting in methyl ester and methyl ether groups and b) the hydrolysis of the ester groups in alkaline solution. The determination of functional groups confirmed that a part of the primary phenolic OH groups were blocked by etherification. As a result of the alkaline saponification of the ester groups, the number of HA carboxylic groups was increased. Thus, the original HA of type M1 was additionally alkaline-saponified to provide a HA with non-modified phenolic OH groups having a comparable number of carboxylic groups (type M1-V) /2/. With these synthetic HA model substances, we investigated the influence of phenolic OH groups on the complexation behavior of HA with  $UO_2^{2+}$  ions at pH 4 by laser-induced fluorescence spectroscopy.

Tab. 1 shows the composition of the investigated uranyl humate solutions. The experimental conditions of the spectroscopic measurements are described in /3/. The experimental data were evaluated applying the charge neutralization model by Kim and Czerwinski /4/.



where HA(II) represents the humic acid ligand and  $UO_2HA(II)$  stands for uranyl humate.

	Type M1-V	Type M1-B
phenolic OH/(meq/g) <sup>a</sup>	1.70 ± 0.10	1.06 ± 0.19
PEC/(meq/g) <sup>b</sup>	2.12 ± 0.06	1.94 ± 0.13
COOH / (meq/g)	2.03 ± 0.02	1.91 ± 0.07
$UO_2^{2+}$ /(μmol/L)	1.1 - 10.3	1.1 - 10.3
HA/(mg/L)	10	10
pH	3.96 ± 0.04	3.94 ± 0.05

<sup>a</sup> radiometrically determined; <sup>b</sup> Proton exchange capacity

Tab. 1: Composition of the investigated uranyl humate solutions (I: 0.1 M NaClO<sub>4</sub>; T: 20 ± 1 °C)

Tab. 2 summarizes the spectroscopically-determined loading capacities (LC) and complexation constants (log  $\beta$ ) for synthetic HA M1-B and M1-V. Fig. 1 illustrates

the loading capacity of both HA with  $UO_2^{2+}$  ions which represents the mole fraction of maximal available complexing sites of the HA under the applied conditions.

	Type M1-V	Type M1-B
LC ± 2F / (%)	34 ± 3	18 ± 2
log $\beta$ ± 2F	6.11 ± 0.33	6.38 ± 0.72

Tab. 2: LC and log  $\beta$  for the complexation of HA type M1-V and M1-B with  $UO_2^{2+}$  (pH 4; I: 0.1 M NaClO<sub>4</sub>)

The complexation constants of HA M1-B and M1-V are comparable within their experimental errors. Nevertheless, HA M1-B shows a significant lower LC at pH 4 than HA M1-V. This indicates that the blocking of the phenolic OH groups changes the complexation behavior of the HA. Therefore, one can conclude that phenolic OH groups are involved in the complexation process with  $UO_2^{2+}$  ions under the applied conditions. At pH 4, the HA phenolic OH groups are likely protonated due to their high pKa values. We assume that intramolecular hydrogen bonds between the hydrogen atoms of the non-modified phenolic OH groups and the oxygen atoms of the  $UO_2^{2+}$  ions are formed.

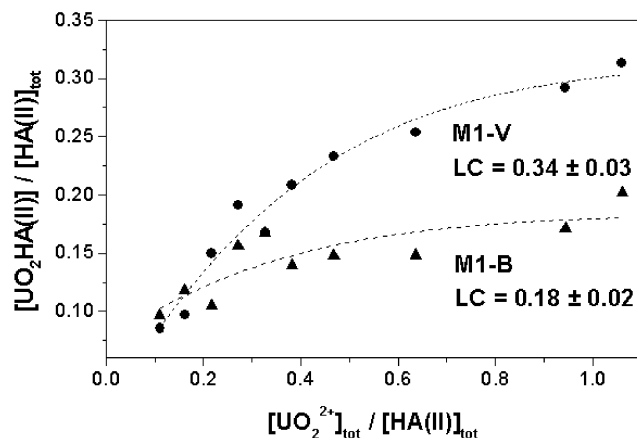


Fig. 1: Loading capacities for HA type M1-B and M1-V

We are currently investigating other modified synthetic and natural HA with blocked phenolic OH groups to confirm this result.

## Acknowledgments

This work was supported by the Bundesministerium für Bildung, Forschung und Technologie (BMBF) under contract number 02 E88150.

## References

- /1/ Pompe, S. et al.; Radiochim. Acta **74**, 135 (1996)
- /2/ Pompe, S. et al.; Report FZR 218 (1998) p.30
- /3/ Pompe, S. et al.; Radiochim. Acta **82**, 89 (1998)
- /4/ Kim, J.I. et al.; Radiochim. Acta **65**, 111 (1994)

# COMPARISON OF THE MODEL HUMIC ACIDS M1 AND M42 WITH ALDRICH HUMIC ACID AND THEIR URANYL COMPLEXES BY INFRARED SPECTROSCOPY

K.H. Heise, R. Nicolai<sup>1</sup>, S. Pompe, M. Bubner, H. Nitsche  
<sup>1</sup>Institute of Bioinorganic and Radiopharmaceutical Chemistry

The infrared spectra of synthetic HA of type M1 and M42 and their uranyl complexes shows good agreement with natural Aldrich HA in the range from 4000 cm<sup>-1</sup> to 50 cm<sup>-1</sup>. For the first time, the UO<sub>2</sub>-vibrational bending frequencies were measured in the far infrared.

## Introduction

Humic acids (HA) are instable and chemically not well-defined substances. Therefore, it is impossible to accurately describe HA containing systems. This fact often limits systematic environmental studies on the interaction between HA and heavy metals. It has been suggested to study stable, humic-acid-like substances /1/. We have introduced melanoidins as model humic acids (MHA) /2/. In this study we have compared the infrared spectra of MHA's M1 and M42 with purified natural Aldrich HA (A2), and their corresponding uranyl humic complexes. A Perkin-Elmer FTIR Spectrometer Mod. 2000 was used.

## Model Humic Acids

The condensation reaction of reducing sugars and  $\alpha$ -amino acids leads to melanoidins. The HA-like melanoidine fractions were isolated by alkaline extraction and acidic precipitation.

M1 was synthesized from a phenyl alanine/glycine mixture and xylose. M1 had 1.02±0.06 meq/g of carboxylic groups, and 2.3±0.1 meq/g phenolic OH-groups. M42 was synthesized from glutamic acid and xylose. M42 had 4.10±0.11 meq/g of carboxylic groups, and 2.3±0.4 meq/g phenolic OH-groups. The purified natural HA A2 had 4.41±0.11 meq/g of carboxylic groups, and 3.4±0.4 meq/g of phenolic OH-groups.

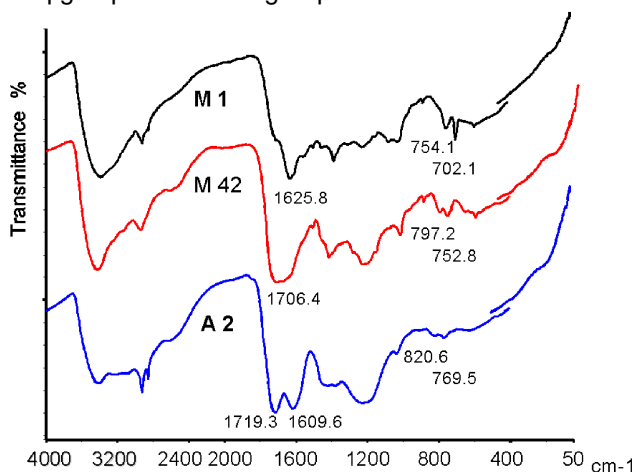


Fig. 1: FTIR spectra (MIR and FIR) of the model humic acids M1 and M42, and Aldrich humic acid A2

Infrared spectra in the range from 4000 cm<sup>-1</sup> to 50 cm<sup>-1</sup> of the three humic acids are fundamentally the same (Fig. 1). However, in middle infrared (MIR), M1 exhibits a clear  $\nu$ (C-H) out of plane-vibration which stems from the aromatic structures of the phenyl alanine precursor. M42 and A2 show more pronounced C=O stretching vibrations than M1 due to their higher carboxylic group content. In addition, bands from aliphatic chain structures can be seen. As expected, the spectra in far infrared (FIR) are exhibit no bands.

## Uranyl Humic Complexes

Preparation of uranyl humic complexes of M1, M42, and A2 have been described before /3/. The infrared spectra from 4000 cm<sup>-1</sup> to 50 cm<sup>-1</sup> are shown in Fig. 2.

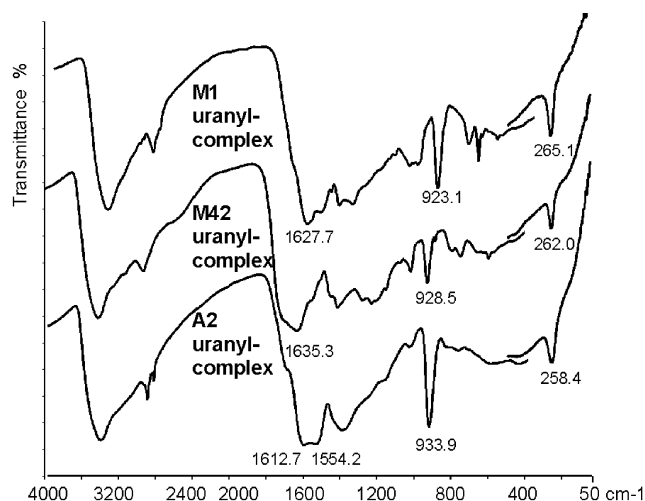


Fig. 2: FTIR spectra (MIR and FIR) of uranyl complexes of the model humic acids M1 and M42, and Aldrich humic acid A2

The asymmetric UO<sub>2</sub> stretching vibration is observed in the MIR range at 923.1 cm<sup>-1</sup> (M1), 928.3 cm<sup>-1</sup> (M42), and 933.1 cm<sup>-1</sup> (A2). They shift significantly to higher wavenumbers with decreasing aromatic character of humic acids. The characteristic UO<sub>2</sub> bending frequencies were detected in the FIR at 265.1 cm<sup>-1</sup> (M1), 262.0 cm<sup>-1</sup> (M42), and 258.4 cm<sup>-1</sup> (A2). These bands shifts significantly to lower wavenumbers with decreasing of the aromatic character of humic acids.

## Conclusions

This infrared spectroscopic study show that the uranium (VI) coordination is comparable for the MHAs and the Aldrich HA. Shifts of the vibrations associated with the uranyl unit in MIR and FIR can be ascribed to differences in the aromaticity of the HAs; however, these differences indicate no significant differences of the uranium (VI) coordination. These results agree with our previous investigations and confirm once more the suitability of melanoidins as stable and chemically well-defined models for basic environmental research on humic acids.

## Acknowledgments

This work was supported by the BMBF under contract number 02E88150.

## References

- /1/ Skytte Jensen, B. et al.; EU Report 16763 EN (1996)
- /2/ Pompe, S. et al.; Radiochim. Acta **74**, 135 (1996)
- /3/ Bubner, M. et al.; Report FZR-180, 22 (1997)

# REDUCTION OF HEXAVALENT URANIUM BY NATURAL POLYELECTROLYTES

A. Abraham, L. Baraniak, G. Bernhard, H. Nitsche

The reduction of uranium(VI) by natural polyelectrolytes such as lignin, humic acid and wood degradation products was studied. The reducing capacity of these substances was obtained from the spectrophotometric determination of (IV) with arsenazo-III.

## Introduction

The process of wood degradation in the flooded uranium mines consumes oxygen and therefore anoxic and reducing conditions are prevailing in deeper mine water layers. Natural polyelectrolytes such as wood degradation products (WDP), lignin (LIG) and humic acids (HUA) are redox active and may be able to change the oxidation state of dissolved metals.

## Experimental

The U(VI) reduction by lignin, humic acid and wood degradation products was studied by the spectrophotometric determination of U(IV) with arsenazo-III /1/. The measurements were carried out with a diode array spectrophotometer (Hewlett Packard, Type 8452A). The lignin and the wood degradation products were prepared at the Institute of Plant and Wood Chemistry, Tharandt (Saxony) and the humic acid was a commercial product (Aldrich).

The samples contained  $1.0 \times 10^{-4}$  M U(VI) and 0.3 to 2.0 g/L organic matter. They were prepared under nitrogen to prevent disturbances by dissolved oxygen. The reduction was studied in the pH range from 2 to 8. Because the reaction is very slow, the equilibration time was about four weeks. After that, the samples were treated with 10 M HCl to precipitate the polyelectrolytes and dissolve the formed U(IV) hydroxide. The concentration of U(IV) was determined spectrophotometrically.

## Results

Tetravalent uranium formed at pH  $\geq 4.5$  (Fig. 1). The amount increases with the pH. A given amount LIG (0.4 g), for example, reduced  $7.5 \times 10^{-7}$  mol U(VI) at pH 4.5 and  $2.2 \times 10^{-6}$  mol at pH 7, meaning a three-fold increase in U(IV).

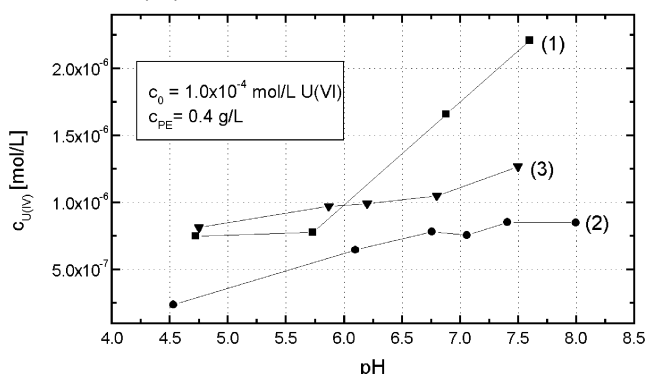


Fig. 1: pH-dependency of the U(VI) reduction by lignin (1), humic acid (2) and wood degradation products (3)

For WDP, we find  $8.1 \times 10^{-7}$  mol at pH 4.5 and  $1.1 \times 10^{-6}$  mol at pH 7, and for HUA  $3.5 \times 10^{-7}$  mol at pH 4.5 and  $7.5 \times 10^{-7}$  mol at pH 7, which is an increase by a factor of 2. From these dates, we calculated reducing capacities (Tab. 1) between  $7.6 \times 10^{-4}$  and  $4.4 \times 10^{-3}$  mmol/g.

	U(IV) [mmol/g] pH 4.5	U(IV) [mmol/g] pH 7.0
Lignin	$1.87 \pm 0.05 \times 10^{-3}$	$5.53 \pm 0.20 \times 10^{-3}$
Humic acid	$6.30 \pm 2.17 \times 10^{-4}$	$1.89 \pm 0.21 \times 10^{-3}$
WDP	$1.92 \pm 0.12 \times 10^{-3}$	$3.02 \pm 0.47 \times 10^{-3}$

Tab. 1: Reducing capacities of natural polyelectrolytes

We determined the following reducing capacities (mmol/g):

pH 7:

LIG ( $5.5 \times 10^{-3}$ )  $\gg$  WDP ( $3.0 \times 10^{-3}$ )  $>$  HUA ( $1.9 \times 10^{-3}$ )

pH 4.5:

LIG ( $1.9 \times 10^{-3}$ )  $>$  WDP ( $1.9 \times 10^{-3}$ )  $>$  HUA ( $0.63 \times 10^{-3}$ )

## Discussion

The interaction was studied in the pH range 2 to 8. Reduction starts at pH  $> 4.5$ . At lower pH no U(IV) was found. This corresponds with the Eh-pH dependency of the uranium system /2/ and that of the organic matter /3/.

Large amounts of wood remain in the uranium mines, that are currently being flooded as a measure of remediation. For example, the amount of wood at the flooded mine at Schlema, Saxony, produces several hundred thousand tons of lignin by wood degradation. If we assume a uranium(VI) reducing capacity of  $2 \times 10^{-3}$  mmol/g, as we have determined in our study, and a total amount of 100 tons of dissolved U(VI) in the mine, it is quite lively that the total U(VI) inventory could be reduced to U(IV) by the lignin and thus precipitate as  $U(OH)_4$  /4/. This process would possibly immobilize U(IV) and substantially limit the availability of uranium that can be transported to the environment.

## Acknowledgments

This study was supported by the Sächsisches Staatsministerium für Wissenschaft und Kunst under contract no. 4-7541.83-FZR/512.

We thank N. Zier and R. Schiene, Technische Universität Dresden, Institute of Plant and Wood Chemistry, Tharandt, for supplying the lignin and the hydrothermal wood leachates.

## References

- /1/ Markow, W.K.; IAEA-SM-133/97
- /2/ Brookins, D.G.; *Eh-pH Diagrams for Geochemistry*. Springer-Verlag Berlin 1988, p. 73
- /3/ Final Report Project 4-7541.83-FZR/512, 1998
- /4/ Ahonen et al.: *Radiochim. Acta* **66/67**, 115 (1994)

# COMPLEX FORMATION OF HEXAVALENT URANIUM WITH PROTOCATECHUIC ACID

L. Baraniak, G. Bernhard, H. Nitsche

The stability of the U(VI) complexes with 3,4-dihydroxybenzoic acid in carbonate-free solutions was determined from potentiometric pH titration curve fitting using the multi-equilibria code "SCOGS".

## Introduction

3,4-Dihydroxybenzoic acid occurs in nature as a monomeric intermediate of lignin degradation. It influences the radionuclide migration at uranium mining sites. The stabilities of the main complex species were determined by recalculation of potentiometric pH titration experiments /1/ with the non-linear curve fitting code "*Stability Constants of General Species*" (version 2) /2/ assuming that acidic species are formed and considering the  $UO_2^{2+}$  hydrolysis.

## Results

Complex formation starts above pH 3 with the occurrence of the acidic 1:1-complex (Fig. 1) according to

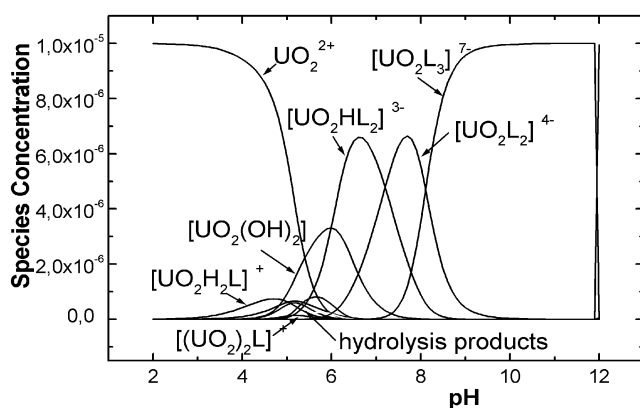
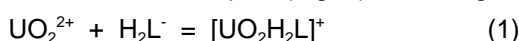


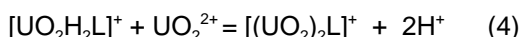
Fig. 1: Speciation of uranium(VI) in the presence of protocatechuic acid ( $10^{-5}$  M  $UO_2^{2+}$  and  $10^{-3}$  M organic complexant)

This equilibrium is characterized by  $\log K = 2.1$ ; the formation constant for the complex is  $\log \beta_{112} = 23.8 \pm 1.6$  (Tab. 1). This complex is followed by the formation of the acidic 1:2-species from the free  $UO_2^{2+}$  in the pH range 5-6 as well as from a second ligand addition onto the 1:1-complex at pH 5-5.5 according to:



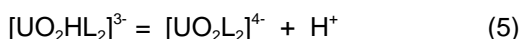
The constants for the two equilibria amount to -10.8 and to -12.9, respectively, and the complex stability is  $\log \beta_{121} = 32.6 \pm 1.8$ .

Between pH 5 and 7 a polynuclear species can occur in that the ligand bridges two  $UO_2^{2+}$  ions at high metal ion to the ligand concentration ratio:



with  $\log K = -5.5$  and  $\log \beta_{21} = 18.3 \pm 1.2$ .

If the pH increases further, the acidic 1:2-complex changes to the neutral complex:



that is dominating above pH 7; the equilibrium constant amounts to  $\log K = -7.2$  and the stability to  $\log \beta_{12} =$

$24.5 \pm 1.1$ .

Under alkaline condition, a 1:3-complex can be deduced from the experiments; the formation of that species can be described by



with  $\log K = -4.5$  and  $\log \beta_{13} = 34.0 \pm 1.6$ .

$[(UO_2)_2L]^+$	$[UO_2H_2L]^+$	$[UO_2HL_2]^3-$	$[UO_2L_2]^4-$	$[UO_2L_3]^7-$
$18.3 \pm 1.2$	$23.8 \pm 1.6$	$32.6 \pm 1.8$	$24.5 \pm 1.1$	$34.0 \pm 1.6$

Tab. 1: Formation constants of  $UO_2^{2+}$  complexes with protocatechuic acid computed by the "SCOGS" code (uranium hydrolysis was considered in the calculations)

Using these stabilities, the speciation (Fig. 1) was calculated for  $10^{-5}$  M  $UO_2^{2+}$  (-2.4 ppm U) and  $10^{-3}$  M protocatechuic acid by the "RAMESSES" code /3/.

Up to pH 5.5, the free  $UO_2^{2+}$  and the acidic 1:1-complex are dominating together with some  $UO_2^{2+}$  hydrolysis products, such as  $UO_2OH^+$ ,  $(UO_2)_2(OH)_2$ ,  $UO_2(OH)_2$ ,  $(UO_2)_3(OH)_4^{2+}$ ,  $(UO_2)_3(OH)_5^+$  and  $(UO_2)_4(OH)_7^+$ . Above pH 5.5 the main species are 1:2-complexes and the experimentally not confirmed 1:3-complex.

## Discussion

The dissociation of the 3,4-dihydroxybenzoic acid starts with the release of  $H^+$  from the carboxyl group ( $pK_1 = 4.26$ ), followed by the stepwise dissociation of the phenolic OH-groups ( $pK_2 = 8.64$  and  $pK_3 = 13.1$ ). The 1:1-complex with U(VI) has a bidentate carboxyl coordination in the equatorial plane of the linear  $UO_2$  arrangement. In the 1:2-complex, however, the  $UO_2^{2+}$  is coordinated by the phenolic groups of the ligand under formation of a five-membered chelate ring of high stability. The change of the carboxylic to the o-diphenolic coordination was experimentally confirmed by EXAFS measurements /4/. The coordination of the 1:1-complex is comparable to that of succinic acid, and the coordination of the 1:2-species corresponds to the complexation with 1,2-dihydroxybenzene (catechol).

The main complexes were determined by the curve fitting. Introducing the species  $[UO_2H_2L]^+$ ,  $[UO_2HL_2]^3-$  and  $[UO_2L_2]^4-$ , the fit showed the highest accuracy ( $F_{fit} \# 0.5\%$ ). The species  $[(UO_2)_2L]^+$  and  $[UO_2L_3]^7-$  are fit-indifferent and the introduction of the neutral 1:1-complex and further acidic complexes reduce the quality of the fit.

## Acknowledgments

This study was supported by the Sächsisches Staatsministerium für Wissenschaft und Kunst under contract no. 4-7541.83-FZR/402.

## References

- /1/ Baraniak, L. et al.: Report FZR-180 (1997) p. 28
- /2/ Sayce, I.G.: Talanta **15**, 1397 (1968)
- /3/ Leung et al.: Talanta **35**, 713 (1988)
- /4/ Roßberg, C. et al.: This report p. 53



## IRON(III) REDUCTION BY SYNTHETIC AND NATURAL HUMIC ACIDS

B. Mack, K.H. Heise, L. Baraniak, G. Bernhard, H.Nitsche

The reducing capacity of various synthetic and natural humic acids was studied with iron(III) at pH 3. It was found that the reducing capacity is not directly correlated with the number of phenolic groups.

Synthetic humic acids are used as model compounds for a better understanding of the chemical behavior of natural humic acids (HA) /1/. The ability of natural HA to reduce several metal ions is well known whereas the mechanism is not understood in detail. We studied the reducing behavior of various synthetic and natural HA against iron(III).

Two types of synthetic and natural HA were examined. The first, gallic acid based HA (GALOP), was synthesized by oxidation of gallic acid using sodium periodate at pH 8 /2/, the second, M 1 humic acid, via the Maillard reaction of xylose, glycine and phenylalanine /1/. The natural humic acids were a purified commercial HA (Aldrich) /3/ and an HA isolated from a bog in Saxony (Kranichsee) /4/.

### Experimental

The reducing capacity (RC) was determined at pH 3, an ionic strength of 0.1 M (KCl) and an initial iron(III) concentration of 5 mmol/L. The HA concentration varied from 0.10 g/L to 0.27 g/L for technical reasons. The solutions were prepared under nitrogen and gently shaken in the dark at room temperature over 6 weeks. The iron(III) reduction was monitored by spectrophotometric determination of iron(II) with 1,10-phenanthroline after separation of the humic acid by precipitation with sulfuric acid. The content of phenolic and carboxyl groups was radiometrically determined. The results are listed in Tab. 1.

Humic acid	Functionality [meq/g]	
	phenolic OH	COOH
GALOP	4.8	2.2
M 1	2.3	1.2
Kranichsee HA	3.9	3.9
Aldrich HA	3.4	3.9

Tab. 1: Functionalities of various humic acids

### Results and discussion

The RC of the humic acids ranges from 1.9 to 11.5 meq/g (Tab. 2).

Humic acid	Reducing capacity [meq/g]
GALOP	11.5
M 1	4.7
Kranichsee HA	3.2
Aldrich HA	1.9

Tab. 2: Reducing capacity of various humic acids

The following sequence of decreasing reducing capacity was found:

GALOP-HA >> M1-HA > Kranichsee-HA > Aldrich-HA.

The GALOP - HA shows the highest RC. This corresponds to the high content of phenolic OH in the matrix unit. These OH groups remained from the 3,4,5-trihydroxy benzoic acid after radicalic polymerization. Since the OH - groups are in o-position to each other on the aromatic ring, the major part of the reducing properties occurs in the oxidation to the o-quinonoid systems.

The natural HA's are characterized by an RC of 2 to 3 meq/g and a phenolic content of 3 to 4 meq/g, relating to a RC / OH ratio of 0.7. This value is low when compared to then GALOP - HA (~ 2.4). This can be explained by the prevailing single-positioned OH groups, i.e., by a small fraction of o-diphenolic groups. The aromatic content of natural HA's from the lignin degradation is generally much lower than of HA that are synthesized from a higher-valent phenol.

The Maillard type HA (M 1) with an RC / OH ratio of 2.0 resembles the GALOP - HA rather than natural HA. Since o-diphenolic groups are not incorporated into the matrix, other mechanisms have to be considered in order to the explain the reducing properties.

The time dependencies (Fig. 1) show a steady slight increase in the RC's. The values discussed here were calculated after a reaction time of 6 weeks.

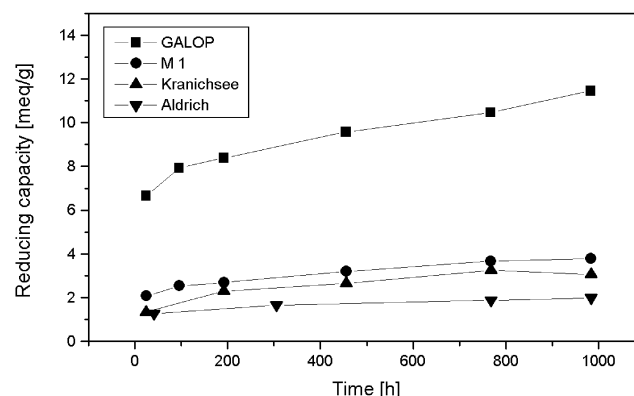


Fig. 1: Reduction of iron(III) by humic acids

### Acknowledgments

We thank Professor R. Klöcking of Jena University's Institute for Antiviral Chemotherapy for supplying the GALOP sample.

### References

- /1/ Pompe, S. et al.; Radiochim. Acta **74** (1996) 136
- /2/ Helbig, B. et al.; Geoderma **36** (1985) 255
- /3/ Kim, J.I. et al.; Report RCM 02188, Institut für Radiochemie, TU München (1988)
- /4/ Schmeide, K. et al.; Report FZKA 6124, Forschungszentrum Karlsruhe (1998)

## EXPERIMENTAL STUDIES FOR THE DISPOSAL OF CARBON-14-LABELED ORGANIC MATERIAL: IV. RESULTS OF THE PHOTOCATALYTIC MINERALIZATION

E. Förster, S. Heller, K.H. Heise, H. Nitsche

*The decomposition of carbon-14-labeled organic material with UV-illuminated titanium dioxide is monitored by on-line measuring of the  $\beta$ -radiation of the produced  $^{14}\text{CO}_2$ .*

### Introduction

Heterogeneous photocatalysis has been established as an effective method for the mineralization of organic compounds in aqueous media. We reported earlier the results of the mineralization of different non-labeled organic model compounds /1/.

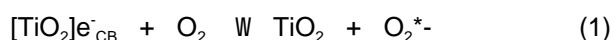
### Experimental

The photocatalytic oxidation of aqueous solutions or suspensions of two carbon-14-labeled organic compounds (4-hydroxy benzoic acid [ring UL- $^{14}\text{C}$ ] and acetic acid [2- $^{14}\text{C}$ ] sodium salt) was studied in a gas recycling reactor using suspended  $\text{TiO}_2$  (Degussa P 25) as photocatalyst in the presence of hydrogen peroxide. The samples were irradiated with a 420 W UV-high pressure lamp (Osram Ultratech 400) having a wavelength range from 315 to 380 nm (UV-A). The reactor consists of a cylindrical vessel with a cooling jacket. The lamp is placed in a quartz tube in the center of the vessel. About 370 kBq (10  $\mu\text{Ci}$ ) of the carbon-14-labeled substance is diluted with the same non-labeled organic substance to obtain an equivalent of 12 millimoles of carbon. The organic compound and a suspension of 0.5 g  $\text{TiO}_2$  in 250 mL water are transferred into the vessel. The reactor is equipped with a magnetic stirrer, a gas inlet tube, and a reflux condenser. The condenser is connected to a cupric oxide filled quartz tube (catalyst) followed by a gas flow cuvette, an air filtration unit (Midisart 2000, Sartorius), and two gas traps each containing 50.0 mL of 0.5 M sodium hydroxide. The cupric oxide catalyst is heated to about 650°C. To measure the radioactivity of  $^{14}\text{CO}_2$  on-line, the gas flow cuvette is connected to a commercial proportional counter tube (type LB 6280, Berthold) which is connected to the radiation counter 20046 (VEB Messelektronik) and a printer. Oxygen gas is essential for the photo mineralization process and it is also used to transfer the produced  $^{14}\text{CO}_2$  from the reactor to the gas traps.

The recovery of radioactivity is determined by LSC (liquid scintillation counter, Beckman model LS 6000 LL) of the solution containing the educt and the  $^{14}\text{CO}_2$ -containing sodium hydroxide solution from the gas traps. Ultima Gold (Packard Instr. Comp.) liquid scintillation cocktail was used.

### Results

The results are shown in Tab. 1 and Fig. 1. Excess electrons in the conduction band of the semiconductor  $\text{TiO}_2$  react with oxygen to form in a first step an oxygen radical:



substance	recovery of activity	
	[MBq]	%
4-Hydroxy benzoic acid [ring UL- $^{14}\text{C}$ ]	0.34	95.5
a. Sodium acetate [2- $^{14}\text{C}$ ]	0.64	110.1
b. Sodium acetate [2- $^{14}\text{C}$ ]	0.39	106.1

Tab. 1: Measured recovery of carbon-14 by photocatalytic mineralization of organic compounds

Hence oxygen is consumed during the mineralization process. A directly proportional correlation exists between the loss of oxygen and the oxidation number of the organic compound and the reaction course. The time progression of the mineralization is shown in Fig. 1. The conversion is completed after approximately 4 hours. No radioactivity was detectable in the remaining reaction mixture.

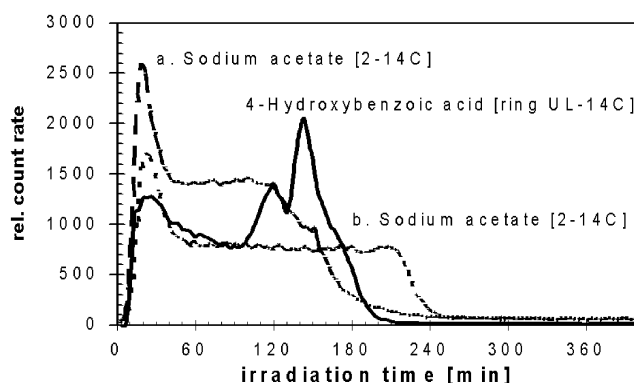


Fig. 1: Kinetics of photocatalytic mineralization of some carbon-14-labeled organic substances by the on-line measuring of the  $\beta$ -radiation of the produced  $^{14}\text{CO}_2$

### Acknowledgments

This study was supported by the Sächsisches Ministerium für Wissenschaft und Kunst under contract No. 4-7581.312/20

### References

/1/ Förster, E., Heise, K.H., Wolf, K., Nitsche, H.: Report FZR-123 (1996) p. 77

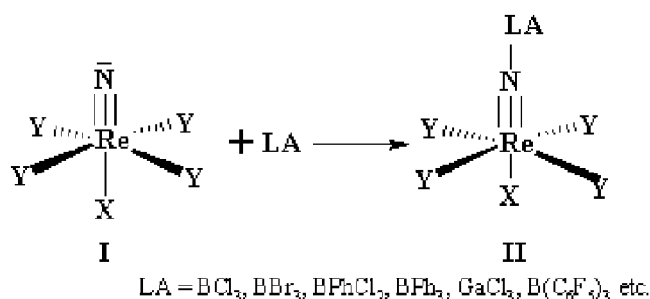
## THE STRUCTURAL *trans*-INFLUENCE - 6-COORDINATION vs. 5-COORDINATION

U. Abram

On the basis of a series of rhenium nitrido complexes mainly electronic in favor of steric factors have been found to be responsible for the strong structural *trans* influence of the multiply bonded "N<sup>3-</sup>" ligand.

Metal nitrides play an important role in the solid state chemistry where a number of novel compounds with extraordinary properties have been developed. Relatively less is known about the reactivity of covalent bonded nitrido ligands which belong to the strongest B-donor ligands and cause a strong structural *trans* influence which weakens the bond to the ligand coordinated *trans* to the multiply bonded "N<sup>3-</sup>". Generally, steric and / or electronic reasons are discussed to be responsible for this result /1,2/ and discussed separately for 5-coordinate and 6-coordinate metal complexes /3/.

The present communication summarizes the results of structural studies on about 20 couples of 5- and 6-coordinate rhenium complexes containing terminal nitrido ligands (I) and covalent nitrido bridges between Re and LEWIS acidic compounds (II) which can be prepared from complexes of type I with LEWIS acids (LA).



The terminal nitrido ligands in I cause a strong *trans* influence which results in a lengthening of the bond to the *trans* situated donor atom (X) by about 0.3-0.4 Å compared with the equatorial ligands. The addition of a LEWIS acid on the coordinated nitrido ligand results in an only slight increase of the Re-N triple bond length (1.1-5.3%). The distance to the *trans* coordinated ligand, however, decreases up to 17% and can not be correlated with the size of the LEWIS acid used (comparably small boron halides have been used as well as the bulky tris(pentafluorophenyl)boron). This suggests, that steric factors should be negligible and the structural *trans* influence should mainly be determined by the electronic situation in the corresponding molecules. The result is supported by N-Re-Y bond angles which are mainly determined by the individual bonding situation in the regarded complexes (monodentate ligands vs. chelate ligands). Even in cases, where the N-Re-Y angles increase, the Re-X bond decreases which clearly disfavors steric effects to cause the *trans* influence in the nitrido complexes under study.

In 5-coordinate nitrido complexes the formation of nitrido bridges which is coupled with a decrease of the *trans* influence results in an "activation" of the non-occupied sixth coordination position and allows the coupling of solvent molecules. When the reactions are performed in non-coordinating solvents, the formation

of binuclear, 6-coordinate compounds has been observed. This can exemplarily be demonstrated on bis(diethyldithiocarbamato)nitridorhenium(V), [ReN(Et<sub>2</sub>dtc)<sub>2</sub>], which forms a 6-coordinate, nitrido-bridged compound upon reaction with B(C<sub>6</sub>F<sub>5</sub>)<sub>3</sub>. This is achieved by dimerisation via a dithiocarbamato ligand.

Details of the bonding situation in the dimer can be obtained from Fig. 1 which represents the results of the crystal structural determination.

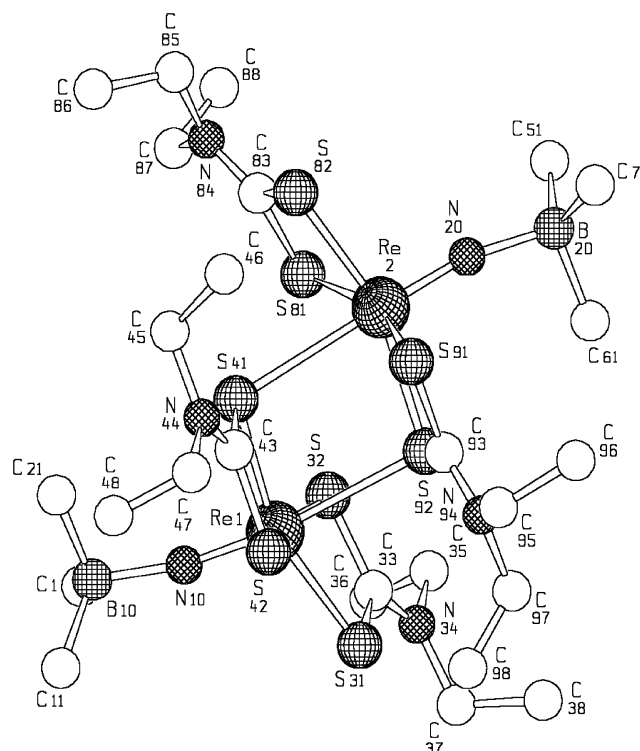


Fig. 1: Representation of the [Re(NB(C<sub>6</sub>F<sub>5</sub>)<sub>3</sub>)(Et<sub>2</sub>dtc)<sub>2</sub>]<sub>2</sub> dimer. C<sub>6</sub>F<sub>5</sub> rings have been omitted for clarity. Bond lengths in Å: Re(1)-N(10) 1.67, Re(1)-S(92) 2.86, Re(2)-N(20) 1.69, Re(2)-S(41) 2.84.

### Acknowledgments

This work is supported by the Deutsche Forschungsgemeinschaft.

### References

- /1/ Appleton, T.G. et al.; *Coord. Chem. Rev.* **10**, 335 (1973)
- /2/ Nugent, W.A. et al.; *Metal Ligand Multiple Bonds*. Wiley, New York, 1988
- /3/ Lyne, P.D. et al.; *J. Chem. Soc. Dalton Trans.* 1635 (1995)

# SYNTHESIS, CHARACTERIZATION AND STRUCTURE OF AMMINETRIS(DIMETHYLPHENYLPHOSPHINE)DIODORHENIUM(III) TRIIODID

B. Schmidt-Brücken, U. Abram

The reaction of  $[\text{ReNCl}_2(\text{Me}_2\text{PhP})_3]$  with an excess of trimethylsilyl iodide results in protonation of the nitrido ligand and the formation of  $[\text{Re}(\text{NH}_3)_2(\text{Me}_2\text{PhP})_3]\text{I}_3$ .

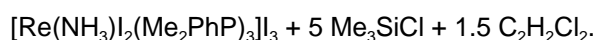
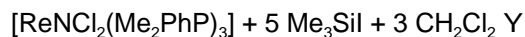
Generally it is not easy to protonate coordinated nitrido ligands. Only a few examples have been reported /1/.

The formation of coordinated  $\text{NH}_3$  has been observed during the reaction of  $[\text{ReNCl}_2(\text{Me}_2\text{PhP})_3]$  with  $\text{Me}_3\text{SiI}$ .

$[\text{ReNCl}_2(\text{Me}_2\text{PhP})_3]$  was dissolved in dry dichloromethane and a twentyfold excess of trimethylsilyl iodide was added. After refluxing for one hour under an atmosphere of dry nitrogen and cooling, the mixture was evaporated to dryness. The residue was dissolved in dichloromethane and put in the refrigerator over night to obtain redbrown crystals (yield >60%).

The IR spectrum shows  $\nu(\text{NH})$  vibrations. The elemental analyses confirms the presence of nitrogen (calc.: 1.1%, found: 1.1%). The mass spectrum (FAB<sup>+</sup>) shows many fragments of the cation  $[\text{Re}(\text{NH}_3)_2(\text{Me}_2\text{PhP})_3]^+$ , including the  $\text{M}^+$ -peak ( $m/z = 871$ ). The compound is expected to be paramagnetic. Its magnetic moment was determined to  $\mu_{\text{eff}} = 2.74$  B.M. This result agrees with the value calculated for two unpaired electrons ( $\mu_{\text{spinonly}} = 2.83$  B.M.). The difference between the theoretical and the experimental value can be explained by a considerable spin-orbit-coupling, which is usually observed for heavy elements.

being prepared from a nitrido complex. This is only possible, when the solvent takes part in the reaction and acts as source for the protons:



Further studies to elucidate the mechanism of the reaction and to analyze the side products are in progress.

## Acknowledgments

The work was supported by the Deutsche Forschungsgemeinschaft.

## References

/1/ Dilworth, J.R. et al.; Inorg. Chim. Acta **71**, 21 (1983)

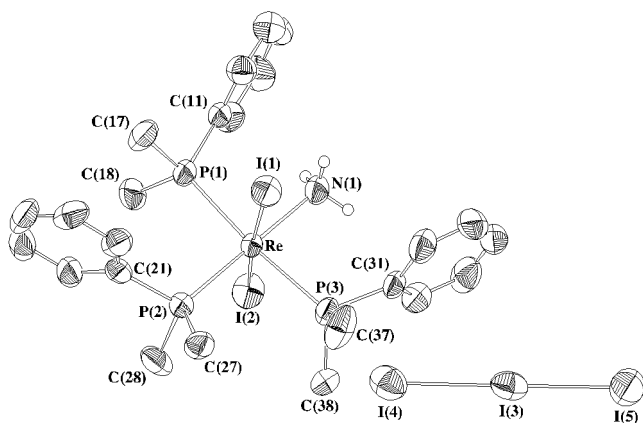


Fig. 1: Ellipsoid plot of  $[\text{Re}(\text{NH}_3)_2(\text{Me}_2\text{PhP})_3]^+$ . H atoms of the phosphines have been omitted for clarity. Selected bond lengths [pm]: Re-N 223.6, Re-P(1) 248.4, Re-P(2) 242.6, Re-P(3) 247.6, Re-I(1) 264.1, Re-I(2) 266.5, I(3)-I(4) 294.0, I(3)-I(5) 288.4.

The X-ray structure determination (Fig.1) finally confirms triiodide as counter ion. All bond lengths and angles are located in the expected range. The Re-N distance (223.6 pm) agrees with the value expected for a Re-N single bond and the significant *trans* influence caused by a nitrido ligand is no longer observed. This is shown by the Re-P(2) distance of 242.6 pm, which is shorter than the Re-P bonds in the equatorial positions.

The title compound is the first rhenium amine complex

# SYNTHESIS, CHARACTERIZATION AND STRUCTURE OF DICHLOROBIS(TRIPHENYLPHOSPHINE)PYRIDINE-2-THIOLATORHENIUM(III) AND DICHLOROBIS(TRIPHENYLPHOSPHINE)PYRIMIDINE-2-THIOLATORHENIUM(III)

B. Schmidt-Brücken, U. Abram

Two different routes are shown leading to novel rhenium(III) complexes with the heterocyclic ligands. The structure of the pyridine-2-thiolato complex is discussed.

Pyridine-2-thiol and pyrimidine-2-thiol are known as very flexible ligands forming countless complexes with transition metals.

$[\text{ReCl}_2(\text{PPh}_3)_2(\text{pyrS-S,N})]$  (pyrS-S,N = pyridine-2-thiolate) and  $[\text{ReCl}_2(\text{PPh}_3)_2(\text{pyrmS-S,N})]$  (pyrmS-S,N = pyrimidine-2-thiolate) have been prepared by the reaction of  $[\text{ReOCl}_3(\text{PPh}_3)_2]$  with two equivalents of the thiol in dichloromethane or acetone. The reduction of the oxo compound is caused by the well known reaction of a displaced triphenylphosphine with the coordinated oxo ligand, resulting in the formation of the phosphine oxide and a  $\text{Re}^{\text{III}}$  center. Due to the mechanism the maximum yield is 50%.

A second route is the ligand exchange reaction with the  $\text{Re}^{\text{III}}$  precursor  $[\text{ReCl}_3(\text{CH}_3\text{CN})(\text{PPh}_3)_2]$  and the thiols in a 1:1 molar ratio in acetonitrile, where better yields have been obtained (Fig. 1).

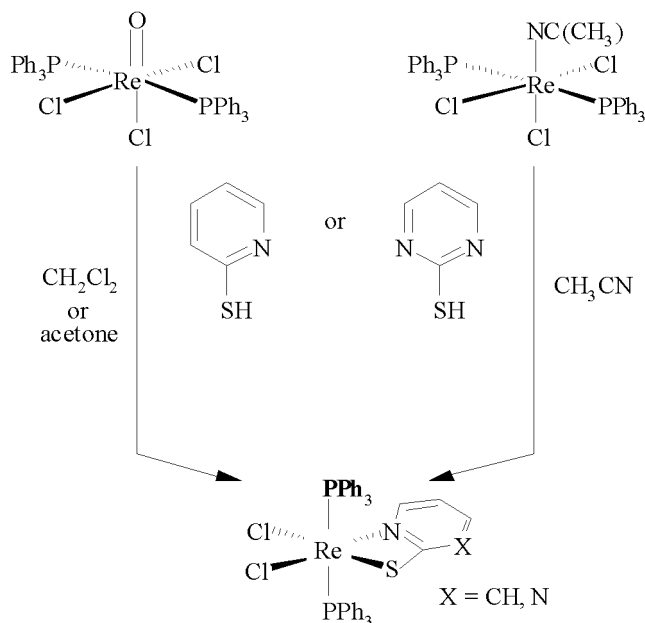


Fig. 1: Reaction scheme

IR spectra and elemental analyses confirm the formation of the products.

$[\text{ReCl}_2(\text{PPh}_3)_2(\text{pyrmS-S,N})]$  is finally identified by the  $\text{M}^+$ -peak in the mass spectrum ( $\text{FAB}^+$ ), which shows an identical isotopic pattern with the calculated  $\text{M}^+$ -peak.

The X-ray structure determination of  $[\text{ReCl}_2(\text{PPh}_3)_2(\text{pyrS-S,N})]$  (Fig. 2) shows the coordinated phosphines in *trans* position to each other. Re, the two chlorine atoms and the thiolate ligand form a mirror plane. The thiolate ligand shows a very small chelate angle  $\text{S}(1)\text{-Re-N}(3)$  ( $67.1^\circ$ ) due to the structural restrictions of the pyridine-2-thiolate.

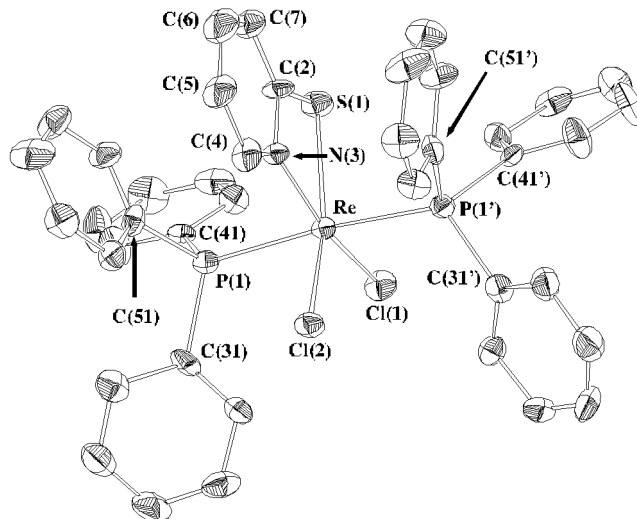


Fig. 2: Ellipsoid plot of  $[\text{ReCl}_2(\text{PPh}_3)_2(\text{pyrS-S,N})]$ . H atoms have been omitted for clarity. Selected bond lengths [pm]:  $\text{Re-S}(1)$  244.7,  $\text{Re-N}(3)$  209.5,  $\text{Re-Cl}(1)$  238.1,  $\text{Re-Cl}(2)$  236.7,  $\text{Re-P}(1)$  245.0,  $\text{Re-P}(1')$  245.0.

## Acknowledgments

The work was supported by the Deutsche Forschungsgemeinschaft.

**[Re(NGaCl<sub>3</sub>)Cl(Me<sub>2</sub>PhP)<sub>2</sub>(H<sub>2</sub>Et<sub>2</sub>tcb)][GaCl<sub>4</sub>]**  
**(H<sub>2</sub>Et<sub>2</sub>tcb = N,N-DIETHYLTHIOCARBAMOYL BENZAMIDINE)**  
**- A COMPLEX WITH A COVALENT Re-N-Ga BRIDGE -**

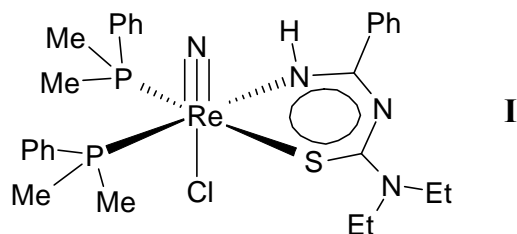
U. Abram, S. Ritter<sup>1</sup>

<sup>1</sup>University of Tübingen, Institute of Inorganic Chemistry

The reaction of [ReN(Cl)(Me<sub>2</sub>PhP)<sub>2</sub>(HEt<sub>2</sub>tcb)] (HEt<sub>2</sub>tcb = N,N-diethylthiocarbamoylbenzamidate, Me<sub>2</sub>PhP = dimethylphenylphosphine) with GaCl<sub>3</sub> yields a nitrogen-bridged binuclear complex with a covalent bond between the nitrido ligand and gallium. This goes along with protonation of the coordinated chelate ligand.

Nitrido ligands belong to the strongest B-donor ligands and stabilize transition metals in high formal oxidation states. "N<sup>3-</sup>" can coordinate terminally or bridging between transition metals and Lewis-acidic compounds /1/.

A covalent Re-N-Ga bridge is formed upon reaction of the Re(V) mixed-ligand complex chloro(N,N-diethylthiocarbamoylbenzamidato)-bis(dimethylphenylphosphine)nitridorhenium(V), [ReN(Cl)(Me<sub>2</sub>PhP)<sub>2</sub>(HEt<sub>2</sub>tcb)] I, with GaCl<sub>3</sub>.



When this reaction is performed in dry dichloromethane, red crystals of [Re(NGaCl<sub>3</sub>)Cl(Me<sub>2</sub>PhP)<sub>2</sub>(H<sub>2</sub>Et<sub>2</sub>tcb)][GaCl<sub>4</sub>] are obtained in good yields.

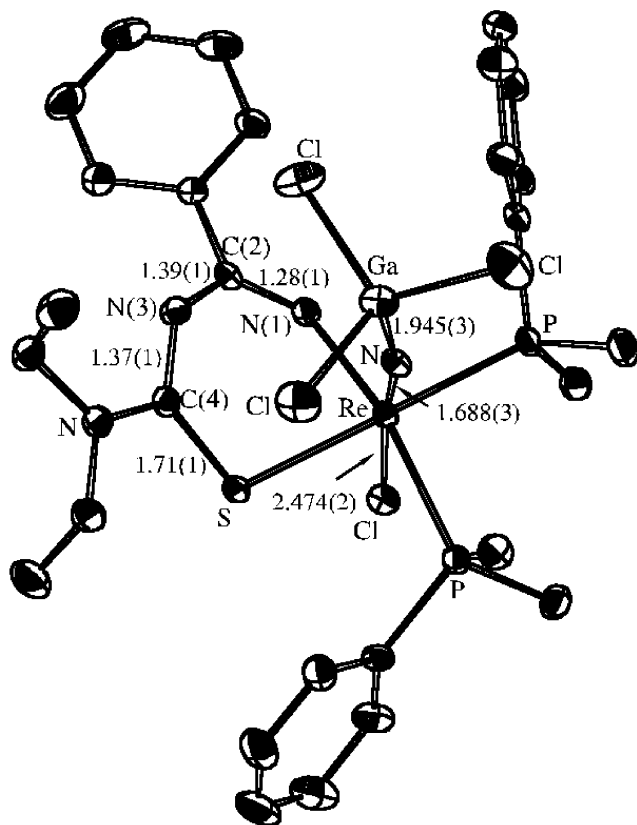


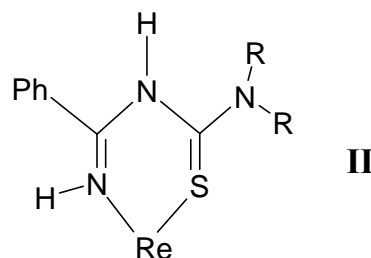
Fig. 1: Ellipsoid representation of the complex cation of [Re(NGaCl<sub>3</sub>)Cl(Me<sub>2</sub>PhP)<sub>2</sub>(H<sub>2</sub>Et<sub>2</sub>tcb)][GaCl<sub>4</sub>]. Bond lengths in Å.

The use of other solvents decreases the yield dramatically or yields other products.

This result and the high yield of the reaction suggests CH<sub>2</sub>Cl<sub>2</sub> as source of the H and Cl atoms which are used to protonate the coordinated chelate ligand and to form the GaCl<sub>4</sub><sup>-</sup> anion. The exact mechanism of the obviously complex reaction has not yet been elucidated. During attempts with CD<sub>2</sub>Cl<sub>2</sub> the expected product [Re(NGaCl<sub>3</sub>)Cl(Me<sub>2</sub>PhP)<sub>2</sub>(HDEt<sub>2</sub>tcb)][GaCl<sub>4</sub>] could only be isolated in very low yields (about 5 per cent).

The most remarkable structural feature is the bonding situation inside the chelate ring. This is due to the protonation of N(3) which results in a non-planar chelate ring. [Re(NGaCl<sub>3</sub>)Cl-(Me<sub>2</sub>PhP)<sub>2</sub>(H<sub>2</sub>Et<sub>2</sub>tcb)][GaCl<sub>4</sub>] is the first example of a metal complex containing a neutral, chelate-bonded N,N-dialkylthiocarbamoylbenzamidate ligand. The extended B-electron system which can be found in I /2/ is disturbed and the N(1)-C(2) and C(4)-S bonds are shortened.

This is in accordance with a formulation as given in II.



Comparison with the situation in [ReN(Cl)(Me<sub>2</sub>PhP)<sub>2</sub>(HEt<sub>2</sub>tcb)] /2/ shows that the equidistance of the C-N bonds and the planarity of the chelate ring disappeared upon protonation. The sum of the bond angles inside the six-membered ring in [Re(NGaCl<sub>3</sub>)Cl(Me<sub>2</sub>PhP)<sub>2</sub>(H<sub>2</sub>Et<sub>2</sub>tcb)]<sup>+</sup> is 690.8° which is lower by about 20° than in the chelate ring of I.

#### Acknowledgments

We acknowledge support from the Deutsche Forschungsgemeinschaft and the Fonds der Chemischen Industrie.

#### References

- /1/ Ritter, S. et al.; Z. Anorg. Allg. Chem. **620**, 1786 (1994)  
 /2/ Abram, U. et al.; Inorg. Chim. Acta **210**, 99 (1993)

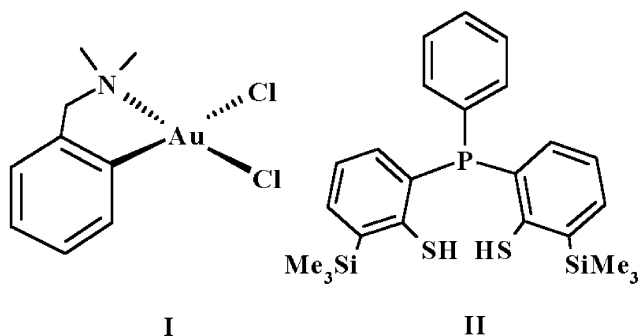
## STABILIZATION OF Au<sup>I</sup> AND Au<sup>III</sup> IN THE SAME COMPLEX MOLECULE

U. Abram, K. Ortner<sup>1</sup>, L. Hilditch<sup>2</sup>, J.R. Dilworth<sup>2</sup>

<sup>1</sup>University of Tübingen, Institute of Inorganic Chemistry; <sup>2</sup>University of Oxford, Inorganic Chemistry Laboratories

The reaction of the organometallic complex [Au<sup>III</sup>(damp-C<sup>1</sup>,N)Cl<sub>2</sub>] (damp = dimethylaminomethylphenyl) with PhP(C<sub>6</sub>H<sub>3</sub>SH-2-SiMe<sub>3</sub>-3)<sub>2</sub>, H<sub>2</sub>L, results in the formation of [Au<sup>III</sup>LCl] and the first binuclear complex where Au<sup>I</sup> and Au<sup>III</sup> is stabilized by the same ligand, [Au<sup>III</sup>L<sub>2</sub>Au<sup>I</sup>].

Relativistic effects which play an important role in the chemistry of the heavy actinide elements have also been observed in the gold chemistry. This encouraged us to study some gold complexes with ligand systems which are scheduled for future actinide studies.



During the reaction of [Au(damp-C<sup>1</sup>,N)Cl<sub>2</sub>] I with the potentially tridentate phosphinothiolate ligand PhP(C<sub>6</sub>H<sub>3</sub>-SH-2-SiMe<sub>3</sub>-3)<sub>2</sub>, H<sub>2</sub>L II, two different products have been isolated, the Au<sup>III</sup> complex [AuLCl] which possesses a strongly distorted square structure (95% yield) and [Au<sup>III</sup>L<sub>2</sub>Au<sup>I</sup>] (Fig. 1) which contains gold atoms in the formal oxidation states "+3" and "+1" (5% yield).

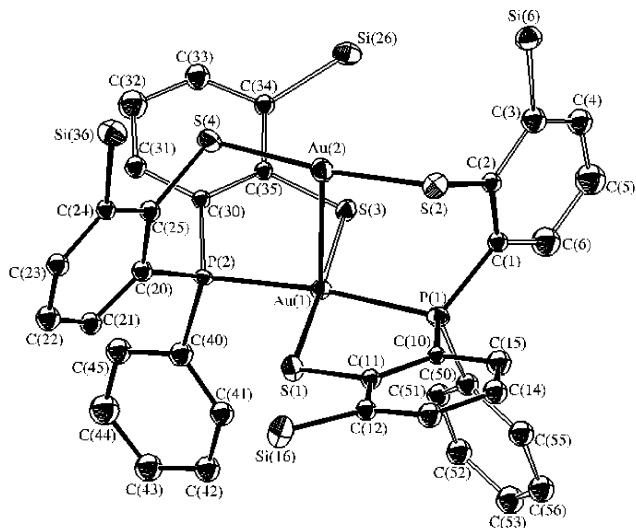
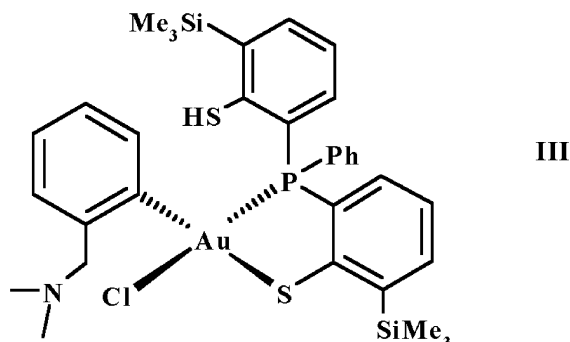


Fig. 1: Ellipsoid representation of [Au<sup>I</sup>L<sub>2</sub>Au<sup>III</sup>] (methyl groups of Me<sub>3</sub>Si have been omitted for clarity). Selected bond lengths (Å) and angles (°): Au(1)-P(1) 2.317(5), Au(1)-P(2) 2.312(5), Au(1)-S(1) 2.331(4), Au(1)-S(3) 2.343(4), Au(2)-S(2) 2.276(5), Au(2)-S(4) 2.275(5), Au(1)-Au(2) 2.919(1), P(1)-Au(1)-P(2) 172.1(2), S(1)-Au(1)-S(3) 178.4(2), S(2)-Au(2)-S(4) 173.1(2).

The linear Au<sup>I</sup> coordination is accomplished by two thiolate groups. The Au(2)-S bond lengths are slightly shorter than those for Au(1)-S, but are in the same range as found in the gold(I) thiolate complexes [(2,4,6-Pr<sup>i</sup><sub>3</sub>C<sub>6</sub>H<sub>2</sub>S)Au]<sub>6</sub> and [NH<sub>4</sub>]-[(2,4,6-Pr<sup>i</sup><sub>3</sub>C<sub>6</sub>H<sub>2</sub>S)<sub>2</sub>Au]

/1/. The Au<sup>III</sup> coordination environment is square-planar with a maximum deviation from a least-square plane formed by P(1), S(1), P(2) and S(3) of 0.074(2) Å. The gold atom is displaced from this plane by 0.081(2) Å towards Au(2). The Au-Au distance is 2.919(1) Å. This contact is comparable with values found in other bi- and multinuclear gold compounds /2/ and is consistent with an aurophilic bonding interaction. The S(2)-Au(2)-S(4) system is in an eclipsed arrangement relative to the P(1)-Au(1)-P(2) unit of the square-planar coordination sphere of Au(1). The atoms P(1), S(2), Au(1), Au(2), P(2) and S(4) fit a plane with a rms. deviation of 0.06 Å resulting in a paddle-wheel like arrangement of the phenyl rings C(1)-C(6) and C(20)-C(25) with the Au(1)-Au(2) vector as hub.

The low yield of the binuclear compound could not be increased by changing the reaction conditions and stoichiometric corresponds. Its formation as opposed to [AuLCl] must depend on the fate of the assumed intermediate III which is formed by the displacement of the



NMe<sub>2</sub> group by P and chloride by thiolate S. The formation of [AuLCl] by replacement of the *cis* phenyl ligand by thiolate is then clearly the preferred reaction. However, there appears to be a small competing reaction involving the reaction of III with a second ligand molecule to give a species with two pendant thiolate groups which then coordinate Au<sup>I</sup> to give the dimeric compound [Au<sup>III</sup>L<sub>2</sub>Au<sup>I</sup>].

### References

- /1/ Schröter, I. et al.; Chem. Ber. **124**, 2161 (1991)
- /2/ Housecroft, C.E.; Coord. Chem. Rev. **164**, 161 (1997)

# **Interaction of Microorganism with Radionuclides**



## BACTERIAL DIVERSITY IN TWO URANIUM MINE WASTE PILES IN SAXONY

S. Selenska-Pobell, K. Flemming

*Rep-APD analysis was used to study bacterial diversity in soil samples from two different uranium waste piles in Saxony. Results obtained by this method are in agreement with our previously published observations that in both waste piles a large number of highly diverse bacteria occurs. There are indications that both wastes may also share common bacterial species.*

Recently, the presence of a large number of diverse bacteria was demonstrated in soil and water samples of two uranium mining waste piles near the region Gittersee (Gitt) and the town Johanngeorgenstadt (JG) in Saxony by the use of ribosomal intergenic spacer amplification (RISA) analysis /1/.

In the present work another molecular method was applied for more precise investigation of bacterial diversity in the same samples. The method named repetitive primer amplified polymorphic DNA (rep-APD) is based on PCR amplification by the use of primers corresponding to the repetitive consensus sequences in bacterial genomes /2, 3/. This method is much more informative than RISA due to the fact that it derives information from the whole bacterial genome and not only from a particular part of it as it is the case of RISA /3/. Two examples of this analysis using an ERIC- and a BOX-primer are shown in Fig. 1 and Fig. 2.

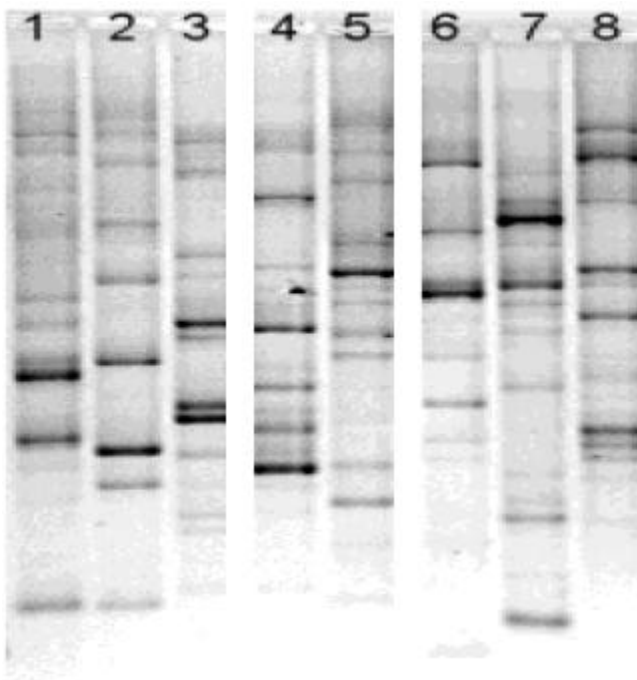


Fig. 1: ERIC-rep-APD in total soil DNA recovered from Gittersee/Coschütz (Gitt.) and from "Haberland-Halde" Johanngeorgenstadt (JG). 1: Gitt.2, 2: Gitt.6, 3: Gitt.7, 4: JG-C 1-2, 5: JG-B 3-4, 6: JG-B 2-3, 7: JG-B 0-1, 8: JG-A 4-5

As seen in Fig. 1 the ERIC-rep-APD patterns for the soil samples studied are sample specific. Sample specific are also the BOX-generated fingerprints, however, for the samples drawn from the same site and depth they share significant similarity (compare Gitt. 2, Gitt. 6, Gitt. 7 in Fig. 2). Less similarity was found between the samples drawn from different depths (one to four meters under the surface) of the same site (compare JG-B 0-1, JG-B 2-3, and JG-B 3-4). Interestingly, common

bands, demonstrating presence of common bacterial genomic structures, were found in the BOX-patterns of many DNA samples (see the black arrows in Fig. 2).

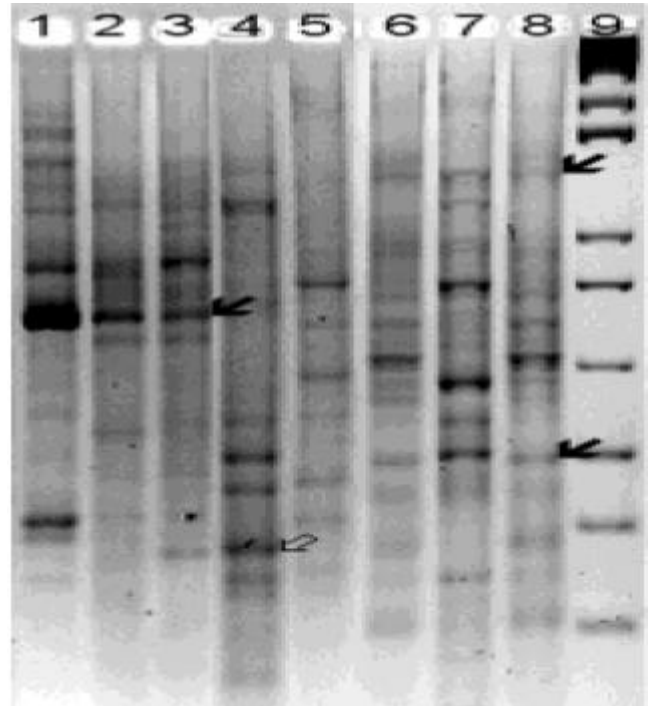


Fig. 2: Box-rep-APD in total soil DNA recovered from Gittersee/Coschütz (Gitt.) and from "Haberland-Halde" Johanngeorgenstadt (JG). 1: Gitt.6, 2: Gitt.7, 3: Gitt.2, 4: JG-C 1-2, 5: JG-B 3-4, 6: JG-B 2-3, 7: JG-B 0-1, 8: JG-A 4-5, 9: 1kb plus ladder (Gibco BRL)

Moreover, in some cases similarity between the BOX-patterns of the samples from the two geographically different waste piles investigated was observed (see the white arrow in Fig. 2). This result is in agreement with those obtained recently in our laboratory by the use of the 16S rDNA retrieval /4/. The latter has demonstrated that, on the background of the high bacterial diversity in the soil samples from the two uranium waste piles studied, several dominant bacterial types might be distinguished.

### Acknowledgments

This work was supported by grant 7531.50-03-FZR/607 from the Sächsisches Staatsministerium für Wissenschaft und Kunst, Dresden, Germany.

### References

- /1/ Kampf, G., Selenska-Pobell, S.; Report FZR-218 (1998) p.59-60
- /2/ Versalovich, J., et al.; Methods Mol. Cell Biol. **5**, 25-40 (1994)
- /3/ Selenska-Pobell, S., et al.; J. Appl. Bacteriol. **80**, 517-528 (1996)
- /4/ Satschanska G., Selenska-Pobell S.; this report p. 40

## DIVERSITY IN NATURAL BACTERIAL COMMUNITIES IN URANIUM WASTES AS EXAMINED BY 16S rDNA RETRIEVAL

G. Satschanska, S. Selenska-Pobell

<sup>1</sup> Institute of Molecular Biology, Bulgarian Academy of Sciences, 1113 Sofia, Bulgaria

A 16S rDNA clone bank was constructed for three different uranium waste piles in Saxony. An analysis of several hundred clones of this bank has indicated an extremely high bacterial diversity in the soil and water samples studied. The presence of 16S rRNA genes representing several dominant bacterial groups was demonstrated in the soil samples of the wastes.

A very important approach to study bacteria in soil and water environments is to extract and directly analyze their DNA, because at present only a few percent of the bacteria living in nature can be handled in laboratory conditions. Using ribosomal intergenic spacer amplification - RISA /1/ and repetitive primer amplified polymorphic DNA - rep-APD /2/ methods, we have demonstrated a high bacterial diversity in a large number of soil and water samples of three different uranium waste piles in Saxony.

Two of the waste piles - Gittersee/Coschütz (Gitt) and Schlema (Schl) are "uranium mill-tailings" from the former uranium production. The third pile near the town Johanngeorgenstadt (JG) stems from uranium mining but no production of uranium was performed there. All of them are highly polluted with uranium and other heavy metals and radionuclides.

In order to investigate which are the main bacterial groups present in these environments, several of the above-mentioned samples were analyzed using 16S rDNA amplification, cloning, RFLP typing, and sequence analysis /3, 4/.

Several hundred clones were obtained possessing bacterial specific 16S rDNA fragments amplified by the use of two alternative primer pairs (see Tab. 1). They represent the bacterial composition of several soil and water samples drawn from different sites and depths of the wastes.

Geographic origin	Number of clones	Primer pair	RFLP analyzed
JG-B 0-1m	70	7f- 1492r	70
JG-B 0-1m	74	63f-1387r	74
JG-B 2-3m	28	7f -1492r	28
JG-B 2-3m	26	63f-1387r	26
Gitt -0-1m	155	7f -1492r	60
Schl/water	120	7f -1492r	12

Tab. 1: 16S rDNA clone library

About 250 of these clones were grouped in RFLP types by the use of the frequently cutting restriction endonucleases *HaeIII*, *MspI* and *RsaI* (see Tab. 1, last column). Many unique 16S RFLP patterns were obtained. However, there were several dominant RFLP types shared by the soil samples drawn from the piles Gittersee/Coschütz and Johanngeorgenstadt (see Tab. 2). These RFLP types were studied in particular.

Geographic origin	RFLP-types	Common types
JG-B 0-1m	30 7f- 1492r	2
JG- B 2-3m	24 7f- 1492r	3
Gitt 0-1m	29 7f- 1492r	2
Schl/water	3 7f- 1492r	not yet found

Tab. 2: RFLP-typing of the 16S rDNA fragments

The most dominant 16S rDNA group was affiliated to the species *Thiobacillus ferrooxidans* (99,6% identity).

Two other groups were affiliated to the *Pseudomonas* group, one as *P. veronii* - 99% identity, and another one as *P. anguilliseptica* - 99% identity.

This is the first report of a direct 16S rDNA retrieval that resulted in an exact determination of several dominating bacterial groups that are common to several uranium waste piles. We suggest that these groups play a significant role in the biotransformation and migration of uranium and other radionuclides in the studied ecosystems. They should be further studied and considered for the development of bioremediation procedures of these polluted environments.

### Acknowledgments

This work was supported by grant 7531.50-03-FZR/607 from the Sächsisches Staatsministerium für Wissenschaft und Kunst, Dresden, Germany.

### References

- /1/ Kampf, G., Selenska-Pobell, S.; Report FZR-218 (1998) p.59-60
- /2/ Selenska-Pobell, S., Flemming, K.; this report p. 39
- /3/ Satschanska G. et al.; Euroconf. Bacterial-Metal/Radionuclide Interactions (BMRI-1); Dresden, Germany (1998)
- /4/ Selenska-Pobell S.; Int. Symp. Microb. Ecolol. '98 (ISME '98); Halifax, Canada (1998)

# INVESTIGATION OF BACTERIAL DIVERSITY IN A SOIL SAMPLE OF A DEPLETED SAXONIAN URANIUM MINING AREA VIA SEQUENCING OF PCR-AMPLIFIED AND TA-CLONED 16S rRNA GENES

C. Puers, S. Selenska-Pobell, H. Nitsche

*The bacterial diversity of a soil sample from site at, 4-5 m depth of the uranium mining area near Johanngeorgenstadt, Saxony, was investigated by sequencing of 100 TA-cloned 16S-rDNA-PCR-amplicons. Affiliations to reference bacterial sequences were determined by BLAST-GenBank and by Sequence Match-RDP-II-database comparisons and phylogenetic analyses.*

## Introduction

One of our approaches to gain more information about bacterial radionuclide/heavy metal interactions and to assess associated environmental problems is to identify bacterial community members that are well adapted to radionuclide/heavy-metal-containing environments. For this purpose, we investigated the bacterial diversity of a soil sample isolated in a pseudo-sterile manner from four-to-five meters depth at the so-called "Site A" of a former Saxonian uranium mining area near Johanngeorgenstadt, Saxony, Germany ("Haberland uranium mining waste pile"). On the surface above "Site A" exists relative acidic (pH 4.5) water which contains an elevated uranium concentration (58 mg/L). We applied the 16S-rDNA PCR amplicon clone library sequencing method [1] for our study. The pCRII-TOPO-vector was used for cloning and 100 randomly selected soil bacteria 16S-969-1406-rDNA clone sequences were compared against GenBank and RDP-II (Ribosomal Database Project II) data base reference sequences using 'Blast 2.0' and 'RDP-II Sequence Match 2.7', respectively. Through RDP-II-'Chimera\_Check' detection nine apparently chimeric sequences, which are PCR amplification artifacts, were excluded from further analyses. For phylogenetic comparisons sequences of 29 representatives (or equivalents of these) of the bacterial domain were chosen from the RDP-II-list with the title "Small Subunit rRNA: Representative Prokaryotic Listing (July 31, 1998)". Twenty seven additional reference sequences were chosen based on the results gained via comparisons against the sequence data bases (data not shown). Hypervariable regions were excluded from multiple sequence alignments essential for phylogenetic tree analysis [2].

## Results

The bacterial affiliations obtained by comparison of clone insert sequences with sequence data bases were mainly identical to the phylogenetic analysis results (not shown). Table 1 shows the distribution of the soil rDNA clones in the Bacteria domain for the investigated soil sample 'A,4-5m' 16S-rDNA-library. Three major taxa are highly represented: Purple bacteria (24 %); Green-non-sulfur bacteria (41 %) and bacteria of the Fibrobacter, Acidobacterium subdivision (19 %). Only 5.5% of the clones belong to the Gram-positive phylum. Eight percent of the clones cluster with the DA052-clone [3]. Felske et al. [3] found that the 16S-rDNA-sequence of the DA052 clone is not closely related to any other known bacterial sequence. Only one clone each was found for the Fusobacterium and relatives division and for the Paraphyletic assemblage, Leptospirillum/ Nitrospira subdivision. The major-

ity of the Purple bacteria belongs to the (-Subdivision (15.4 %), while 4.4 % each of the clones are associated with the  $\alpha$ - and  $\beta$ -subdivision. Within the Gram-positive phylum clones, three of the five clones (3.3 %) are High-G+C-subdivision members. The phylogenetic affiliation of nine clones remains uncertain (Tab. 1).

Division, Subdivision	Number of clones	(%)
Purple bacteria	22	24.18
$\alpha$ -Subdivision	4	4.4
$\beta$ -Subdivision	4	4.4
$\gamma$ -Subdivision	14	15.38
$\delta$ -Subdivision	0	0
$\epsilon$ -Subdivision	0	0
Green non-sulfur bacteria, Chloroflexus Subdivision	37	40.66
Fibrobacter, Acidobacterium Subdivision	9+8* = 17	9.9+8.8* = 18.7
DA052 cluster	8	8.8
Fusobacteria and relatives	1*	1.1*
Paraphyletic Assemblage, Leptospirillum/Nitrospira-Subd.	1	1.1
Gram-positive Phylum	5	5.5
Sporomusa and relatives	1	1.1
High-G+C-Subdivision	3	3.3
Thermoanaerobacter and relatives	1	1.1
Total	91	100

Tab. 1: Distribution of bacteria identified in the rDNA library made from the soil sample "A, 4-5m" DNA. The DA052 clone [3] could not be affiliated to any known taxon yet. It branches of the Fibrobacter phylum, Acidobacterium subdivision. (\*: uncertain affiliation).

## Acknowledgments

This work was partly supported by grant 7531-50-03-FZR/607 of the Sächsisches Staatsministerium für Wissenschaft und Kunst. We thank Sabine Kutschke, Forschungszentrum Rossendorf, Germany for helping to isolate the soil sample, Dr. Gudrun Kampf for bacterial DNA isolation and Dr. Waltraut Wiesner, Forschungszentrum Rossendorf for performing the ICP-MS measurements.

## References

- [1] Lane D.J., et al.: Proc. Natl. Acad. Sci. USA 82: 6955-6959 (1985)
- [2] Byers H., et al.: FEMS Microbiol. Ecol. 25, 391-403 (1998)
- [3] Felske A., et al.: Appl. Envir. Microbiol. 64, 871-879 (1998)

## COMPARISON OF ENVIRONMENTAL *DESULFOVIBRIO* ISOLATES USING RAPD AND rep-APD ANALYSES

J. Wober, S. Selenska-Pobell

The genomic relationship between five *Desulfovibrio* isolates was studied using RAPD and rep-APD analyses. All isolates are able to grow on medium with pH 4, and they form a group with high genomic similarity. The strains of this group have genomic fingerprints which differ significantly from those of the phylogenetically related strain *D. vulgaris (oxamicus)* 1925<sup>T</sup>.

### Introduction

Five natural strains, anaerobic sulfate-reducing bacteria belonging to the genus *Desulfovibrio*, isolated from soils and sediments of different environments, were analyzed by Random Amplified Polymorphic DNA (RAPD) and Repetitive Primer Amplified Polymorphic DNA (rep-APD) analyses. Two of them, JG-1 (UFZ B490) and Sediment 5, were recovered from a uranium waste pile near Johanngeorgenstadt in Saxony, Germany. Two isolates, UFZ B378 and UFZ B406, were isolated from waste water ponds. The isolate UFZ B393 was obtained from a copper mine in Averøy, Norway /1/.

### Experimental

The reference strain *Desulfovibrio vulgaris (oxamicus)* 1925<sup>T</sup> was obtained from the Deutsche Stammsammlung. The environmental isolates were supplied by UFZ Leipzig-Halle. The total bacterial DNA was isolated by NucleoSpin C+T Kit (Macherey-Nagel).

RAPD and rep-APD were performed as described by Selenska-Pobell et al. /2/. For the RAPD analysis the primers AP1, AP21, and AP22 were used. The rep-APD analysis was performed using single repetitive primers corresponding to the A subunit of the BOX element (BOX), to the enterobacterial repetitive intergeneric consensus (ERIC), and to the REP consensus (REP). The resulting patterns were analyzed by the software RFLP-Scan/Treecon.

### Results

The genomic fingerprints of the five natural isolates were compared to that of the reference strain *Desulfovibrio vulgaris (oxamicus)* 1925<sup>T</sup>. The choice of the strain *D. vulgaris (oxamicus)* 1925<sup>T</sup> as a reference strain was based on the fact that this strain was phylogenetically affiliated together with the strains JG-1 and Sediment 5 /3/.

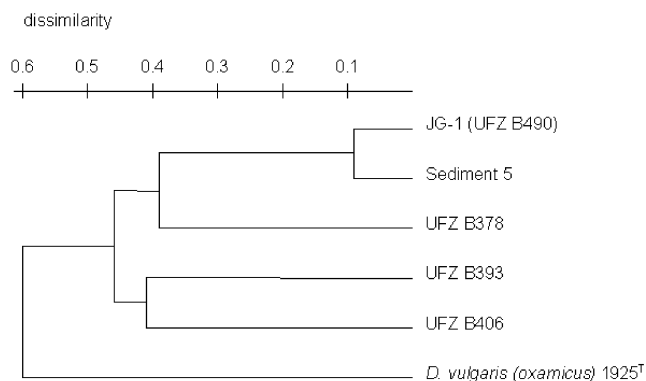


Fig. 1: Dendrogram showing the genomic relationships between the strains studied by RAPD analysis with the primers AP1, AP21, and AP22.

The resulting dendrograms of RAPD (Fig. 1) and rep-APD (Fig. 2) show high relatedness between the strains compared. It was demonstrated that all isolates are members of a group with high genomic similarity. *D. vulgaris (oxamicus)* 1925<sup>T</sup> is not very related to these strains, whereas the pile isolates JG-1 and Sediment 5 are very closely related to each other. They have identical patterns in the RAPD analysis with the primer AP21, and in the rep-APD analysis with the primers BOX and ERIC. UFZ B378 is the next related strain to these isolates from the uranium waste pile. The strains UFZ B393 and UFZ B406 form a particular group.

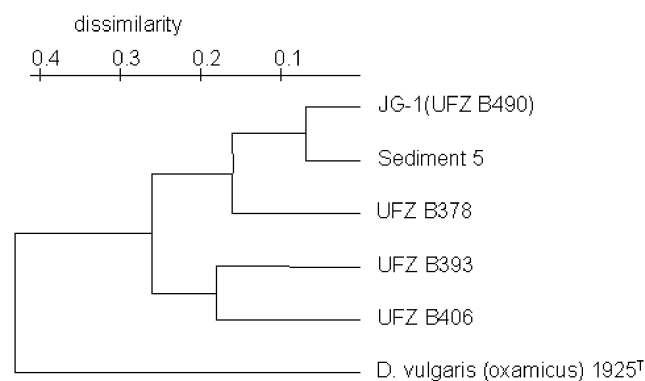


Fig. 2: Dendrogram showing the genomic relationships between the strains studied by rep-APD analysis with the primers BOX, ERIC, and REP.

The close genomic relationships between the five strains studied may be explained by the fact that all of them were cultured from their environmental samples using the same Postgate derived medium with pH 4 as modified by Hard and Babel /4/.

Our analyses demonstrate that the five natural *Desulfovibrio* isolates form a particular genomic group which is related to the subspecies *Desulfovibrio vulgaris (oxamicus)*.

### Acknowledgements

This work was supported by grant 7531.50-03-FZR/607 from the Sächsisches Staatsministerium für Wissenschaft und Kunst Dresden, Germany.

### References

- /1/ Hard, B.C. et al.; Microbiol. Res. **152**, 63-73 (1997)
- /2/ Selenska-Pobell, S. et al.; System. Appl. Microbiol. **18**, 425-438 (1995)
- /3/ Flemming, K. et al.; this report p.43
- /4/ Hard, B.C., Babel, W.; J. Basic Microbiol. **35**, 385-392 (1995)

# CLASSIFICATION OF *DESULFOVIBRIO* ISOLATES RECOVERED FROM A URANIUM WASTE PILE

K. Flemming, J. Wober, B. Hard<sup>1</sup>, S. Selenska-Pobell

<sup>1</sup>UFZ-Center for Environmental Research Leipzig-Halle, 04301 Leipzig, Germany

Two *Desulfovibrio* isolates from a uranium waste pile were compared to 25 *Desulfovibrio* reference strains by the use of ARDREA. Both strains were very closely related to the reference strain *D. vulgaris* (*oxamicus*) 1925<sup>T</sup>.

## Introduction

A large variety of bacteria was demonstrated to be present in soil and sediment samples of a uranium waste pile near the town Johanngeorgenstadt in Saxony, Germany. Anaerobic sulfate-reducing bacteria belonging to the genus *Desulfovibrio* were found among them. These *Desulfovibrio* isolates which are indigenous for the waste, were classified by the use of the Amplified Ribosomal DNA Restriction Endonucleases Analysis (ARDREA) of the 16S rDNA /1/ and the intergenic spacer region (IGS) between the 16S and 23S rDNA genes /2/. 25 reference strains (from the Deutsche Stammsammlung (DSM) and the American Type Culture Collection (ATCC)) and the two natural isolates were involved in these analyses. The latter, JG-1 (UFZ B 490) and Sediment 5, represent a large number of pile isolates recovered from the uranium waste pile.

## Results

The phylogenetic relationship between the strains studied, evaluated on the basis of the highly conservative 16S rDNA, is shown in Fig. 1. The dendrogram presented in the figure was obtained by the unweighted pair group method with averages (UPGMA). The RFLP patterns of the pile isolate Sediment 5 were identical to those of the reference strain *D. vulgaris* (*oxamicus*) 1925<sup>T</sup>. However, it was possible to discriminate these two strains by the ARDREA of the more variable IGS region (shown in Fig. 2) and by Random Amplified Polymorphic DNA (RAPD) and Repetitive Primer Amplified Polymorphic DNA (rep-APD) analyses /3/. The other pile isolate (JG-1) - from a different site of the same pile - is very closely related to Sediment 5 and *D. vulgaris* (*oxamicus*) 1925<sup>T</sup>.

Interestingly, some of the known *Desulfovibrio* strains, classified as very closely related on the basis of their physiological and biochemical properties, showed lower phylogenetical relationship (e.g. *D. desulfuricans* (*desulfuricans*) 642<sup>T</sup> and *D. desulfuricans* (*aestuarii*) 29578<sup>T</sup>). On the other hand in both dendrograms the strains *D. halophilus* 5663<sup>T</sup> and *D. oxycliniae* 11498<sup>T</sup> were very closely related.

## Acknowledgments

This work was supported by grant 7531.50-03-FZR/607 from the Sächsisches Staatsministerium für Wissenschaft und Kunst, Dresden, Germany.

## References

- /1/ Laguerre, G., et al.; Appl. Environ. Microbiol. **60**, 56-63 (1994)
- /2/ Selenska-Pobell, S., et al.; J. Appl. Bacteriol. **80**, 517-528 (1996)
- /3/ Wober, J., Selenska-Pobell, S., this report p.42

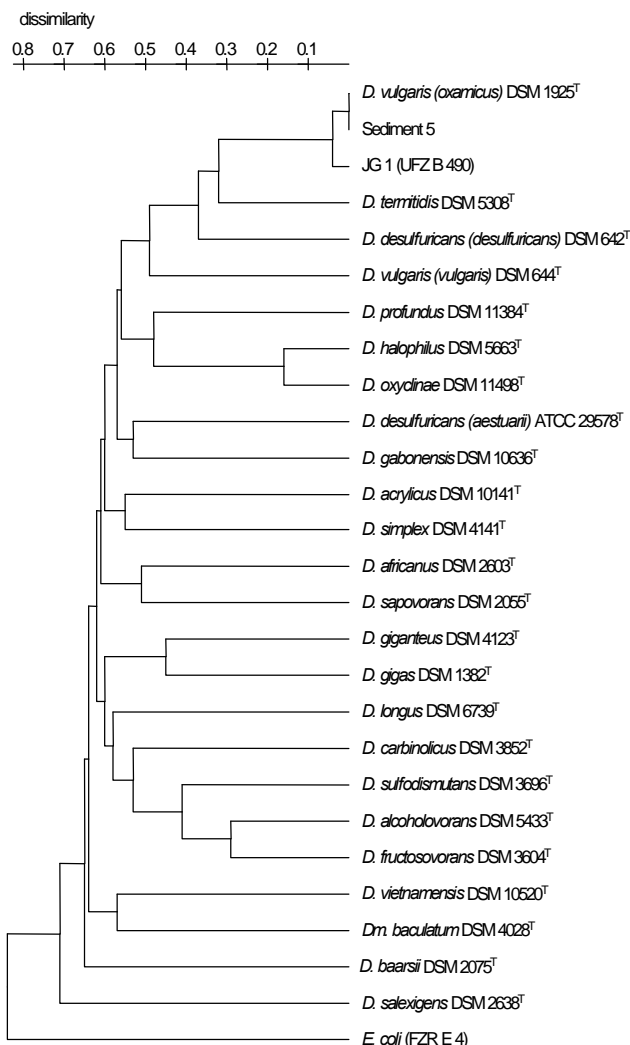


Fig. 1: Dendrogram showing the phylogenetical relationship between the *Desulfovibrio* reference strains and the isolates obtained by 16S-ARDREA

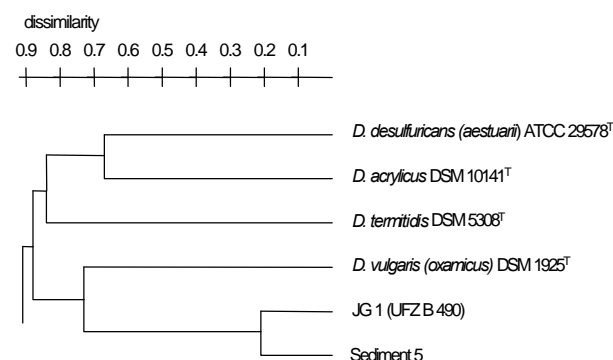


Fig. 2: Dendrogram showing the phylogenetical relationship between some *Desulfovibrio* reference strains and the isolates obtained by IGS-ARDREA

# MOLECULAR CHARACTERIZATION OF *THIOBACILLUS* STRAINS RECOVERED FROM A URANIUM MINING WASTE PILE

S.Kutschke, V.Groudeva<sup>1</sup>, S.Selenska-Pobell

<sup>1</sup>Department of General and Industrial Microbiology, University of Sofia, Sofia, Bulgaria

*Thiobacillus* strains, isolated from a former uranium mine in Saxonia, Germany, were characterized by pulsed-field gel electrophoresis and repetitive primer-amplified polymorphic DNA as *Thiobacillus ferrooxidans*. The six pile isolates show a high relation to the strain *Thiobacillus ferrooxidans* ATCC 33020 recovered from a uranium waste pile in Japan.

Bioleaching involves solubilization of metals from minerals by metabolic activity of mixed microbial populations. *Thiobacillus ferrooxidans* is the most frequently used bacterium for commercial leaching of metals such as copper, uranium, and gold from sulphide-containing ores. Thiobacilli as well as many other acidophilic chemoautotrophic and heterotrophic bacteria have been found in uranium mines/1/. *Thiobacillus*-strains recovered from a former uranium mine in Saxony, Germany, were characterized using pulsed-field gel electrophoresis (PFGE) /2/ and repetitive primer-amplified polymorphic DNA (rep-APD) fingerprinting /3/.

These methods yield information from the whole bacterial genome. In the case of PFGE, the embedded bacterial cells were lysed and the intact genome DNA was digested by the use of a rarely cutting endonuclease *Xba*I. The obtained DNA fragments were separated in an alternating electrical field. Genomic fingerprinting by rep-APD is based on the use of special oligonucleotide primers complementary to interspersed bacterial repetitive sequences and PCR. As a result DNA fragments of different size consisting of sequences laying between these elements will be obtained. The latter are fractionated by electrophoresis /4/.

Using the above-mentioned methods, six newly isolated *Thiobacillus* isolates were characterized. As shown in Fig. 1, the PFGE fingerprints of the waste isolates were sample specific. The sampling sites had different

depths and metal compositions. Three of the isolates, TFSS1, TFSS2, and TFSS6 were recovered from a sample drawn from a depth of about one meter below the surface where the concentration of uranium was low. The three other samples TFSS3, TFSS4, TFSS5 were recovered from a depth between two and three meters. The concentration of uranium at this site was estimated to be three times higher than that in the other above-mentioned sample.

The six novel *Thiobacillus ferrooxidans* isolates are from a particular rep-APD group which is closely related to the strain *Thiobacillus ferrooxidans* ATCC 33020 that was recovered from a uranium mine in Japan (see Fig. 2).

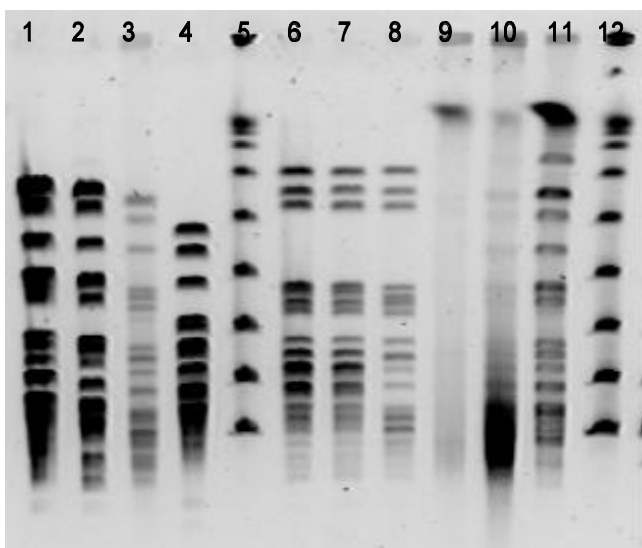


Fig. 1: PFGE- Fingerprint of the strains:

1, *Thiobacillus ferrooxidans* ATCC 19859; 2, *Thiobacillus ferrooxidans* ATCC 21834; 3, *Thiobacillus ferrooxidans* ATCC 23270; 4, *Thiobacillus ferrooxidans* ATCC 33020; 5, 8 Ladder PFG Marker; 6, Pile isolate TFSS1; 7, Pile isolate TFSS2; 8, Pile isolate TFSS6; 9, Pile isolate TFSS3; 10, Pile isolate TFSS4; 11, Pile isolate TFSS5; 12, 8 Ladder PFG Marker

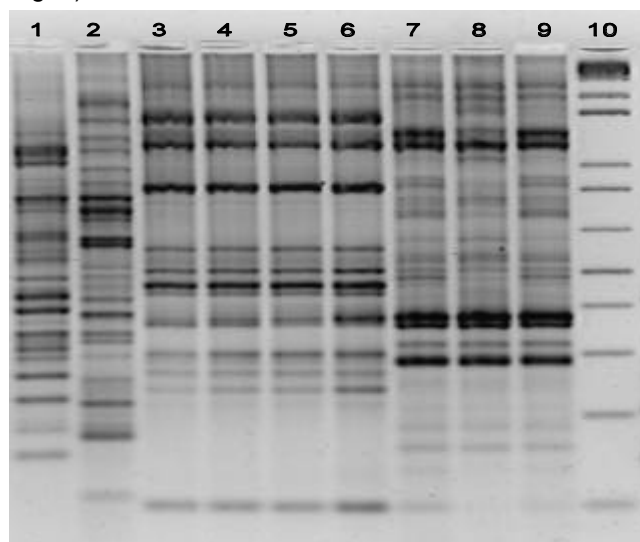


Fig. 2: Genomic rep-APD fingerprint of the strains:

1, *E. coli*; 2, *Thiomonas cuprina* DSM5495; 3, Pile isolate TFSS6; 4, Pile isolate TFSS2; 5, Pile isolate TFSS1; 6, *Thiobacillus ferrooxidans* ATCC33020; 7, *Thiobacillus ferrooxidans* ATCC23270; 8, *Thiobacillus ferrooxidans* ATCC21834; 9, *Thiobacillus ferrooxidans* ATCC 19859; 10, 1Kb Plus DNA Ladder

## Acknowledgments

This study was supported by grant 7531.50-03-FZR/607 from the Sächsisches Staatsministerium für Wissenschaft und Kunst, Dresden, Germany.

## References

- Goebel, B.M. et al.; *Bacterial Diversity and Systematics*. Eds. Priest, F.G. et al., Plenum Press, New York 1994
- Kondrat'eva, T.F., et al.; *Mol. Gen. Microbiol. Virusol.*, 19-22 (1993)
- Selenska-Pobell, S., et al.; *J. Appl. Microbiology* **84**, 1085-1091 (1998)
- Versalovic, J., et al.; *Methods Mol. Cell Biol.* **5**, 25-40 (1994)

## CHARACTERIZATION OF THE SURFACE LAYER PROTEIN OF THE *BACILLUS SPHAERICUS* ISOLATE JG A-12 FROM A URANIUM WASTE PILE

J. Raff, R. Kirsch<sup>1</sup>, S. Kutschke, T. Maier<sup>2</sup>, M. Mertig<sup>1</sup>, S. Selenska-Pobell, G. Bernhard, U. Hahn<sup>2</sup>, W. Pompe<sup>1</sup>

<sup>1</sup>Institute of Material Science, Technische Universität Dresden, 01062 Dresden, Germany

<sup>2</sup>Institute of Biochemistry, Universität Leipzig, 04103 Leipzig, Germany

*The bacterial surface layer of a natural Bacillus isolate JG A-12, which was recovered from a uranium waste pile near the town Johanngeorgenstadt in Saxony, was analyzed and compared to the surface layer of a reference strain (Bacillus sphaericus NCTC 9602). Both protein monomers show equal chemical and physical properties.*

Many bacteria possess a crystalline protein or glycoprotein surface layer (S-layer) as the outermost component of their cell wall. The function of this protein lattice in different bacteria is not uniform and has been studied in detail only in some cases. The protein layer may act as a protective coat, molecular sieve, ion trap. It may also represent a framework or a structure for cell adhesion and surface recognition /1, 2/. In addition, it was demonstrated that the isolated lattice interacts with metal ions by forming metal clusters /3/. The latter may be used for developing biotechnological procedures to remediate heavy-metal-contaminated wastes. In this work natural bacterial isolates, recovered from the uranium waste pile "Haberland", were analyzed for the presence of surface layer proteins.

The natural isolate JG A-12 was phylogenetically affiliated to the species *Bacillus sphaericus* by use of the RFLP analysis of the PCR-amplified 16S rDNA. The genomic macro-fingerprints of the two *B. sphaericus* strains obtained by pulsed-field gel electrophoresis were strain specific.

*B. sphaericus* NCTC 9602 and the isolate JG A-12 were grown in batch culture until the end of their exponential growth, harvested by centrifugation, and stored at -20 °C. S-layers were isolated as follows: first the cells were disrupted with glass beads in a mixer mill. After that the pure S-layer sheets were produced by centrifugation of the crude extract and successive treatment of the pellet with Triton X-100 and lysozyme. The purity and the apparent molecular weight were examined with a denaturing polyacrylamid gel electrophoresis. The molecular weights of the S-layer proteins of both, the reference strain NCTC 9602 and the strain JG A-12, were estimated to be approximately 135 kDa. This size is about 10 kDa larger than the one published for the S-layer protein of another *B. sphaericus* strain 2362 /5/. The first 20 amino acids at the N-termini of the 135 kDa proteins of the strains 9602 and JG A-12 were identical. However, no similarity to the oblique *B. sphaericus* 2362 S-layer protein was found /1, 3/. Interestingly, in the case of the uranium waste isolate, in addition to the S-layer a second, smaller protein with a size of 30 kDa was co-purified. The amino acid sequence of the N-terminus of the 30 kDa protein was significantly different from those of the S-layer proteins. This small protein possesses a similarity to many flagellins of different bacteria. The highest similarity was found to flagella protein from *Leptospira interrogans* and *B. subtilis*. The lattice structures of the S-layers of the reference strain *B. sphaericus* NCTC 9602 and of the uranium waste isolate JG A-12 were also characterized using transmission electron microscopy.

Fig. 1 shows the isolated and negatively stained (with uranyl acetate) tetragonally arranged S-layer from the isolate.

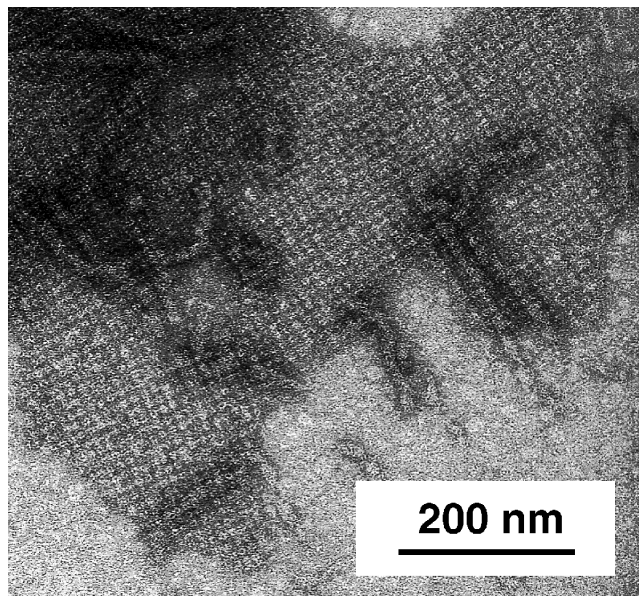


Fig. 1: S-layer of the *Bacillus sphaericus* isolate JG A-12.

JG A-12 is the first *B. sphaericus*-strain recovered from an uranium-contaminated environment and tested for the presence of S-layer. Surprisingly, both *B. sphaericus* strains 9602 and JG A-12 seem to possess the S-layer protein with the same structure. Proteolytical cleavage and sequencing of the internal protein fragments will be applied to prove this first observation. Further studies of S-layers from other isolates (especially thiobacilli) recovered from the uranium waste pile "Haberland" are in progress.

### Acknowledgments

This study was supported by grant 4-7531.50-03-0370/708 from Sächsisches Staatsministerium für Wissenschaft und Kunst, Dresden, Germany.

### References

- /1/ Sidhu, M.S., Olsen, I.: S-layer of *Bacillus* species. *Microbiol.* **143**, 1039-1052 (1997)
- /2/ Kirsch, R.: *Metallische Nanostrukturen auf biomolekularen Templaten*. Dissertation TU Dresden, Institut für Werkstoffwissenschaften (1998)
- /3/ Bowditch, R. D., Baumann, P., Yousten, A. A.: Cloning and Sequencing of the Gene Encoding a 125-Kilodalton Surface-Layer Protein from *Bacillus sphaericus* 2362 and of a Related Cryptic Gene. *J. Bacteriol.* **171**, 4178-4188 (1989)

## COMPLEX FORMATION OF *THIOBACILLUS FERROOXIDANS* WITH U(VI)

P. Panak, S. Kutschke, S. Selenska-Pobell, G. Bernhard, H. Nitsche

Uranium (VI) accumulation of several strains of *Thiobacillus ferrooxidans* recovered from different environments was studied. Extraction with sulfuric acid and EDTA provided information on the strength and reversibility of the binding.

In uranium deposits a number of acidophilic chemolithoautotrophic bacteria have been identified which are able to oxidize sulphide minerals, elemental sulfur, ferrous iron, and in presence of uranium minerals also U(IV). The mechanism of the uranium oxidation was extensively studied, but only little information is available on the complexes formed with U(VI) /1/. We studied the bioaccumulation of U(VI) by several strains of *Thiobacillus ferrooxidans* drawn from environments with different mineral compositions. Strains *T. ferrooxidans* ATCC 23270<sup>T</sup> and ATCC 21834 were recovered from two different coal mines in USA and Japan, *T. ferrooxidans* ATCC 19859 from a Canadian copper mine, and *T. ferrooxidans* ATCC 33020 from a uranium mine in Japan. We compared the results obtained with *T. ferrooxidans* strains to those obtained with another acidophilic strain, *Thiomonas cuprina* DSM 5495<sup>T</sup>, which does not belong to the genus *Thiobacillus* but was isolated from a German uranium mine. Sorption studies have shown that the origin of the strains has a significant influence on their capability to accumulate uranium. The amount of uranium bound to the biomass increases in the order *Thiobacillus ferrooxidans* ATCC 19859 (copper mine), ATCC 23270<sup>T</sup> (coal mine) and ATCC 33020 (uranium mine). *Thiomonas cuprina* shows the highest uranium uptake (Fig. 1).

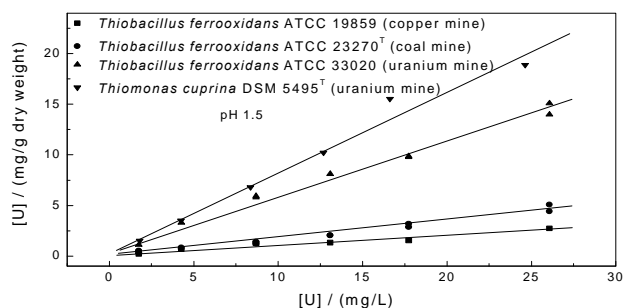


Fig. 1: Accumulation of U(VI) by *Thiobacillus ferrooxidans* strains and *Thiomonas cuprina* at pH 1.5

In order to get information on the binding strength and the reversibility, we tried to remove the accumulated uranium from the biomass by different extractants. First we measured the distribution of the U(VI) between the solution and the cell material by washing the biomass with H<sub>2</sub>SO<sub>4</sub> at pH 1.5. After separating the cells by centrifugation and removing one half of the washing solution, an equivalent volume of sulfuric acid was added to the bacterial suspension. This procedure was repeated five times. Fig. 2 shows the results of the extraction studies for the strain *Thiobacillus ferrooxidans* ATCC 33020. The U(VI) concentration in the solution decreases quickly with each dilution step whereas the amount of uranium fixed to the biomass does not change, not even after five extraction steps.

Extraction with EDTA released a small fraction of the U(VI) accumulated by *Thiobacillus ferrooxidans* strains

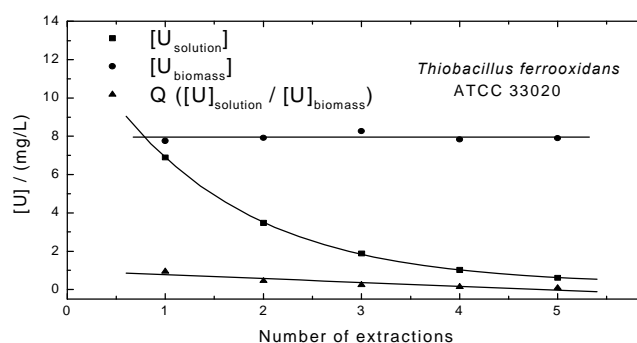


Fig. 2: Distribution of U(VI) between H<sub>2</sub>SO<sub>4</sub> (pH 1.5) and the cell material as a function of the number of extractions

(Fig. 3). For higher uranium concentrations, a saturation of sorption sites on the surface responsible for the weak binding of uranium was observed. The results of the extraction studies show that the main part of the uranium forms strong complexes with the bacteria. *Thiomonas cuprina* has different surface properties which lead to a different complexation behavior towards uranium. The total amount of accumulated U(VI) for this strain is higher than for the *Thiobacillus ferrooxidans* strains, but the binding is weaker. A larger amount of the uranium could be released from the biomass by EDTA-treatment.

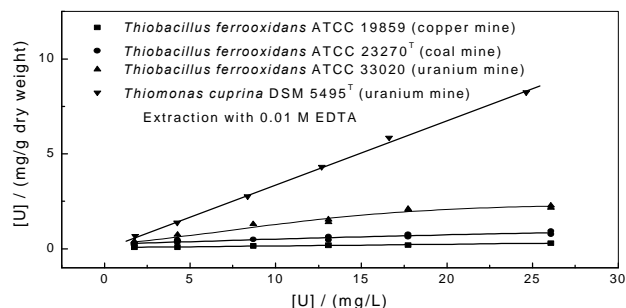


Fig. 3: U(VI) extracted from the biomass with 0.01M EDTA solution

In accordance with genetic results /2/, the two strains isolated from uranium mines show a substantially higher uptake than the strains from coal and copper mines. Therefore, natural isolates from the contaminated areas are of particular importance for bioremediation purposes because they are already adapted to harsh conditions in the natural system and to high concentrations of the contaminants.

### References

- /1/ DiSpirito, A.A., Talnagi Jr., J.W., Tuovinen, O.H.; Arch. Microbiol. **135**, 250-253 (1983)
- /2/ Selenska-Pobell, S., Otto, A., Kutschke, S.; J. Appl. Bacteriol. **84**, 1085-1091 (1998)



# SPECTROSCOPIC CHARACTERIZATION OF U(VI)-COMPLEXES WITH *THIOBACILLUS FERROOXIDANS*

P. Panak, S. Kutschke, S. Selenska-Pobell, G. Geipel, G. Bernhard, H. Nitsche

The formation of stable inner-sphere complexes of three *Thiobacillus ferrooxidans* strains and a *Thiomonas cuprina* strain with U(VI) was proved by time-resolved laser fluorescence spectroscopy. The spectroscopic properties of the formed U(VI)-complexes correspond well to the accumulation capability of the strains.

## Experimental

The uranyl fluorescence was measured in aqueous biomass solutions (0.27-0.30 g dry weight/L) with  $1.67 \cdot 10^{-5}$  M U(VI) in 0.032 M HClO<sub>4</sub>. For a better determination of the fluorescence properties of the bacterial UO<sub>2</sub><sup>2+</sup>-complexes, we removed the uranyl in solution and uranyl weakly adsorbed to the surface of the cells by extracting the biomass with 0.01 M EDTA/TRIS solution. For TRLFS-measurement, a Nd-YAG (model GCR, Spectra Physics, USA) pumped OPO-system (MOPO 730, Spectra Physics, USA) was used. The details of the TRLFS-spectrometer are given elsewhere /1/. Emission spectra were recorded from 408 to 634 nm using an excitation wavelength of 266 nm and a delay time from 0.1 μs to 20 μs.

## Results

Fig. 1 shows the emission spectra of U(VI) bound to bacterial cells of the strains *Thiobacillus ferrooxidans* ATCC 19859, 21834, 33020, and *Thiomonas cuprina* in comparison to the spectrum of the aqueous uranyl ion. The spectroscopic results are summarized in Tab. 1.

Tab. 1:	Emission maxima/Halfwidths(nm)				Lifetime (ns)
UO <sub>2</sub> <sup>2+</sup> <sub>aq</sub>	488.6	510.2	533.4	559.8	1540 ± 139
	(11.4)	(11.5)	(15.6)	(14.1)	
<i>Thiobacillus ferrooxidans</i>					
ATCC 19859	493.6	514.9	537.1	565.7	2778 ± 250
	(13.9)	(13.1)	(17.0)	(14.3)	
ATCC 21834	494.3	515.7	538.3	567.4	
	(12.3)	(14.0)	(16.3)	(13.4)	3116 ± 280
ATCC 33020	495.1	516.5	539.5	568.4	3911 ± 352
	(13.9)	(12.5)	(16.0)	(13.1)	
<i>Thiomonas cuprina</i>					
DSM 5495 <sup>T</sup>	494.1	516.5	538.5	566.9	2314 ± 208
	(12.7)	(11.0)	(13.0)	(13.0)	

The interaction with the biomass causes a strong bathochrome shift of the emission bands between 3.7 to 8.5 nm, indicating the formation of inner-sphere complexes for all strains examined. Additional important information can be obtained from life time measurements. The decrease of fluorescence intensity can be fitted by a bi-exponential function. The bacterial uranyl complexes show a fast decaying time component  $\tau_1$  in the range of 86 to 373 ns that is much smaller than the life time of the aqueous uranyl ion. This is due to a quenching process via intramolecular energy transfer from the metal ion to electronic levels of the ligand. The second life time  $\tau_2$ , calculated from the bi-exponential fit, describes the fluorescence decay of the respective bacterial UO<sub>2</sub><sup>2+</sup>-complex. The complexation with the cells causes an increase of life time by a factor of 1.8 for *Thiobacillus ferrooxidans* ATCC 19859, 2.0 for *Thiobacillus ferrooxidans* ATCC 21834, 2.5 for *Thiobacillus ferrooxidans* ATCC 33020, and 1.5 for *Thiomonas cuprina* DSM 5495<sup>T</sup>.

Furthermore, the analysis of the time dependence of the fluorescence spectra demonstrates that the samples contained only one complexed uranyl species. The wavelength of the emission spectra did not shift with increasing delay time as it is expected if several complexes with different life times coexist. Therefore, the formation of various complexes with chemically different functional groups of the cells or a different number of binding sites can be excluded. The results of the laser fluorescence measurements are in good correlation with the quantitative studies on the U(VI) accumulation /2/. Except for *Th. cuprina*, the red shift of the emission bands and the fluorescence life time of the bacterial complexes increase in the same order as the capability of the strains to accumulate uranium. Given that these changes of spectroscopic parameters are a consequence of the influence of the ligands on the coordination sphere of the uranyl ion, the binding strength increases in the order *T. ferrooxidans* ATCC 19859 (copper mine), ATCC 23270<sup>T</sup> (coal mine) and ATCC 33020 (uranium mine), whereas *Thiomonas cuprina* forms less stable complexes with U(VI).

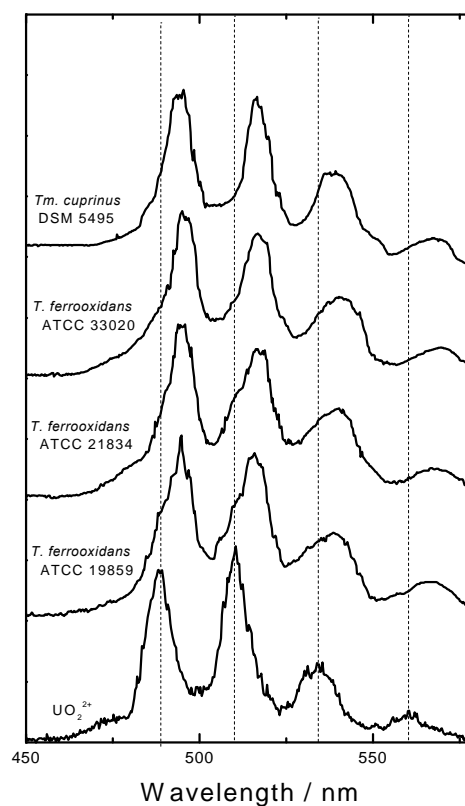


Fig. 1: TRLF-spectra of the UO<sub>2</sub><sup>2+</sup>-bacterial complexes

## References

- /1/ Bernhard, G., et al.; Radiochim. Acta **74**, 87 (1996)
- /2/ Panak, P., et al.; this report p.46

# INTERACTION OF *BACILLUS* ISOLATES FROM A URANIUM MINING WASTE PILE WITH U(VI)

P. Panak, V. Miteva, I. Boudakov, S. Selenska-Pobell, G. Bernhard, H. Nitsche

The accumulation of U(VI) by three different *Bacillus* isolates from a uranium mining waste pile in Saxony, Germany, classified as *B. cereus*, *B. sphaericus*, and *B. megaterium*, was studied. Information on the binding strength and the reversibility were obtained from extraction studies with 0.01 M EDTA-solution

The genus *Bacillus* consists of more than 70 species of Gram-positive, aerobic or facultatively anaerobic spore-forming rod-shaped bacteria [1,2]. Because of the high resistance of their spores, *Bacilli* were found in a large variety of natural habitats. Recently, various *Bacillus* species have been isolated from a uranium mining waste pile in Saxony, Germany (Haberlandhalde, Johannegeorgenstadt) [3]. For our accumulation studies with U(VI), we used vegetative cells and spores of three *Bacillus* isolates (JG-A 30, JG-A 12, JG-A 22, classified as *Bacillus cereus*, *Bacillus sphaericus*, *Bacillus megaterium*) from this uranium mining waste pile and their corresponding reference strains. The sorption studies have shown (Fig. 1 and 2) that *Bacilli* can accumulate high amounts of uranium.

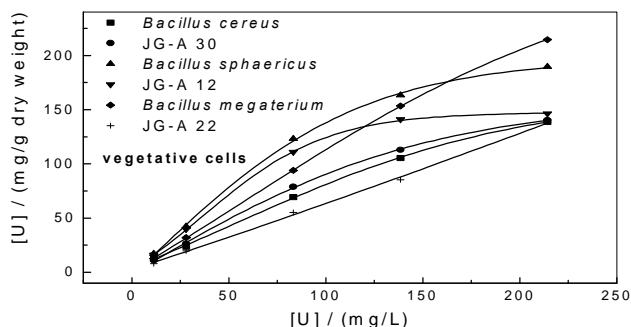


Fig. 1: Accumulation of U(VI) by the vegetative cells of the *Bacilli* isolates and their reference strains

In the concentration range examined (11 – 214 mg/L), the uranium is taken up linearly with increasing initial uranium concentration by the isolate JG-A 22 and its *B. megaterium* reference strain (vegetative cells and spores). In the cases of the other strains, the amount of

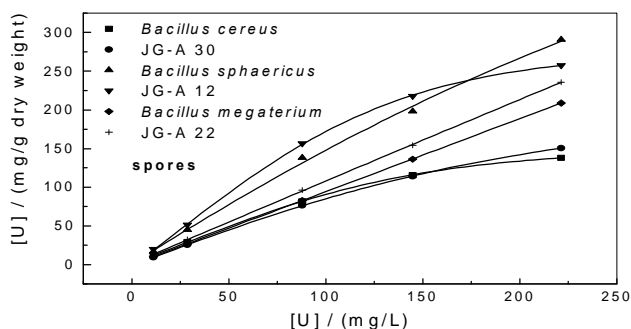


Fig. 2: Accumulation of U(VI) by the spores of the *Bacilli* isolates and their reference strains

uranium bound to the biomass approaches a limiting value for higher uranium concentrations (> 80 mg/L). Comparing the sorption behavior of the vegetative cells and the spores, for JG-A 30 and *Bacillus cereus* no significant differences could be observed. In the case of JG-A12/*Bacillus sphaericus*, the spores show a higher uranium accumulation related to the dry weight of the

biomass. For *Bacillus megaterium*, sorption properties of the vegetative cells and the spores are almost identical whereas in the case of the corresponding isolate the capability to accumulate uranium increases with sporulation.

Contrary to the results of the *Thiobacilli* [4], the uranium bound to the vegetative cells was released almost quantitatively by EDTA-extraction. Fig. 3 shows the percentage of the extractable uranyl for an initial uranium concentration of 214 mg/L. In agreement with the similar sorption behavior of the vegetative cells and the spores of the pair JG-A 30/*Bacillus cereus*, also comparable amounts of uranium were extracted.

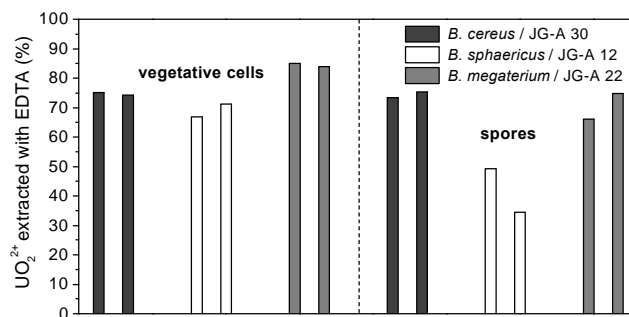


Fig. 3: Amount of uranium (%) extracted with 0.01 M EDTA (initial uranium concentration: 214 mg/L)

For the other strains, the part of the non-extractable uranium on the biomass increased with the formation of the spores. Especially in the case of JG-A 12/*Bacillus sphaericus*, strains forming very small circular spores, the fraction of extractable uranium was smaller than 40% / 50 %, respectively.

The characterization of the formed bacterial- $UO_2^{2+}$ -complexes by time-resolved laser fluorescence spectroscopy has proved the formation of inner-sphere complexes with the biomass for all strains examined. In accordance to the results of the *Thiobacilli*, the fluorescence spectra of the bacterial complexes show a strong red shift compared to the hydrated uranyl ion, and the life time of the fluorescence emission increases.

## Acknowledgments

This work was supported by a grant (No: 7531.50-03-FZR/607) from the Sächsisches Staatsministerium für Wissenschaft und Kunst, Dresden, Germany.

## References

- 1/ Bacterial Nomenclature Up-to-Date, October 1997, Deutsche Stammsammlung von Mikroorganismen und Zellkulturen GmbH, Braunschweig, Germany
- 2/ Slepecky, R., et al., The Prokaryotes, p.1663 (1991)
- 3/ Selenska-Pobell, S., et al., FEMS Microbiol. Ecol. (accepted)
- 4/ Panak, P., et al., this report p.46

# SELECTIVE ACCUMULATION OF METAL IONS IN A DRAIN WATER OF A URANIUM MINING WASTE PILE BY INDIGENOUS *BACILLUS* ISOLATES

P. Panak, V. Miteva, I. Boudakov, S. Selenska-Pobell, G. Bernhard, H. Nitsche

The interaction of three *Bacillus* isolates recovered from a uranium mining waste pile and of their reference strains with different metal ions in an original groundwater of the pile was studied. Selective accumulation of U, Pb, Cu, Cd and Al was observed for all strains examined.

Bacteria in soil, sediment, and water can have a significant influence on the transport of radionuclides and other heavy metals in nature. Certain bacterial strains can selectively take up various metal ions from aqueous systems, and are therefore important for the regulation of environmental pollution and remediation purpose. In order to examine which metal ions are accumulated by the *Bacilli* isolates (JG-A 30, JG-A 12, JG-A 22, classified as *Bacillus cereus*, *Bacillus sphaericus*, *Bacillus megaterium* /1/) recovered from the uranium mining waste pile "Haberlandhalde", Johanngeorgenstadt, Saxony, Germany, an original drain water of the pile was used for accumulation studies. The pH of the water sample was 4.6. It was air-saturated and contained the following metal ions: Al (1018 µg/L), Si (9460 µg/L), Cr (1.9 µg/L), Fe (< 20 µg/L), Mn (1050 µg/L), Co (43.2 µg/L), Ni (247 µg/L), Cu (124 µg/L), Zn (3975 µg/L), Ga (7.0 µg/L), As (< 0.5 µg/L), Rb (18.6 µg/L), Sr (65 µg/L), Cd (15.4 µg/L), Sn (1.6 µg/L), Cs (1.7 µg/L), Ba (17.7 µg/L), Pb (18.6 µg/L), and U (72.1 µg/L). The interactions with the metal ions of the drain water were studied using vegetative cells and spores of the isolates and their corresponding reference strains.

U, Cu, Pb, Al and Cd were preferably accumulated by the vegetative cells of all strains examined (Fig. 1) which is in agreement with the results of Nakajima et al. /2/,

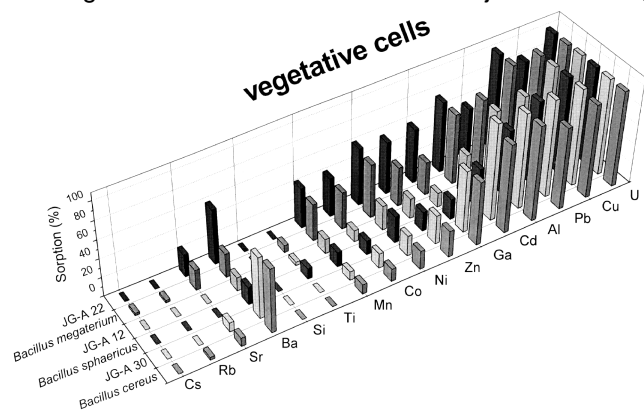


Fig. 1: Selective accumulation of metal ions of a drain water by vegetative cells of *Bacilli*

except for Cd. Comparing the accumulation properties of the corresponding pairs, *B. cereus*/JG-A30 accumulated higher amounts of Ba, Cd, and Ga, whereas the pair *B. megaterium*/JG-A22 accumulated more Co, Mn, Ni, and Zn. All these elements were only weakly accumulated by *B. sphaericus*/JG-A 12.

Comparing the corresponding members of the pairs, *B. cereus*/JG-A30 and *B. sphaericus*/JG-A 12 have shown almost the same binding capability to each particular metal ion. In the case of *B. megaterium*/JG-A22 the isolate accumulated Ba, Ga, and Zn to a higher, and Al and Cu to a smaller extent compared to the *B. megaterium* reference strain.

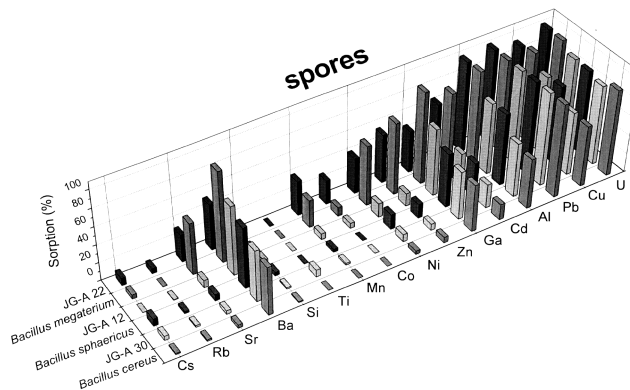


Fig. 2: Selective accumulation of metal ions of a drain water by spores of *Bacilli*

The spores of the strains followed a very similar tendency. Ga, Cd, Al, Pb, Cu, and U were selectively removed from the drain water. In comparison to the spores of the other strains and to their own vegetative cells, the spores of *B. cereus*/JG-A30 possess a lower capability to accumulate Cd, whereas the spores of *B. sphaericus*/JG-A 12 were able to bind more Ba than the vegetative cells. In good agreement with the results of the vegetative cells, the spores of the corresponding members of the pairs *B. cereus*/JG-A30 and *B. sphaericus*/JG-A 12 have shown a very similar accumulation behavior, whereas the spores of *B. megaterium*/JG-A22 interacted differently to the metal ions studied. The spores of the isolate accumulated smaller amounts of Sr, Ba, Ni, Zn, Ga, and Cd, and higher amounts of Cs, Rb, Mn, and Co than those of the reference strain. In general, the spores of the pair *B. megaterium*/JG-A22 possess a higher binding capability than the spores of the other four strains. In order to get information on the binding strength, desorption studies with 0.01 M EDTA-solution were performed. According to the results of the interaction of these strains with uranium /3/, most of the metal ions were easily released from the vegetative cells by EDTA-extraction. Some of the metals, however, were irreversibly bound by the spores. Significant amounts of Ba, Ni, Cd, and U could not be extracted from the spores with EDTA. Especially strong was the binding of U, Al, and Cd observed for the spores of the isolate JG-A 22.

## Acknowledgments

This work was supported by a grant (No: 7531.50-03-FZR/607) from the Sächsisches Staatsministerium für Wissenschaft und Kunst, Dresden, Germany

## References

- /1/ Selenska-Pobell, S., et al., FEMS Microbiol. Ecol. (accepted)
- /2/ Nakajima, A., et al., Appl. Microbiol. Biotechnol. **24**, 59 (1986)
- /3/ Panak, P., et al., this Report p.48

# **Application of X-Ray Absorption Spectroscopy**

# THE RADIOCHEMISTRY END STATION FOR XAS MEASUREMENTS AT THE ROSSENDORF BEAMLINE (ROBL)

T. Reich, G. Bernhard, M.A. Denecke, S. Dienel<sup>1</sup>, H. Funke, C. Hennig, H. Krug<sup>1</sup>, W. Neumann<sup>1</sup>, W. Oehme<sup>1</sup>, H. Nitsche

<sup>1</sup> Department for Experimental Facilities and Information Technology

*The radiochemistry end station at ROBL has been designed to perform a variety of x-ray absorption spectroscopy experiments on radionuclides.*

## Design goals

The end station has been designed for x-ray absorption spectroscopy of solid and liquid samples containing the following radioactive elements: Tc, Po, Ra, Th, Pa, U, Np, Pu, and Am. Their absorption edges to perform EXAFS spectroscopy are in the energy range of 9 - 21 keV. Therefore, concentrated samples can be measured in transmission. Environmental samples often contain the radionuclide at low concentrations. The XAS spectra of these samples have to be recorded in fluorescence mode. The anticipated capabilities of the radiochemistry end station can be summarized as follows: XANES and EXAFS spectroscopy between 5 - 35 keV; spectrum measurement in transmission or fluorescence modes; sample temperature control between 10- 295 K; remote control of sample positioning; time-resolved XAFS measurements (Quick-EXAFS); spatially resolved XAFS using a focused beam.

For the measurements the following equipment is available: gas ionization chambers of various lengths (OHOYO KOKEN KOGYO); four pixel Ge solid state fluorescence detectors (Lawrence Berkeley National Laboratory); fluorescence x-ray ion chamber detector (Lytle detector, EXAFS Company); closed-cycle He cryostat (Oxford Instruments); various remote controlled sample positioners (FZR).

## Description of the construction

According to the safety requirements, the radioactive samples are positioned inside a glove box (Mbraun, FZR). The glove box is equipped with five 125  $\mu\text{m}$  thick polyimide windows which are transparent to the incoming and transmitted x-ray beams and the fluorescence radiation. All detectors, e.g., gas ionization chambers and fluorescence detectors, are mounted on an optical bench outside the glove box. This arrangement allows a direct and easy access to the detectors.

Inside the glove box three different remote controlled sample positioners can be used depending on the sample geometry and type of experiment. The first sample positioner can hold up to eight solid and/or liquid samples for transmission and/or fluorescence measurements. With this sample holder it is possible to switch automatically from one sample to another without need for the experimenter to enter the Radiochemistry Hutch. The second sample positioner holds the closed-cycle He cryostat. For measurements of very dilute samples, a third sample holder can incline the sample 45° with respect to the beam between two polyimide windows which are perpendicular to the beam. These windows allow the simultaneous recording of the fluorescence spectrum by two Ge solid state fluorescence detectors. Since the samples are safely contained in the glove box, it is possible to modify the chemical conditions of liquid

samples just before or during the XAS measurement by adding non-radioactive substances like acid, base, or complexing agents.

For energy calibration purpose, the XAS spectrum of a non-radioactive reference sample is recorded simultaneously with the sample using the gas ionization chambers or the Lytle detector outside the glove box.

The glove box is mounted on a support frame which allows to move the glove box in horizontal direction out of the beam leaving the position of the optical bench and the detectors unchanged. This has the advantage that non-radioactive samples do not need to be brought into the glove box for XAS measurements since they can easily be mounted on the optical bench outside the glove box.

## End station commissioning

First XAFS measurements using metals foils to calibrate the energy in the range of 5 - 35 keV were done in March 1998.

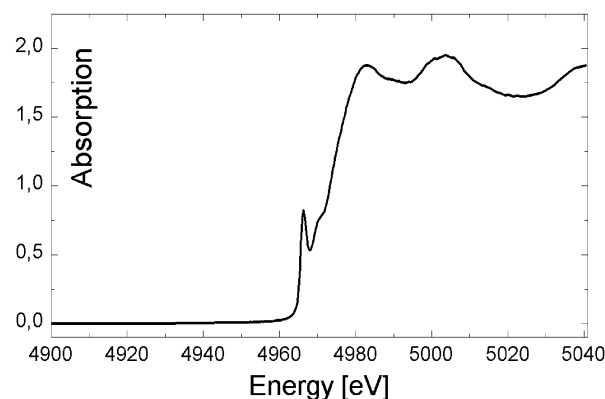


Fig. 1: Ti K-edge XANES spectrum of a 6  $\mu\text{m}$  thick metal foil.

The pre-edge feature in the Ti K-edge XAFS spectrum given in Fig. 1 indicates the good energy resolution of the Si(111) double-crystal monochromator. After installation of the radiochemistry end-station (glove box, optical bench, support frame, detectors, sample positioners) in May 1998, the commissioning of the end-station components started. The movement of the second Si(111) crystal in fixed-exit mode parallel to the beam introduced beam intensity variations on the sample. To avoid distortions in the EXAFS signal, the beam stability was significantly improved using a monochromator feed-back system developed at Hasylab /1/. The quality of the obtained EXAFS spectrum can be judged by the examples given in this report. In the immediate future the end-station commissioning will continue and the XAFS measurements will be extended to Np and Tc.

## References

/1/ Krolzig, et al.; Nucl. Instr. Meth. **219**, 430 (1984)

## AN EXAFS STUDY OF URANIUM(VI) SORPTION ONTO FERRIHYDRITE

T. Reich, T. Arnold, C. Hennig, M.A. Denecke, G. Bernhard, H. Nitsche

*The structural parameters for the uranium coordination shells indicate formation of inner-sphere, mononuclear uranyl complexes at the ferrihydrite surface.*

### Experimental

Three samples labeled Fe1-Fe3 were prepared in air at room temperature from 2 L suspensions of six-line ferrihydrite ( $10^{-3}$  M as Fe). Samples Fe1 and Fe2 were obtained at pH 5.8 and sample Fe3 at pH 7.8. The uranium(VI) concentration in suspension Fe1 was adjusted to  $10^{-4}$  Mol/L. For suspensions Fe2 and Fe3, the uranium(VI) concentration was  $10^{-5}$  Mol/L. Before and after adding uranyl nitrate stock solution to the suspensions, the pH was adjusted to the desired values. After 50 hours of continuous stirring, the pH of the suspension had not changed.

For the EXAFS measurements, the samples were separated by centrifugation and transferred as a wet paste into polyethylene cuvettes of 3 mm diameter. The cuvettes were hermetically sealed to prevent the pastes from drying. Uranium  $L_{III}$ -edge x-ray absorption (XAS) spectra were collected simultaneously in transmission and fluorescence modes at room temperature at the Stanford Synchrotron Radiation Laboratory (SSRL) and at Hamburger Synchrotronstrahlungslabor (HASYLAB) using Si(220) and Si(311) double-crystal monochromators, respectively. Further details on sample preparation, EXAFS measurements, and data analysis are given in /1/.

### Results

To obtain the structural parameters given in Tab. 1, a four-shell fit to the experimental EXAFS data was utilized.

In samples Fe1-Fe3 uranium is surrounded by two  $O_{ax}$  atoms at  $1.81 \pm 0.02$  Å. Approximately five  $O_{eq}$  atoms are coordinated to the uranyl group at 2.36-2.39 Å in the equatorial plane. The large Debye-Waller (DW) factor observed for this shell indicates a rather broad distribution of U- $O_{eq}$  distances. For sample Fe3, one iron atom is detected at a U-Fe distance of 3.42 Å. For samples Fe1 and Fe2, the coordination number of the U-Fe shell was held constant at unity to obtain a stable fit. Note that the U- $O_{ax}$  MS interaction at 3.6 Å, which was accounted for in all fits, interferes with the U-Fe interaction. As Table 1 shows, the U-Fe DW factor for samples Fe1 and Fe2 is twice that of sample Fe3. Since the U-Fe coordination number was the same in all fits, one can argue that the disorder in the U-Fe shell of samples Fe1 and Fe2 results from the presence of more than one surface species. However, the observation of U-Fe interaction for all samples indicates the formation of an inner-sphere surface complex. Since this shell could not be fit as U-U interaction, we conclude that multinuclear uranyl species are not sorbed at the surface.

The theoretical fits to the data improved when uranium interaction with a light scatterer like oxygen or carbon

was included. The U-O/C distance of about 2.9 Å found in this study is too large for a direct bond between uranium and oxygen or carbon. In case of carbon,  $2.93 \pm 0.02$  Å matches the U-C distance observed for a bidentate coordination of the  $CO_3^{2-}$  group to  $UO_2^{2+}$ . Detection of the U-C interaction may indicate the formation of a ternary complex such as  $(1 FeO_2)UO_2CO_3^{2-}$  /2/.

Sample	Shell	R(Å)	N	$\sigma^2(\text{Å}^2)$
Fe1	U- $O_{ax}$	1.81	2	0.0022
	U- $O_{eq}$	2.39	6(1)	0.019
	U-C	2.93	1 <sup>*</sup>	0.002
	U-Fe	3.48	1	0.013
Fe2	U- $O_{ax}$	1.81	2	0.0018
	U- $O_{eq}$	2.39	4.4(6)	0.014
	U-C	2.93	1 <sup>*</sup>	0.002
	U-Fe	3.47	1	0.013
Fe3	U- $O_{ax}$	1.81	2	0.0028
	U- $O_{eq}$	2.36	5.9(8)	0.018
	U-C	2.93	1 <sup>*</sup>	0.001
	U-Fe	3.42	1.0(5)	0.0063

<sup>\*</sup>) N was held constant at the closest integer value determined in a fit to the  $k^2$ -weighted data.

Tab. 1: EXAFS structural parameters for uranyl sorbed onto ferrihydrite.

Based on the U-Fe interaction and the absence of a U-U interaction, we conclude that a mononuclear inner-sphere complex is formed at the ferrihydrite surface. Additionally, the EXAFS results show evidence of U-C/O interaction at 2.9 Å.

Future studies will determine if this interaction results from the formation of ternary surface complexes involving  $CO_3^{2-}$ .

### References

- /1/ Reich, T., et al.; J. Electron Spectroscopy Related Phenom. in press
- /2/ Waite, T.D., et al.; Geochim. Cosmochim. Acta **58**, 5465 (1994)

# EXAFS INVESTIGATIONS OF THE COMPLEXATION BEHAVIOR OF $\text{UO}_2^{2+}$ WITH MODEL COMPOUNDS OF PHENOLIC WOOD DEGRADATION PRODUCTS

A. Roßberg, T. Reich, C. Hennig, L. Baraniak, G. Bernhard, H. Nitsche

Uranium  $L_{III}$ -edge EXAFS was studied on the of aqueous uranyl complexes with protocatechuic acid (3,4-dihydroxy-benzoic acid, PCS), catechol (2-hydroxyphenol, BCT), pyrogallol (1,2,3-trihydroxybenzol, PYR), vanillin (4-hydroxy-3-methoxy-benzaldehyde, VAN), and with vanillic acid (4-hydroxy-3-methoxy-benzoic acid, VNS). The structural parameters of these uranyl complexes are compared and the influence of the phenolic hydroxy and carboxy groups on the uranyl(VI) binding is determined.

## Experimental

Baraniak et al. /1/ determined the complex formation constants of uranium(VI) with PCS, VAN and VNS. The complex formation constants of uranium(VI) with PYR and BCT are from /2/. The speciation of the complexes in absence of  $\text{CO}_2$  was calculated with the computer-program RAMESSES at 0.1M ionic strength ( $\text{NaClO}_4$ ) and 25 EC. The metal concentration was 1 mM  $\text{UO}_2(\text{ClO}_4)_2$  and the ligand concentrations for PCS, BCT, PYR and VAN were 50 mM. To avoid precipitation in the VNS solution, the metal concentration was 0.5 mM and the ligand concentration was 5 mM.  $\text{UO}_2^{2+}$  hydrolysis was included in the calculations. The U  $L_{III}$ -edge spectra of these complexes were measured at the HASYLAB beam line RÖMO II and at the SSRL beam line 4-1. Because of the low  $\text{UO}_2^{2+}$  concentration, the fluorescence signal was measured using a 4-pixel-germanium detector.

## Results and Discussion

### Uranyl complexes with PCS, BCT and PYR:

The EXAFS spectrum and the coordination parameters of the 1:3 uranyl BCT complex are identical with the EXAFS spectrum of the 1:3 uranyl PCS complex at pH 10 and comparable with the EXAFS spectrum of the 1:2 uranyl PYR complex at pH 8 (Fig. 1, Tab. 1).

Ligand(L), $\text{UO}_2^{2+}:\text{L}$	U-X equatorial				
	pH	Atom	R	$F^2 \cdot 10^{-3}$	N
PYR, 1:2	8.0	O	2.38	7	4.9
BCT, 1:3	10.0	O	2.37	6	5.7
PCS, 1:3	10.0	O	2.38	6	5.4
PYR, 1:1	4.8	O	2.40	7	4.8
BCT, 1:1	5.0	O	2.39	8	5.6
PCS, 1:1	4.3	O	2.46	6	4.8
		C	2.87	2	1.8
VNS, 1:1	4.1	O	2.44	5	4.8
VAN, 1:2	6.7	O	2.35	27.0	6.1
		U	3.88	1.2	1.4

Tab. 1: Fit results for the second coordination shells, (N - coordination number, R - radial distance in Å,  $F^2$  - Debye-Waller factor in Å<sup>2</sup>)

EXAFS results of the 1:1 uranyl PCS complex at pH 5 indicate that the carboxylic group coordinates in a bidentate fashion with the uranyl cation (Tab. 1). Structural elements of uranyl triacetate, detected by EXAFS spectroscopy /3/, are comparable to this 1:1 uranyl PCS complex. The EXAFS results shows that the carboxylic group from PCS is not involved in the complexation behavior at pH 10 and only the neighboring phenolic OH groups interact with the uranyl cation.

### Uranyl complexes with VAN and VNS:

The equatorial oxygen is not visible in the Fourier transform of the EXAFS spectra of the 1:2 uranyl VAN complex at pH 6.7 and a second coordination shell exist with uranium as backscatterer (Fig. 2). A destructive interference between equatorial oxygen with large different radial distances is not improbable. The long radial U- $\text{O}_{\text{eq}}$  distance in the 1:1 uranyl VNS complex at pH 4.1 indicates a bidentate coordination behavior of the ligand with the uranyl cation (Tab. 1).

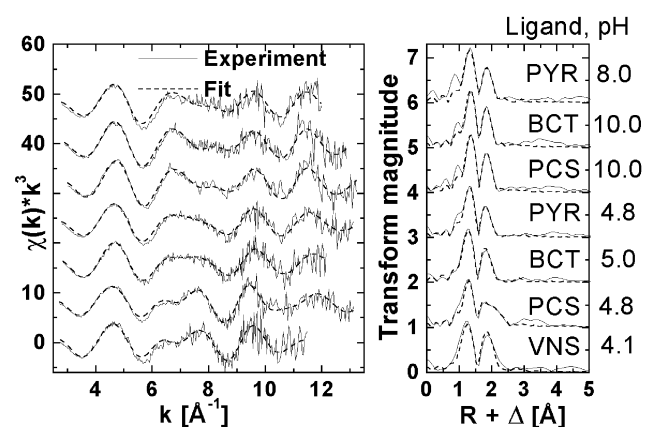


Fig. 1: Raw  $k^3$ -weighted EXAFS spectra of uranyl complexes

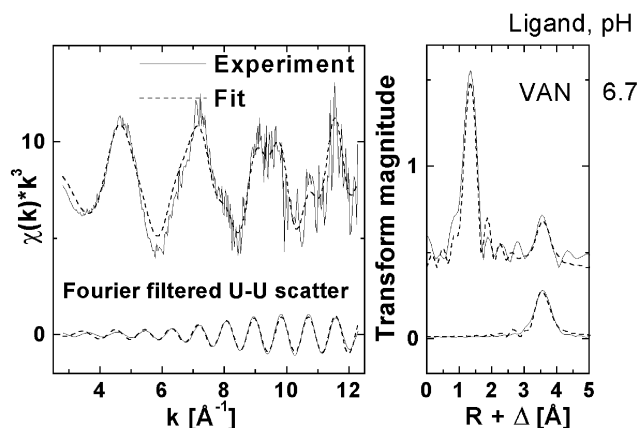


Fig. 2: Raw  $k^3$ -weighted EXAFS spectra with FT filtered U-U scatter from the VAN complex

## References

- /1/ Baraniak, L., et al.; Report FZR-180 (1997), p. 28
- /2/ Martell, A.E., et al.; *Critically Selected Stability Constants Of Metall Complexes Database Version 2.0*. Texas A & M University, (1995)
- /3/ Denecke, M.A., et al.; J. Phys. IV France 7, C2-637 (1997)

# EXAFS INVESTIGATIONS OF URANIUM COMPLEXES IN PLANT SAMPLES

A. Günther, A. Roßberg, T. Reich, G. Bernhard, H. Nitsche

We determined the structure of uranium complexes in various contaminated plant samples by EXAFS.

## Experiments

To investigate the chemical speciation on and in plant materials, uranium-containing aqueous solution was injected into selected roots and shoot axes of blue lupin and dandelion which were grown in uranium-containing solution. Then the plants and the appropriate pieces of plants were washed, dried and pulverized. EXAFS measurements were performed on beam line 4-1 at the Stanford Synchrotron Radiation Laboratory (SSRL). The samples were measured in fluorescence mode by a 4-pixel-Ge-fluorescence detector. The EXAFS spectra were analyzed according to standard procedures using the suite of programs EXAFSPAK and theoretical scattering phases and amplitudes calculated with the scattering code FEFF7/1/.

## Results

The sample treatment conditions and the results of the EXAFS study are listed in Tab.1 and shown in Figs. 1 and 2.

plant sample	U - O <sub>ax</sub>		U - O <sub>eq</sub>		
	R [D]	* [D <sup>2</sup> ]	N	R [D]	* [D <sup>2</sup> ]
blue lupin, root (A) <sup>1)</sup>	1.79	0.002	3.3	2.29	0.002
blue lupin, shoot axis (B) <sup>1)</sup>	1.80	0.001	3.2	2.30	0.003
dandelion, root (C) <sup>2)</sup>	1.78	0.002	5.1	2.36	0.013
dandelion, root (D) <sup>3)</sup>	1.80	0.001	3.9	2.36	0.009

<sup>1)</sup> 10<sup>-2</sup>M UO<sub>2</sub>(NO<sub>3</sub>)<sub>2</sub> solution injected

<sup>2)</sup> grown in UO<sub>2</sub>(CH<sub>3</sub>COO)<sub>2</sub> solution

<sup>3)</sup> grown in UO<sub>2</sub>(NO<sub>3</sub>)<sub>2</sub> solution

Tab.1: EXAFS structural parameters for samples A - D

In all samples, the first and second coordination shells were clearly identified as uranium-oxygen-coordination in axial (U-O<sub>ax</sub>) and equatorial (U-O<sub>eq</sub>) position. The equatorial U-O distance of the complexes formed in samples A and B is clearly smaller than that in samples C and D. The difference in the parameter sets may be due to the varying influence of the plant metabolism or/and the type of plants. Samples C and D have an equatorial coordination distance of 2.36D which is typical for a monodentate coordination of UO<sub>2</sub><sup>2+</sup> with carboxylic groups. The third coordination shell of the samples A and B is quite distinguished, but we cannot assign any physical meaning to it at this time.

One can assume direct sorption of uranium (VI) or complexation with metabolic or plant growth products /2/. Through EXAFS investigations of model compounds

with variously arranged functional groups and by comparing with the results obtained from the plant samples, it's possible to determine the ligands which are able to form complexes with uranium in or at the plants.

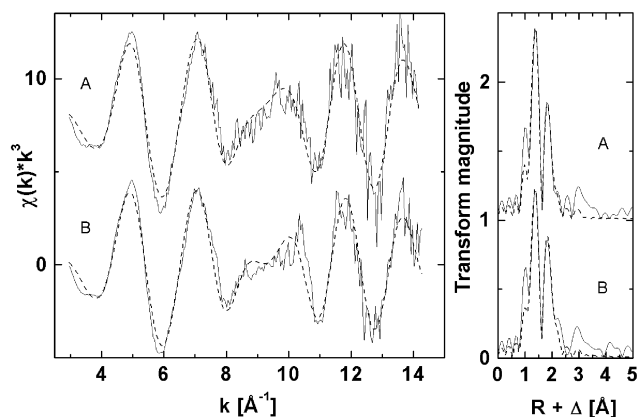


Fig. 1: Raw k<sup>3</sup>-weighted EXAFS-spectra of plants samples  
A) root, injected with 10<sup>-2</sup>M UO<sub>2</sub>(NO<sub>3</sub>)<sub>2</sub>-solution  
B) shoot axis, injected with 10<sup>-2</sup>M UO<sub>2</sub>(NO<sub>3</sub>)<sub>2</sub> solution  
---- Experiment - - - Fit

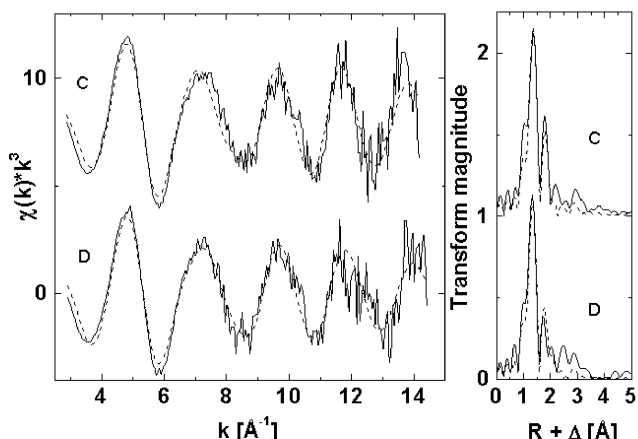


Fig. 2: Raw k<sup>3</sup>-weighted EXAFS-spectra of root samples  
C) root, plantgrown in 10<sup>-2</sup>M UO<sub>2</sub>(CH<sub>3</sub>COO)<sub>2</sub> solution  
D) root, plant grown in 10<sup>-2</sup>M UO<sub>2</sub>(NO<sub>3</sub>)<sub>2</sub> solution  
---- Experiment - - - Fit

## References

- Zabinsky, S.I., Rehr, J.J., Ankudinov, A., Albers, R.C., Eller, M.J.: Multiple-scattering calculations of x-ray-absorption. Phys.Rev. **B52**, 2995 (1995)
- Nultsch, W.: *Allgemeine Botanik*, Georg Thieme Verlag Stuttgart, New York, 1996



# CRYSTAL STRUCTURE COMPARISON OF URANYL ARSENATES USING EXAFS

C. Hennig, T. Reich, M. Rutsch, A. Roßberg, H. Funke, G. Geipel, G. Bernhard, H. Nitsche

The crystal structures of natural meta-zeunerite and synthetic hydrogen uranyl arsenate hydrate were compared using EXAFS spectroscopy. The different interlayer cations have no influence on the bond length in the uranyl arsenate layers.

## Experimental

First EXAFS measurements were taken on the new Rossendorf Beamline (ROBL) at the European Synchrotron Radiation Facility (ESRF) in Grenoble. The monochromator, equipped with a Si(111) water cooled double-crystal system, was used in the cancel-cut mode. Higher harmonics were rejected by Pt coated mirrors. U  $L_{III}$ -edge and As K-edge EXAFS spectra were collected in transmission. The Cu K-edge EXAFS spectrum was measured with a multichannel Ge fluorescence detector /1/. Two or three scans were obtained in transmission mode and 32 single accumulations were taken for the Cu K-edge fluorescence spectra. The measurements were carried out with a sample orientation of  $0^\circ$  and  $45^\circ$  to the beam direction to investigate the influence of polarization effects (not discussed here). For energy calibration of the uranium spectra, we used the first inflection point of Zr at 17996eV. The samples are natural meta-zeunerite from Wheal Basset, Cornwall, and hydrogen uranyl arsenate hydrate, prepared according to the literature /2/.

## Results

Uranyl arsenates like meta-zeunerite,  $\text{Cu}[\text{UO}_2\text{AsO}_4]_2 \cdot 8\text{H}_2\text{O}$ , and hydrogen uranyl arsenate hydrate,  $\text{H}[\text{UO}_2\text{AsO}_4] \cdot 4\text{H}_2\text{O}$ , are built of stable layers of  $[\text{UO}_2]^{2+}$  and  $[\text{AsO}_4]^{3-}$  units. The charge neutrality is achieved by different interlayer cations like  $\text{Cu}^{2+}$ ,  $\text{H}^+$  and  $\text{H}_3\text{O}^+$ . We used EXAFS measurements to compare the crystal structures. The results of the curve fitting to the  $k^3$ -weighted EXAFS data are shown in Figs. 1-3.

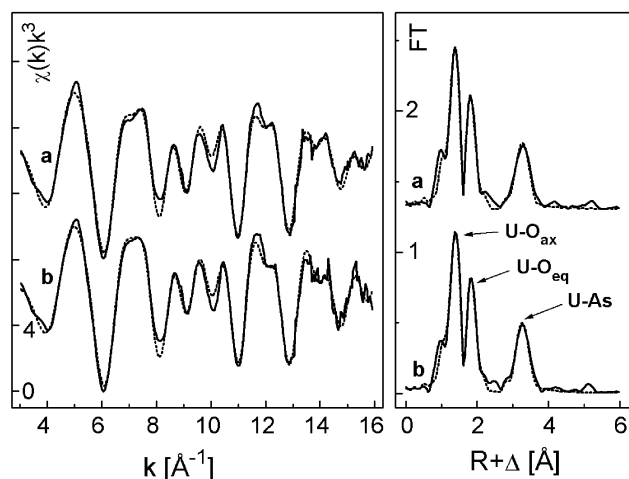


Fig. 1: U  $L_{III}$ -edge EXAFS spectra of  $\text{H}[\text{UO}_2\text{AsO}_4] \cdot 4\text{H}_2\text{O}$  (a), and  $\text{Cu}[\text{UO}_2\text{AsO}_4]_2 \cdot 8\text{H}_2\text{O}$  (b)

All figures show at the left the  $k^3$ -weighted EXAFS spectra and at the right the corresponding Fourier transforms, the solid lines are measured data, the dotted lines are calculated values. The first shell of the U  $L_{III}$ -edge EXAFS of meta-zeunerite (Fig. 1), represents

the axial oxygen atoms ( $\text{O}_{ax}$ ) at a distance of 1.79Å. The second shell corresponds to the equatorial atoms with a distance of 2.28Å, and the third shell originates from the arsenic atoms with a distance of 3.67Å. Using As as absorbing atom (Fig. 2), the As-U distance was confirmed to 3.68Å and the As- $\text{O}_{eq}$  distance was determined to 1.68Å. The measurements at two near-neighbor absorber atoms allows to calculate the bond angle U- $\text{O}_{eq}$ -As to  $135.34^\circ$ . The interlayer Cu-O distance in meta-zeunerite was measured by Cu K-edge EXAFS (Fig. 3) to 1.95Å. The EXAFS data of the uranyl arsenate layer on  $\text{H}[\text{UO}_2\text{AsO}_4] \cdot 4\text{H}_2\text{O}$  are quite similar within the error of 0.02Å. In conclusion, the uranyl arsenate layer structure is nearly independent from the interlayer cation arrangement. Furthermore, our investigation demonstrates the possibility to compensate the lost angle information in EXAFS using the radial distribution functions at various absorption edges.

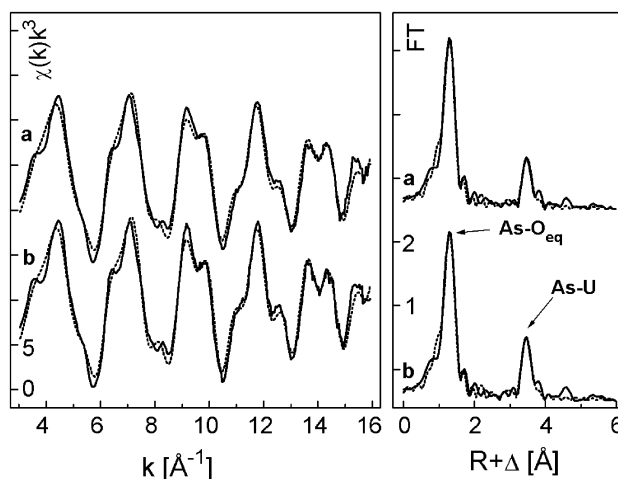


Fig. 2: As K-edge EXAFS spectra of  $\text{H}[\text{UO}_2\text{AsO}_4] \cdot 4\text{H}_2\text{O}$  (a), and  $\text{Cu}[\text{UO}_2\text{AsO}_4]_2 \cdot 8\text{H}_2\text{O}$  (b)

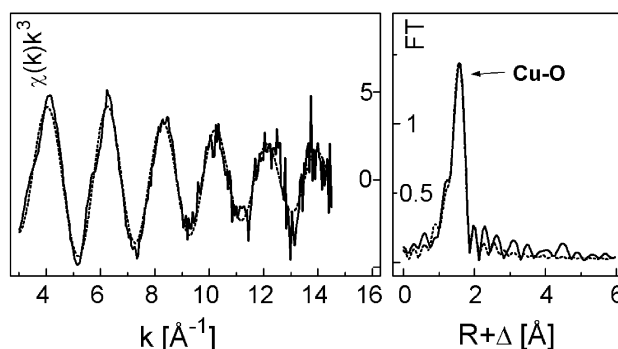


Fig. 3: Cu K-edge EXAFS spectrum of  $\text{Cu}[\text{UO}_2\text{AsO}_4]_2 \cdot 8\text{H}_2\text{O}$

## References

- /1/ Bucher, J.J., et al.; Rev. Sci. Instrum. **67**, 1 (1996)
- /2/ Weiss, A., et al.; Z. Naturforsch. **12b**, 669 (1957)

## COORDINATION GEOMETRY OF FERRIHYDRITE

C. Hennig, T. Reich, H. Funke, T. Arnold, H. Nitsche

EXAFS spectra on ferrihydrite show a preferred octahedral coordination in the first shell and a short range disorder in the second shell. The structural order in 6-line ferrihydrite is higher than in 2-line ferrihydrite.

### Experimental

The coordination geometry in ferrihydrite was studied by EXAFS measurements at the new Rossendorf Beamline (ROBL) at the European Synchrotron Radiation Facility (ESRF) in Grenoble. Iron K-edge EXAFS spectra were collected in transmission mode.

### Results

Ferrihydrite (FH) occurs during weathering processes of iron-containing rocks as a metastable compound which transforms into crystalline and stable goethite ( $\alpha$ -FeOOH) and/or hematite ( $\alpha$ -Fe<sub>2</sub>O<sub>3</sub>). FH precipitates from aqueous Fe(III) solutions in particles of various nanometer sizes. Differences of peak numbers in X-ray diffraction patterns lead to a distinction between two general FH structure types: the so-called 2-line (2L-FH) and the 6-line (6L-FH) ferrihydrite. The structural and genetic relationship between 2L-FH and 6L-FH is still under discussion. Several structural models have been suggested for FH based on similarities with hematite structure /1/. Therefore, we compared the EXAFS of 2L-FH and 6L-FH with hematite (Fig. 1).

tion of a preferred octahedral coordination geometry in FH. But the radial distribution function for the Fe-O in FH is broadened to higher R-values, which indicates additional longer Fe-O bonds. The Fe-O octahedra in hematite are connected about 1 face ( $R_{\text{Fe-Fe1}}=2.89\text{\AA}$ ), 3 edges ( $R_{\text{Fe-Fe2}}=2.97\text{\AA}$ ), 3 corners ( $R_{\text{Fe-Fe3}}=3.36\text{\AA}$ ) and 6 corners ( $R_{\text{Fe-Fe4}}=3.70\text{\AA}$ ) /2/. This coordination gives a splitting of the second feature in the EXAFS radial distribution function of hematite into two asymmetric peaks (Fig. 1a). It is difficult to isolate these bond distances by numerical fits. However, Fourier filtering shows, that the first peak corresponds to the 2.89Å and 2.97Å shells and the second peak results mainly from the 3.70Å shell including additional Fe-O distances. In contrast, the maximum of the second shell in FH is located at  $R^+=2.7\text{\AA}$  with a shoulder at  $R^+=3.0\text{\AA}$ , which gives after phase correction Fe-Fe distances of 3.1Å and 3.4Å. This is a significant difference to hematite. The lowered peak height in the EXAFS Fourier transform of FH results from a short range disorder. Therefore, in connection to the broadened Fe-O Fourier transformed peak, a simple octahedral coordination geometry is not expected. In contrast to hematite, preferred bond lengths of 3.1Å to 3.2Å are obtained. Only small differences are found between the EXAFS spectra of 2L-FH and 6L-FH. In the spectra of the 6L-FH, the peak height of the second shell is slightly increased in comparison to the 2L-FH. This is due to a lowering of the Debye-Waller factor and means that the structural ordering increases from 2L-FH to 6L-FH.

### Acknowledgments

We thank J. Friedl (TU München) for the preparation of the ferrihydrite samples.

### References

- /1/ Drits, V.A., et al.; Clay Min. **28**, 185 (1993)
- /2/ Blake, R.L., et al.; Am. Min. **51**, 123 (1966)

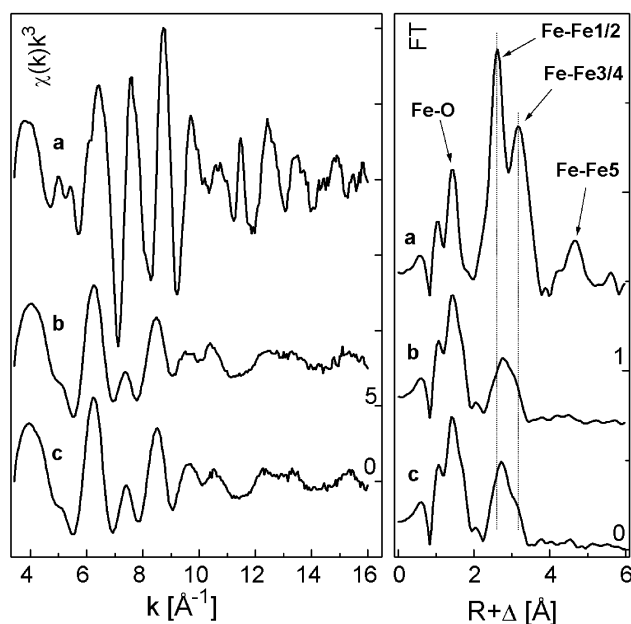


Fig. 1: Left  $k^3$ -weighted Fe K-edge EXAFS spectra of  $\alpha$ -Fe<sub>2</sub>O<sub>3</sub> (a), 2L-ferrihydrite (b) and 6L-ferrihydrite (c). Right: the corresponding Fourier transformed EXAFS. Only the measured spectra are shown here.

In hematite, the iron is octahedrally coordinated by oxygen. The first coordination shell includes two bonding distances: Fe-O1=1.94Å and Fe-O2=2.11Å /2/. These bond length differences are too small to be distinguishable by EXAFS. Ferrihydrite in comparison shows a very similar radial distribution function for the Fe-O distance and the coordination number. This leads to the assump-

# CHROMIUM(III) SULFATE - COLLAGEN INTERACTION: AN EXAFS-STUDY

T. Reich, A. Roßberg, C. Hennig, M.A. Denecke, G. Reich<sup>1</sup>  
<sup>1</sup> Forschungsinstitut für Leder- und Kunstledertechnologie, Freiberg

*First experimental evidence has been obtained for the cross-linking of collagen fibrils in leather due to the formation of binuclear chromium complexes.*

## Introduction

Chrome tanning of animal hides and skins for the production of high-quality leather is a well established industrial process. About 90% of the leather produced worldwide is chrome tanned. Therefore, an understanding of the multistep process whereby complex salts of trivalent chromium cross-link collagen fibrils is of great interest.

From a theoretical point of view it has been confirmed that the cross-linking effect is based on the formation of a bi- or polynuclear chromium complex bound to the carboxylate side chains of asparaginic and glutaminic acids /1/. Computer modeling /2, 3/ showed that such a reaction should be possible at an intrafibrillar level. Up to now there has been no direct evidence that such a postulated mechanism takes place in leather.

## Experimental

We measured Cr K-edge EXAFS spectra in transmission mode at 20 K of the following samples using the Si(111) double-crystal monochromator EXAFS II at the Hamburger Synchrotronstrahlungslabor (HASYLAB): chromium alum (solid 1 and 0.2 mol Cr/L solution 2), a technical chrome tanning agent (solid 3 and 0.2 mol Cr/L solution 4 of a 33% basic chromium sulfate „Chromosal”), chrome leather 5, and gelatin 6, both treated with "Chromosal". The chrome leather was tanned with an offer of 1.5% Cr<sub>2</sub>O<sub>3</sub> per pelt weight, intensively washed and acetone dehydrated. The gelatin was „tanned” with different offers of Cr<sub>2</sub>O<sub>3</sub>. The aim of our EXAFS experiments was to determine the structural parameters of the chromium near-neighboring environment and to see whether a Cr-Cr interaction indicative of binuclear complexes is present.

## Results and Conclusions

The EXAFS structural parameters of the leather sample 5 are given in Tab. 1.

The first coordination shell consists of six oxygen atoms surrounding the chromium atom at a distance of 1.98±02 Å. The second coordination shell corresponds to one chromium atom at a distance of 2.97±02 Å from the absorbing chromium atom. The detection of one Cr-Cr interaction at 2.97 Å is direct evidence of the presence of a binuclear chromium complex in the leather sample.

Tab. 1 compares the obtained EXAFS structural parameters with values measured for the dimeric unit (H<sub>2</sub>O)<sub>4</sub>Cr(μ-OH)<sub>2</sub>Cr(OH)<sub>2</sub>)<sub>4</sub><sup>4+</sup> 7 in a crystalline salt by XRD /4/. Our structural parameters are in excellent agreement with the interatomic distances measured by XRD for the binuclear complex.

The Cr-Cr distance of 2.97 Å in leather is also in good

agreement with the value of 2.71 Å obtained by computer modeling /2,3/. Our results confirm the assumptions from computer modeling and are in so far the first experimental proof of the common opinion about chromium complex binding on collagen in leather.

Sample	O			Cr		
	N	R(Å)	σ <sup>2 a)</sup>	N	R(Å)	σ <sup>2 a)</sup>
<u>1</u>	5.6	1.97	1.7	-		
<u>2</u>	6.3	1.98	3.8	-		
<u>3</u>	5.6	1.97	2.7	2.0	3.07	0.9
<u>4</u>	6.0	1.97	3.8	0.7	3.00	0.5
<u>5</u>	6.0	1.98	3.2	1.2	2.97	0.4
<u>6</u>	5.9	1.98	3.2	1.2	2.97	0.4
<u>7</u>	6	1.97 <sup>b)</sup>	-	1	3.00	-

a) σ<sup>2</sup> in units of 10<sup>-3</sup> Å<sup>2</sup>, b) average value of 2 x 1.94 Å and 4 x 1.98 Å calculated using XRD results /4/

Tab. 1: EXAFS data of samples 1-6 compared with XRD data of sample 7 /4/

Additional conclusions can be drawn from the EXAFS structural parameters given in Tab. 1.

- 1) Chromium alum both as solid 1 and in solution 2 does not show evidence of a Cr-Cr interaction and therefore exists as a mononuclear chromium complex.
- 2) In solid Chromosal 3, the coordination number for the Cr-Cr interaction at 3.07 Å is two. Therefore, solid Chromosal is polynuclear. In solution 4 the Cr-Cr coordination number is approximately one, indicative of a binuclear chromium complex.
- 3) The same mechanism of cross-linking as in leather occurs in gelatin 6 notwithstanding the complete other structural conditions.

In conclusion, the first examples given here show how EXAFS as a modern and highly sophisticated method can contribute to elucidate the chrome tannage mechanism at a molecular level.

## References

- /1/ Heidemann, E.: *Fundamentals of Leather Manufacturing*. E. Roether KG, Darmstadt 1993
- /2/ Fennen, J.; Soc. Leather Technologists and Chemists **82**, 51 (1998)
- /3/ Buttar, D., et al.; J. Amer. Leather Chemists Ass. **92**, 185 (1997)
- /4/ Spiccia, L., et al.; Inorg. Chem. **26**, 474 (1987)

# TEXTURE ANALYSIS OF POWDER SAMPLES USING THE RIETVELD METHOD

C. Hennig, W. Kraus<sup>1</sup>, G. Nolze<sup>1</sup>

<sup>1</sup> Federal Institute for Materials Research and Testing, Unter den Eichen 87, D-12205 Berlin

*Texture in powder samples influences polarization dependent EXAFS measurements. The Rietveld method was used to analyze the texture of such powder samples.*

Many EXAFS measurements are carried out on polycrystalline samples. It is known that powdered samples are characterized by a more or less strong texture caused by an axial pressure during sample preparation. Due to the polarized synchrotron radiation, this leads to an incorrect determination of the coordination number  $N_j$ , in particular for compounds with an anisotropic coordination center. Exemplarily, a strong polarization dependence can be detected in EXAFS spectra for oriented single crystals containing a uranyl coordination center [1]. The effect of the preferred orientation in EXAFS measurements on powder samples using linear polarized synchrotron radiation will be shown for polycrystalline uranyl phosphate. The effect in EXAFS measurements is demonstrated by an angle variation between the beam direction  $\underline{k}$  respective to the sample normal vector  $\underline{n}$  about  $\beta=45^\circ$  and  $0^\circ$ . A strong difference at the Fourier transform (FT) peak height is obtained by coarse-grained powder of  $\text{Ba}[\text{UO}_2\text{PO}_4]_2 \cdot n\text{H}_2\text{O}$  in boron nitride (Fig. 1).

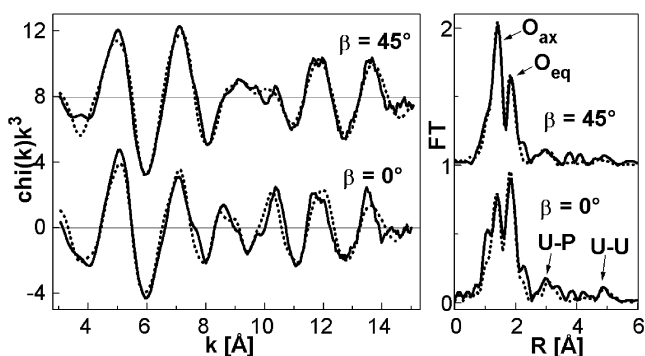


Fig. 1: Left  $k^3$ -weighted U  $L_{III}$ -edge EXAFS spectra of  $\text{Ba}[\text{UO}_2\text{PO}_4]_2 \cdot n\text{H}_2\text{O}$  and right: the corresponding Fourier transformed EXAFS. The solid line is the experimental data, and the dashed line represents the theoretical fit of the data.

The amplitude function of the EXAFS formula describes this polarization dependency with the term

$$N_j^{\text{eff}} = 1/2 N_j (1 + 3 \cos^2 2_j) \quad (1)$$

where  $2_j$  is the angle between the polarization vector  $\underline{g}$  of the synchrotron radiation and the interatomic vector  $\underline{l}$  between the absorber and backscatterer. For simplification, this term is often set to 1, which is strictly only correct for perfect statistics. Especially the exact calculation of the coordination number  $N_j$  is difficult because of its strong correlation with the Debye-Waller factor. Additional difficulties will be caused by an anisotropic orientation distribution of the crystallites in powder samples. A way to determine this texture is to use X-ray diffraction measurements. One of the commonly used descriptions of a simple preferred orientation is given by March and Dollase [2]. There, the preferred orientation is characterized by a single vector and the degree of preferred ori-

entation:

$$I_{\text{corr}} = I_{\text{str}} (G^2 \cos^2 \theta_k + G^{-1} \sin^2 \theta_k)^{-2/3} \quad (2)$$

For a given reflection  $hkl$ , this formula describes the relation between the corrected intensity  $I_{\text{corr}}$  and the integral intensity  $I_{\text{str}}$  resulting from well-known crystal structure data.  $I_{\text{str}}$  will be corrected by the preferred orientation in dependence of the orientation parameter  $G$  and the angles  $\theta_k$  between the scattering vectors  $\underline{H}_k$  of all symmetry-equivalent lattice planes and the preferred orientation vector  $\underline{H}_p$  assumed as lattice vector. In contrast, the orientation parameter  $G$  is valid for all reflections and must be fitted in a special refinement procedure. The March-Dollase function can be used in Rietveld refinement calculations [3]. As an example, the 2/22 diffraction pattern is obtained on a  $\text{Cu}[\text{UO}_2\text{PO}_4]_2 \cdot n\text{H}_2\text{O}$  sample with 200 mg h-BN.

The experimental and calculated diffractograms are shown in Fig. 2. These calculations give a preferred orientation  $\underline{H}_p$  of 001 and an orientation parameter  $G$  of 0.53. Both the preferred orientation vector  $\underline{H}_p$  and the orientation parameter  $G$  should be introduced as additional amplitude correction terms in the calculation of polarization sensitive EXAFS measurements on powder samples.

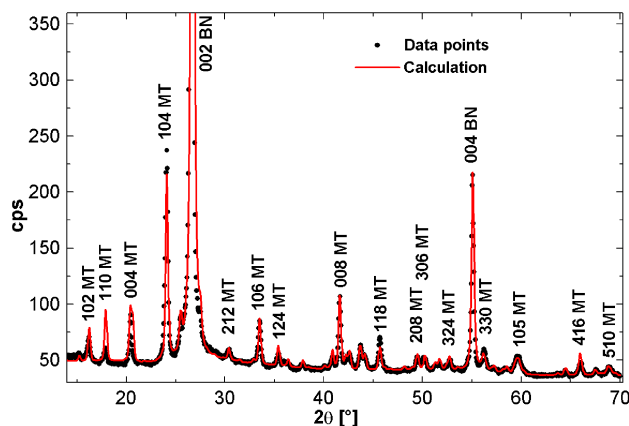


Fig. 2: Experimental and calculated X-ray diffractograms of  $\text{Cu}[\text{UO}_2\text{PO}_4]_2 \cdot n\text{H}_2\text{O}$ , metatorbernite (MT), and boron nitride (BN) in a pellet sample (Cu-K $\alpha$  radiation) with  $hkl$  indices.

## Acknowledgments

This work was supported by a NATO Collaborative Research Grant. We thank W. Matz for measuring time at the X-ray diffractometer.

## References

- /1/ Hennig, C., et al.; Z. Krist. Suppl. **15**, 156 (1998)
- /2/ Dollase, W.A.; J. Appl. Cryst. **19**, 267 (1986)
- /3/ Rietveld, H.M.; J. Appl. Cryst. **2**, 65 (1969)

# **Behavior of Colloids and Aerosols**

## DYNAMIC LIGHT SCATTERING ON FILTERED HUMIC ACID SOLUTIONS

H. Zänker, G. Hüttig, M. Böttger, H. Nitsche

PCS demonstrates that two out of four particle classes observed by SFM are existing also in solution: submicron chunks and the humic acid molecules. This is in contrast to the micelle hypothesis.

Two hundred ppm solutions of purified Aldrich humic acid were investigated by photon correlation spectroscopy (PCS). In /1/ we had shown that scanning force microscopy (SFM) on deposits obtained by spin-coating of such solutions on freshly cleaved mica yields four particle classes with the following spherical equivalent diameters:

Submicron chunks (Class 1):	100 to 150 nm
Elongated agglomerates (Class 2):	30 to 40 nm
Disk-like agglomerates (Class 3):	10 to 25 nm
Subunits (Class 4):	1.5 to 8 nm.

The aim of our light scattering experiment was to elucidate which of these objects found on the mica are representative of states in solution and which are only formed on the substrate during the spin-coating process. Particle Class 1 can be classified relatively easy as to exist also in aqueous solution. These particles show physico-chemical properties different from those of the other particle classes: they are chemically inert, i. e., they do not change when humic acid concentration or solution pH are changed. Fig. 1 shows particles of the remaining classes: elongated agglomerates (Class 2) and disk-like agglomerates (Class 3) that consist of small subunits (Class 4). If the concentration of the

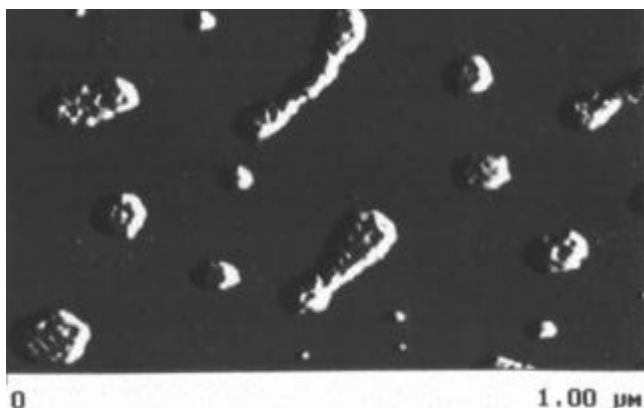


Fig. 1: SFM image of spin-coated humic acid. Height of the deposits: 1.5 to 2 nm.

humic acid solution is low enough, the subunits appear in their fully disintegrated state (not shown in Fig. 2; see /1/). We classify the subunits as the humic acid molecules. The still open question was if the Class 2 and Class 3 agglomerates exist in solution or if the original humic acid solution consists of the individual molecules. PCS on the unfiltered solutions gives particle sizes of 100 to 150 nm, i. e., PCS finds exclusively the submicron chunks (Class 1). This is because the smaller particles are optically masked by the chunks, although these chunks provide only about 10 % of the humic acid material. The idea was to investigate the humic acid solution after removing the disturbing submicron chunks. Fig. 2a shows an example of the autocorrelation functions obtained on a 1000-nm filtrate whose deconvolution yields the 100- to 150-nm particles. The shape of the autocorrelation function changes com-

pletely after the filtration through the 50-nm filter (Fig. 2b).

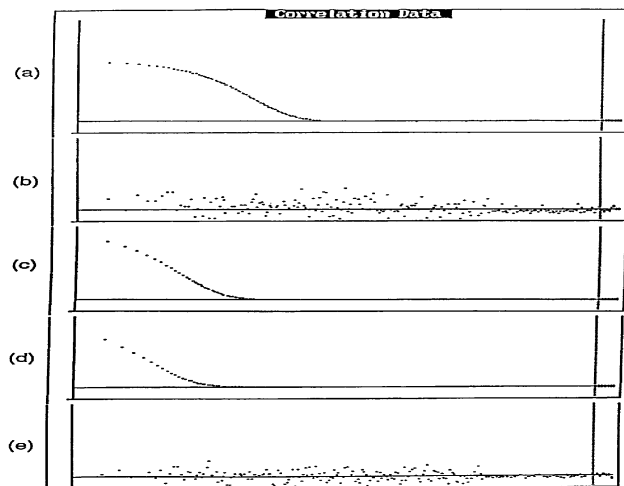


Fig. 2: Autocorrelation functions. Ordinate: autocorrelation function,  $C(J)$ ; abscissa: delay time,  $J$  (range 5  $\mu$ s to 1 s). (a) 1000-nm filtrate of humic acid. (b) 50-nm filtrate of humic acid. (c) 28-nm polystyrene latex particles. (d) 12-nm silica particles. (e) Toluene.

The deconvolution of this autocorrelation function, however, is not possible for mathematical reasons: the decay is much too small compared to the quality of the counting statistics. Nevertheless, the upper limit of the particle size can be deduced indirectly from PCS measurements on suspensions of standard particles. Figs. 2c to 2e show the results for 28-nm and 12-nm particles, and for toluene. The autocorrelation function of the 50-nm filtrate is different from those of the 28-nm and the 12-nm standard particles and resembles the autocorrelation function of pure toluene, a Rayleigh scatterer that consists of particles (molecules) of less than 1 nm. We conclude that the humic acid particles in the 50-nm filtrate must be significantly smaller than 12 nm. It follows that the elongated and the disk-like particles (Classes 2 and 3) do not exist in solution. The Class 2 and 3 particles result from agglomeration processes during the deposition on the mica surface. Thus, the particles representative of the aqueous solution are the chemically inert submicron chunks and the humic acid molecules. Several authors (see, e. g. /2/) hypothesized that micelles are formed in humic acid solutions. Micelles react very sensitively to changes in the solution conditions. Our experiment does not support the micelle hypothesis (for humic acid concentrations # 500 ppm).

### References

- /1/ Zänker, H., et al.; Photon Correlation Spectroscopy and Scanning Force Microscopy on Humic Acid. In: Report FZR-218, p. 78, (1997)
- /2/ Skytte Jensen, B., et al.; *The Role of colloids in the migration of radioelements*. Report EUR 16763 EN, 1996.

# MIGRATION BEHAVIOR OF URANIUM IN A HUMIC-COLLOIDS-RICH AQUIFER SYSTEM: LABORATORY STUDIES WITH COLUMN EXPERIMENTS

S. Pompe, R. Artinger<sup>1</sup>, K. Schmeide, K.H. Heise, J.I. Kim<sup>1</sup>, H. Nitsche  
<sup>1</sup> Forschungszentrum Karlsruhe, Institute of Nuclear Waste Management

We investigated the migration behavior of uranium in a sandy aquifer system rich in humic substances as a function of uranium/groundwater equilibration time, groundwater flow velocity and column length. The results show that the migration of uranium is strongly influenced by kinetically controlled processes.

We used a pleistocene aeolian quartz sand and groundwater GoHy-532 (DOC: 29.9 mg C/L; pH 7.2±0.1; Eh: -220 mV) from Gorleben /1/ to study the migration behavior of uranium in a sandy aquifer system rich in humic substances. The column experiments were performed in a glove box with equilibrated columns under anaerobic conditions (Ar + 1% CO<sub>2</sub>). <sup>232</sup>U(VI) (<sup>232</sup>UO<sub>2</sub>Cl<sub>2</sub>: 4·10<sup>-7</sup> - 5·10<sup>-7</sup> mol/L) was used as tracer. Tritiated water (HTO) was also applied as conservative tracer to determine the hydraulic properties of the columns. The experiments were performed as a function of the <sup>232</sup>U/groundwater equilibration time before injection into the column, the flow velocity and the column length. Due to the low Eh value of the groundwater one cannot exclude that U(VI) is reduced to U(IV) during the experiment. The experimental parameters and the results of the experiments are summarized in Tab.1.

Exp. No.	Equilibration time [d]	Column length [cm]	Flow velocity [m/d]	Recovery <sup>a</sup> [%]	R <sub>f</sub> <sup>b</sup>
1	0.04	25	0.32	0.4±0.1	0.97
2	0.62	25	0.31	1.4±0.3	0.97
3	11	25	0.31	3.4±0.8	0.96
4	82	25	0.31	7.8±2.0	0.96
5	5	25	2.03	6.5±1.6	0.95
6	6	25	0.04	1.6±0.4	0.97
7	5	50	0.24	2.5±0.6	0.97
8	5	75	0.24	2.1±0.5	0.96

<sup>a</sup>humic colloid-borne <sup>232</sup>U; <sup>b</sup>retardation factor R<sub>f</sub> (± 0.01)

Tab. 1: Experimental conditions and results

From the R<sub>f</sub> values in Tab. 1 and the breakthrough curves depicted in Fig. 1, we can conclude that a part of

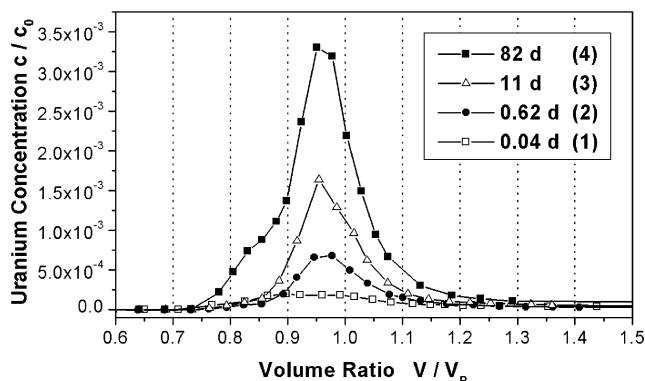


Fig. 1: <sup>232</sup>U breakthrough curves in dependence on <sup>232</sup>U/groundwater equilibration time (1-4: number of experiment).

the injected <sup>232</sup>U migrates slightly faster than groundwater (HTO: R<sub>f</sub> = 1). The observed migration behavior can be explained that a fraction of the <sup>232</sup>U is associated with humic colloids, which move faster due to size exclusion processes. The colloid-borne transport of <sup>232</sup>U was also confirmed by ultrafiltration experiments. This phenomenon was observed earlier in americium migration experiments /1/. The recovery of humic colloid-bound transported <sup>232</sup>U increases with increasing equilibration time before injection into the column (Fig. 1, Tab. 1).

This fact suggests that <sup>232</sup>U is bound stronger to humic colloids with increasing equilibration time and, therefore, less available for interaction with the sediment. The recovery of colloid-borne non-retarded <sup>232</sup>U decreases with decreasing groundwater flow velocity and increasing column length, i.e., increasing residence time in the column (Fig. 2, Tab. 1).

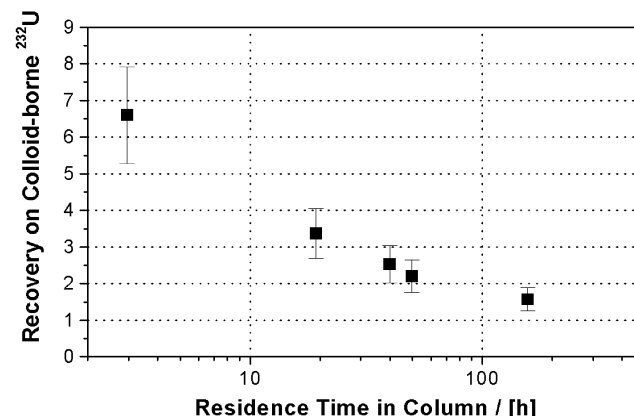


Fig. 2: Recovery of <sup>232</sup>U bound on humic colloids in dependence on the residence time in the column.

This dependence may be due to a time-dependent dissociation of uranium from the humic colloids and sorption onto the sediment surface.

The results of the column experiments show that some of uranium migrates humic colloid-bound up to 5 % faster than water in a groundwater/sediment system that is rich in humic substances. The migration behavior of uranium is strongly influenced by kinetically controlled processes, such as association of uranium onto and dissociation of uranium from humic colloids.

## Acknowledgments

This work was supported by the Bundesministerium für Bildung, Forschung und Technologie (BMBF) under contract number 02 E88150.

## References

/1/ Artinger, R., et al.; J. Contam. Hydrol., accepted

# CHARACTERIZATION OF COLLOID PARTICLES IN MINING WATER (ROTSCHÖNBERGER STOLLN)

W. Richter, H. Zänker, H. Nitsche

**Abstract:** Measurements in a mining water of the Erzgebirge proved that water contains approximately 1 mg/L colloid particles. These submicron particles were characterized by photon correlation spectroscopy (PCS), scanning electron microscopy (SEM) and ICP-MS/AAS.

## Experimental

Water from the mouth of the Rothschönberger Stolln /1/ was filtered through filters of varying pore size to characterize submicron particles. The filtrates were investigated by PCS (BI-90 from Brookhaven Instruments Corp.) and by ICP-MS and/or AAS (Perkin Elmer) to analyze the particle size distribution and the concentration of cationic elements, respectively. The dried filters were weighed, coated with carbon and examined by SEM with energy dispersive X-ray analysis (EDX).

## Results

The gravimetric analysis of the filter cake revealed that the colloid concentration in the drainage water amounts to about 1 mg/L. According to the elemental analysis by ICP-MS/AAS of the filters and the filtrates, the elements Fe, Al, As, Pb, and Cu are colloid-borne /1/. The elements Mg, Si, Ca, Mn, Zn, Cd, Sn, U, pass through all filters and are consequently ionic. The measurement of the particle size distribution by PCS is intricate for natural waters because of the strong dependence of the scattered light intensity on the particle radius ( $r^6$  dependence) /2/. Due to this relation, large particles should be removed by filtration (5  $\mu\text{m}$  filter) prior to PCS measurement. Fig.1 shows a typical PCS result of the 5  $\mu\text{m}$  fil-

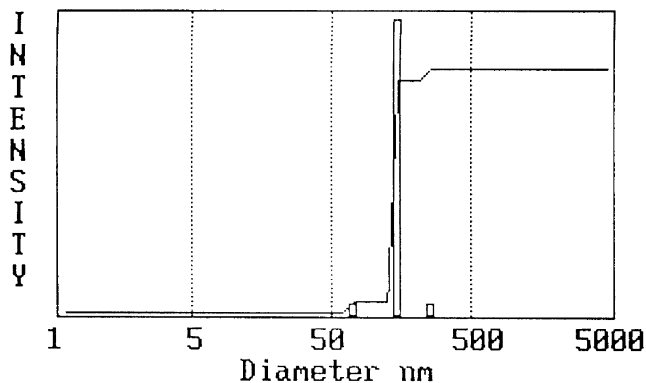


Fig. 1: Typical PCS particle size distribution of a water from Rothschönberger Stolln. Prefiltration through a 5  $\mu\text{m}$  filter. Particles were found in a range from 100 to 300 nm with the light intensity peak at 180 nm.

trate. The presence of particles of about 180 nm in diameter is obvious. Fig. 2 gives a scanning electron micrograph of the deposits on the 5  $\mu\text{m}$  filter that confirms the existence of particles of the size range of 100 to 300 nm found by PCS. They are arranged on the filter in the form of agglomerates of several  $\mu\text{m}$ . These agglomerates are probably formed during the filtration caused by self-coagulation of colloids on the membrane's surface /3/. PCS shows that the micron-sized agglomerates do not exist in solution. The filtered particles were further characterized by detailed EDX investigations. Fig. 3 shows an EDX-spectrum of an agglomerate of typical

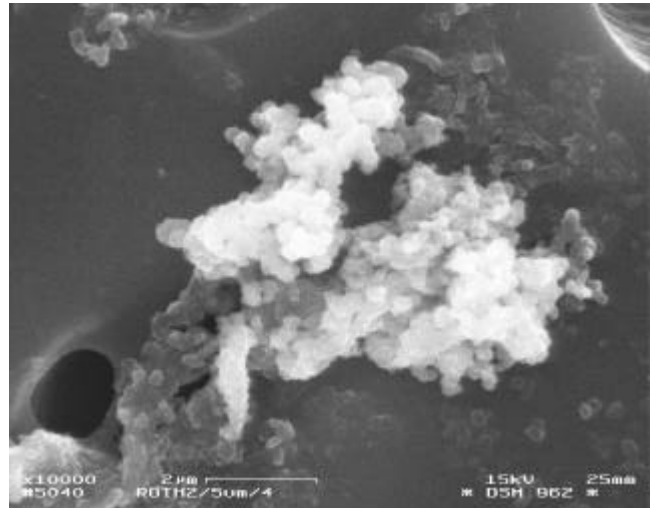


Fig. 2: SEM micrograph of a particle agglomerate on a 5  $\mu\text{m}$  Nuclepore filter

particles depicted in Fig. 2. Corresponding to the results of ICP-MS/AAS /1/, the elements Fe and Al are the main constituents of the oxidhydroxide colloid particles. This Fe-Al matrix contains adsorbed trace elements like Pb, Cu, and Zn. The high carbon peak in Fig. 3 is caused by the filter surface and is thus an artifact.

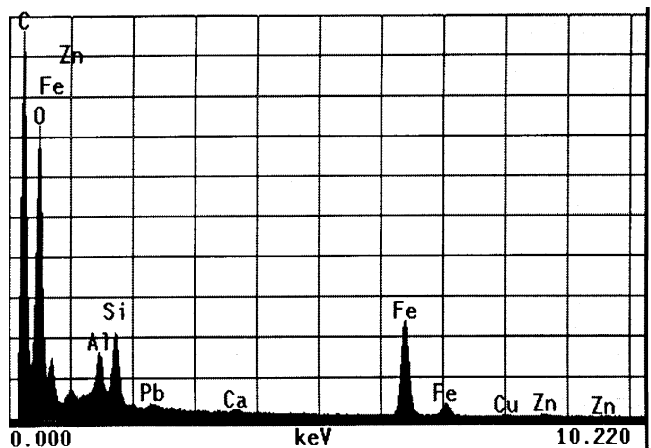


Fig. 3: EDX-Spectrum of the particle agglomerate in Fig. 2

## Acknowledgments

The work has been partly funded by the Deutsche Forschungsgemeinschaft.

## References

- /1/ Zänker, H., Brendler, V., Richter, W., Nitsche, H.: this report p.62
- /2/ Schurtenberger, P., Newman, M.E.: Characterization of Biological and Environmental Particles Using Static and Dynamic Light Scattering. *Environmental Particles*, Vol. 2, p. 37, Lewis Publishers (1993)
- /3/ Buffle, J., Leppard, G.G.: *Environ. Sci. Technol.* **29**, 2176 (1995)



# COLLOID-BORNE HEAVY METALS IN THE WATER OF A MINING DRAINAGE GALLERY (ROTSCHÖNBERGER STOLLN)

H. Zänker, V. Brendler, W. Richter, H. Nitsche

The colloid-borne heavy metals in the water of a mining drainage gallery are distinguished from the dissolved ones. The experiment demonstrates how EQ6 calculations can be made more realistic.

The Rothschönberger Stolln is the main drainage gallery of the Freiberg (Saxony) abandoned mining area. The water at its mouth contains about 1 mg/L of colloidal particles with a size of 75 to 300 nm /1/. We tested 25 elements for their colloidal/non-colloidal states in the drainage water by filtration/ultrafiltration through filters of varying pore size and by centrifugation at varying centrifugal forces. Tab. 1 gives a comparison between the concentrations of several components in the raw water and in the 3-kD (about 1-nm) ultrafiltrate. The results show that the elements Fe, Al, As, Pb, and Cu are colloid-borne. They also show that the colloids consist obviously of a Fe-Al matrix that contains certain trace elements. This was confirmed by using filters of larger pore size (50-nm filters) and by centrifugation experiments.

Component	Concentration [Mol/L]	
	Raw Sample	3-kD Filtrate
Fe	1.5 · 10E-05	< 1.8 · 10E-07
Al	1.1 · 10E-05	1.6 · 10E-07
Pb	1.2 · 10E-07	< 2.4 · 10E-09
As	2.0 · 10E-07	< 1.3 · 10E-08
Cu	6.0 · 10E-07	1.2 · 10E-07
Zn	7.4 · 10E-05	5.0 · 10E-05
Mg	1.1 · 10E-03	1.1 · 10E-03
Ca	2.7 · 10E-03	2.7 · 10E-03
Si	1.9 · 10E-04	2.0 · 10E-04
Cd	2.6 · 10E-07	2.2 · 10E-07
U	7.0 · 10E-09	7.5 · 10E-09
Mn	4.2 · 10E-05	4.3 · 10E-05
Sulphate	3.65 · 10E-03	na
Carbonate	1.75 · 10E-03	na

na: not analyzed

Tab. 1: Results of ICP/MS, AAS and Ion Chromatography on the Raw Water and on the 3-kD Ultrafiltrate

Tab. 2 presents the results of calculations with the geochemical code EQ6 for the raw sample analysis given in Tab. 1. EQ6 predicts that the chemical compounds in column 1 of this table are oversaturated.

Product	Amount of Precipitate [Mol/L]		
	Results without exclusions	Results after exclusion on all high-temperature Phases	Results after exclusion of all Si and Mn species
Cerussite (PbCO <sub>3</sub> )	3.7 · 10E-08	3.7 · 10E-08	3.7 · 10E-08
CoFe <sub>2</sub> O <sub>4</sub>	3.1 · 10E-07	-	-
Diaspore (" -AlOOH)	8.7 · 10E-06	8.6 · 10E-06	1.1 · 10E-05
Nontronite-Ca (Ferri-Montmorillonite)	7.0 · 10E-06	7.4 · 10E-06	-
Pyrolusite (\$-MnO <sub>2</sub> )	4.2 · 10E-05	4.2 · 10E-05	-
Quartz	6.2 · 10E-05	6.1 · 10E-05	-
Rutil (TiO <sub>2</sub> )	1.0 · 10E-07	-	-
Hematite (Fe <sub>2</sub> O <sub>3</sub> )	-	-	7.4 · 10E-06

Tab. 2: Oversaturated Species in the Drainage Water According to EQ6

However, high-temperature phases such as rutil and CoFe<sub>2</sub>O<sub>4</sub> are very unlikely to occur because the colloid formation process in the Rothschönberger Stolln is the precipitation of heavy metal oxidhydroxides due to changes of the oxygen content and the pH. When these

phases are excluded, the substances in column 2 are identified as oversaturated. Given our experimental results, however, the EQ6 calculations shown in column 2 must be further corrected. In column 3 the undissolved species of Si and Mn are also excluded because Si and Mn proved to be non-colloidal in the experiment. The erroneous calculations for Si and Mn are obviously attributable to insufficient consideration of the kinetics in the chemical model. Under the colloid formation conditions of the Rothschönberger Stolln (precipitation of secondary minerals), the system is far from its thermodynamic equilibrium. Thus, the equilibrium solubility of nontronite-Ca or quartz, for instance, is probably not solubility-determining for Si. Natural waters often show stable silica concentrations of 5 @ 10<sup>-4</sup> Mol/L or even more governed by the solubility of amorphous silica /2/. For Fe and Al, too, the calculations underestimate the solubility. They predict the presence of the thermodynamically most stable compounds, i. e., of hematite and diaspore. However, the precipitation of these products is kinetically hampered; their formation proceeds via intermediates such as ferrihydrite, goethite, gibbsite or boehmite. Nevertheless, the error is negligible in this case because the solubility of these intermediates is also extremely low. This does obviously not apply to Mn. Here, the calculations result in the formation of pyrolusite. A fresh precipitate of Mn(II) in the presence of oxygen, however, does not consist of pyrolusite; the formation of hausmannite (Mn<sub>3</sub>O<sub>4</sub>), feiticnechtite (\$-MnOOH) etc. that rapidly age to (-MnOOH is to be expected /3/. These products are still non-colloidal at the Mn concentrations given. The comparison between the model calculations and the experiment also allows conclusions on the binding states of typical toxicants onto the colloids. Oversaturated and, thus, actual sources of colloids are only the toxicants Al and Pb. As and Cu are not oversaturated. Their colloidal behavior is exclusively attributable to the adsorption onto existing colloidal particles (pseudocolloids). The experiment demonstrates how EQ6 calculations applied to a real geochemical problem can be made more realistic.

## Acknowledgments

This work has been partly funded by the Deutsche Forschungsgemeinschaft.

## References

- /1/ Richter, W., Zänker, H., Nitsche, H.: this report p.61
- /2/ Iler, R.K.: *The chemistry of Silica*. John Wiley & Sons, 1979
- /3/ De Vitre, R.R., Davison, W.: Manganese Particles in Freshwaters. *Environmental Particles* (ed. J. Buffle, H.P. van Leeuwen) Vol. 2. p. 317. Lewis Publishers, 1993

# ROTSCHÖNBERGER STOLLN: MODELING OF REACTION PATHWAYS WITH EQ3/6

V. Brendler, H. Zänker, W. Richter

We modeled the development of speciation patterns in the gallery "Rothschönberger Stolln" with the reaction path option of the EQ3/6 speciation software. The reducing environment at the origin of the gallery changes to oxidizing conditions at its junction into an open river system. The calculated uranium speciation was compared with analytical results from test samples.

## Methodology

The gallery "Rothschönberger Stolln" is the main drainage of the mining area around Freiberg / Saxony. It collects drainage and surface waters of various origin. After a distance of 13.5 km, the outflow to a tributary of the river Elbe is reached. In connection with the investigation of colloids (see previous article), the change in composition of both the aqueous phase and the accompanying minerals along the flow path was also of interest. To obtain further insights into basic processes, the reaction-path modeling feature of the geochemical speciation software EQ3/6 /1/ was utilized. Another aim was to find explanations of the pH-dependence of uranium sorption in such waters.

The basic model setup for the water composition at the mouth of the gallery with regard to the presence of various minerals was explained in the previous article. There also a summary of the analytical results and the filtering experiments is given.

## Results

A pH scan for the uranium distribution (with EQ3NR and a revised COM thermodynamic data base) produced the speciation patterns shown in Figure 1.

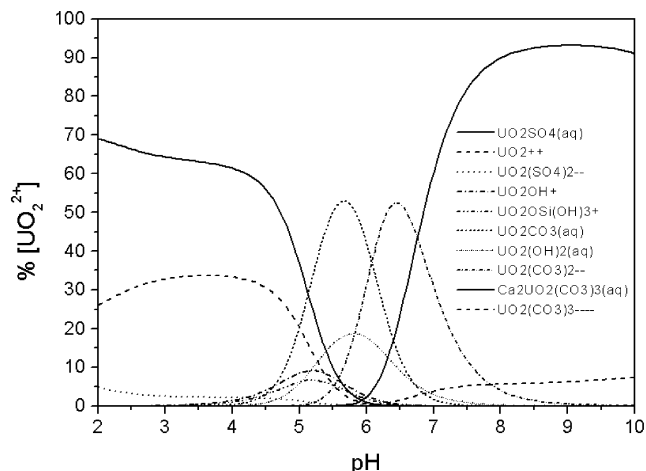


Fig. 1: Uranyl speciation in waters leaving the gallery "Rothschönberger Stolln", computed with EQ3NR

Whereas negatively charged uranyl carbonate species make up a considerable part of the uranyl species at pH 7.3 (as measured at the gallery mouth), at pH 5.1 the speciation shifts to mostly positively charged species. The latter sorb much better onto hydrous ferric oxides and aluminium oxides, see, e.g., Dzombak and Morel /2/, which are the major colloidal particles in the investigated solutions as pointed out in the previous article. This explains the much stronger binding of uranyl ions onto colloids at pH 5.1, as found in filtering experiments after acidification of the original pH 7.3 water. Whereas the original water did not contain any uranium attached to the colloidal particles, after acidifi-

cation only 26.5 % of the total uranium remained dissolved.

The reaction path is inversely modeled with EQ6, starting from the known final composition of the gallery water at its mouth. Oxygen is defined as a reactant with a negative reaction rate, leading to the depletion of oxygen from the solution, which in turn decreases the redox potential. The Eh changed from the initial 816 mV to a value of -200 mV, which represents the anoxic waters leaving the mines. This decrease in Eh is accompanied by a slight increase in pH. Figure 2 shows

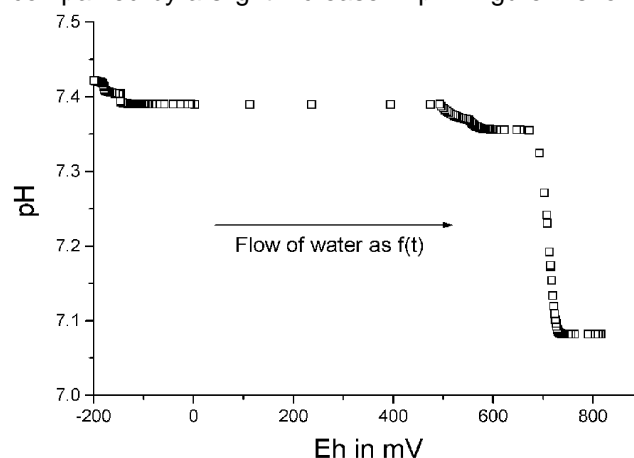


Fig. 2: Waters from the "Rothschönberger Stolln" gallery: pH as a function of the redox potential Eh, computed with EQ6

the Eh-pH dependence. The following modeling results were obtained for the main metal ions:

- manganese is fully dissolved at Eh < 570 mV, pyrolusite is the thermodynamically stable (but kinetically hindered) mineral phase at higher Eh.
- aluminium will quantitatively precipitate over the whole redox range as diaspore, boehmite or gibbsite.
- iron will precipitate as ferrihydrite (which slowly transforms into more stable phases such as hematite) for Eh > -100 mV
- several sulfide minerals will dissolve when the redox potential approaches -100 mV: chalcocite is stable for Eh < -110 mV, sphalerite for Eh < -120 mV, and galena for Eh < -110 mV.

## Acknowledgments

This work was partly funded by the DFG.

## References

- /1/ Wolery, T.J., UCRL-MA-110662 Part I, Lawrence Livermore National Laboratory, Livermore, 1992
- /2/ Dzombak, D.A., Morel, F.M.M., *Surface complexation modeling*. Hydrous ferric oxide; Wiley, New York, 1990

# DETECTION OF IRON AND ALUMINIUM HYDROXIDE COLLOIDS IN A SUSPENSION OF GROUND PHYLLITE

H. Zänker, G. Hüttig, T. Arnold, T. Zorn, H. Nitsche

*Colloidal submicron particles of Fe and Al hydroxides could be characterized in the presence of large amounts of coarse rock particles. Toxic trace metals such as U, As, Pb, and Cu can adsorb onto such particles.*

One of the mineralogical constituents of phyllite is chlorite, a mineral containing ferrous iron. The iron becomes partly oxidized during the weathering of phyllite. It is an open question if all freshly formed ferric iron is kept at the site of its generation or if some forms a relatively stable colloid in the water. Ten grams of ground phyllite from the western Erzgebirge mountains were suspended in 250 mL of water. This mixture was shaken for 1 day. The detection of fine heavy metal colloids in such a system is a non-trivial colloid-chemical problem. Most methods of colloid characterization (dynamic or static light scattering, laser breakdown spectroscopy, throughflow single particle counting, scanning or transmission electron microscopy, atomic force microscopy) would fail under the conditions of a turbid slurry. To solve the problem, a separation technique had to be applied to remove the coarse particles from the submicron ones prior to identifying the hypothetical small particles. We decided to remove the coarse particles by centrifugation. The concentration of Na, K, Mg, Ca, Mn, Si, Fe, and Al in the centrifugates at varying centrifugal acceleration were determined by ICP-MS and/or AAS. Fig. 1 gives some examples. The behavior of these elements divides them into 3 groups:

- Group 1: Na;
- Group 2: K, Mg, Si, Ca, Mn;
- Group 3: Al, Fe.

The Group 1 element, Na, shows hardly any response to the centrifugations. Obviously, the sodium occurs primarily as the Na<sup>+</sup> ion in the phyllite suspension. The Group 2 elements reach a constant concentration at the first centrifugation step and are not further influenced when applying higher centrifugal force. These elements represent the behavior of the undissolved ground rock particles. Most of the rock particles are removed by the 500 x g centrifugation. The remaining concentrations of Mg, Si, Ca and Mn, that can not be further decreased, represent the chemically dissolved ions of these elements. Two of the rock-forming elements, Fe and Al, clearly deviate from the scheme of the Group 2 elements. The Fe and Al remaining after the removal of the rock particles does not primarily exist in the form of ions. From the centrifugal behavior of Fe and Al at higher centrifugal accelerations, a particle size of the Fe and the Al submicron particles of 6 to 25 nm for Fe and 13 to 33 nm for Al, assuming spherical particles and densities of 2.7 and 4.0 g cm<sup>-3</sup> for the Al and Fe particles, respectively, were obtained. The experiment demonstrates that ferric iron produced by the weathering of phyllite can form a stable colloid in the contact water. Moreover, also Al forms a stable colloid. Mineralogically, the Fe and Al colloids should probably be classified as ferrihydrite and gibbsite/boehmite. The existence of fine hydroxide colloids in oxic waters from phyllite environments should be taken into account when assessing the transport of

toxic heavy metals via the water path through a phyllite environment because they may significantly influence the transport behavior of certain trace elements. U(VI), for instance, is described to be attached to ferrihydrite /1/. As, Pb, and Cu, too, are very prone to adsorption onto Fe or Al hydroxide colloids /2/.

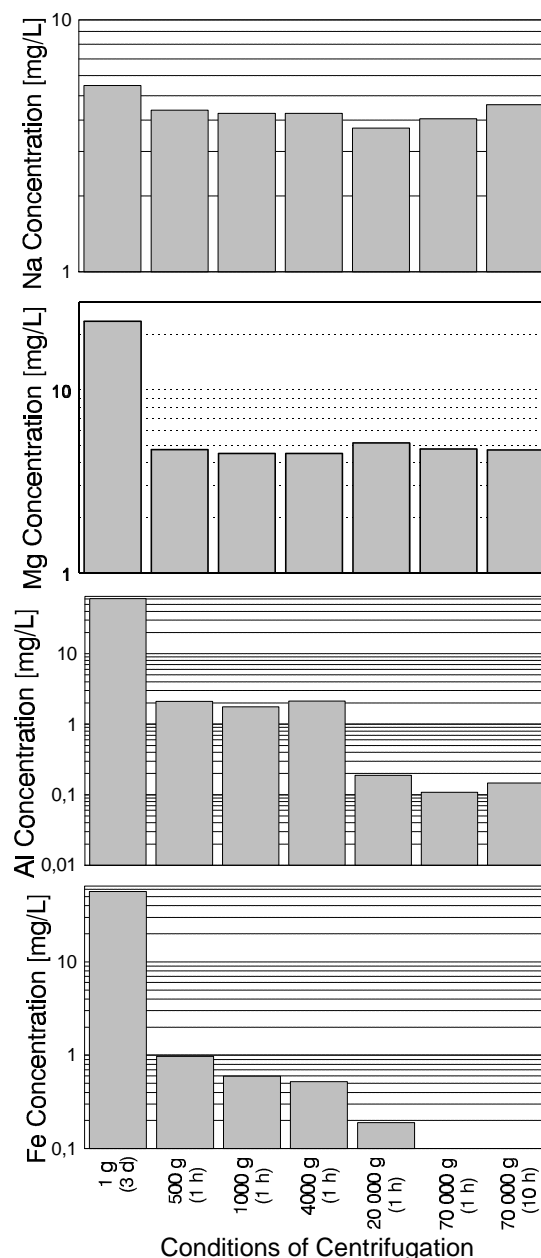


Fig. 1: Elemental concentration of the centrifugates in dependence on the centrifugal acceleration and the centrifugation time (examples).

### References

- /1/ Bruno, J., De Pablo, J., Duro, L., Figuerola, E.; *Geochim. Cosmochim. Acta* **59**, 4113 (1995).
- /2/ Zänker, H., Brendler, V., Richter, W., Nitsche, H.; this report p.62

# PHOTOLYSIS OF SILICIC ACID AND NEW PARTICLE FORMATION

D. Rettig, V. Berghof<sup>1</sup>, P. Merker, N. Schwentner<sup>1</sup>

<sup>1</sup>Freie Universität Berlin, Institute of Experimental Physics

The emission of charge-free particles from fused silica that was UV-irradiated in a moist gas environment was examined as a function of residence time, relative humidity of the gas, and photon energy and flux density. Conclusions are drawn on the importance of the process for atmospheric reactions.

Recently, we noticed a particle emission from fused silica surfaces which were irradiated by a low pressure mercury lamp in a humid gas environment /1/. In the present work, we investigated the dependence of the particle production rate on the following parameters:

- (1) Residence time of the gas in a fused silica vessel irradiated with a mercury lamp (8W electric power, wavelengths 185 nm | 6.7eV and 254 nm | 5eV).
- (2) Gas humidity at a residence time of 108s and irradiation with the same lamp (Fig.1). Filtered air or high purity N<sub>2</sub> or He were used as gases without showing any significant differences on the results.
- (3) Photon flux density from three different lasers (ArF 193 nm | 6.4 eV, KrF 248 nm | 5eV, XeCl 308 nm | 4eV) applying a small vessel, a small beam cross section and a residence time of 8s (Fig.2).

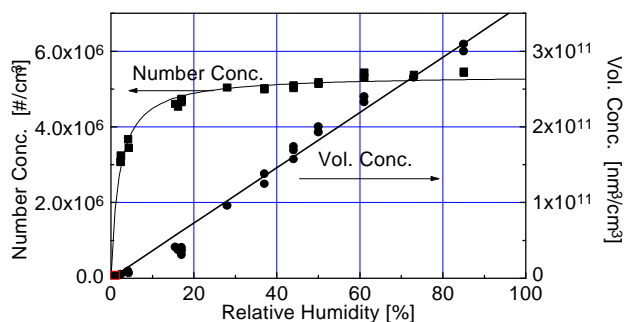


Fig. 1: Dependence of volume and number concentration of the particles on the humidity of nitrogen

At mean residence times ranging between 20 and 200s, aerosol particles with median diameters between 10 and 20 nm were formed. They could be measured without significant losses. The aerosol volume concentration increased linearly with the humidity of the gas, whereas the number concentration reached a constant value at high humidity (Fig.1). The aerosol is in the accumulation mode under these conditions. At low humidities (Fig.1) and at residence times below 20s, which also prevailed in the laser experiments (Fig.2), the particles are in the nucleation mode. In addition, the smallest particles were lost in the tubing connected to the particle counter.

The aerosol particles are spheric, amorphous, electrical charge-free, and contain silicon as the main constituent as was found by SEM, TEM, XRD, XRF, EDX and ICPMS analysis of filtered particles.

In summary, the findings are discussed in the following way: The formation of charge-free particles is in accordance with the high band gap energy of amorphous silica (8.9eV) which cannot be supplied by the irradiation to form ions. However, three-fold coordinated silicon and paramagnetic electrons near oxygen are well known defects formed by UV radiation. Single =Si(OH)<sub>2</sub>,

or -Si(OH)<sub>3</sub> groups are reported to be formed by water chemisorption at the SiO<sub>2</sub> surface. Both processes can be combined to formulate a photolytic dissociation process with formation of ≡Si(OH)<sub>3</sub> or ≡O-Si(OH)<sub>3</sub> radicals or Si(OH)<sub>4</sub> molecules. These are emitted into space and can travel like gas molecules. If they meet each other in a collision-controlled process, they can form nuclei without serious hindrance and grow in the accumulation process. In this step voluminous spheric particles are formed by the loss of water molecules.

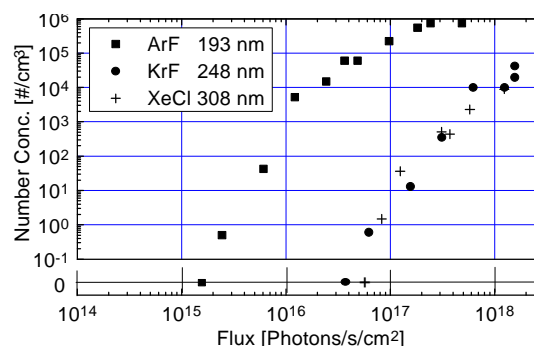


Fig. 2: Concentration of the generated particles vs. photon flux density from the ArF, KrF, and XeCl laser

First conclusions on the importance of the reaction were drawn in /1/ for particle generation and UV lamp degradation. In addition, the process should be taken into consideration to fill a gap in recent interpretations of meteorological and climatic observations. Silica is always found in upper atmospheric layers in the form of coarse particles. Radiation from the sun can reach the stratosphere in the window (180-220 nm) between the oxygen and the ozone absorption bands. The photolytic process, the reverse nucleation and accumulation process, and the nature of the amorphous loosely packed spheric particles may offer the properties which are looked for the interpretation of many phenomena. The particles can develop from the gas like radicals during night time or in polar winter. They may again be photolyzed under sun irradiation. They have catalytic properties for the photolytic decomposition of chloromethanes, they can take up water and hydrochloric acid, and they enable chemical reactions in their electrolytic phase. They are cloud condensation nuclei.

In the global modeling of aerosol live cycles involving a gas-to-particle conversion step, only sulfur compounds and carbon have been considered so far /2/. Silica should be involved in this group.

## References

- /1/ Rettig, D., et al.; J. Aerosol Sci. **29**, Suppl.1, 921 (1998), and Report FZR-218, p.80 (1998)
- /2/ Heintzenberg, J., et al.; Beitr. Phys. Atmosph. **69**, 261 (1996)

# **Chemistry of the Heaviest Elements**

# PHYSICO CHEMICAL CHARACTERIZATION OF SEABORGIUM AS OXIDE HYDROXIDE

S. Hübener, A. Vahle, S. Taut, H. Nitsche for a University Bern - FLNR Dubna - GSI Darmstadt - TU Dresden - GH Kassel - University Mainz - Forschungszentrum Rossendorf - PSI Villigen collaboration

*High-temperature on-line gas chromatography of oxidehydroxides was used to characterize the physico-chemical properties of seaborgium. The results indicate the formation of a low volatile seaborgium oxide hydroxide.*

In continuation of experiments with seaborgium oxychlorides /1/ the goal of the present gas chemistry experiment of the seaborgium-collaboration was to show that Sg forms low volatile oxide hydroxides.

The **High-Temperature on-line Gas chromatography Apparatus HITGAS** developed for studying low volatile oxide hydroxides is shown schematically in Fig. 1. Considering the low rate of the basic reactions of the gas chromatography of group 6 oxide hydroxides in quartz glass columns /2/, reasonable short open tubular chromatography columns were used and directly coupled with the GSI **Rotating Wheel Multidetector Analyzer ROMA**: The chromatography furnace was flanged onto the ROMA and a separate deposition chamber was placed between column and rotating wheel, as described earlier in detail /3/. In test experiments with short-lived Mo- and W-isotopes retention times as short as 8 s and chemical yields of about 60 % were achieved /3,4/. On-line alpha spectroscopy was carried out with a resolution of 25 keV. However, 1  $\mu\text{m}$  collection foils, to be applied for 4B alpha spectroscopy, which were stable in pure He carrier gas, were immediately destroyed when the reactive gas  $\text{H}_2\text{O}/\text{O}_2$  was added. Considering the results of the test experiments and potential interferences of short-lived Po-isotopes, we decided to study  $^{266}\text{Sg}$  ( $T_{1/2} = 21$  s) instead of the shorter-lived  $^{265}\text{Sg}$  ( $T_{1/2} = 7.4$  s) and detect it in 2B geometry by registration of  $^{266}\text{Sg}$   $\alpha$ -decay and time correlated spontaneous fission events of the  $^{262}\text{Rf}$  daughter.

The seaborgium experiments were performed at the GSI UNILAC accelerator with a mixed  $^{248}\text{Cm}/^{152}\text{Gd}$  target (GSI,  $820 \mu\text{g}/\text{cm}^2$   $^{248}\text{Cm}$ ,  $85 \mu\text{g}/\text{cm}^2$   $^{152}\text{Gd}$ ) at a  $^{22}\text{Ne}$  beam energy of 118 - 120 MeV. Assuming a cross section of 80 pb for the  $^{248}\text{Cm} (^{22}\text{Ne}, 4n) ^{266}\text{Sg}$ -reaction the production rate was about one  $^{266}\text{Sg}$  atom per hour. A  $\text{He}/\text{MoO}_3$ -jet was used to transport the nuclear reaction products with a gas flow rate of 2.0 l/min to the HITGAS. The temperature of the chromatography columns was 1325 K in the reaction and 1300 K in the isothermal zone. At the column entrance, 0.5 l/min  $\text{O}_2$ , moistened with  $\text{H}_2\text{O}$  at 323 K, were added as reactive gas. 25  $\mu\text{m}$  Al-foils were used to collect the species under study. The ROMA was operated with a cycle-time for collection and detection of 10 s. 15 equidistantly positioned PIPS detectors were used to detect spontaneous fission and  $\alpha$ -decay events /5/. Short-lived W-isotopes were monitored with a HPGe detector. The yield of W oxide hydroxides and the separation of interfering spontaneously fissioning actinides were watched continuously. The quartz-glass columns were replaced when the spontaneous fission rates were above 2 cph and/or W-yields were lower than 40 %.

The spectrum in Fig. 2 was summarized from the single spectra of 10 PIPS detectors, accumulated during 43 h beam time. We detected two correlated  $^{266}\text{Sg}$ - $^{262}\text{Rf}$ -decay chains :

chain	$E_{\alpha}$ [MeV]	life time $^{266}\text{Sg}$ [s]	life time $^{262}\text{Rf}$ [s]
1	8.66	84.9	7.0
2	8.70	4.8	3.7

A careful statistic evaluation of the background events in the spectra yielded 0.4 random chains.

We interpret this result with the formation of a low volatile seaborgium oxide hydroxide as typical for group 6 elements.

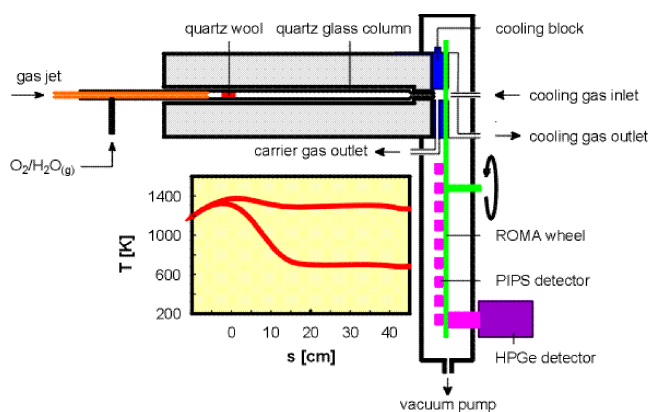


Fig. 1: On-line gas chromatography apparatus, schematically

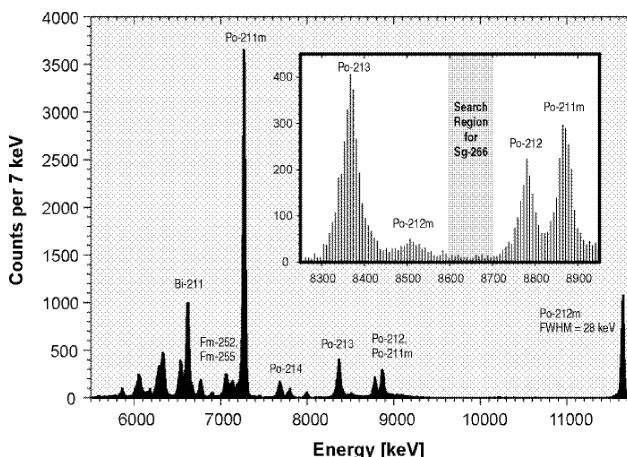


Fig. 2: Summary alpha spectrum of 43 h beam time

## Acknowledgments

The support by the BMBF and the GSI under contracts 06 DR 824 and DRNITK is gratefully acknowledged.

## References

- /1/ Schädel, M., et al.; Nature **388**, 55 (1997)
- /2/ Vahle, A., et al.; Radiochim. Acta **78**, 53 (1997)
- /3/ Hübener, S., et al.; Report FZR-218, 87 (1998)
- /4/ Vahle, A., et al.; Report FZR-218, 85 (1998)
- /5/ Taut, S.; this report p.68



# CORA – A NEW CONTROL PROGRAM FOR THE ROMA DETECTION SYSTEM

S. Taut

The new computer program CORA has been developed for the **C**ontrol of the **G**SI **R**otating **W**heel **M**ulti **D**etector **A**nalyzer (ROMA) running under Windows 95 and Windows NT 4.0. It can be customized with high flexibility to many different detection tasks.

The ROMA apparatus /1/ has been used successfully for many chemical investigations of heavy elements. In preparation of our seaborgium experiment at GSI in the summer of 1998 /2/, a new control program had to be developed, because the old code could not fulfill our experimental demands. This new program is written in C++ based on the Virtual Component Library using the Borland C++ Builder 1.0 programming environment.

The program has to carry out the following tasks:

- control of the ROMA wheel movements according to the actual experiment;
- start and stop of the nuclear spectroscopy data acquisition;
- sending information about the actual ROMA status to the spectroscopy data acquisition hardware;
- processing control requests of the data acquisition hardware (e. g., switching in "daughter mode" /3/);
- processing user input (e. g., experiment and wheel setup dialog boxes).

The program consists mainly of four software modules as shown in Fig. 1. The DLL *Hardware\_IO.dll* implements an interface for all interactions with the hardware. All other parts, organizing the experiment on a more abstract level, use exclusively this interface for controlling the hardware.

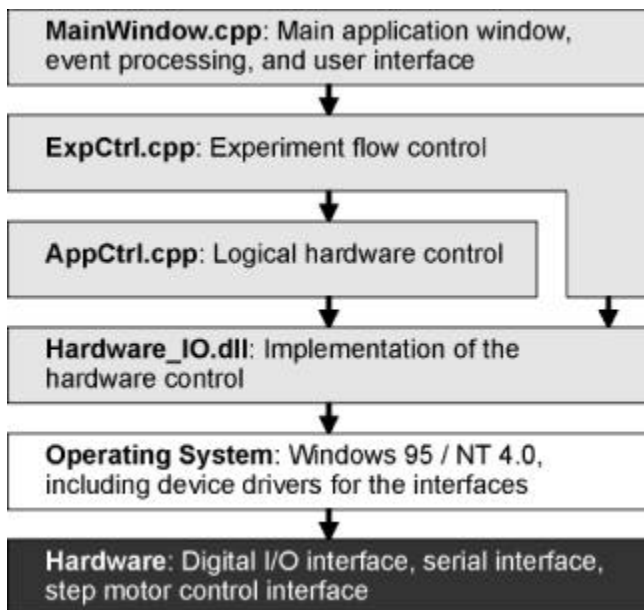


Fig. 1: Simplified Layer Scheme of the Program

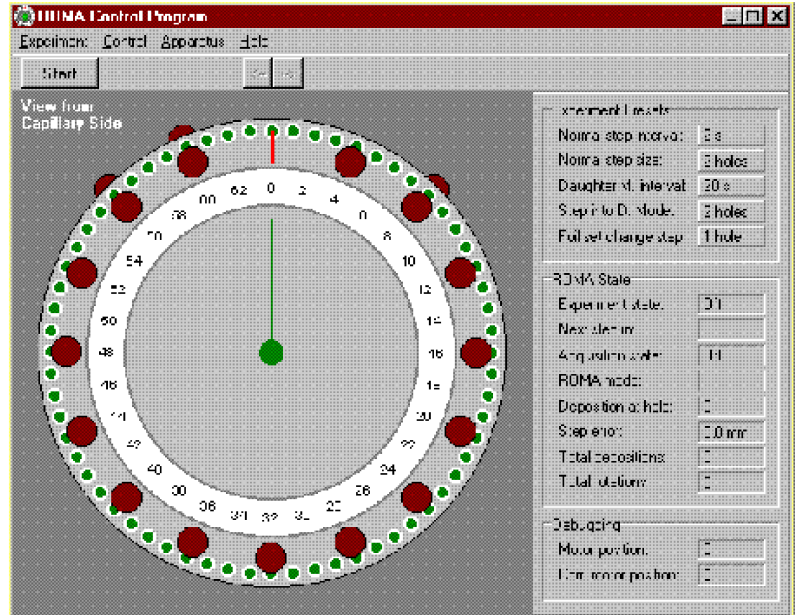


Fig. 2: Main Window of the Program

Thus, the program can be adopted to similar detection systems with very low programming effort: only the *Hardware\_IO.dll* must be adapted to the other hardware. This is planned for the new GSI multi detector apparatus which is currently in development.

The program has a very comfortable user interface, Fig. 2 shows the main application window. It is almost self explanatory. Control can be accessed easily with dialog boxes, even by inexperienced users. Critical hardware settings are hidden, but all program settings can be modified in initialization files (Windows 3.x style) with a normal editor.

It is possible to control the experiment related parts of the program completely by a digital I/O interface without direct user input. With this feature, the program can be used in fully automated systems.

In our seaborgium experiment /2/ the program controlled the ROMA apparatus for the first time. The following ROMA configuration was used: 15 PIPS detectors were mounted in the vacuum chamber equidistantly over the whole wheel circumference. The cycle time for each collection/detection period was 10 seconds.

## Acknowledgments

This work was supported by BMBF, 06DR824

## References

- /1/ Sümmerer, K. et al.; GSI Annual Report 1983, **84-1**, 246 (1984)
- /2/ Hübener, S. et al.; this report p.67
- /3/ Türlér, A. et al.; Phys. Rev. C **57**, 1648 (1998)

## **II. PUBLICATIONS, PATENTS, LECTURES AND POSTERS**



## PUBLICATIONS

Abram, S., Maichle-Mößmer, C., Abram, U.

Synthesis and characterization of indium(III) complexes with tri- and pentadentate thiosemicarbazones. Crystal and molecular structure of  $[\text{InCl}_2(\text{HDAPTSC})] \cdot 2\text{DMSO}$ ,  $\{\text{O}[\text{In}(\text{HDAPTSC})(\text{OH})_2] \cdot 5\text{MeOH}$ ,  $[\text{InCl}_2(\text{APTSC})(\text{MeOH})]$ ,  $[\text{In}(\text{APTSC})_2](\text{PF}_6)$  and  $(\text{H}_2\text{APTSC})[\text{InCl}(\text{APTSC})(\text{mnt})] \cdot 0.5\text{H}_2\text{O}$  ( $\text{H}_2\text{DAPTSC}$  = 2,6-diacetylpyridinebis(thiosemicarbazone),  $\text{HAPTSC}$  = 2-acetylpyridinethiosemicarbazone,  $\text{mnt}^{2-}$  = 1,2-dicyanoethene-1,2-dithiolate)  
*Polyhedron* **17**, 131 (1998)

Abram, U.

A man-made element's brilliant career  
*Science Spectra* **12**, 58 (1998)

Abram, U., Braun, M., Abram, S., Kirmse, R., Voigt, A.

$[\text{NBu}_4][\text{ReNCl}_4]$ : Facile synthesis, structure, electron paramagnetic resonance spectroscopy and reactions  
*J. Chem. Soc. Dalton Trans.* **1998**, 231

Abram, U., Mack, J., Ortner, K., Müller, M.

Reactions of Dichloro[2-(dimethylaminomethyl)phenyl-C<sup>1</sup>,N]gold(III),  $[\text{Au}(\text{damp-C}^1, \text{N})\text{Cl}_2]$ , with heterocyclic thiols. Evidence for Au-N bond cleavage and protonation of the dimethylamino group  
*J. Chem. Soc. Dalton Trans.* **1998**, 1011

Abram, U., Abram, S., Schibli, R., Alberto, R., Dilworth, J.R.

Synthesis and structures of technetium(I) and rhenium(I) tricarbonyl complexes with bis(diphenylthiophosphoryl)-amide,  $\{\text{M}[(\text{Ph}_2\text{PS})_2\text{N}](\text{CO})_3(\text{CH}_3\text{CN})\}$  (M = Tc, Re)  
*Polyhedron* **17**, 1303 (1998)

Abram, U., Kohl, F.J., Öfele, K., Herrmann, W.A., Voigt, A., Kirmse, R.

$(\text{Bu}_4\text{N})[\text{Re}\{\text{NB}(\text{C}_6\text{F}_5)_3\}\text{Cl}_4(\text{OH}_2)]$  - Struktur und EPR-Spektren  
*Z. anorg. allg. Chem.* **624**, 934 (1998)

Abram, U., Voigt, A., Kirmse, R.

Synthesis, Structure and EPR spectra of  $(\text{NBu}_4)_2[(\text{OH}_2)\text{Br}_4\text{ReNReBr}_4\text{NReBr}_4(\text{OH}_2)]$   
*Inorg. Chem. Communication* **1**, 213 (1998)

Abram, U., Ortner, K., Hübener, R., Voigt, A., Kirmse, R., Caballho Rias, R., Vazquez Lopez, E.

Darstellung, Strukturen und EPR-Spektren der Rhenium(II)-Nitrosylkomplexe  $[\text{Re}(\text{NO})\text{Cl}_2-(\text{PPh}_3)(\text{OPPh}_3)(\text{OReO}_3)]$ ,  $[\text{Re}(\text{NO})\text{Cl}_2(\text{OPPh}_3)_2(\text{OReO}_3)]$  und  $[\text{Re}(\text{NO})\text{Cl}_2(\text{PPh}_3)_3][\text{ReO}_4]$   
*Z. anorg. allg. Chem.* **624**, 1662 (1998)

Arnold, T., Zorn, T., Bernhard, G., Nitsche, H.

Sorption of uranium (VI) onto phyllite  
*Chem. Geol.* **151**, 129 (1998)

Baraniak, L., Mack, B., Abraham, A., Bernhard, G., Nitsche, H.

Untersuchung des Einflusses der in Grubenwässern gelösten organischen Verbindungen auf den Valenzzustand von Radionukliden und Schwermetallen im Hinblick auf den Flutungsprozeß der sächsischen Uranbergwerke  
Abschlußbericht SMWK-Förderprojekt 4-7541.83-FZR/512, (1998)

Bernhard, G., Geipel, G., Brendler, V., Nitsche, H.

Uranium speciation in waters of different uranium mining areas  
*J. Alloys and Compounds* **271-273**, 201 (1998)

Bonfada, E., Strähle, J., Abram, U.

Darstellung, Strukturen und Photolyse von Rheniumisocyanato-Komplexen  
*Z. anorg. allg. Chem.* **624**, 757 (1998)

Bubner, M., Meyer, M., Fuksova, K., Matucha, M., Heise, K.H., Nitsche, H.

Synthesis of Uniformly <sup>13</sup>C and <sup>14</sup>C Labelled PCB-Congeners  
*Ecological Chem. (Russia)* **7**, 65 (1998)

Denecke, M.A., Reich, T., Pompe, S., Bubner, M., Heise, K.H., Nitsche, H., Allen, P.G., Bucher, J.J., Edelstein, N.M., Shuh, D.K., Czerwinski, K.R.

EXAFS Investigations of the Interaction of Humic Acids and Model Compounds with Uranyl Cations in Solid Complexes  
*Radiochim. Acta* **82**, 103 (1998)

Denecke, M.A., Reich, T., Bubner, M., Pompe, S., Heise, K.H., Nitsche, H., Allen, P.G., Bucher, J.J., Edelstein, N.M., Shuh, D.K.

Determination of structural parameters of uranyl ion complexed with organic acids using EXAFS  
*J. Alloys and Compounds* **271-273**, 123 (1998)

- Geipel, G., Bernhard, G., Brendler, V., Nitsche, H.  
Complex formation between  $\text{UO}_2^{2+}$  and  $\text{CO}_3^{2-}$  studied by laser-induced photoacoustic spectroscopy (LIPAS)  
Radiochim. Acta **82**, 59 (1998)
- Griffiths, D.V., Parrott, J., Togrou, M., Dilworth, J.R., Zheng, Y., Ritter, S., Abram, U.  
Synthesis and Crystal Structures of the Novel Tetrameric Nitrido Complexes  $[\{\text{cyclo-ReN}\}_4 (\text{S}_2\text{CNEt}_2)_6 (\text{MeOH})_2 (\text{PPh}_3)_2][\text{BPh}_4]_2 \cdot \text{CH}_2\text{Cl}_2 \cdot 2 \text{H}_2\text{O}$  and  $[\{\text{cyclo-ReN}\}_4 (\text{S}_2\text{CNEt}_2)_4 \text{Cl}_4 (\text{Pme}_2\text{Ph})_4] \cdot 2 \text{acetone}$   
Z. anorg. allg. Chem. **624**, 1409 (1998)
- Heise, K.H., Pompe, S., Schmeide, K., Bubner, M., Nitsche, H.  
Die Rolle von Huminsäuren in der Umwelt  
Jahresbericht 1997 FZ Rossendorf e.V., S. 30-35 (1998)
- Hennig, C., Denecke, M.A., Roßberg, A., Zahn, G., Reich, T., Nitsche, H.  
 $\text{U L}_{\text{III}}$  Polarized XAFS Studies on  $\text{Ba}[\text{UO}_2\text{PO}_4]_2 \cdot 8\text{H}_2\text{O}$   
Suppl. Z. Krist. **15**, 156 (1998)
- Hennig, C., Denecke, M.A., Roßberg, A., Zahn, G., Reich, T., Bernhard, G., Nitsche, H.  
Uranium  $\text{L}_{\text{III}}$  XANES and EXAFS on the Uranyl Unit in a Single Crystal with Linear Polarized Synchrotron Radiation  
HASYLAB Annual Report 1997, 823 (1998)
- Hennig, C., Hallmeier, K.H., Szargan, R.  
XANES Investigation of Chemical States of Nitrogen in Polyaniline  
Synthetic Metals **92/2**, 161 (1998)
- Jankowsky, R., Kirsch, S., Reich, T., Spies, H., et al.  
Solution Structures of Rhenium (V) Oxo Peptide Complexes of Glycylglycylcysteine and Cysteinylglycine as Studied by Capillary Electrophoresis and X-ray Absorption Spectroscopy  
J. Inorg. Biochem. **70**, 99 (1998)
- Kirmse, R., Voigt, A., Abram, U.  
 $[\text{ReNF}_4]$  - an EPR study  
Inorg. Chem. Communications **1**, 141 (1998)
- Kuhn, N., Kotowski, H., Maichle-Mößmer, C., Abram, U.  
Synthese und Kristallstruktur von  $[\text{Fe}(\text{MeCN})_6][\text{Fe}_2\text{OCl}_6]$   
Z. anorg. allg. Chem. **624**, 1653 (1998)
- Matasyoh, J.C., Abram, U., Schuler, P., Stegmann, H.B.  
Synthesis and Stereochemistry of the Spin Adducts of a New Chiral Spin Trap, 3,5-Diphenyl-5-methylpyrroline-1-oxide  
J. Magnet. Resonance **36**, 422 (1998)
- Matz, W., Schell, N., Funke, H., Bernhard, G.  
ROBL (German Beamline) on BM20: Structural and Radiochemical Investigations  
ESRF Newsletter **30**, 45 (1998)
- Moll, H., Geipel, G., Brendler, V., Bernhard, G., Nitsche, H.  
Interaction of uranium(VI) with silicic acid in aqueous solutions studied by time-resolved laser-induced fluorescence spectroscopy (TRLFS).  
J. Alloys and Compounds **271-273**, 765 (1998)
- Nebelung, C., Nitsche, H., Bernhard, G.  
A fast method for low-level actinide measurement in concrete  
J. Alloys and Compounds **271-273**, 42 (1998)
- Nefedov V.I., Teterin Yu.A., Lebedev A.M., Teterin A.Yu., Dementjev A.P., Bubner, M., Reich T., Pompe S., Heise K.H., Nitsche, H.  
Electron spectroscopy for chemical analysis investigation of the interaction of uranyl and calcium ions with humic acids  
Inorg. Chim. Acta **273**, 234 (1998)
- Ortner, K., Abram, U.  
Reactions of Dichloro[2-(dimethylaminomethyl)phenyl- $\text{C}^1, \text{N}$ ]gold(III),  $[\text{Au}(\text{damp-}\text{C}^1, \text{N})\text{Cl}_2]$ , with aromatic thiosemicarbazones. Structures and spectroscopical data of the first gold(III) thiosemicarbazone complexes  
Inorg. Chem. Communications **1**, 251 (1998)
- Panak, P., Hard, B., Pietzsch, K., Kutschke, S., Röske, K., Selenska-Pobell, S., Bernhard, G., Nitsche, H.  
Bacteria from uranium mining waste pile: Interactions with U(VI)  
J. Alloys and Compounds **271-273**, 262 (1998)

- Pompe, S., Brachmann, A., Bubner, M., Geipel, G., Heise, K.H., Bernhard, G., Nitsche, H.  
Determination and comparison of uranyl complexation constants with natural and model humic acids  
Radiochim. Acta **82**, 89 (1998)
- Reich, T., Hudson, E.A., Denecke, M.A., Allen, P.G., Nitsche, H.  
Structural Analysis of Uranium(VI) Complexes by X-ray Absorption Spectroscopy  
Surface Investigations **13**, 557 (1998)
- Rettig, D., Merker, P., Nitsche, H.  
Particle emission from UV-irradiated silica surfaces  
J. Aerosol Sci. **29**, 921 (1998)
- Schibli, R., Alberto, R., Abram, U., Abram, S., Egli, A., Schubiger, P.A., Kaden, Th.A.  
Coordination Behavior of the *fac*-[Tc(CO)<sub>3</sub>]<sup>+</sup> Moiety towards Macrocyclic Thioethers of Various Ring Size: Synthesis and Structure of the Complexes *fac*-[Tc(9-ane-S<sub>3</sub>)(CO)<sub>3</sub>]Br, *fac*-[Tc<sub>2</sub>(tos)<sub>2</sub>(18-ane-S<sub>6</sub>)(CO)<sub>6</sub>] and *fac*-[Tc<sub>2</sub>(20-ane-S<sub>6</sub>-OH)(CO)<sub>6</sub>][tos]<sub>2</sub>  
Inorg. Chem. **37**, 3509 (1998)
- Schmeide, K., Zänker, H., Heise, K.H., Nitsche, H.  
Isolation and Characterization of Aquatic Humic Substances from the Bog "Kleiner Kranichsee".  
Forschungszentrum Karlsruhe, Report FZKA 6124, 161-195 (1998)
- Schulz-Lang, E., Pradella Ziani, J., Abram, U.  
Tris(selenophenyl)methane  
Acta Cryst. **C55**, 1010 (1998)
- Schulz-Lang, E., Abram, U., Strähle, J., Vázquez-López, E.M.  
Synthesis and Crystal Structures of [TeI<sub>3</sub>][Gal<sub>4</sub>] and [TeI<sub>3</sub>][InI<sub>4</sub>]  
Z. anorg. allg. Chem. **624**, 999 (1998)
- Schumann, D., Andrassy, M., Nitsche, H., Novgorodov, A.F., Misiak, R., Schädel, M., Brüchle, W., Schausten, B., Kratz, J.V., Bruchertseifer, H.  
Sorption behaviour of W, Hf, Lu, U, and Th on ion exchangers from HCl/H<sub>2</sub>O<sub>2</sub> solutions. Model experiments for chemical studies of Seaborgium (Sg)  
Radiochim. Acta **80**, 1 (1998)
- Schumann, D., Nitsche, H., Taut, S., Jost, D.T., Gäggeler, H.W., Yakushev, A.B., Buklanov, G.V., Domanov, V.P., Din Thi Lien, Kubica, B., Misiak, R., Szegłowski, Z.  
Sorption behaviour of rutherfordium and thorium from HCl/Hf containing aqueous solution  
J. Alloys and Compounds **271-273**, 307 (1998)
- Selenska-Pobell, S., Otto, A., Kutschke, S.  
Identification and Discrimination of Thiobacilli using ARDREA, RAPD, and Rep-APD  
Journal of Applied Bacteriology **84**, 1085 (1998)
- Selenska-Pobell, S., Döring, H.  
Sequences around the fragmentation sites of the large subunit rRNA in the family Rhizobiaceae  
Antonie van Leeuwenhoek **43**, 55 (1998)
- Taut, S., Hübener, S., Eichler, B., Türler, A., Gäggeler, H.W., Timokhin, S., Zvara, I.  
Thermochromatography of Heavy Actinides - Adsorption of No-259 on Ti, V, Nb, Ta, and Mo  
J. Less-Common Met. **271-273**, 316 (1998)
- Teterin, Yu.A., Ivanov, K.E., Baev, A.S., Nefedov, V.I., Geipel, G., Reich, T., Nitsche, H.  
X-ray Photoelectron Study of the Interaction of UO<sub>2</sub>(ClO<sub>4</sub>)<sub>2</sub> with Calcite and Diabase Minerals in Water Solutions  
Surface Investigations **13**, 613 (1998)
- Trautmann, N., Pompe, S., Heise, K.H., Bernhard, G., Bubner, M., Nitsche, H., Beck, H.P., Wagner, H., Keuth, U., Schank, M., Mansel, A., Seibert, A., Keller, H., Kratz, J.V.  
Einfluß von Huminstoffen auf das Migrationsverhalten von Schadstoffen  
Forschungszentrum Karlsruhe, Report FZKA-PTE Nr. 5, 147-172 (1998)
- Türler, A., Dressler, R., Eichler, B., Gäggeler, H.W., Jost, D.T., Schädel, M., Brüchle, W., Gregorich, K.E., Trautmann, N., Taut, S.  
Decay properties of <sup>256</sup>Sg(Z=106) and <sup>266</sup>Sg(Z=106)  
Phys. Rev. C **57**, 1648 (1998)
- Türler, A., Buklanov, G.V., Eichler, B., Gäggeler, H.W., Grantz, M., Hübener, S., Jost, D.T., Lebedev, V.Y., Piguet, D., Timokhin, S.N., Yakushev, A.B., Zvara, I.

Evidence for Relativistic Effects in the Chemistry of Element 104  
J. Alloys Comp. **271-273**, 287 (1998)

Voigt, A., Abram, U., Strauch, P., Kirmse, R.  
An electron paramagnetic resonance study of tetrabutylammoniumtetrabromonitridorhenate(VI),  $[(n-C_4H_9)_4N][ReNBr_4]$   
Inorg. Chim. Acta **271**, 199 (1998)

Voigt, A., Kirmse, R., Abram, U.  
EPR spectroscopic evidence for  $[Re\{NC(C_6H_5)_3\}X_4]$  complexes (X = Cl, Br)  
Inorg. Chem. Communications **1**, 203 (1998)

## PATENTS

Förster, E., Eisold, B., Hiller, B., Heise, K.H., Nitsche, H.  
Vorrichtung zum Öffnen von Glasampullen  
Patent registered by Deutsches Patentamt; Az. 198 41 722.5

## LECTURES

Abram, U.  
Crystal Structure Determination for Everybody  
University of Santiago de Compostela, Spain, 03.02.1998

Abram, U.  
Terminal Nitrido Ligands - Lewis Bases for the Coordination Chemist  
University of Graz, Austria, 14.05.1998

Allen, P.G., Shuh, D.K., Bucher, J.J., Edelstein, N.M., Reich, T.  
Applications of XAFS Spectroscopy to Speciation Problems in Environmental Radiochemistry  
Euroconference and NEA Workshop: Actinide-XAS-98  
Grenoble, France, 04.-06.10.1998

Arnold, T.  
Sorption of Uranium(VI) onto Phyllite  
Workshop: "The Münster Workshop on Mineral Surface Science"  
Münster, Germany, 18.-20.03.1998

Arnold, T.  
Sorption of Uranium(VI) onto Phyllite  
Workshop: "Surface Reactivity" Meeting  
University of Manchester, Department of Earth Sciences  
Manchester, UK, 30.03.-1.04.1998

Arnold, T., Bernhard, G., Nitsche, H.  
Sorption of Uranium(VI) onto schwertmannite  
European Research Conference "GEOCHEMISTRY OF CRUSTAL FLUIDS. Characterization of Reactive Transport in Natural Systems"  
Aghia Pelaghia, Greece, 22.-27.05.1998

Baraniak, L., Mack, B., Abraham, A.  
Untersuchungen zum Redoxverhalten von Lignin und Huminsäure  
Workshop "Einfluß von Huminstoffen auf das Migrationsverhalten radioaktiver und nichtradioaktiver Schadstoffe unter naturnahen Bedingungen"  
Mainz, Germany, 11.-12.03.1998

Brendler, V., Bernhard, G., Nitsche, H.  
Coupling Geochemical Speciation to Risk Assessment Codes  
Uranium Mining and Hydrogeology II  
Freiberg, Germany, 15.-17.09.1998

Bubner, M., Pompe, S., Meyer, M., Heise, K.H., Nitsche, H.  
Isotopically Labelled Humic Acids for Heavy Metal Ion Complexation - Advantages and Limitations  
Joint European International Isotope Society Conference  
Bad Soden, Germany, 24.- 26.06.1998

Funke, H.  
The Radiochemistry Experimental Station at the Rossendorf Beamline (ROBL)  
Euroconference and NEA Workshop: Actinide-XAS-98  
Grenoble, France, 04.-06.10.1998

Funke, H.  
The Radiochemistry Safety System at ROBL  
14th CRG Club Meeting  
Grenoble, France, 19.-20.10.1998

Geipel, G., Rutsch, M., Bernhard, G., Brendler, V., Nitsche, H.  
Speciation of Uranium - Determination and Calculation under Natural Conditions  
Uranium Mining and Hydrogeology II  
Freiberg, Germany, 15.-17.09.1998

Geipel, G., Bernhard, G., Rutsch, M., Brendler, V., Nitsche, H.  
Laserspektroskopie in der Nuklearchemie - Möglichkeiten und Grenzen  
GDCh-Fachtagung, FG Nuklearchemie  
Dresden, Germany, 07.-09.09.1998

Geipel, G., Bernhard, G., Rutsch, M., Brendler, V., Thieme, M.  
Speciation in Water Released from Mining and Milling Facilities  
NATO Workshop on Global Solutions to Disarmament Involving Management of Radionuclides  
Cracow, Poland, 09.-13.11.1998

Heise K.H., Bubner M., Pompe S., Nitsche H.  
Synthetic Humic Acids for Radioecological Environmental Research  
Joint European International Isotope Society Conference  
Bad Soden, Germany, 24.- 26.06.1998

Hennig, C.  
A Monochromator Feedback System  
14th CRG Club Meeting  
Grenoble, France, 19.-20.10.1998

Hübener, S.  
Physikochemische Charakterisierung des Seaborgiums: Experimentelle Vorbereitung am U-120  
Kolloquium "40 Jahre Rossendorfer Zyklotron U-120"  
Rossendorf, Germany, 18.09.1998

Kutschke, S., Selenska-Pobell, S., Otto, A., Panak, P., Geipel, G., Bernhard, G., Nitsche, H.  
Molecular Characterization of *Thiobacillus* Strains Recovered from Uranium Waste Heaps  
Uranium Mining and Hydrogeology II  
Freiberg, Germany, 15.-17.09.1998

Kutschke, S., Groudeva, V., Selenska-Pobell, S.  
Molecular characterization of several *Thiobacillus ferrooxidans* strains recovered from an uranium mine waste pile in Germany  
Euroconference: Bacterial-Metal/Radionuclide Interaction  
Rossendorf/Dresden, Germany, 02.-04.12.1998

Nitsche, H.  
Data transferability into numerical models and sources of uncertainty  
EC-Cluster Workshop "Radionuclide Transport/Retardation Processes"  
Brussels, Belgium, 19.-20.03.1998

Nitsche, H., Brendler, V.  
Radionuclide Migration and Transport in the Vadose Zone: R&D Needs in Measurements and Modelling  
Fourth Intern. Symposium and Exhibition on Environmental Contamination in Central and Eastern Europe  
Warsaw, Poland, 15.-17.09.1998

Nitsche, H.  
Application of Synchrotron Radiation Techniques to Radionuclide Studies  
Euroconference and NEA Workshop: Actinide-XAS-98  
Grenoble, France, 04.-06.10.1998

Nitsche, H.  
Environmental Nuclear Chemistry: Uranium Speciation by Laser Fluorescence and X-ray Absorption Spectroscopy  
European Synchrotron Radiation Facility (ESRF)  
Grenoble, France, Oct. 1998

Panak, P.  
Bacteria from uranium mining waste piles: Complex formation of *Thiobacillus ferrooxidans* with U(VI)  
Uranium Mining and Hydrogeology II  
Freiberg, Germany, 15.-17. 09.1998

Panak, P., Miteva, V., Boudakov, I., Hard, B.C., Pietsch, K., Kutschke, S., Selenska-Pobell, S., Bernhard, G., Nitsche, H.  
 Interactions of Bacteria from a Uranium Mining Waste Pile with U(VI)  
 Uranium Mining and Hydrogeology II  
 Freiberg, Germany, 15.-17.09.1998

Pietsch, K., Panak, P., Hard, B.C., Babel, W.  
 Characterization of a Sulfate-Reducing Bacterium which is able to Reduce Uranium  
 Uranium Mining and Hydrogeology II  
 Freiberg, Germany, 15.-17.09.1998

Pompe, S., Artinger, R.  
 Erste Ergebnisse aus Säulenexperimenten zur Untersuchung des Migrationsverhaltens von Uran(VI) im System  
 GoHy-532 / Gorlebensand  
 BMBF-Projektmeeting Universität Mainz, Institut für Kernchemie  
 Mainz, Germany, 12.03.1998

Pompe S., Heise K.H., Bernhard G., Nitsche, H.  
 Einfluß von Huminstoffen auf das Migrationsverhalten radioaktiver und nichtradioaktiver Schadstoffe unter  
 naturnahen Bedingungen. (IFR-Teilbericht zum BMBF-Verbundprojekt-Abschluß)  
 BMBF-Projektmeeting, FZ Karlsruhe  
 Karlsruhe, Germany, 22.-23.10.1998

Pompe, S., Artinger, R., Schmeide, K.  
 Investigation of the Migration Behavior of Uranium in an Aquifer System Rich in Humic Substances - Column  
 Experiments-  
 Fourth Project Meeting of the EU project "Effects of Humic Substances on the Migration of Radionuclides:  
 Complexation and Transport of Actinides"  
 Leuven, Belgium, 19.-20.11.1998

Pompe, W., Mertig, M., Kirsch, R., Raff, J., Selenska-Pobell, S.  
 Metal cluster formation on bacterial surface layer proteins  
 Euroconference: Bacterial-Metal/Radionuclide Interaction  
 Rossendorf/Dresden, Germany, 02.-04.12.1998

Puers, C., Kampf, G., Selenska-Pobell, S.  
 Bacterial Diversity in Soil of a Depleted Saxonian Uranium Mine as Revealed by 16S rRNA Gene and 16S/23S  
 Intergenic Spacer Analyses  
 Uranium Mining and Hydrogeology II  
 Freiberg, Germany, 15.-17.09.1998

Reich, T.  
 Anwendung der Röntgenabsorptionsspektroskopie in der Radioökologie  
 Zentrumsseminar "Anwendung der Synchrotronstrahlung"  
 Forschungszentrum Rossendorf e.V.  
 Rossendorf, Germany, 08.01.1998

Reich, T., Bernhard, G., Nitsche, H.  
 Application of X-ray Absorption Spectroscopy in Radioecology  
 13th Radiochemical Conference  
 Mariánské Lázně, Czech Republic, 19.-24.04. 1998

Reich, T.  
 X-ray Absorption Fine Structure Studies of Uranium in Environmental Systems  
 Lawrence Berkeley National Laboratory  
 Berkeley, CA, USA, 19.05. 1998

Reich, T.  
 Synchrotronstrahlungsuntersuchungen an Radionuklidensystemen  
 GDCh-Fachtagung, FG Nuklearchemie  
 Dresden, Germany, 07.-09.09.1998

Reich, T.  
 EXAFS Studies of Uranium(VI) Sorption on Mineral Surfaces  
 Euroconference and NEA Workshop: Actinide-XAS-98  
 Grenoble, France, 04.-06.10.1998

Reich, T.  
 Speziationsbestimmung von Uran in umweltrelevanten Systemen mittels Röntgenabsorptionsspektroskopie  
 Universität Leipzig, Fakultät für Chemie und Mineralogie

Leipzig, Germany, 19.10.1998

Rettig, D., Merker, P., Nitsche, H.  
Photolysis of silicic acid and new particle formation  
5th International Aerosol Conference  
Edinburgh, Scotland, 12.-18.09.1998

Roßberg, A., Denecke, M.A., Reich, T., Hennig, C., Nitsche, H.  
Determination of Molecular-Level Structural Information of Uranium in Environmentally Relevant Samples by EXAFS  
Uranium Mining and Hydrogeology II  
Freiberg, Germany, 15.-17.09.1998

Schmeide, K., Geipel, G., Zänker, H., Heise, K.H., Nitsche, H.  
Complexation of Uranyl(VI) by Humic Substances in Absence and Presence of Sulfate  
EC Project Meeting, Centre d'Études de Saclay  
Paris, France, 11.-12.05.1998

Schmeide, K., Zorn, T., Zänker, H., Heise, K.H., Nitsche, H.  
Effect of Humic Substances on the Sorption of Uranium(VI) onto Site-Specific Rock Material  
EC Project Meeting, Centre d'Études de Saclay  
Paris, France, 11.-12.05.1998

Schmeide, K., Geipel, G., Heise, K.H., Nitsche, H.  
Case-Study: Uranium-Mining Rock Pile No. 250 in the Region Schlema/Alberoda (Saxony, Germany)  
EC Project Meeting  
Katholieke Universiteit Leuven  
Leuven, Belgium, 19.-20.11.1998

Schmeide, K., Pompe, P., Heise, K.H., Nitsche, H.  
Effect of Humic Acid on the Uranium Sorption on Phyllite and its Constituents  
EC Project Meeting  
Katholieke Universiteit Leuven  
Leuven, Belgium, 19.-20.11.1998

Selenska-Pobell, S.  
Analysis of the culturable members of the natural bacterial communities in uranium waste piles  
Dept. of Geomicrobiology, University of Sofia  
Sofia, Bulgaria, 06.06.1998

Selenska-Pobell, S.  
Selective accumulation of heavy metals in drain waters of a uranium waste pile by three indigenous Bacillus strains  
Institute of Microbiology, Bulgarian Academy of Sciences  
Sofia, Bulgaria, 25.06.1998

Selenska-Pobell, S.  
Diversity in natural bacterial populations in the uranium wastes as examined by a 16S rDNA retrieval  
Inst. of Molecular Biology, Bulgarian Academy of Sciences  
Sofia, Bulgaria, 07.10.1998

Selenska-Pobell, S.  
Molecular studies on bacterial diversity in uranium wastes  
Internat. Symposium on Microbial Ecology  
Halifax, Canada, 09.-14.08.1998

Selenska-Pobell, S.  
Molecular studies of the culturable and non-culturable bacteria in uranium wastes  
Uranium Mining and Hydrogeology II  
Freiberg, Germany, 15.-17.09.1998

Selenska-Pobell, S., Boudakov, I., Flemming, K., Kampf, G., Kutschke, S., Miteva, V., Otto, A., Puers, C., Wober, J.  
Molecular Studies of Bacterial Diversity in Uranium Wastes  
Uranium Mining and Hydrogeology II  
Freiberg, Germany, 15.-17.09.1998

Selenska-Pobell, S.  
Bakterielle Diversität in uranhaltigen Abraumhalden und Absetzbecken  
Wissenschaftliche Konferenz: BIODIVERSITÄT der WGL  
Berlin, Germany, 17.-19.11.1998

Taut, S., Hübener, S., Eichler, B., Eberhardt, K., Trautmann, N., Peterson, Y.R.

Thermochromatography of Elemental Einsteinium  
13th Radiochemical Conference  
Mariánské Lázně, Czech Republic, 19.-24.04.1998

Wober, J., Flemming, K., Hard, B.C., Pietzsch, K., Selenska-Pobell, S.  
Comparison of *Desulfovibrio* Isolates Recovered from a Uranium Waste Heap and other Environments  
Uranium Mining and Hydrogeology II  
Freiberg, Germany, 15.-17.09.1998

Zänker, H., Richter, W., Nitsche, H.  
Charakterisierung der Kolloidpartikel in den Wasserfließsystemen stillgelegter sächsischer Bergbauanlagen.  
4. Kolloquium des DFG-Schwerpunktprogramms "Geochemische Prozesse mit Langzeitfolgen im anthropogen beeinflussten Sickerwasser und Grundwasser"  
Freiberg, Germany, 26.-27.04.1998

Zänker, H.  
Photonenkorrelationsspektroskopie und Rasterkraftmikroskopie an Huminsäure.  
TU Dresden, Institut für Werkstoffwissenschaft  
Dresden, Germany, 17.12.1998

## POSTERS

Abraham, A., Mack, B., Baraniak, L., Nitsche, H.  
Vergleich der Sorption von Eisen und Uran an Erzgebirgsmetamorphiten und Elbtalsedimenten unter aeroben und anaeroben Bedingungen und unter dem Einfluß organischer Grubenwasserinhaltsstoffe  
GDCh-Fachtagung, FG Nuklearchemie  
Dresden, Germany, 07.-09.09.1998

Abraham, A., Mack, B., Baraniak, L., Nitsche, H.  
Einfluß von Grubenholzabbauprodukten auf die Redoxsituation in Flutungswässern und auf das Sorptionsverhalten von Eisen und Uran an Erzgebirgsmetamorphiten und Elbtalsedimenten  
Uranium Mining and Hydrogeology II  
Freiberg, Germany, 15.-17.09.1998

Baraniak, L., Jelen, K., Schiene, R., Fischer, K., Bernhard, G., Nitsche, H.  
Hydrothermal Wood Decomposition and Influence of the Degradation Products on the Uranium Adsorption on Metamorphic Rocks and Sediments  
Uranium Mining and Hydrogeology II  
Freiberg, Germany, 15.-17.09.1998

Baraniak, L., Jelen, K., Schiene, R., Fischer, K., Bernhard, G., Nitsche, H.  
Influence of Mine Wood Degradation Products on the Adsorption of Uranium, Thorium, Iron and Lead on ore Mountain Rocks and Elbe Valley Sediments  
GDCh-Fachtagung, FG Nuklearchemie  
Dresden, Germany, 07.-09.09.1998

Bernhard, G., Geipel, G., Brendler, V., Reich, T., Nitsche, H.  
Validation of Complex Formation of  $\text{Ca}^{2+}$ ,  $\text{UO}_2^{2+}$ , and  $\text{CO}_3^{2-}$   
Euroconference and NEA Workshop: Actinide-XAS-98  
Grenoble, France, 04.-06.10.1998

Brendler, V., Bernhard, G., Nitsche, H., Stiglund, Y., Nordlinder, S.  
Coupling geochemical speciation to risk assessment codes  
Uranium Mining and Hydrogeology II  
Freiberg, Germany, 15.-17.09.1998

Bubner, M., Pompe, S., Meyer, M., Heise, K.H., Nitsche, H.  
Die Synthese isotopmarkierter Modellhuminsäuren  
GDCh-Fachtagung, FG Nuklearchemie  
Dresden, Germany, 07.-09.09.1998

Förster, E., Heller, S., Heise, K.H., Nitsche, H.  
Mineralisierung von Kohlenstoff-14-haltigen Reststoffen durch anodische Oxidation  
GDCh-Fachtagung, FG Nuklearchemie  
Dresden, Germany, 07.-09.09.1998

Friedrich, H., G. Bernhard, H. Nitsche  
Neues Radiochemisches Laborgebäude im Forschungszentrum Rossendorf  
-Bauliche und Strahlenschutztechnische Aspekte-  
GDCh-Fachtagung, FG Nuklearchemie  
Dresden, Germany, 07.-09.09.1998



Heise, K.H., Nicolai, R., Pompe, S., Bubner, M., Nitsche, H.  
 Melanoidins as Model Humic Acids in Radioecological Research  
 13<sup>th</sup> Radiochemical Conference  
 Mariánské Lázně-Jachymov, Czech Republic, 20.-24.04.1998

Heise, K.H., Nicolai, R., Pompe, S., Bubner, M., Nitsche, H.  
 FTIR-Untersuchungen zur Komplexbildung von Uran(V) durch huminsäureähnliche Melanoidine  
 GDCh-Fachtagung, FG Nuklearchemie  
 Dresden, Germany, 07.-09.09.1998

Heise, K.H., Pompe, S., Nicolai, R., Schmeide, K., Bubner, M., Reich, T., Nitsche, H.  
 Huminsäureforschung im FZR - Melanoidine als Modell-Huminsäuren  
 Uranium Mining and Hydrogeology II  
 Freiberg, Germany, 15.-17.09.1998

Heise, K.H., Pompe, S., Schmeide, K., Bubner, M., Schuster, G., Nicolai, R., Zänker, H., Reich, T., Geipel, G.,  
 Baraniak, L., Bernhard, G., Nitsche, H.  
 Humic Acid Research at FZR  
 Uranium Mining and Hydrogeology II  
 Freiberg, Germany, 15.-17.09.1998

Hennig, C., Denecke, M.A., Roßberg, A., Zahn, G., Reich, T., Nitsche, H.  
 U L<sub>III</sub> Polarized XAFS Studies on Ba[UO<sub>2</sub>PO<sub>4</sub>]<sub>2</sub>·8H<sub>2</sub>O  
 6. Jahrestagung der Deutschen Gesellschaft für Kristallographie (DGK)  
 Karlsruhe, Germany, 02.-05.03.1998

Hennig, C.  
 Korrektur der Koordinationszahlbestimmung für die Uranylgruppe aus EXAFS-Messungen pulverförmiger Proben  
 GDCh-Fachtagung, FG Nuklearchemie  
 Dresden, Germany, 07.-09.09.1998

Hennig, C., Arnold, T., Roßberg, A., Reich, T., Nitsche, H.  
 Uran L<sub>III</sub>-EXAFS Messungen zur Untersuchung der Uranyl-Adsorption an Ferrihydrit  
 GDCh-Fachtagung, FG Nuklearchemie  
 Dresden, Germany, 07.-09.09.1998

Hennig, C., Denecke, M.A., Roßberg, A., Zahn, G., Reich, T., Nitsche, H.  
 U L<sub>III</sub> Polarized XAFS Studies on Ba[UO<sub>2</sub>PO<sub>4</sub>]<sub>2</sub>·8H<sub>2</sub>O  
 Euroconference and NEA Workshop: Actinide-XAS-98  
 Grenoble, France, 04.-06.10.1998

Hennig, C., Kraus, W., Nolze, G.  
 The Problem of Preferred Orientation in EXAFS Measurements - Solvable with X-ray Diffraction?  
 Euroconference and NEA Workshop: Actinide-XAS-98  
 Grenoble, France, 04.-06.10.1998

Hennig, C., Reich, T., Arnold, T., Roßberg, A., Nitsche, H.  
 EXAFS Investigations of Uranyl Sorption on Ferrihydrite  
 Euroconference and NEA Workshop: Actinide-XAS-98  
 Grenoble, France, 04.-06.10.1998

Hübener, S., Brüchle, W., Dressler, R., Eichler, B., Gäggeler, H.W., Grantz, M., Heyne, H., Jäger, E., Jost, D.T.,  
 Kirbach, U., Nitsche, H., Piquet, D., Schädel, M., Schimpf, E., Taut, S., Trautmann, N., Türler, A., Vahle, A.,  
 Yakushev, A.B.  
 Seaborgium: Charakterisierung als Oxidhydroxid  
 GDCh-Tagung, FG Nuklearchemie  
 Dresden, Germany, 07.-09.09.1998

Kutschke, S., Panak, P., Selenska-Pobell, S., Geipel, G., Bernhard, G., Nitsche, H.  
 Molecular characterization of Thiobacillus strains recovered from uranium waste piles  
 Uranium Mining and Hydrogeology II  
 Freiberg, Germany, 15.-17.09.1998

Kutschke, S., Panak, P., Groudeva, V., Selenska-Pobell, S., Bernhard, G., Nitsche, H.  
 Molecular and radiochemical analysis of *Thiobacillus ferrooxidans* strains recovered from a uranium waste pile in  
 Saxony  
 Euroconference: Bacterial-Metal/Radionuclide Interaction  
 Rossendorf/Dresden, Germany, 02.-04.12.1998

Mack, B., Abraham, A., Baraniak, L., Bernhard, G., Nitsche, H.  
 Characterization of the Redox Behaviour of Spruce-Wood Lignin and Humic Acid  
 13<sup>th</sup> Radiochemical Conference  
 Mariánské Lázně-Jachymov, Czech Republic, 20.-24.04.1998

Miteva, V., Mitev, V., Selenska-Pobell, S.  
 RAPD and Rep-APD analysis of *Bacillus sphaericus*  
 8th Int. Symposium on Genetics of Industrial Microorganisms  
 Israel, 28.06.-03.07.1998

Nebelung, C., Nitsche, H., Henniger, J., Mann, G.  
 Vergleich von berechneten und gemessenen Alpha-Spektren von extrem dünnen Betonmeßpräparaten zur Freigabeentscheidung  
 GDCh-Tagung, FG Nuklearchemie  
 Dresden, Germany, 07.-09.09.1998

Panak, P., Kutschke, S., Selenska-Pobell, S., Geipel, G., Bernhard, G., Nitsche, H.  
 Wechselwirkung von U(VI) mit Bakterien aus Uranhalden  
 GDCh-Tagung, FG Nuklearchemie  
 Dresden, Germany, 07.-09.09.1998

Panak, P., Kutschke, S., Selenska-Pobell, S., Geipel, G., Bernhard, G., Nitsche, H.  
 Bacteria from a uranium mining waste pile: interaction with U(VI)  
 Euroconference: Bacterial-Metal/Radionuclide Interaction  
 Rossendorf/Dresden, Germany, 02.-04.12.1998

Panak, P., Selenska-Pobell, S., Boudakov, I., Miteva, V., Bernhard, G., Nitsche, H.  
 Selective accumulation of heavy metals in drain waters of a uranium waste pile by indigenous *Bacilli*  
 Euroconference: Bacterial-Metal/Radionuclide Interaction  
 Rossendorf/Dresden, Germany, 02.-04.12.1998

Pompe, S.  
 Erste Ergebnisse aus Säulenexperimenten zur Untersuchung des Migrationsverhaltens von U(VI) im System Gohy 532/Gorlebensand  
 Workshop Institut für Kernchemie der Universität Mainz  
 Mainz, Germany, 13.03.1998

Pompe, S., Bubner, M., Geipel, G., Heise, K.H., Nitsche, H.  
 Modified Synthetic Humic Acids for the Investigation of Humic Acids Complexation Behavior with Uranyl(VI) Ions  
 13<sup>th</sup> Radiochemical Conference  
 Mariánské Lázně-Jachymov, Czech Republic, 20.-24.04.1998

Pompe, S., Artinger, R., Schmeide, K., Heise, K.H., Nitsche, H., Kim, J.I.  
 Säulenexperimente zur Untersuchung des Einflusses von Huminstoffen auf das Migrationsverhalten von Uran(VI) in einem sandigen Sediment  
 GDCh-Fachtagung, FG Nuklearchemie  
 Dresden, Germany, 07.-09.09.1998

Puers, C., Selenska-Pobell, S.  
 Investigation of bacterial diversity in soil sample of a depleted uranium mining area nearby Johanngeorgenstadt, Saxonia, via 16S-RDNA-sequence analysis  
 Euroconference: Bacterial-Metal/Radionuclide Interaction  
 Rossendorf/Dresden, Germany, 02.-04.12.1998

Puers, C., Kampf, G., Selenska-Pobell, S.  
 Investigation of bacterial diversity in soil of a depleted Saxonian uranium mine via 16S rRNA gene and 16S/23S intergenic spacer analyses  
 Intern. Symposium on Microbial Ecology  
 Halifax, Canada, 09.-14.08.1998

Raff, J., Kirsch, R., Kutschke, S., Maier, T., Mertig, M., Selenska-Pobell, S., Bernhard, G., Hahn, U., Pompe, W.  
 Characterization of the surface layer of the *Bacillus sphaericus* isolate JG-A12 from a uranium waste pile  
 Euroconference: Bacterial-Metal/Radionuclide Interaction  
 Rossendorf/Dresden, Germany, 02.-04.12.1998

Reich, T., Denecke, M.A., Pompe, S., Otto, A., Brendler, V., Bubner, M., Heise, K.H., Nitsche, H., Allen, P.G., Bucher, J.J., Edelstein, N.M., Shuh, D.K.  
 Structural Analysis of the Interaction of Uranium(VI) with Humic Acid and Simple Carboxylic Acids Using EXAFS  
 Euroconference and NEA Workshop: Actinide-XAS-98  
 Grenoble, France, 04.-06.10.1998

Rettig, D., Merker, P., Nitsche, H.  
Particle emission from UV-irradiated silica surfaces  
Edinburgh, Scotland, 12.-18.09.1998

Richter, W., Zänker, H., Nitsche, H.  
Charakterisierung anorganischer und organischer Kolloide in bergbaurelevanten Wässern.  
4. Kolloquium des DFG-Schwerpunktprogramms "Geochemische Prozesse mit Langzeitfolgen im anthropogen beeinflussten Sickerwasser und Grundwasser"  
Freiberg, Germany, 26.-27.03.1998.

Richter, W., Zänker, H., Nitsche, H.  
Charakterisierung der Kolloidpartikel im Entwässerungsstollen des Freiburger Bergbaureviere (Rothschönberger Stolln).  
GDCh-Fachtagung, FG Nuklearchemie  
Dresden, Germany, 07.-09.09.1998

Roßberg, A., Reich, T., Hennig, C., Denecke, M.A., Baraniak, L., Bernhard, G., Nitsche, H.  
Determination of Molecular-Level Structural Information of Uranium in Environmentally Relevant Samples by EXAFS  
Uranium Mining and Hydrogeology II  
Freiberg, Germany, 15.-17.09.1998

Roßberg, A., Reich, T., Hennig, C., Denecke, M.A., Baraniak, L., Bernhard, G., Nitsche, H.  
Determination of Molecular-Level Structural Information of Uranium in Environmentally Relevant Samples by EXAFS  
Euroconference and NEA Workshop: Actinide-XAS-98  
Grenoble, France, 04.-06.10.1998

Rutsch, M., Geipel, G., Brendler, V., Bernhard, G., Nitsche, H.  
Interaction of uranium(VI) with arsenate studied by time-resolved laser-induced fluorescence spectroscopy  
13<sup>th</sup> Radiochemical Conference  
Mariánské Lázně-Jachymov, Czech Republic, 20.-24.04.1998

Rutsch, M., Geipel, G., Brendler, V., Bernhard, G., Nitsche, H.  
Komplexierung von Uran(VI) mit Arsen  
GDCh-Fachtagung, FG Nuklearchemie  
Dresden, Germany, 07.-09.09.1998

Satschanska, G., Kampf, G., Selenska-Pobell, S.  
Molecular bacterial diversity in soils and waters of three East German uranium mining waste piles  
Intern. Symposium on Microbial Ecology  
Halifax, Canada, 09.-14.08.1998

Satschanska, G., Kampf, G., Selenska-Pobell, S.  
Molecular bacterial diversity in soils and waters of three East German uranium mining waste piles  
Uranium Mining and Hydrogeology II  
Freiberg, Germany, 15.-17.09.1998

Satschanska, G., Kampf, G., Flemming, K., Selenska-Pobell, S.  
Molecular bacterial diversity in soils of two East German uranium waste piles  
Euroconference: Bacterial-Metal/Radionuclide Interaction  
Rossendorf/Dresden, Germany, 02.-04.12.1998

Satschanska, G., Kampf, G., Flemming, K., Selenska-Pobell, S.  
Molekulare Untersuchungen bakterieller Diversität in Erdproben aus uranhaltigen Abfallhalden  
Wissenschaftliche Konferenz: BIODIVERSITÄT der WGL  
Berlin, Germany, 17.-19.11.1998

Schmeide, K., Geipel, G., Zänker, H., Heise, K.H., Nitsche, H.  
Complexation of U(VI) with Aquatic Humic Acid Isolated from Bog Water  
13<sup>th</sup> Radiochemical Conference  
Mariánské Lázně-Jachymov, Czech Republic, 20.-24.04.1998

Schmeide, K., Geipel, G., Brendler, V., Heise, K.H., Nitsche, H.  
Einfluß von Sulfat auf die Uranyl-Humat-Komplexierung  
GDCh-Fachtagung, FG Nuklearchemie  
Dresden, Germany, 07.-09.09.1998

Schuster, G., Bubner, M., Pompe, S., Jander, R., Henkel, K., Heise, K.H., Nitsche, H.  
Thermoanalytische Untersuchungen an Huminsäuren und ihren Uran(VI)- und Eisen(III)- Komplexen  
GDCh-Fachtagung, FG Nuklearchemie  
Dresden, Germany, 07.-09.09.1998

Taut, S., Hübener, S., Eichler, B., Türler, A., Gäggeler, H.W., Timokhin, S.N., Zvara, I.  
Einsteinium: Entropien und Enthalpien der Adsorption auf Niobium, Tantal und Titanium  
GDCh-Fachtagung, FG Nuklearchemie  
Dresden, Germany, 07.-09.09.1998

Wober, J., Flemming, K., Hard, B., Pietsch, K., Selenska-Pobell, S.  
Comparison of *Desulfovibrio* isolates recovered from a uranium mining waste pile and other environments  
Uranium Mining and Hydrogeology II  
Freiberg, Germany, 15.-17.09.1998

Wober, J., Flemming, K., Pietsch, K., Hard, B., Selenska-Pobell, S.  
Comparison of *Desulfovibrio* isolates recovered from a uranium mining waste pile and other environments  
Euroconference: Bacterial-Metal/Radionuclide Interaction  
Rossendorf/Dresden, Germany, 02.-04.12.1998

Zänker, H., Hüttig, G., Richter, W., Schmeide, K., Nitsche, H.  
Colloid Characterization in a Humic-Rich Environmental Water Containing Varying Concentrations of Uranyl(VI) Ions  
13<sup>th</sup> Radiochemical Conference  
Mariánské Lázně-Jachymov, Czech Republic, 20.-24.04.1998

Zänker, H., Hüttig, G., Richter, W., Schmeide, K., Nitsche, H.  
Wechselwirkung von Moorwasserkolloiden mit Uranyl(VI)-Ionen  
GDCh-Fachtagung, FG Nuklearchemie  
Dresden, Germany, 07.-09.09.1998

Zorn, T., Arnold, T., Bernhard, G., Nitsche, H.  
Sorption of Uranium (VI) onto Phyllite and its Mineral Constituents  
GDCh-Fachtagung, FG Nuklearchemie  
Dresden, Germany, 07.-09.09.1998

### **III. SEMINARS, CONFERENCES AND WORKSHOPS**

## **INSTITUTE SEMINARS**

Dr. Lars Carlsen, DSc.

National Environmental Research Institute, Department of Environmental Chemistry, Research Department, Roskilde, Denmark

The role of humics in the migration of pollutants. How can radiolabeling bring us new information.

02.04.1998

Dr. Veneta Groudeva

University of Sofia, Department of Microbiology, Sofia, Bulgaria

Distribution of Thiobacilli in different copper mines in Bulgaria.

08.04.1998

Dr. Isabelle Billard

University of Strasbourg, Laboratoire de Chimie Nucleaire, Strasbourg, France

An overview about the scientific activities of the laboratory.

15.04.1998

Muriel Bouby

University of Strasbourg, Laboratoire de Chimie Nucleaire, Strasbourg, France

Uranium complexation by a biological molecule and by an organic industrial complexant.

15.04.1998

Prof. Dr. Shinya Nagasaki

University of Tokyo

Complexes of uranyl and organic substances by molecular orbital calculations

27.04.1998

Dr. Solange Hubert

Universite de Paris-Sud, Institut de Physique Nuclaire, Paris, France

Research on phosphate materials for nuclear waste storage

07.05.1998

Prof. Dr. Nicolai B. Mikheev

Russische Akademie der Wissenschaften, Institut für Physikalische Chemie, Moskau

Niedere Oxidationsstufen von f-Elementen

17.06.1998

Prof. Dr. Jean Fuger

University of Liège, Department of Radiochemistry

Liège, Belgium

Actinide chemical thermodynamics: Overview and perspective

12.10.1998

Dr. Dirk Bosbach

Universität Münster, Institut für Mineralogie

Wachstum und Auflösung von Mineralen: In-situ Beobachtungen im molekularen Maßstab

21.10.1998

Dr. Francis Livens

Department of Chemistry, University of Manchester, UK

Speed, speciation, and spectroscopy - kinetic and surface reactions in Geochemistry

19.11.1998

Dr. Henry Moll

The Royal Institute of Technology, Department of Chemistry, Stockholm, Sweden

Solution coordination chemistry of uranium and thorium in binary and ternary systems

30.11.1998

## **INTERNAL SEMINARS (open for the public)**

S. Amayri

Synthese und Charakterisierung von Liebigit

11.02.1998

L. Baraniak

Zur Redoxsituation im Hochmoor Kranichsee und der Grube Schlema

16.03.1998

G. Geipel

Uranminerale und ihre Fluoreszenzeigenschaften

13.05.1998

V. Brendler

Gewinnung thermodynamischer Standard-Daten

06.07.1998

H. Zänker

Nachweis eines feinen Eisen- und Aluminiumhydroxidkolloids in einer Aufschlämmung gemahlener Phyllits

17.7.1998

W. Richter

Charakterisierung der Kolloidpartikel im Wasser des Rothschnberger Stollns

13.8.1998

M. Rutsch

Zeitaufgelöste Laserfluoreszenzspektroskopie mit ultrakurzen Pulsen

02.09.1998

S. Pompe

Einfluß von Huminstoffen auf das Migrationsverhalten radioaktiver und nichtradioaktiver Schadstoffe unter natur-nahen Bedingungen - Zusammenfassender Bericht über die Arbeiten des Instituts für Radiochemie innerhalb des BMBF-Verbundprojekts 02E88150

20.10.1998

G. Mainka

Charakterisierung der Oberflächen von Biotit und Muskovit

02.11.1998

H. Zänker

Photonenkorrelationsspektroskopie und Rasterkraftmikroskopie an Huminsäure

17.11.1998

D. Rettig

Photolyse von Kieselsäure

09.12.1998

J. Raff

Die Hüllproteine des Bacillus sphericus Haldenisolates JG A-12

10.12.1998

## **CONFERENCES / WORKSHOPS** (organized by Institute of Radiochemistry)

GDCh-Fachtagung, FG Nuklearchemie

Dresden, Germany, 07.-09.09.1998

- Kernchemische Grundlagenforschung
- Actinidenchemie
- Radioanalytik
- Nuklearchemie in den Lebenswissenschaften
- Radiochemie in der Nuklearenergie-Technologie
- Nuklearchemie in der nuklearen Entsorgung
- Anwendung von Radioindikatoren in der Technik
- Nuklearchemie in Geowissenschaften und Kosmochemie
- Strahlenschutz / Radioökologie / Radionuklide in der Umwelt
- Tritiumchemie in der Fusionstechnologie

Euroconference and NEA Workshop "Speciation, Techniques, and Facilities for Radioactive Materials at Synchrotron Light Sources"

Grenoble, France, 04.-06.10.1998

- Introduction to Synchrotron Radiation Techniques
- Applications of Synchrotron Techniques
- Use of Radionuclides at Synchrotron Facilities, Present and Future

Euroconference "Bacterial-Metal/Radionuclide Interaction: Basic Research and Bioremediation"

Rosendorf/Dresden, Germany, 02.-04.12.1998

- Bacterial diversity in uranium wastes
- Oxidation, reduction, and accumulation of heavy metals/radionuclides by bacteria
- Environmental challenges of the nuclear fuel cycle and nuclear incidents
- Bioremediation for radionuclides and heavy metals
- Genetics of bacteria interacting with radionuclides/heavy metals

## **IV. PERSONNEL**



## PERSONNEL

### Director

Univ.-Prof. Dr. H. Nitsche (until October 31, 1998)  
PD Dr. G. Bernhard (acting, since November 1, 1998)

### Administrative Staff

G. Kreuzel\*  
K. Wünsche

A. Nagel

H. Pospischil

### Scientific Staff

Prof. Dr. U. Abram  
Dr. T. Arnold\*  
Dr. L. Baraniak  
PD Dr. G. Bernhard  
DC D. Birnstein  
Dr. V. Brendler\*  
Dr. M. Böttger\*  
Dr. M. Bubner  
Dr. H.-J. Engelmann  
DBC K. Flemming\*  
Dr. E. Förster\*  
Dr. H. Funke  
Dr. G. Geipel

Dr. A. Günther\*  
Dr. K.H. Heise  
Dr. C. Hennig\*  
Dr. S. Hübener  
Dr. G. Kampf\*  
Dr. K. Krogner  
Dr. G. Mainka\*  
Dr. P. Merker  
DC C. Nebelung  
DI K. Nicolai\*  
Dr. P. Panak\*  
Dr. S. Pompe\*

Dr. C. Puers\*  
Dr. T. Reich  
Dr. D. Rettig  
Dr. W. Richter\*  
Dr. S. Selenska-Pobell\*  
Dr. K. Schmeide\*  
Dr. G. Schuster\*  
Dr. S. Taut\*  
Dr. A. Vahle\*  
Dr. W. Wiesener  
DBC J. Wober\*  
Dr. H. Zänker

### Technical Staff

DI(FH) B. Barz\*  
DI(FH) C. Eckardt  
B. Eisold  
J. Falkenberg  
DI(FH) H. Friedrich  
Ch. Fröhlich  
DI(FH) G. Grambole  
G. Heinz

S. Heller\*  
DI(FH) K. Henkel  
B. Heschel  
H. Heyne  
B. Hiller  
DI(FH) G. Hüttig  
DI(FH) R. Jander  
P. Kluge

DI(FH) M. Meyer  
Ch. Müller  
H. Neubert  
DC(FH) A. Otto  
A. Rumpel  
R. Ruske  
DI(FH) U. Schaefer

### Graduate Students

DC A. Abraham  
DC S. Amayri  
DBT S. Kutschke  
DC B. Mack

DB J. Raff  
DC A. Roßberg  
DC M. Rutsch

DBC G. Sachanska\*  
DC B. Schmidt-Brücken  
DC T. Zorn

### Trainee

S. Grünert

C. Heidel

S. Wallner

\* post doc  
\* term contract

DC: Dipl.-Chem.  
DI: Dipl.-Ing.  
DP: Dipl.-Phys.

DBC: Dipl.-Biochem.  
DBT: Dipl.-Biotech.

DB: Dipl.-Biol.  
DM: Dipl.-Mineral.

## **V. ACKNOWLEDGMENTS**

## ACKNOWLEDGMENT OF FINANCIAL SUPPORT

The Institute is part of the Forschungszentrum Rossendorf e.V., which is financed in equal parts by the Federal Republic of Germany and the Free State of Saxony.

Four projects were supported by the Bundesministerium für Bildung, Wissenschaft, Forschung und Technologie (BMBF):

- Stilllegung und Rückbau: Direktmessung  $\alpha$ -aktiver Nuklide in Bauschutt zur Freigabeentscheidung.  
Contract No. BMBF 02 S 7655 A8
- Chemie der schwersten Elemente:  
Hochtemperaturgaschromatographie der Elemente 106 und 107  
Contract No. BMBF 06 DR 824 (2)
- Influence of humic acids on migration behavior of radioactive and non-radioactive heavy elements under natural conditions.  
Contract No. BMBF 02 E 88150
- Biosorption of uranium by bacillus for remediation of uranium wastes  
Contract No. DRL: BUL-014-97

Four projects were supported by Commission of the European Communities:

- Restoration Strategies for Radioactive Contaminated Sites and their Close Surroundings (RESTRAT).  
In collaboration with:  
SCK-CEN Mol, Belgium; Studsvik Ecosafe AB, Sweden; Riso National Laboratory, Denmark; Westlakes Research Institutes, Great Britain  
Contract No. F14P-CT95-0021
- Cooperative Network Matching EU and FSU Activities in the Field of Nuclear Fission Safety (NET-WORK/NNFS).  
In collaboration with:  
JRC Ispra, Italy; SIEVERT Moscow, Russia; UIOP Kiew, Ukraine; INTERPROJECT Minsk, Weißrußland  
Contract No. F14C-CT96-0016
- Effects of Humic Substances on the Migration of Radionuclides: Complexation and Transport of Actinides.  
In collaboration with:  
FZ Karlsruhe, Inst. f. Nukleare Entsorgungstechnik, Germany; British Geological Survey, Nottingham, United Kingdom; Centre d' Etudes des Saclay, CEA, France; Katholieke Universiteit Leuven, Labor voor Colloid-chemie, Heverlee, Belgium; Loughborough University, Dept. of Chemistry, Leicestershire, United Kingdom; University of Manchester, Dept. of Chemistry, Manchester, United Kingdom; National Environmental Research Institute, Roskilde, Denmark; GSF Forschungszentrum für Umwelt und Gesundheit, Oberschleißheim, Germany; Université de Nantes, Laboratoire de Biochimie at Radiochimie, Nantes, France  
Contract No. F14W-CT96-0027
- Joint European Thermodynamic Database for Environmental Modeling (JETDEM).  
In collaboration with:  
FZ Karlsruhe, Germany; RCM Environmental Ltd., United Kingdom; Kungliga Tekniska Hogskolan, Department of Chemistry, Sweden; University of Aberdeen, Department of Chemistry, United Kingdom; Quantisci, Spain; Uppsala University, Institute of Earth Sciences, Sweden  
Contract No. F14W-CT96-0029

The Sächsisches Staatsministerium für Wissenschaft und Kunst provided support for the following projects:

- Mine-water Induced Wood Decomposition and Influence of the Degradation Products on Radionuclide Speciation, Sorption and Migration.  
Contract No. SMWK 4-7541.83-FZR/402
- Influence of Natural Water-borne Organic Substances on the Valency of Radionuclides and Toxic Heavy Metals.  
Contract No. SMWK 4-7541.88-FZR/512
- Soil-Plant Transfer Factors for Uranium.  
Contract No. SMWK 4-7531.50-03-VKTA/601
- Wechselwirkung von Mikroorganismen mit Uran und ausgewählten Radionukliden: Charakterisierung der Biosorption und ihrer genetischen Grundlagen mit Hinblick auf Ausbreitungsverhalten und Bioremediation.  
Contract No. SMWK 4-7531.50-03-FZR/607
- Wechselwirkung zwischen Proteinen und Metalloberflächen. Teilvorhaben C: Wechselwirkung von bakteriellen Zellhüllenproteinen mit Metallclustern.  
Contract No. SMWK 4-7531.50-03-0370/708

- Untersuchung der Bildung von kolloidalen organischen Partikeln in Bergwerkswässern.  
Contract No. SMWK 4-7533.70-FZR/704
- Chemical conversion of <sup>14</sup>C-labeled products to [<sup>14</sup>C]Barium carbonate for long-time disposal.  
Contract No. SMWK 4-7581.312/20
- Vortragstagung der GDCh-Fachgruppe Nuklearchemie  
Contract No. SMWK 4-7531.50-05-98/35

One project was supported by Sächsisches Staatsministerium für Wirtschaft und Arbeit:

- Festelektrolytensensoren für die Messung von Verunreinigungen in flüssigem Stahl.  
In cooperation with Herbst GmbH Wärmekeramik, Dürrröhrsdorf.  
Projekt Nr. 1500/309

Six projects were supported by Deutsche Forschungsgemeinschaft (DFG):

- Experimentelle Untersuchung der Eigenschaften schwerer Actinoide im elementaren Zustand mittels chromatographischer Methoden.  
Contract No. DFG HU 642/1-2
- Nitridbrücken zwischen Übergangsmetallen und Hauptgruppenelementen.  
Contract No. DFG AB 67-4/1
- Nitridbrücken zwischen Rhenium und Elementen der 3. Hauptgruppe.  
Contract No. DFG AB 67-4/2
- Charakterisierung der Kolloidpartikel in den Wasserfließsystemen stillgelegter sächsischer Bergwerke  
Contract No. DFG NI 210/4-1
- Untersuchungen zur Sorption von Uranylionen an Huminsäurebioschichten auf Phyllit und seinen mineralischen Bestandteilen  
Contract No. DFG NI 210/5-1
- Untersuchung der Sorptionsmechanismen von Uran(VI) auf Gesteins- und Mineraloberflächen. Identifizierung und Modellierung der sorbierten Oberflächenspezies auf molekularer Ebene.  
Contract No. DFG NI 210/6-1

Ten projects were supported by the following sponsors:

- Development of experimental arrangements and methods for on-line high temperature gas-chromatography of the heaviest elements.  
In cooperation with GSI.  
GSI DRNIK.
- INTAS: Spectroscopic study of particles emitted by nuclear fuel under different accident scenarios.  
Contract No. INTAS 96-1927
- Complexation and Sorption Phenomena of Uranium in Environmentally-Relevant Systems. Stanford Synchrotron Radiation Laboratory SSRL; U.S. Department of Energy  
Contract No. 2362 MP
- XAFS-Untersuchungen umweltrelevanter Uranylkomplexverbindungen und deren Sorbate.  
Hamburger Synchrotronstrahlungslabor HASYLAB am Deutschen Elektronen-Synchrotron DESY.  
Contract No. II-97-18
- EXAFS-Untersuchungen umweltrelevanter Cr(III) Verbindungen.  
Hamburger Synchrotronstrahlungslabor HASYLAB am Deutschen Elektronen-Synchrotron DESY.  
Contract No. II-97-17
- Fundamental Technetium, Rhenium and Gold Chemistry.  
Contract No. DAAD ARC-XI-97/1
- Molecular analysis of natural bacterial communities in uranium wastes.  
ESF scientific programme: "Ground water pollution"  
Contract No. Gpoll/9816
- Euroconference "Speciation, techniques, and facilities for radioactive materials at synchrotron light sources"  
Contract No. EU/ERBFMMACT98-0331
- Euroconference "Bacterial-Metal/Radionuclide Interaction: Basic Research and Bioremediation"  
Contract No. EU/ERBFMMACT98-0339
- NATO Collaborative Research Grant "Speciation of radionuclides in environmentally relevant systems by XAFS spectroscopy"  
Contract No. SA.5-2-05(CRG.971641)